

**PHYSICOCHEMICAL PROPERTIES OF BIOPOLYMER-  
STABILIZED COLLOIDAL PARTICLES: MICROFIBRILLATED  
CELLULOSE-STABILIZED EMULSIONS AND  
 $\beta$ -LACTOGLOBULIN-COATED GOLD NANOPARTICLES**

**THUNNALIN WINUPRASITH**

**A THESIS SUBMITTED IN PARTIAL FULFILLMENT  
OF THE REQUIREMENTS FOR  
THE DEGREE OF DOCTOR OF PHILOSOPHY  
(BIOTECHNOLOGY)  
FACULTY OF GRADUATE STUDIES  
MAHIDOL UNIVERSITY  
2014**

**COPYRIGHT OF MAHIDOL UNIVERSITY**

Thesis  
entitled

**PHYSICOCHEMICAL PROPERTIES OF BIOPOLYMER-  
STABILIZED COLLOIDAL PARTICLES: MICROFIBRILLATED  
CELLULOSE-STABILIZED EMULSIONS AND  
β-LACTOGLOBULIN-COATED GOLD NANOPARTICLES**

.....  
Miss Thunnalin Winuprasith  
Candidate

.....  
Assoc. Prof. Manop Suphantharika,  
Ph.D.  
Major Advisor

.....  
Lect. Pairoj Luangpituksa,  
Dr.Agr.Chem.  
Co-advisor

.....  
Asst. Prof. Anadi Nitithamyong,  
Ph.D.  
Co-advisor

.....  
Asst. Prof. Promluck Somboonpanyakul,  
Ph.D.  
Co-advisor

.....  
Prof. Banchong Mahaisavariya,  
M.D., Dip. Thai Board of Orthopedics  
Dean  
Faculty of Graduate Studies  
Mahidol University

.....  
Assoc. Prof. Sittiwat Lertsiri,  
Ph.D.  
Program Director  
Doctor of Philosophy Program in  
Biotechnology  
Faculty of Science, Mahidol University

Thesis  
entitled

**PHYSICOCHEMICAL PROPERTIES OF BIOPOLYMER-  
STABILIZED COLLOIDAL PARTICLES: MICROFIBRILLATED  
CELLULOSE-STABILIZED EMULSIONS AND  
β-LACTOGLOBULIN-COATED GOLD NANOPARTICLES**

was submitted to the Faculty of Graduate Studies, Mahidol University  
for the degree of Doctor of Philosophy (Biotechnology)  
on  
June 13, 2014

.....  
Miss Thunnalin Winuprasith  
Candidate

.....  
Asst. Prof. Utai Klinkesorn,  
Ph.D.  
Member

.....  
Asst. Prof. Somchai Chauvatcharin,  
Ph.D.  
Chair

.....  
Lect. Pairoj Luangpituksa,  
Dr.Agr.Chem.  
Member

.....  
Assoc. Prof. Manop Supphantharika,  
Ph.D.  
Member

.....  
Asst. Prof. Anadi Nitithamyong,  
Ph.D.  
Member

.....  
Asst. Prof. Promluck Somboonpanyakul,  
Ph.D.  
Member

.....  
Prof. Banchong Mahaisavariya,  
M.D., Dip. Thai Board of Orthopedics  
Dean  
Faculty of Graduate Studies  
Mahidol University

.....  
Prof. Skorn Mongkolsuk,  
Ph.D.  
Dean  
Faculty of Science  
Mahidol University

## ACKNOWLEDGEMENTS

I would like to express my deepest gratitude and appreciation to my advisor, Assoc. Prof. Manop Suphantharika, for his helpful guidance, instruction, supervision, and encouragement throughout this study. All his kindness and courtesy will be long remembered with respect. I am also grateful to the all members of the advisory committee, Dr. Pairoj Luangpitaksa, Asst. Prof. Anadi Nitithamyong, Asst. Prof. Promluck Somboonpanyakul, and Asst. Prof. Utai Klinkesorn for all of their helpful suggestions and advice over the thesis and for serving on my committee.

My sincerely gratitude is given to Prof. Dr. David Julian McClements who was my supervisor when I was an exchange student at Department of Food Science, University of Massachusetts (Amherst), USA. It would not have been possible without his consistent guidance and invaluable advises for my work there. I would also like to thank Dr. Lili He for her suggestion especially in the use and interpretation of SERS experiment. Moreover, I am particularly grateful to all Thai students and all friends in UMASS, Amherst for their friendship, helps and support. I would say they never made me feel homesick when I was there. These will be in my memory as long.

I am very grateful to the Thailand Research Fund and Mahidol University for the financial support through the Royal Golden Jubilee Ph.D. Program. This research is also partially supported by AG-BIO/PERDO-CHE. I am grateful to Metrohm Siam Ltd for providing the rheometer used in these experiments.

I am thankful to all members of the room BT204, and all staffs for their encouragement, friendship, and providing the facilities during my study.

Last but not least, I cannot find any word or phrase to express how lucky I am to be a part of my family. Without their supporting, I cannot reach this point, indeed. Thank you.

Thunnalin Winuprasith

**PHYSICOCHEMICAL PROPERTIES OF BIOPOLYMER-STABILIZED COLLOIDAL PARTICLES: MICROFIBRILLATED CELLULOSE-STABILIZED EMULSIONS AND  $\beta$ -LACTOGLOBULIN-COATED GOLD NANOPARTICLES**

THUNNALIN WINUPRASITH 5238128 SCBT/D

Ph.D. (BIOTECHNOLOGY)

THESIS ADVISORY COMMITTEE: MANOP SUPHANTHARIKA, Ph.D., PAIROJ LUANGPITUKSA, Dr.Agr.Chem., ANADI NITITHAMYONG, Ph.D., PROMLUCK SOMBOONPANYAKUL, Ph.D.

**ABSTRACT**

This research focused on stabilization of colloidal particles using biopolymers. Two biopolymer-stabilized colloidal systems were studied; i.e. microfibrillated cellulose (MFC)-stabilized oil-in-water (o/w) emulsions and  $\beta$ -lactoglobulin ( $\beta$ Lg)-coated gold nanoparticles (GNPs). This research consists of four parts.

The first part investigated the effect of number of passes (1-20 passes) through a homogenizer used for MFC preparation on properties of MFC itself and also the properties and stability of o/w emulsions stabilized by MFC. MFC was prepared from mangosteen (*Garcinia mangostana* L.) rind using hot sodium hydroxide extraction, hydrogen peroxide bleaching, and then shearing using a homogenizer. The crystallinity index, degree of polymerization, viscoelasticity, and viscosity of the MFC decreased as the number of homogenization passes increased, indicating that fiber degradation occurred. The 30% o/w emulsions stabilized by MFC (0.7% w/w MFC, pH = 6.8-7.2) obtained at the higher number of homogenization passes exhibited smaller oil droplets, stronger three-dimensional network structures, and were more stable to creaming than those stabilized by MFC obtained at the lower number of homogenization passes. The creaming stability was reduced at low pH or at high salt concentration. Thermal treatment had little influence on the creaming stability of these emulsions. The second part focused on the effect of MFC concentration (0.05-0.70% w/w) on the properties and stability of 10% o/w emulsions (pH = 6.8-7.2). In this study, MFC obtained at 20 homogenization passes was chosen due to its highest emulsion stabilizing properties. The results show that the oil droplet size, color intensity, viscoelasticity, and stability of the MFC-stabilized emulsions increased with MFC concentration. SEM and confocal micrographs revealed that MFC stabilized emulsion by Pickering mechanism. In addition, the rheological data provided evidence for network formation in the emulsions with increasing MFC concentration. All emulsions were stable to coalescence but the stability of creaming decreased with decreasing MFC concentration. These results provided understanding of the influence of processing conditions for MFC preparation as well as its concentration on properties and stability of MFC-stabilized emulsions, leading to a new application in food industry.

The third part was aimed to prepare the  $\beta$ Lg-coated GNPs (pH 3) and to study the influence of  $\beta$ Lg concentration on protein conformational changes and GNPs aggregation. The surface charge of GNPs changed from negative to positive with increasing  $\beta$ Lg concentration, indicating that the globular protein molecules adsorbed to the surfaces of the particles. Extensive particle aggregation occurred when  $\beta$ Lg did not saturate the GNP surfaces, which was attributed to electrostatic bridging flocculation. Modifications in LSPR and SERS spectra after addition of  $\beta$ Lg to the GNP suspensions supported the adsorption of  $\beta$ Lg to the surfaces. Moreover, SERS highlighted the importance of specific functional groups in the binding interaction, and suggested conformational changes of the globular protein after adsorption. The fourth part focused on the interactions between  $\beta$ Lg-coated GNP interfaces and bile salts (BS) at pH 7 by primarily focusing on the physicochemical and interfacial compositional changes of protein at the particle surfaces. The BS was shown to adsorb to the  $\beta$ Lg-coated GNP surfaces and alter the interfacial composition, charge, and structure. SERS spectra of  $\beta$ Lg-coated GNP after BS addition contained bands from both  $\beta$ Lg and BS, indicating that the  $\beta$ Lg was not fully displaced by the BS. The impact of the bile salts could be described by an orogenic mechanism: mixed interfaces were formed that consisted of islands of aggregated proteins surrounded by a sea of bile salts. These results provided fundamental information about the interaction between globular protein, colloidal particles, and surface active bile salts that can be used as database for interface science in food emulsion application.

**KEY WORDS: MICROFIBRILLATED CELLULOSE / EMULSION /  $\beta$ -LACTOGLOBULIN / GOLD NANOPARTICLES / SURFACE-ENHANCED RAMAN SCATTERING**

คุณสมบัติทางเคมีกายภาพของอนุภาคคอลลอยด์ที่เสถียรด้วยโพลีเมอร์ชีวภาพ:  
 ระบบอิมัลชันที่เสถียรด้วยเส้นใยเซลลูโลส และ อนุภาคทองคำระดับนาโนที่เคลือบด้วยโปรตีนเบต้า-แลคโทโกลบูลิน  
 PHYSICOCHEMICAL PROPERTIES OF BIOPOLYMER-STABILIZED COLLOIDAL PARTICLES:  
 MICROFIBRILLATED CELLULOSE-STABILIZED EMULSIONS AND  $\beta$ -LACTOGLOBULIN-COATED GOLD NANOPARTICLES

ธัญญ์นลิน วิทยุประสิทธิ์ 5238128 SCBT/D

ปรด. (เทคโนโลยีชีวภาพ)

คณะกรรมการที่ปรึกษาวิทยานิพนธ์: มานพ สุพรรณธริกา, Ph.D., ไพโรจน์ หลวงพิทักษ์, Dr.Agr.Chem., อาภาณี นิตินธรรมขง, Ph.D.,  
 พร้อมลักษณ์ สมบูรณ์ปัญญากุล, Ph.D.

บทคัดย่อ

งานวิจัยนี้สนใจการทำให้อนุภาคคอลลอยด์เสถียรโดยใช้โพลีเมอร์ชีวภาพ ซึ่งศึกษาใน 2 ระบบ ได้แก่ ระบบอิมัลชันที่คงตัวโดยการ  
 ใช้เส้นใยเซลลูโลสระดับไมโคร และการเคลือบอนุภาคทองคำระดับนาโนด้วยโปรตีนเบต้า-แลคโทโกลบูลิน โดยงานวิจัยนี้ประกอบไปด้วย 4 ส่วนหลัก  
 ส่วนแรกศึกษาผลของจำนวนรอบ (1-20 รอบ) ในการผ่านเครื่องโฮโมจิไนเซอร์ของเส้นใยเซลลูโลสต่อคุณสมบัติของเส้นใย  
 เซลลูโลสเอง รวมทั้งคุณสมบัติและความเสถียรของระบบอิมัลชันที่เตรียมโดยใช้เส้นใยดังกล่าว เส้นใยเซลลูโลสสามารถสกัดได้จากเปลือกมังคุด โดย  
 การใช้โซเดียมไฮดรอกไซด์ร่วมกับฟอกสีด้วยไฮโดรเจนเปอร์ออกไซด์ และแยกเส้นใยโดยใช้เครื่องโฮโมจิไนเซอร์ ผลการทดลองพบว่า ดัชนี  
 ความเป็นผลึก, อันดับการพอลิเมอไรเซชัน, สมบัติหุ่ยนหืดและความหนืดของเส้นใยเซลลูโลสลดลง เมื่อจำนวนรอบในการผ่านเครื่องโฮโมจิไนเซอร์  
 เพิ่มขึ้น บ่งชี้ได้ว่าเส้นใยเกิดการแตกสลายในกระบวนการเตรียมดังกล่าว ระบบอิมัลชันชนิดน้ำมันในน้ำ (น้ำมัน 30%, เส้นใยเซลลูโลส 0.7% ค่าความ  
 เป็นกรดต่าง = 6.8-7.2) ที่คงตัวด้วยเส้นใยเซลลูโลสที่ได้จากการผ่านเครื่องโฮโมจิไนเซอร์ที่จำนวนรอบมากนั้น มีขนาดอนุภาคไขมันเล็ก, มีโครงสร้าง  
 คาข่ายสามมิติที่แข็งแรง, และมีความเสถียรต่อการเกิดคริมมากกว่าระบบอิมัลชันที่คงตัวด้วยเส้นใยที่ได้มาจากการผ่านเครื่องโฮโมจิไนเซอร์ที่จำนวน  
 รอบน้อย ความเสถียรต่อการเกิดคริมจะลดลงเมื่ออิมัลชันมีสถานะเป็นกรดหรือมีความเข้มข้นของเกลือสูง ส่วนอุณหภูมิมีผลต่อการเกิดคริมเพียงเล็กน้อย  
 ส่วนที่สองได้ศึกษาถึงอิทธิพลของความเข้มข้นของเส้นใยเซลลูโลส (0.05-0.70%) ต่อคุณสมบัติและความเสถียรของระบบอิมัลชันชนิดน้ำมันในน้ำ  
 (ไขมัน 10%, ค่าความเป็นกรดต่าง = 6.8-7.2) ในการทดลองนี้ใช้เส้นใยเซลลูโลสที่ผ่านเครื่องโฮโมจิไนเซอร์ 20 รอบ เนื่องจากให้ความคงตัวของ  
 อิมัลชันสูงสุด ผลการทดลองพบว่าขนาดอนุภาคไขมัน, ความเข้มข้นของลิ, สมบัติหุ่ยนหืดและความเสถียรของระบบอิมัลชันเพิ่มขึ้น เมื่อเส้นใยเซลลูโลส  
 ในระบบเพิ่มขึ้น ภาพจากกล้องจุลทรรศน์อิเล็กตรอนแบบส่องกราดและแบบคอนโฟคอลชนิดที่ใช้เลเซอร์ แสดงให้เห็นว่า เส้นใยเซลลูโลสทำให้ระบบ  
 อิมัลชันเสถียรด้วยกลไก “Pickering” นอกจากนี้ ข้อมูลเกี่ยวกับคุณสมบัติการไหลชี้ให้เห็นว่าการสร้างร่างแหในอิมัลชันเมื่อความเข้มข้นของเส้นใย  
 เซลลูโลสเพิ่มขึ้น โดยสรุปผลการทดลองข้างต้นเป็นประโยชน์ในการเพิ่มความเข้าใจในอิทธิพลของกระบวนการเตรียมเส้นใยเซลลูโลสต่อคุณสมบัติ  
 ของเส้นใยเอง รวมถึงคุณสมบัติและความเสถียรของระบบอิมัลชันที่ใช้เส้นใยเซลลูโลสเพื่อนำไปใช้ในอุตสาหกรรมอาหารต่อไป

ในส่วนที่สามมุ่งเน้นถึงการเตรียมอนุภาคทองคำระดับนาโนที่เคลือบด้วยโปรตีนเบต้า-แลคโทโกลบูลินที่ความเป็นกรดต่างเท่ากับ 3  
 และยังศึกษาถึงการเปลี่ยนแปลงรูปร่างของโปรตีนและการเกิดการรวมกันของอนุภาคทองคำ พบว่า การดูดซับของโปรตีนบนผิวของอนุภาคขึ้นไปได้  
 จากการเปลี่ยนแปลงสเปกตรัมของ LSPR และ SERS รวมทั้งการเปลี่ยนแปลงประจุของอนุภาคจากลบเป็นบวก เมื่อปริมาณโปรตีนในระบบเพิ่มขึ้น การ  
 รวมกันของอนุภาคทองคำจะเกิดขึ้นเมื่อพื้นผิวของอนุภาคไม่ได้เชื่อมด้วยโมเลกุลของโปรตีน โดยกลไกการเชื่อมของอนุภาคด้วยไฟฟ้าสถิตย์  
 นอกจากนี้สเปกตรัม SERS ยังบ่งชี้ว่าเกิดการเปลี่ยนแปลงรูปร่างของโปรตีนหลังจากดูดซับบนพื้นผิวของอนุภาค โดยมีหมู่ฟังก์ชันจำเพาะของโปรตีน  
 เกี่ยวข้องในปฏิกิริยาดังกล่าว ส่วนที่สี่ได้ศึกษาถึงปฏิกิริยาของเกลือน้ำดีต่อคุณสมบัติทางเคมีกายภาพและการเปลี่ยนแปลงของโปรตีนบนผิวสัมผัสของ  
 อนุภาคทองคำระดับนาโนที่เคลือบด้วยโปรตีนเบต้า-แลคโทโกลบูลิน โดยศึกษาที่ความเป็นกรดต่างเท่ากับ 7 พบว่า มีการดูดซับของเกลือน้ำดีลงบน  
 อนุภาคดังกล่าว ซึ่งส่งผลให้เกิดการเปลี่ยนแปลงองค์ประกอบของผิวสัมผัส ประจุ และโครงสร้าง การใช้เทคนิค SERS แสดงให้เห็นว่าในระบบที่มีเกลือ  
 น้ำดีและอนุภาคที่เคลือบด้วยโปรตีน โดยรูปแบบของสเปกตรัมจะเป็นการผสมผสานระหว่างสเปกตรัมของโปรตีนและเกลือน้ำดี แสดงว่าเกลือน้ำดี  
 สามารถเข้าแทนที่โปรตีนบนอนุภาคได้เป็นบางส่วน ซึ่งกลไกดังกล่าวเรียกว่ากลไก “Orogenic” คือ การแทนที่ของโปรตีนบนผิวสัมผัสด้วยเกลือน้ำดี  
 โดยโปรตีนจะเกิดการรวมตัวเป็นก้อนท่ามกลางผิวสัมผัสของเกลือน้ำดีโดยรอบ โดยสรุปผลการทดลองนี้เป็นข้อมูลพื้นฐานเพื่ออธิบายเกี่ยวกับ  
 ปฏิกิริยาระหว่างโปรตีน อนุภาค และเกลือน้ำดี และสามารถใช้เป็นฐานข้อมูลด้านวิทยาศาสตร์ผิวสัมผัสของอิมัลชันในอาหารต่อไป

## CONTENTS

	<b>Page</b>
<b>ACKNOWLEDGEMENTS</b>	<b>iii</b>
<b>ABSTRACT</b>	<b>iv</b>
<b>ABSTRACT (THAI)</b>	<b>v</b>
<b>LIST OF TABLES</b>	<b>xiii</b>
<b>LIST OF FIGURES</b>	<b>xiv</b>
<b>LIST OF ABBRIVIATIONS</b>	<b>xxi</b>
<b>CHAPTER I INTRODUCTION</b>	<b>1</b>
<b>CHAPTER II LITERATURE REVIEW</b>	<b>6</b>
2.1 Biopolymers stabilized colloidal systems	6
2.2 Microfibrillated cellulose stabilized oil-in-water emulsions	7
2.2.1 Microfibrillated cellulose	7
2.2.1.1 Sources of microfibrillated cellulose	9
2.2.1.2 Preparation of microfibrillated cellulose	10
2.2.1.3 Properties of Microfibrillated cellulose	17
2.2.1.4 Potential applications of microfibrillated cellulose	22
2.2.1.5 Limitation of using MFC	23
2.2.2 Emulsions	24
2.2.2.1 Definition and classification	24
2.2.2.2 Pickering emulsion	25
2.2.2.3 Emulsion formation	29
2.2.2.4 Emulsion properties	31
2.2.2.5 Emulsion stability	40
2.2.3 Emulsion stabilized by cellulose materials	50
2.3 $\beta$ -lactoglobulin coated gold nanoparticles	51
2.3.1 $\beta$ -lactoglobulin ( $\beta$ Lg)	51
2.3.2 Protein adsorption onto particle surfaces	52

## CONTENTS (cont.)

	<b>Page</b>
2.3.3 Gold colloidal nanoparticles	53
2.3.3.1 Gold nanoparticle formation and properties	53
2.3.3.2 Formation of conjugated gold-protein	56
2.4 Raman spectroscopy	58
2.4.1 Basic principles	58
2.4.2 Surface-enhanced Raman scattering (SERS)	61
2.4.2.1 SERS substrate preparation	61
2.4.2.2 Critical factors of SERS experiment	62
2.4.3 Applications of Raman spectroscopy in Foods	63
2.4.4 Interpretation of Raman spectra related to protein	65
2.4.4.1 Aromatic amino acid side chains	65
2.4.4.2 Aliphatic amino acid residues	68
2.4.4.3 Charged amino acid residues	68
2.4.4.4 Amide (peptide) bond	68
<b>CHAPTER III EXPERIMENTAL METHODS</b>	<b>70</b>
3.1 Preparation of microfibrillated cellulose	70
3.2 Characterization of microfibrillated cellulose	71
3.2.1 Chemical analysis	71
3.2.2 X-ray powder diffraction (XRD) analysis	71
3.2.3 Determination of degree of polymerization	72
3.3 Preparation of MFC-stabilized emulsions	72
3.4 Characterization of MFC-stabilized emulsions	73
3.4.1 Particle size determination	73
3.4.2 Scanning electron microscopy	73
3.4.3 Confocal laser scanning microscopy	74
3.4.4 Rheology measurements	74
3.4.5 $\zeta$ -potential measurements	75
3.4.6 Visual assessment of creaming	75

## CONTENTS (cont.)

	<b>Page</b>
3.4.7 Statistical analysis	76
3.5 Preparation of $\beta$ Lg-coated GNPs	76
3.6 $\beta$ Lg-coated GNPs interaction with bile salts	77
3.7 Characterization of $\beta$ Lg coated GNPs systems	77
3.7.1 Particle size and charge measurement	77
3.7.2 UV–visible spectrophotometer	77
3.7.3 Transmission electron microscopy (TEM)	78
3.7.4 Surface-enhanced electron microscopy (SERS)	78
<b>CHAPTER IV MICROFIBRILLATED CELLULOSE FROM MANGOSTEEN</b> <b>(<i>Garcinia mangostana</i> L.) RIND: PREPARATION, CHARACTERIZATION,</b> <b>AND EVALUATION AS AN EMULSION STABILIZER</b>	<b>79</b>
4.1 Abstract	79
4.2 Introduction	80
4.3 Materials and methods	82
4.3.1 Materials	82
4.3.2 Microfibrillated cellulose preparation	83
4.3.3 Characterization of microfibrillated cellulose	83
4.3.3.1 Chemical analysis	83
4.3.3.2 X-ray powder diffraction (XRD) analysis	83
4.3.3.3 Determination of degree of polymerization	84
4.3.4 Preparation of MFC-stabilized emulsions	84
4.3.5 Characterization of MFC-stabilized emulsions	84
4.3.5.1 Particle size determination	84
4.3.5.2 Scanning electron microscopy	84
4.3.5.3 Confocal laser scanning microscopy	85
4.3.5.4 Rheology measurements	85
4.3.5.5 $\zeta$ -potential measurements	85
4.3.5.6 Visual assessment of creaming	85

## CONTENTS (cont.)

	<b>Page</b>
4.3.5.7 Stability to environmental stresses	85
4.3.6 Statistical analysis	86
4.4 Results and Discussions	86
4.4.1 Purified cellulose and microfibrillated cellulose	86
4.4.1.1 Chemical compositions	86
4.4.1.2 X-ray diffraction patterns	87
4.4.1.3 Degree of polymerization ( <i>DP</i> )	88
4.4.1.4 Rheological properties	89
4.4.2 Characterization of MFC-stabilized o/w emulsions	91
4.4.2.1 Particle diameter and particle size distribution	91
4.4.2.2 Microstructure	92
4.4.2.3 Rheological properties	94
4.4.2.4 $\zeta$ -potential	99
4.4.2.5 Creaming stability	101
4.4.2.6 Environmental stresses	104
4.5 Conclusions	106
<b>CHAPTER V PROPERTIES AND STABILITY OF OIL-IN-WATER EMULSIONS STABILIZED BY MICROFIBRILLATED CELLULOSE FROM MANGOSTEEN RIND</b>	<b>108</b>
5.1 Abstract	108
5.2 Introduction	109
5.3 Materials and methods	111
5.3.1 Materials	111
5.3.2 Preparation of microfibrillated cellulose	111
5.3.3 Preparation of MFC-stabilized emulsions	111
5.3.4 Particle size determination	112
5.3.5 Color measurement	112
5.3.6 Optical microscopy	112

## CONTENTS (cont.)

	<b>Page</b>
5.3.7 Scanning electron microscopy	113
5.3.8 Confocal laser scanning microscopy	113
5.3.9 Rheology measurements	113
5.3.10 Visual assessment of creaming	114
5.3.11 Statistical analysis	114
5.4 Results and Discussion	114
5.4.1 Particle size and size distribution	114
5.4.2 Color of emulsions	118
5.4.3 Microstructure of emulsions	119
5.4.4 Rheological properties	120
5.4.5 Emulsion stability	126
5.4.5.1 Stability against coalescence	126
5.4.5.2 Stability against creaming	126
5.5 Conclusions	129
<b>CHAPTER VI SPECTROSCOPIC STUDIES OF CONFORMATIONAL</b>	
<b>CHANGES OF <math>\beta</math>-LACTOGLOBULIN ADSORBED ON GOLD</b>	
<b>NANOPARTICLE SURFACES</b>	
6.1 Abstract	130
6.2 Introduction	131
6.3 Materials and methods	133
6.3.1 Materials	133
6.3.2 $\beta$ Lg Solution preparation	133
6.3.3 Gold nanoparticle (GNPs) interaction with $\beta$ Lg	133
6.3.4 Particle size and charge measurement	134
6.3.5 UV–visible spectrophotometer	134
6.3.6 Transmission electron microscopy (TEM)	134
6.3.7 Surface-enhanced electron microscopy (SERS)	134
6.4 Results and discussion	134

## CONTENTS (cont.)

	<b>Page</b>
6.4.1 Properties of bare GNPs	134
6.4.2 Particle charge characteristics	135
6.4.3 Particle size and aggregation	137
6.4.4 UV–visible absorption spectra	139
6.4.5 Transmission electron microscopy (TEM)	141
6.4.6 Surface-enhanced Raman spectroscopy (SERS)	142
6.5 Conclusions	146
<b>CHAPTER VII ALTERATIONS IN PROTEIN CORONA AROUND NANOPARTICLES BY BIOLOGICAL SURFACTANTS: IMPACT OF BILE SALTS ON <math>\beta</math>-LACTOGLOBULIN-COATED GOLD NANOPARTICLES</b>	
7.1 Abstract	147
7.2 Introduction	148
7.3 Materials and methods	151
7.3.1 Materials	151
7.3.2 $\beta$ Lg Solution preparation	151
7.3.3 GNPs interaction with $\beta$ Lg and bile salts	151
7.3.4 Particle size and charge measurements	152
7.3.5 UV–visible spectrophotometer	152
7.3.6 Transmission electron microscopy (TEM)	152
7.3.7 Surface-enhanced Raman microscopy (SERS)	152
7.4 Results and discussion	153
7.4.1 Properties of bare GNPs	153
7.4.2 Properties of $\beta$ Lg-coated GNPs	153
7.4.3 Influence of bile salts on protein-coated GNPs	155
7.4.3.1 Particle charge characteristics	155
7.4.3.2 Particle diameter	157
7.4.3.3 UV–visible absorption spectra	159
7.4.3.4 Transmission electron microscopy (TEM)	162

**CONTENTS (cont.)**

	<b>Page</b>
7.4.3.5 Surface-enhanced Raman spectroscopy	164
7.5 Conclusions	167
<b>CHAPTER VIII CONCLUSIONS</b>	<b>169</b>
<b>REFERENCES</b>	<b>173</b>
<b>APPENDIX</b>	<b>193</b>
<b>BIOGRAPHY</b>	<b>195</b>

## LIST OF TABLES

<b>Table</b>	<b>Page</b>
2.1 Examples of cellulose micro/nano-fiber preparation procedures.	13
2.2 Example of microparticles and nanoparticles of biological origin stabilized o/w emulsions by Pickering mechanism.	28
2.3 Examples of Raman spectroscopy applications in food systems.	64
2.4 Raman bands useful in the interpretation of protein structure.	67
4.1 Chemical compositions of untreated mangosteen rind and its purified cellulose.	87
4.2 The Herschel-Bulkley rheological parameters of emulsions stabilized by MFC (30% w/w oil, 0.7% w/w MFC in aqueous phase) obtained with different number of passes through the homogenizer.	98
5.1 Influence of MFC concentration on surface-weighted ( $d_{32}$ ) and volume-weighted ( $d_{43}$ ) mean droplet diameters of 10% o/w MFC-stabilized emulsions measured after storage for 1 day and 80 days at room temperature.	116
5.2 Influence of MFC concentration on color ( $L^*$ , $a^*$ , $b^*$ ) of fresh 10% o/w MFC-stabilized emulsions.	116
5.3 Influence of MFC concentration on the Herschel-Bulkley parameters of fresh 10% o/w MFC-stabilized emulsions.	123

## LIST OF FIGURES

<b>Figure</b>	<b>Page</b>
2.1 From the cellulose sources to the cellulose molecules: details of the cellulosic fiber structure with emphasis on the cellulose microfibrils.	8
2.2 Scanning electron micrograph showing the fibril aggregates in a bleached wood fiber.	8
2.3 From fibers suspensions to microfibrillated cellulose (MFC) with their various terminologies.	11
2.4 Basic design of a high-pressure homogenizer.	16
2.5 TEM image of MFC gel showing cellulose nanofibers and bundles (left). AFM image of corn cobs MFC obtained after 8 passes through a homogenizer (right).	18
2.6 X-ray powder diffraction of ground corn cobs and purified corn cob cellulose.	20
2.7 Schematic representation of Pickering stabilization of o/w emulsion by spherical particles. (a) Single hydrophilic particle at the oil-water interface, with contact angle $\theta$ formed at the junction of the three phases: particle (p), oil (o), and water (w). Quantities $\gamma_{po}$ , $\gamma_{pw}$ , and $\gamma_{ow}$ are the tension at the three boundaries. (b) Close-packed monolayer of particles at surface of dispersed oil droplet.	26
2.8 Schematic representations of alternative stabilizing arrangements of particles in a thin film between closely approaching emulsion droplets: (a) separate closely packed monolayers on the two oil–water interfaces; (b) single dense layer of bridging particles; and (c) low-density network layer of aggregated particles.	27
2.9 Homogenization can be divided into primary and secondary homogenization. Primary homogenization is the conversion of two bulk liquids into an emulsion, while secondary homogenization is the reduction in size of the droplets in an existing emulsion.	30

**LIST OF FIGURES (cont.)**

<b>Figure</b>	<b>Page</b>
2.10 High-pressure valve homogenizers are used to produce emulsions with fine droplet sizes.	31
2.11 Schematic representation of monodisperse and polydisperse emulsions.	32
2.12 Example of bimodal and multimodal distributions of o/w emulsions stabilized by fish gelatin at various concentrations.	33
2.13 Apparent viscosity as a function of rate of shear strain or shear stress.	39
2.14 Different types of measurement cells commonly used with dynamic shear rheometers.	40
2.15 Physical instability of emulsion.	41
2.16 Time dependence of droplet creaming in o/w emulsions. Droplets move upward until they cannot move any further and then form a “creamed” layer. Larger droplets tend to move upward faster than smaller ones.	42
2.17 Types of instability that occur after mixing a colloidal dispersion with a polymer solution, including bridging and depletion flocculation.	44
2.18 Schematic diagram of events that occur during the shearing of a flocculated emulsion and their effect on emulsion viscosity.	46
2.19 Droplet coalescence leads to a growth in the mean droplet diameter and may eventually lead to complete separation of the oil and aqueous phases.	47
2.20 Ostwald ripening involves the growth of large droplets at the expense of smaller ones due to diffusion of dispersed phase through the continuous phase.	49
2.21 An illustration showing $\beta$ -lactoglobulin structure.	52
2.22 Plasmon absorption spectrum of GNPs and the optical image of cast GNPs on glass and dried in air.	55
2.23 Various size of GNPs solution.	55

## LIST OF FIGURES (cont.)

<b>Figure</b>	<b>Page</b>
2.24 Schematic representations of several likely arrangements of bovine serum albumin (BSA) at the interface; (A) monolayer, side-on (axis parallel to the surface), not close-packed; (B) monolayer, side-on, close-packed; (C) bilayer, side-on, second layer less concentrated than A; D, E, and F are the same as A, B, and C, but for end-on (axis perpendicular to the surface) orientations. Other possibilities include arrangements similar to C and F, but with first layer not close-packed, and other orientations with the axis neither parallel nor perpendicular	57
2.25 Energy level diagram depicting light scattering processes.	60
2.26 Raman spectrum of solid BSA (a) and SERS spectrum of bioconjugates gold nanospheres–BSA (b).	60
2.27 DXR Raman spectroscopy (left), and gold multi-spot microscope slide (right).	61
4.1 X-ray diffraction patterns of dried ground mangosteen rind, purified cellulose, and mechanical treated (20 passes through the homogenizer) cellulose, i.e. microfibrillated cellulose (MFC).	88
4.2 Influence of number of passes through the homogenizer on rheological properties of 1% w/w fresh MFC suspensions, measured at 25 °C (A) mechanical spectra, i.e. storage modulus, $G'$ , (closed symbols) and loss modulus, $G''$ , (open symbols) as a function of angular frequency, measured at 0.5% strain; (B) Apparent viscosity ( $\eta_a$ ) (calculated from the downward flow curve data) as a function of shear rate. Refer to Table 4.2 for the sample codes of MFC obtained from various homogenization passes.	90
4.3 Influence of number of passes through the homogenizer of MFC on (A) particle size distribution and (B) average particle size ( $d_{43}$ ) of MFC-stabilized o/w emulsions (30% w/w oil, 0.7% w/w MFC in aqueous phase). Refer to Table 4.2 for the sample codes of MFC obtained with various homogenization passes.	92

## LIST OF FIGURES (cont.)

<b>Figure</b>	<b>Page</b>
<p>4.4 SEM micrographs of o/w emulsions stabilized by MFC (30% w/w oil, 0.7% w/w MFC in aqueous phase) obtained with 1 pass (A, C) and 20 passes (B, D) through the homogenizer. CLSM micrograph (E) of emulsion droplets stabilized by MFC obtained with 20 homogenization passes.</p>	94
<p>4.5 Influence of number of passes through the homogenizer of MFC on (A) mechanical spectra, i.e. storage modulus, <math>G'</math>, (closed symbols) and loss modulus, <math>G''</math>, (open symbols) as a function of angular frequency, measured at 0.5% strain and (B) flow curves, i.e. shear stress as a function of shear rate, in which closed symbols represent the ascending part and open symbols represent the descending part of the flow curves of fresh o/w emulsions stabilized by MFC (30% w/w oil, 0.7% w/w MFC in aqueous phase), measured at 25 °C. Particle size distributions (C) of 20P-MFC-stabilized emulsion before and after steady flow tests. Refer to Table 4.2 for the sample codes of MFC obtained with various homogenization passes.</p>	97
<p>4.6 Effects of (A) pH and (B) NaCl concentration on <math>\zeta</math>-potential of MFC suspensions and MFC-stabilized o/w emulsions (30% w/w oil, 0.7% w/w MFC in aqueous phase). The 20-pass MFC (20P-MFC) was used in these experiments.</p>	101
<p>4.7 Creaming profiles (A) and photographs (B) of MFC-stabilized o/w emulsions (30% w/w oil, 0.7% w/w MFC in aqueous phase) during storage at room temperature (25 °C) for 80 days. Refer to Table 4.2 for the sample codes of MFC obtained with various homogenization passes.</p>	103
<p>4.8 Influences of environmental stresses, i.e. (A) pH, (B) NaCl concentration, and (C) temperature, on creaming profiles of 10% o/w emulsions stabilized by MFC at different concentrations. The 20-pass MFC (20P-MFC) was used in these experiments.</p>	105

## LIST OF FIGURES (cont.)

<b>Figure</b>	<b>Page</b>
5.1 Particle size distributions of 10% o/w emulsions stabilized by MFC at different concentrations, i.e. 0.05% (A), 0.10% (B), 0.30% (C), 0.50% (D), and 0.70% (E), measured after storage for 1 day and 80 days at room temperature. The insets represent optical micrographs (40×; scale bars represent 20 μm) of the 1-day stored emulsions.	117
5.2 SEM and CLSM micrographs of fresh 10% o/w emulsions stabilized by MFC at different concentrations, i. e. 0.05% (A, D), 0.30% (B, E), and 0.70% (C, F).	120
5.3 Influence of MFC concentration on (A) mechanical spectra, i. e. storage modulus, $G'$ , (closed symbols) and loss modulus, $G''$ , (open symbols) as a function of angular frequency, (B) loss tangent ( $\tan \delta$ ) as a function of angular frequency, (C) flow curves, i. e. shear stress as a function of shear rate, in which closed symbols represent the upward curves and open symbols represent the downward curves, and (D) apparent viscosity, $\eta_a$ , as a function of shear rate of fresh 10% o/w MFC-stabilized emulsions. All measurements were performed at 25 °C.	122
5.4 Influence of MFC concentration on (A) Cox-Merz plot, i. e. complex viscosity, $\eta^*$ , (closed symbols) versus steady shear viscosity or apparent viscosity, $\eta_a$ , (open symbols) and (B) shift factors of fresh 10% o/w MFC-stabilized emulsions.	125
5.5 Influence of MFC concentration on creaming profiles of 10% o/w MFC-stabilized emulsions during storage at room temperature for 80 days (A). Photographs of the 1- and 80-day stored emulsions (B). Arrow marks cream-serum boundary.	128
6.1 $\zeta$ -Potential of bare GNPs and $\beta$ Lg-coated gold nanoparticles with varying $\beta$ Lg concentrations.	136
6.2 Diameter of bare GNPs and $\beta$ Lg-coated GNPs with varying $\beta$ Lg concentrations. The inset shows visual observation of $\beta$ Lg–GNP mixtures.	138

## LIST OF FIGURES (cont.)

<b>Figure</b>	<b>Page</b>
6.3 Absorption spectra of $\beta$ Lg solution at concentration of 1000 $\mu$ M, bare GNPs in solution and $\beta$ Lg-coated GNPs at 5000 $\mu$ M $\beta$ Lg concentration.	139
6.4 Influence of $\beta$ Lg concentration on (A) absorption spectra of $\beta$ Lg-coated GNPs at 1000, 2500 and 5000 $\mu$ M $\beta$ Lg concentration, and (B) absorbance at 400 nm of $\beta$ Lg-coated GNPs suspensions.	140
6.5 Transmission electron microscopy of $\beta$ Lg-coated GNPs at 1000 $\mu$ M (A), 2500 $\mu$ M (B), and 5000 $\mu$ M (C) $\beta$ Lg concentrations. A representative of TEM micrograph of $\beta$ Lg-coated GNPs with a layer contour of protein corona (D).	142
6.6 Raman spectrum of $\beta$ Lg in solution (A) and SERS spectra of $\beta$ Lg-coated GNP at 1000 $\mu$ M (C), 2500 $\mu$ M (D), and 5000 $\mu$ M (E) $\beta$ Lg concentrations. Bare GNPs was used as a negative control (B).	143
7.1 $\zeta$ -Potential (A) and particle diameter (B) of bare GNPs, GNPs- $\beta$ Lg, GNPs-BS, and GNPs- $\beta$ Lg-BS mixtures. The concentrations of the different components used were $6.86 \times 10^8$ particles/mL GNPs, 0.098 mM $\beta$ Lg, and 10 mg/mL BS.	154
7.2 The change in $\zeta$ -potential of GNPs- $\beta$ Lg-BS on addition of bile salt (10 mg/mL) as a function of time (A) and as a function of bile salt concentration after treatment for 2 h (B). The initial concentrations in the system were $6.86 \times 10^8$ particles/mL GNPs, and 0.098 mM $\beta$ Lg.	157
7.3 The change in particle diameter of GNPs- $\beta$ Lg-BS on addition of bile salt (10 mg/mL) as a function of time (A) and as a function of bile salt concentration after treatment for 2 h (B). The initial concentrations in the system were $6.86 \times 10^8$ particles/mL GNPs, and 0.098 mM $\beta$ Lg.	159
7.4 Absorption spectra of $\beta$ Lg solution, bare GNPs in solution, GNPs- $\beta$ Lg, GNPs- $\beta$ Lg-BS, and BS solutions (A) and absorbance at 279 nm of supernatant obtained from GNPs- $\beta$ Lg-BS with varying bile salt concentrations (B).	161

**LIST OF FIGURES (cont.)**

<b>Figure</b>	<b>Page</b>
7.5 Transmission electron microscopy of GNPs (A), GNPs- $\beta$ Lg (B), GNPs- $\beta$ Lg-BS (C).	163
7.6 Surface-enhanced Raman scattering (SERS) spectra of GNPs (A), GNPs- $\beta$ Lg (B), GNPs- $\beta$ Lg-BS (C), and GNPs-BS (D). The vertical dashed lines in the spectra highlight regions where key functional groups occur in the bile salts or proteins. The original spectra are shown in Appendix.	165
A.1 Original surface-enhanced Raman scattering (SERS) spectra of GNPs (A), GNPs- $\beta$ Lg (B), GNPs- $\beta$ Lg-BS (C), and GNPs-BS (D).	194

## LIST OF ABBREVIATIONS

$a^*$	Redness-greenness
AOAC	Association of Official Analytical Chemists
ANOVA	Analysis of Variance
$\beta$ Lg	Beta-lactoglobulin
$b^*$	Yellow-blueness
BS	Bile salts
cm	Centimeter
$CI$	Creaming index, %
CLSM	Confocal laser scanning microscopy
$C_{Sat}$	Mass of material adsorbed to the surface, $\text{kg m}^{-3}$
$d$	Particle diameter
$d_{32}$	Surface-weighted mean diameter
$d_{43}$	Volume-weighted mean diameter
$DP$	Degree of polymerization
DLS	Dynamic light scattering
g	Gram
GNPs	Gold nanoparticles
$G'$	Storage modulus, Pa
$G''$	Loss modulus, Pa
h	Hour
$H_S$	Height of serum layer
$H_T$	Total height of emulsion
Hz	Hertz
$K$	Consistence coefficient, $\text{Pa s}^n$
kDa	Kilodalton
$L^*$	Lightness

## LIST OF ABBREVIATIONS (cont.)

MFC	Microfibrillated cellulose
mg	Milligram
mL	Milliliter
mM	Millimolar
mV	Millivolt
min	Minute
$n$	Flow behavior index, dimensionless
nm	nanometer
$\eta^*$	Complex viscosity, Pa s
$\eta_a$	Apparent viscosity, Pa s
$[\eta]$	Intrinsic viscosity, dL/g
o/w	Oil-in-water emulsion
Pa	Pascal
pH	Power of hydrogen
pI	Isoelectric point
rpm	Round per minute
$R^2$	Coefficient of determination
s	Second
SD	Standard deviation
SEM	Scanning electron microscopy
SERS	Surface-enhanced Raman scattering
SLS	Static light scattering
SPSS	Statistical package for the social science
$\tan \delta$	Tan delta, dimensionless
TEM	Transmission electron microscopy
$\Gamma_{\text{Sat}}$	Surface load at saturation
$\mu\text{L}$	Microliter
$\mu\text{m}$	Micrometer
$\mu\text{M}$	Micromolar

**LIST OF ABBREVIATIONS (cont.)**

w/o	Water-in-oil emulsion
w/v	Weight by volume
w/w	Weight by weight
°C	Degree Celsius
$\alpha$	Shift factor
$\dot{\gamma}$	Shear rate, s <sup>-1</sup>
$\sigma$	Shear stress, Pa
$\sigma_0$	Yield stress, Pa
$\emptyset$	Disperse phase volume fraction
$\omega$	Angular frequency, rad s <sup>-1</sup>
$\zeta$ -potential	Zeta-potential, mV

## **CHAPTER I**

### **INTRODUCTION**

Biopolymers are polymers produced by living organisms and contain monomeric units that are covalently bonded to form larger structures. It can be classified according to their monomeric units, for example, *proteins*, which are macromolecules, consisting of one or more long chains of amino acid residues covalently linked together by peptide bonds and *polysaccharides*, which are polymeric carbohydrate molecules composed of long chains of monosaccharide units bound together by glycosidic bonds. These biopolymers range in structure from linear to highly branched. Biopolymers can be used in many aspects (e.g. reinforcing or strengthening agents, fat replacers, and stabilizing agents, etc.). Nowadays, utilization of natural ingredients in food products is becoming importance due to the increasing health awareness of toxic from using synthetic chemical ingredients. Therefore, the research efforts are being focused on the finding of the new types of natural ingredients that are not only effective in term of their function, but also acceptable for used in food products in terms of safety to consumer health (Dickinson, 2010).

Microfibrillated cellulose (MFC) or cellulose gel is a polysaccharide biopolymer, which is isolated and purified cellulose fibers recovered from original cellulose filamentous structure, as cellulose fibers consist of nanometer-scale microfibrils (2-10 nm thick, several tens of micrometers length) (Lavoine, Desloges, Dufresne, & Bras, 2012; Siró & Plackett, 2010). MFC can thus be regarded as nanofibers. MFC can be prepared from several agricultural crops and by-products, such as corn cobs, bamboo pulp, and sugar beet pulp, etc. In this study, MFC was extracted from mangosteen (*Garcinia mangostana* L.) rind using chemical pre-treatments (i.e. hot sodium hydroxide and hydrogen peroxide), followed by mechanical treatment using a high-pressure homogenizer. It is with great interest that MFC can be extracted from low value by-products of the fruit canning industry. Thus, the economic value of these by-products could be increased by finding new applications and markets for them. In addition, the mangosteen rind waste has about

60-70% cellulose content comparable to those of the other agricultural by-products such as raw banana, jute, and pineapple leaf (Abraham, Deepa, Pothan, Jacob, Thomas, Cvelbar, et al., 2011). Hence for the cost effective production of MFC, the mangosteen rind is a potential candidate. MFC can be used for several interesting applications as emulsion stabilizers and rheology modifiers in foods, paints, cosmetics, and pharmaceutical products (Turbak, Snyder, & Sandberg, 1983) and as fillers in composite materials (Lavoine et al., 2012; Siró & Plackett, 2010).

An emulsion is a dispersed system that consists of two immiscible liquids with one of liquids dispersed as small spherical droplets in the other and stabilized by emulsifiers (McClements, 2005). Since the original work of Ramsden (1904) and Pickering (1907), emulsion stability can be efficiently obtained using solid colloidal particles as an emulsifier. This type of emulsion system is commonly called “Pickering emulsion”. The mechanism of colloidal particles stabilized emulsion is the accumulation of dispersed particles at the oil-water interface to form mechanical (steric) barriers around the emulsion droplets, which prevents their coalescence (Dickinson, 2012). Over the past 10 years, there is a lot of research conducted on Pickering emulsions. Research efforts are being focused on the production of nanoparticles and microparticles that are not only effective to stabilized emulsions, but also acceptable for used in food products (Dickinson, 2010). Natural particles are becoming an interesting source of particulate material for food use, for examples, hydrophobically modified starch granules (Yusoff & Murray, 2011), chitin nanocrystal particles (Tzoumaki, Moschakis, Kiosseoglou, & Biliaderis, 2011), and bacterial cellulose nanocrystals (Kalashnikova, Bizot, Cathala, & Capron, 2011, 2012). However, there is no report on the effect of preparation conditions and concentration of MFC on the emulsion stabilizing properties of MFC from mangosteen rind. Therefore, in this study, the effect of preparation conditions (i.e. number of passes through a high-pressure homogenizer) of MFC on MFC properties itself, and properties and stability of emulsions stabilized by MFC were tested in order to explore the feasibility of using MFC as emulsion stabilizers. The effect of concentration of MFC obtained at an appropriated homogenization pass, which gave the highest emulsion stability, on the properties and stability of emulsions was then investigated.

As mentioned above, protein is a polypeptide biopolymer, which is widely used in the food and pharmaceutical industries as emulsifiers and stabilizing agents. The adsorption of globular proteins to particle surfaces is important in a number of physicochemical and biological phenomena relevant to the development of food and pharmaceutical products. Proteins adsorb to the surfaces of oil droplets and gas bubbles during the production of emulsions and foams, respectively which plays an important role in their stability to particle growth and aggregation (Dickinson, 2003; McClements, 2005; Kralova & Sjöblom, 2009). Proteins adsorb to the surfaces of ice crystals during their formation and subsequent growth, which is important in the development of anti-freeze systems (Venketesh & Dayananda, 2008). Proteins may adsorb to the surfaces of inorganic nanoparticles (such as gold, silver, or titanium dioxide), (Wilde & Chu, 2011; Talbert & Goddard, 2012) which may alter their gastrointestinal fate (e.g., absorption by epithelium cells or interactions with gut microbiota). In addition, in the gastrointestinal tract, the intestinal fluids may also contain a mixture of different surface active agents, such as bile salts, phospholipids, and proteins. It is therefore important to understand the influence of protein adsorption onto particle surfaces on both protein and particle properties, and also the interaction between protein-coated interfaces and surfactants (Dickinson, 2010).

In this study, we used  $\beta$ -lactoglobulin ( $\beta$ Lg) as a model globular protein and gold nanoparticles (GNPs) as model colloidal particles to form protein-stabilized nanoparticles.  $\beta$ -Lactoglobulin is a major globular protein in bovine milk and is widely used in the food industry as an emulsifier (McClements, 2005). This protein usually exists as a dimer at neutral pH with a molecular weight of nearly 36 kDa, but dissociates into monomers below pH 3. Its three-dimensional structure consists of a  $\beta$ -sheet (54%) with an  $\alpha$ -helix (17%) (Link, Mohamed, & El-Sayed, 1999; Van Der Zande, Böehmer, Fokkink, & Schöenenberger, 2000; El-Sayed, 2001). GNPs are attractive for many biological and medical applications due to their chemical stability, biocompatibility, and unique optical properties (Iosin, Canpean, & Astilean, 2011). We used  $\beta$ -lactoglobulin-coated GNPs (200 nm) as model systems for protein-coated lipid droplets that are found in many food and pharmaceutical systems. We also would like to take an advantage of the surface enhanced Raman scattering (SERS) characteristics of GNPs to study the effect of  $\beta$ Lg concentration and bile salts addition

on the interfacial structure of  $\beta$ Lg-coated nanoparticles. The GNPs were used instead of oil droplets to overcome the limitation of using Raman spectroscopy with real emulsion system. Normally, the Raman intensity of protein adsorbed at oil surfaces is very weak or disappears because of the interference of oil peaks. The common way to enhance the Raman intensity through electromagnetic enhancement and chemical/charge transfer mechanisms is the technique called surface-enhanced Raman scattering (SERS) (Aroca, 2005).

Recently, a number of research groups have developed new techniques for identification and characterization of molecule conformation. Surface-enhanced Raman scattering (SERS) is a derivative of Raman spectroscopic technique that can be used for sensitive molecular identification and structural characterization (Kudelski, 2008). Enhanced Raman scattering occurs when an analyte is on or in close proximity of a SERS active surface, such as silver or gold nanoparticles. To study the conformation of biomolecules such as protein, Raman spectroscopy can provide information related to protein backbone conformation and the molecular environment of certain side chains, as well as transitions from ordered to disordered structure upon protein denaturation (Li-Chan, 1996; Wang, He, Labuza, & Ismail, 2013). Raman scattering is also sensitive to changes in covalent bonds, such as disulfide linkages, and non-covalent bonds, such as electrostatic and hydrophobic interactions (Li-Chan, 1996). Enhanced with nanotechniques, SERS is, therefore, a sensitive and promising technique to observe the molecular conformation of biopolymers or substances on a nanosubstrate. This technique provides the capability to analyze compounds in aqueous solutions with minimal interference from water adsorption, which is a critical factor when considering biological applications.

In summary, this study focused on the use of biopolymers for stabilizing colloidal systems, including microfibrillated cellulose (polysaccharide)-stabilized oil-in-water emulsions and  $\beta$ -lactoglobulin (protein)-coated gold colloids. For MFC, this study shows the feasibility of using mangosteen rind as a new potential lignocellulosic precursor for production of MFC in an attempt to convert this waste into value-added products and also shows the feasibility of using MFC as a new type of emulsion stabilizer (Chapters IV and V). For protein-GNPs system, SERS technique was performed to explain the conformation of protein after adsorption onto hydrophobic

nanoparticles as well as the effect of bile salts addition, in order to provide fundamental information about the interaction between globular protein and colloidal particles that can be used as database for interface science in food emulsion application (Chapters VI and VII).

## **Objectives**

### **General objective**

To study the properties and stability of colloidal particles stabilized by biopolymers, namely microfibrillated cellulose, i.e. MFC-stabilized oil-in-water emulsions and  $\beta$ -lactoglobulin, i.e.  $\beta$ Lg-coated gold nanoparticles.

### **Specific objectives**

(i) To explore the feasibility of using mangosteen rind as a new potential lignocellulosic precursor for production of microfibrillated cellulose (MFC). The influence of processing condition, i.e. the number of passes through a high-pressure homogenizer, on physicochemical and rheological properties of MFC was studied.

(ii) To investigate the effect of the number of passes through a high-pressure homogenizer of MFC and the effect of MFC concentration on physical and rheological properties and stability of the MFC-stabilized o/w emulsions.

(iii) To prepare the  $\beta$ -lactoglobulin ( $\beta$ Lg)-coated gold nanoparticles (GNPs). The influence of  $\beta$ Lg concentration on protein conformational changes and gold nanoparticle aggregation was studied.

(iv) To unravel the mechanisms of interactions between  $\beta$ Lg-coated GNP interfaces and surface active bile salts by primarily focusing on the physicochemical and interfacial compositional changes at the particle surfaces.

## CHAPTER II

### LITERATURE REVIEW

#### 2.1 Biopolymers stabilized colloidal systems

Biopolymers are polymers produced by living organisms; in other words, they are polymeric biomolecules. Since they are polymers, biopolymers contain monomeric units that are covalently bonded to form larger structures. There are three main classes of biopolymers, classified according to the monomeric units used and the structure of the biopolymer formed, for examples, *polynucleotides* (RNA and DNA), which are long polymers composed of 13 or more nucleotide monomers; *polypeptides*, which are short polymers of amino acids; and *polysaccharides*, which are often linear bonded polymeric carbohydrate structures. In addition, cellulose is the most common organic compound and biopolymer on Earth. About 33 percent of all plant matter is cellulose. The cellulose content of cotton is 90 percent, while wood's is 50 percent. Two types of biopolymers, including microfibrillated cellulose (polysaccharide) and  $\beta$ -lactoglobulin (polypeptide) were used in this study.

A dispersion is a system of discrete particles in a continuous liquid. When the particles are gaseous, it is called a foam; with liquid particles, it is called an emulsion (i.e. oil-in-water and water-in-oil emulsions); and with the solid particles, it is named a suspension (i.e. gold colloidal suspension). A *colloid* is usually defined as a dispersion containing particles that are larger than small molecules or too small to be visible. The size range is about 10 nm to 0.1 mm. The colloids can be classified into two types, including lyophilic (solvent loving) and lyophobic (solvent hating). The lyophobic consists of two or more phases, such as oil, water, or various materials (Walstra & van Vliet, 2008). Lyophobic colloids, such as emulsion, do not form spontaneously. It costs energy to disperse the one phase into the other phase and the stabilizer (i.e. small molecule surfactants, proteins, polysaccharides) is then applied to form and stabilize the system. In this study, we are focusing in two types of colloidal systems, which are emulsions and gold colloidal nanoparticles. These two systems are

the microfibrillated cellulose stabilized oil-in-water emulsion and the  $\beta$ -lactoglobulin stabilized gold nanoparticles.

## **2.2 Microfibrillated cellulose stabilized oil-in-water emulsions**

### **2.2.1 Microfibrillated cellulose**

Cellulose is one of the most important biopolymers available worldwide, occurring in wood, agricultural crops, and microorganism. An estimated natural production is about  $10^{12}$  tons/year. It is considered as an almost inexhaustible source of raw materials and a key source of sustainable materials on an industrial scale (Klemm, Heublein, Fink, & Bohn, 2005; Cao, Wu, Zhang, Li, Zhang & He, 2009; Siró & Plackett, 2010; Klemm, Kramer, Moritz, Lindström, Ankerfors, Gray, et al., 2011). The structure of cellulose is a linear homopolymer of D-glucopyranose units linked by  $\beta$ -1,4-glycosidic bonds ( $C_{6n}H_{10n+2}O_{5n+1}$ ). In general, cellulose is the main composition of cell wall in lignocellulosic plants (~23-53% dry basis). Its content depends on the plant species, maturity, and growing environment. Cellulose naturally exists as microfibrils of identified length and varying degree of crystallinity and is embedded in a matrix composed of lignin, hemicellulose, and other carbohydrate polymers (Yu, Liu, Shen, Jiang, & Huang, 2005). Currently, the isolation, characterization, and research for application of these nano/micro-materials, such as nanocrystals, whiskers, nanofibrils, and microfibrillated cellulose, has gained increasing attention due to their high strength and stiffness combined with low weight, biodegradability, and renewability (Siró & Plackett, 2010).

“*Microfibrillated cellulose (MFC)*” or “*cellulose gel*” is isolated and purified cellulose fibers recovered from original cellulose filamentous structure, as cellulose fibers consist of nanometer-scale microfibrils (2–10 nm thick, several tens of micrometers length). The MFC typically consists of partially disintegrated microfibril aggregates with a lateral dimension in the scale of tens of nanometers (typically in the range of 20–40 nm) and lengths of several micrometers (Lavoine, Desloges, Dufresne, & Bras, 2012; Siró & Plackett, 2010), and can thus be regarded as nanofibers. The cellulose chains are stabilized laterally by hydrogen bonds between hydroxyl groups.

Figures 2.1 and 2.2 illustrate the organization of cellulose chain microfibrils and fibril aggregates.

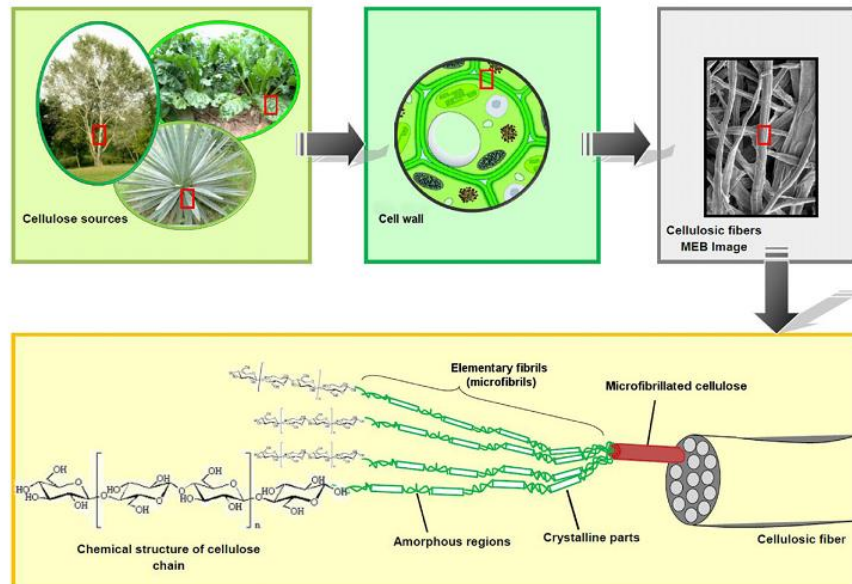


**Figure 2.1** From the cellulose sources to the cellulose molecules: details of the cellulosic fiber structure with emphasis on the cellulose microfibrils (Lavoine et al., 2012).

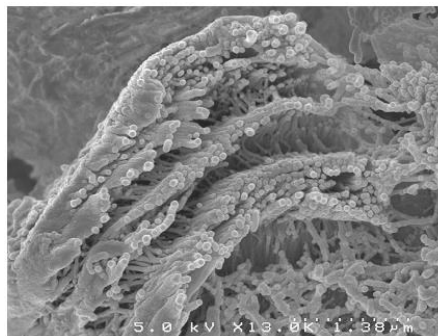


**Figure 2.2** Scanning electron micrograph showing the fibril aggregates in a bleached wood fiber (modified from Klemm et al., 2011).

Novel methods for their production range from top-down methods involving enzymatic, chemical, and physical methodologies for their isolation from

wood and agricultural crops to the bottom-up production of cellulose microfibrils from glucose by microorganisms (Klemm et al., 2011).

### **2.2.1.1 Sources of microfibrillated cellulose**

#### **(i) Wood**

The isolation of cellulose fibril aggregates from wood pulp (Figure 2.2) has first been described by Turbak, Snyder, and Sandberg (1983) using cyclic mechanical extraction method in a high-pressure homogenizer. Through a homogenization process, wood pulp is disintegrated, giving a material whose fibers are moderately degraded and opened into their substructural fibrils and microfibrils (Andresen, Johansson, Tanem, & Stenius, 2006). The resulting MFC gels consist of strongly entangled and disorder network. Kraft pulp has widely used as a raw material for research on MFC production (Iwamoto, Nakagaito, Yano, Nogi, 2005; Saito, Hirota, Tamura, Kimura, Fukuzumi, Heux, et al., 2009). The drawback of using wood as a starting material is that MFC gel can be obtained at higher number of passes through a high-pressure homogenizer because wood highly contains hemicellulose and pectin, which act as a binder between microfibrils, so that pre-treatment step and high energy for production are required (Siró & Plackett, 2010).

#### **(ii) Agricultural crops and by-products**

Although wood is normally the most important industrial source of cellulosic fiber, other sources from plants and their by-products are becoming new candidate for cellulosic material production. These non-wood plants contain less hemicellulosic substances than wood and therefore bleaching and pretreatment processes are less demanding (Siró & Plackett, 2010). In addition, the cellulose microfibrils in agricultural crops are less tightly wound in the primary cell wall than in the secondary wall in wood, therefore fibrillation to product MFC should be less energy demanding (Dinand, Chanzy, & Vignon, 1996). The examples of agricultural by-products which can be used as starting materials for MFC production are corn cobs (Shogren, Peterson, Evans, & Kenar, 2011), banana rachis (Zuluaga, Putaux, Restrepo, Mondragón, & Ganan, 2007), and sugar beet pulp (Dinand, Chanzy, & Vignon, 1996), soy hulls (Alemdar & Sain, 2008), etc.

### **(iii) Bacterial cellulose**

Bacteria, belonging to the genera *Acetobacter*, *Agrobacterium*, *Pseudomonas*, *Rhizobium*, and *Alcaligenes*, can extracellularly secrete the cellulose fibers (El-Saied, Basta, & Gobran, 2004). *Acetobacter xylinum* is considered as the most efficient producer of bacterial cellulose (BC). In contrast to other sources, BC is produced by bacteria through cellulose biosynthesis and the building up of bundles of microfibrils (Nakagaito & Yano, 2005). The structure of BC is a ribbon-shape fibril and less than 100 nm wide, which is composed of finer 2-4 nm fibrils (Brown & Laborie, 2007). Compared with cellulose from plants, BC also exhibits higher water retention capacity, higher degree of polymerization and a finer web-like network (Klemm, Schumann, Kramer, Hessler, Hornung, Schmauder, et al., 2006; Barud, Barrios, Regiani, Marques, Verelst, Dexpert-Ghys, et al., 2008).

#### **2.2.1.2 Preparation of microfibrillated cellulose**

Novel methods for their production range from top-down methods involving enzymatic, chemical, and physical methodologies for their isolation from wood and agricultural crops to the bottom-up production of cellulose microfibrils from glucose by microorganisms (Klemm et al., 2011). Here, we are focusing on the top-down methods, including pre-treatment step for isolation of cellulose from starting materials and then mechanical treatment is applied to produce MFC (Figure 2.3). The nature of raw materials and fibrillation techniques are the major factors which influence the cellulose degree polymerization, morphology, and aspect ratio (Svagan, Samir, & Berglund, 2008). Examples of cellulose micro/nano-fiber preparation procedures are shown in Table 2.1.

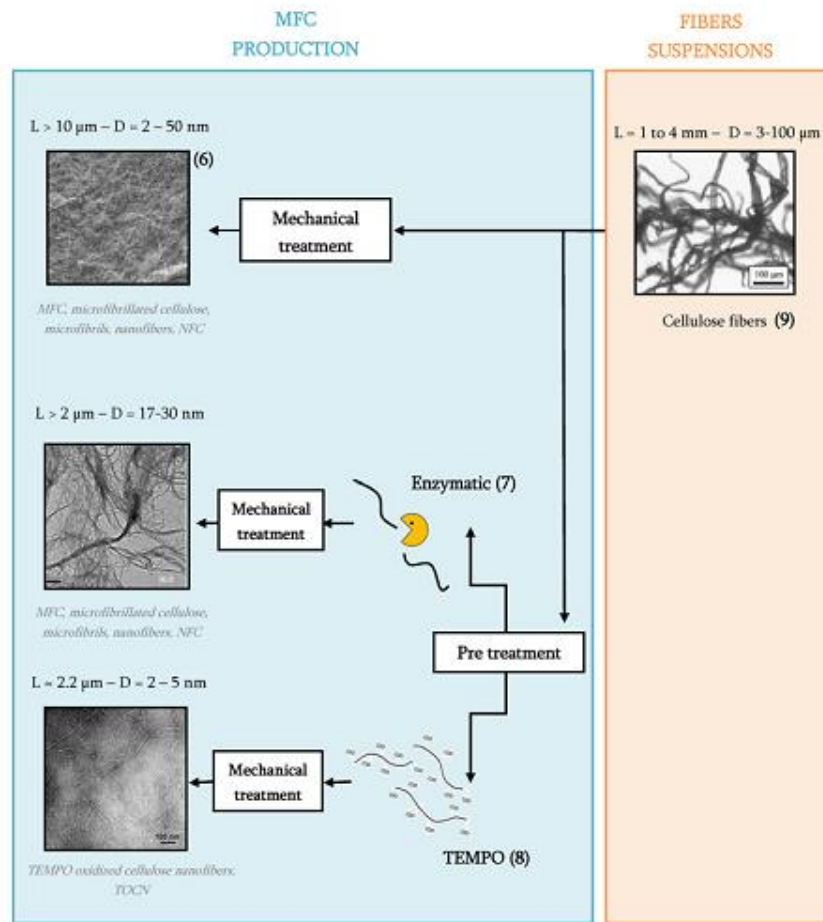


**Figure 2.3** From fibers suspensions to microfibrillated cellulose (MFC) with their various terminologies (modified from Lavoine et al., 2012).

**Table 2.1** Examples of cellulose micro/nano-fiber preparation procedures.

Method	Raw material	Procedure	Fiber dimension	References
Mechanical treatment	Kraft pulp	Passing through a refiner with a gap of 0.1 mm 30 times, then passing through a high-pressure homogenizer 2-30 times	~5 nm in width	Habibi, Mahrouz, & Vignon, 2009
	Soybean stock	Cryocrushing followed by 20 passes through a defibrillator at 500-1,000 bar	50-100 nm in width and several µm in length	Iwamoto, Nakagaito, & Yano, 2007
	Dried sugar beet pulp chips	Disintegration by an Ultra-Turrax mixer at 24,000 rpm followed by homogenization using a high-pressure homogenizer at 300 bar for 10-15 passes	30-100 nm and several µm in length	Leitner, Hinterstoisser, Wastyn, Keckes, & Gindl, 2007
Enzymatic pre-treatment	Bleached sulfite softwood cellulose pulp	Refining to increase the accessibility of the cell wall to the subsequent monocomponent endoglucanase treatment; second refining stage; high-pressure homogenizer	5-30 nm in diameter	Pääkkö et al., 2007
	Softwood sulfite pulp	Beating in a PFI-mill; enzymatic treatment with endoglucanase; second beating; high-pressure homogenizer	5-30 nm in diameter	Henriksson et al., 2007

### **(i) Pre-treatment**

Pre-treatment is aimed to produce purified cellulose which can then be further processed. It also helps to reduce energy demand in mechanical treatment step. By combining the mechanical treatment with appropriate pre-treatments (e.g. chemical or enzyme), it is possible to decrease energy consumption to the level of 1,000 kWh/ton from 20,000-30,000 kWh/ton (Ankerfors & Lindström, 2007).

#### Alkaline-peroxide pre-treatment

The most common chemical process which is widely used is alkaline pre-treatment by using combination of sodium hydroxide (NaOH) with hydrogen peroxide (H<sub>2</sub>O<sub>2</sub>). It is well known that sodium hydroxide has ability to remove non-cellulosic material, such as fat and protein (Prakongpan, Nitithamyong & Luangpituksa, 2002) whereas hydrogen peroxide reacts with lignin under alkaline conditions has ability to disrupt the lignin structure, resulting in separation of the structural linkage between lignin and carbohydrates and also bleaching high-lignin materials (Wang, Sain, & Oksman, 2007). The bleaching ability of H<sub>2</sub>O<sub>2</sub> to react with various colored carbonyl-containing structures in lignin. This reaction can be explained through the reactions of the hydrogen peroxide anion (HOO<sup>-</sup>) which formed in an alkaline medium. The alkaline-peroxide pre-treatment is the critical step in production of cellulosic materials because the alkaline extraction needs to be carefully controlled the concentration of NaOH and pH to avoid undesirable cellulose degradation and to ensure that hydrolysis occurs only at the fiber surface, so that intact microfibrils can be extracted (Wang & Sain 2007). In 2003, Sun, Sun, Tomkinson, and Baird reported that the extraction of wheat straw using 2% H<sub>2</sub>O<sub>2</sub> and 2% NaOH solution at 45°C and 50°C for 5 h resulted in left 53.8 and 53.3% cellulose and about 80% lignin and hemicellulose were removed.

#### Enzymatic pre-treatment

Energy consumption in MFC production can be reduced by using an enzymatic pre-treatment before passing cellulosic material through mechanical step. In nature, cellulose is not degraded by a single enzyme but a set of cellulase enzymes are involved. Cellulase can be classified as cellobiohydrolases

(A- and B-type cellulases) and endoglucanases (C- and D-type cellulases). The cellobiohydrolases are able to attack highly crystalline cellulose, while endoglucanases generally require some disorder in the structure in order to degrade cellulose (Henriksson, Christiernin, & Agnemo, 2005). Both cellobiohydrolases and endoglucanases exhibit strong synergistic effects (Henriksson, Berglund, & Lindström, 2007). Isolated cellulases have been added during MFC preparation in order to modify rather than degrade the cellulose. In 2007, two groups of researchers, Henriksson group (Henriksson et al., 2005, 2007) and Pääkkö group (Pääkkö et al., 2007) confirmed that endoglucanase pre-treatment facilitates disintegration of wood fiber pulp into MFC nanofibers. In addition, pretreated fibers were successfully disintegrated using low enzyme concentration only 0.02% while molecular weight and fiber length were well preserved.

## **(ii) Mechanical treatment**

### ***High-pressure homogenization***

As mentioned in Section 2.1.1.1, the production of MFC using a high-pressure homogenizer has first been described by Turbak, Snyder and Sanberg (1983). Currently, the manufacture of MFC is generally performed using a combination of refining and high pressure homogenizing process steps (Pääkkö et al., 2007). The mechanical treatment made irreversible changes in the fibers, increasing their bonding potential by modification of morphology and size (Nakagaito & Yano, 2005). During homogenization, the slurries are fed through a spring-loaded valve assembly under high pressure (Figure 2.4). This valve opens and closes in rapid succession, resulting in the fibers are subjected to a large pressure drop with shearing and impact forces. As a consequence, these forces promote a high degree of microfibrillation of the fibers, which is MFC. Such mechanical dispersion of fibers lead to fibril structures with a lateral dimension in the scale of tens of nanometers (typically in the range of 20–40 nm) and lengths of several micrometers (Lavoine, Desloges, Dufresne, & Bras, 2012; Siró & Plackett, 2010). Normally, the homogenization process is often repeated several times in order to increase the degree of fibrillation. The number of passes through the high pressure homogenizer required easily runs to 10 and can even reach as high as 30 (Lavoine et al., 2012).

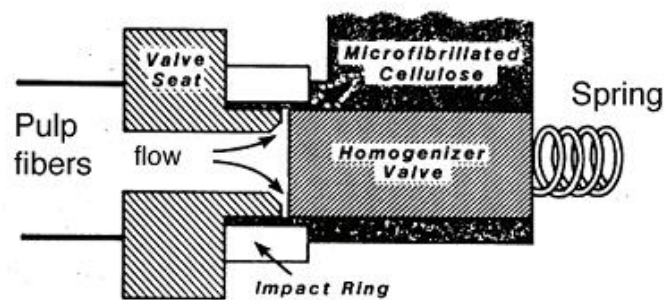


**Figure 2.4** Basic design of a high-pressure homogenizer (Turbak, Snyder, & Sandberg, 1983).

### Cryocrushing

Cryocrushing is an alternative method for producing MFC in which fibers are frozen using liquid nitrogen and then high shear forces are applied. The principle of this method is when high impact forces are applied to the frozen fibers, ice crystals exert pressure on the cell walls, causing them to rupture and thereby liberating microfibrils (Wang & Sain, 2007). In 2007, Wang and Sain demonstrated the use of cryocrushing with a high-pressure fibrillation process for the isolation of microfibrils with diameters in the range between 50 and 100 nm from soybean stock.

### Grinding

Modified commercial grinders with specially disks have been used in order to fibrillate cellulose fiber. This instrument can be operated by passing cellulose slurry between a static grind stone and a rotating grind stone revolving about 1,500 rpm. The principle of this technique is that the cell wall structure consisting of micro/nano-fibers in a multilayered structure and hydrogen bonding are broken down by the shearing forces generated by the grinding stones and then nanosized fibers are individualized from the pulp (Klemm et al., 2011). In 2005 and 2007, Iwamoto et al. reported that the fibril bundles with uniform fibrils 50-100 nm wide could be fibrillated by repeating cryocrushing step for 10 times. The major drawback of this technique is that the shearing force generated by the grinding stone can degrade the fibers, which may affect the reinforcing potential of MFC and also affect the physical properties of composite based on the MFC.

### **2.2.1.3 Properties of microfibrillated cellulose**

#### **(i) Morphology**

As mention before, the diameter and the length of MFC vary according to the pre-treatments and mechanical treatments that are applied. The typical dimensions of MFC produced are 20–40 nm in width and several micrometers in length. The direct techniques, including scanning electron microscopy (SEM), transmission electron microscopy (TEM), and atomic force microscopy (AFM), are the common approaches used to observe MFC and to measure its diameter. Currently, the width of MFC is quite well characterized, while the length of MFC is typically too long to be measured in its entirety within the microscope reading section (Lavoine et al., 2012). From Table 2.1, mechanical treatment and pre-treatment seem to have a certain impact on the MFC morphology. It also remains difficult to accurately compare all the different dimensions obtained since the raw materials are different. Depending on the source of cellulose, the initial fibers have different qualities, lengths, microfibril angles, and amounts of lignin and hemicellulose residues. In addition, the presence of lignin and hemicellulose also affect the diameter of produced MFC. For a low lignin content softwood (about 9%), the width was 30.8 nm, while for a higher lignin content (about 14%), the diameter was 34.4 nm. It can be concluded that the diameter of MFC produced from lignin-containing pulp is larger, regardless of the origin of the pulp used (Spence, Venditti, Habibi, Rojas, & Pawlak, 2010).

Focusing on image analysis instruments and sample preparation methods, TEM obtains the highest degree of precision in MFC characterization, followed by SEM with a field emission gun (FEG), and then AFM. Indeed, the preparation steps involved in TEM are complicated, though the technique gives precise micrographs. In contrast, AFM preparation steps are easier but the precision and resolution of micrographs are not good as those TEM (Lavoine et al., 2012). Bondeson, Mathew, and Oksman (2006) and Fukuzumi, Saito, Iwata, Kumamoto, and Isogai (2009) pointed out that the fibril diameters may be overestimated by FE-SEM because it requires that the surface be covered with a conductive metallic layer. Figure 2.5 presents TEM and AFM micrographs of MFC.

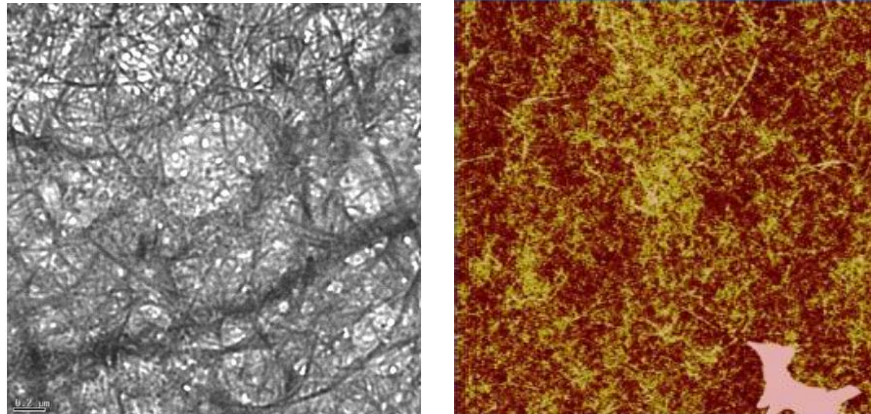


**Figure 2.5** TEM image of MFC gel showing cellulose nanofibers and bundles (left). AFM image of corn cobs MFC obtained after 8 passes through a homogenizer (right).

Recently, Ishii, Saito, and Isogai (2011) demonstrated a viscoelastic evaluation of the average length of MFC by measuring the storage and loss moduli. The theory of linear viscoelasticity was then applied (equation 2.1).

$$\tau = \frac{\pi \times \eta_s \times L^3}{[18 \times k_B \times T \times \ln(L/d)]} \quad (2.1)$$

where  $\tau$  is the longest relaxation time (s) of a semiflexible polymer chain,  $L$  is the chain length ( $\mu\text{m}$ ),  $d$  is the chain diameter (nm),  $T$  is absolute temperature (K),  $\eta_s$  is the solvent viscosity (mPa s), and  $k_B$  is the Boltzmann constant ( $1.3807 \times 10^{-23}$  J/K).

### (ii) Degree of polymerization

The degree of polymerization ( $DP$ ) is strongly correlated with the molecular weight, aspect ratio and also the length of the nanofibers. To evaluate the  $DP$  of MFC, a number of research groups generally use a viscosity method with a cupri-ethylene diamine ( $\text{C}_2\text{H}_6\text{CuN}_2$ ) solution. The average  $DP$  is then calculated from the intrinsic viscosities  $[\eta]$  of the corresponding solutions at 25 °C, using the relationship between intrinsic viscosity and degree of polymerization (Dinand, Chanzy, & Vignon 1999).

By using this relationship, Zimmermann, Bordeanu, and Strub (2010) proved that the disintegration process dramatically reduced the  $DP$  of MFC. The initial pulp had a  $DP$  of 2249, while MFC produced

from softwood sulfite pulp had a *DP* of 825. In addition, it is interesting to note that the strength properties of the ensuring nanocomposites (e.g. film) decrease with a decrease in the *DP* of the MFC. Therefore, the *DP* can be used as a tool for evaluation the performance of MFC as a reinforcing component in various matrices (Zimmermann et al., 2010; Lavoine et al., 2012).

### **(iii) X-ray diffraction (XRD) pattern and degree of crystallinity**

MFC composed of both crystalline and amorphous regions, and measurement of the degree of crystallinity and XRD pattern could explain the structure, behavior, and properties of the materials (Lavoine et al., 2012). X-ray diffraction allows for the measurement of the degree of crystallinity of cellulose, but other methods can also be applied, for example, a peak intensity approach (Segal, Creely, Martin, & Conrad, 1959) and a peak area approach (He, Cui, & Wang, 2008). For XRD pattern, peaks of several cellulosic materials are generally observed around 16 and 23 degree of two theta, as shown in Figure 2.6. This pattern is the characteristic of cellulose I which is a crystal form of native cellulose (Abraham, Deepa, Pothan, Jacob, Thomas, Cvelbar, et al., 2011), such as corn cobs (Shogren et al., 2011), and sugar beet pulp (Agoda-Tandjawa, Durand, Berot, Blassel, Gaillard, Garnier, et al., 2010). The presence of lignin and hemicellulose in the native cellulosic materials influences the XRD pattern to become broader due to the non-crystalline structure of these components.

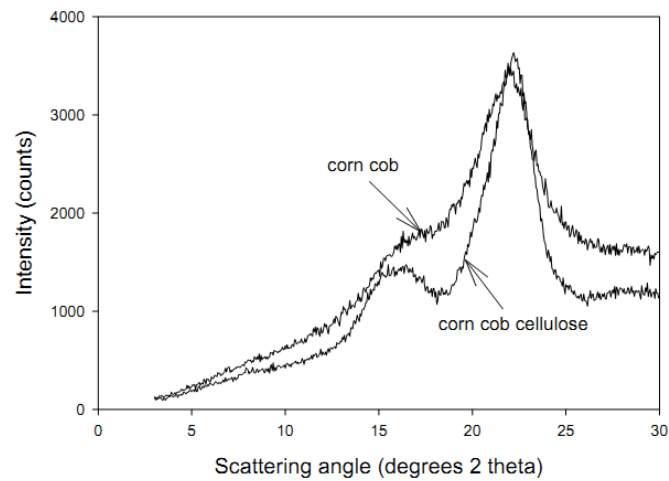


**Figure 2.6** X-ray powder diffraction of ground corn cobs and purified corn cob cellulose (Shogren et al., 2011).

The crystallinity index is the ratio of the diffraction portion from the crystalline part of the sample to the total diffraction of the same sample (Lavoine et al., 2012). The degree of crystallinity depends on the source used for preparation of the MFC. For example, a high crystallinity index around 78% has been obtained for wheat straw MFC (Alemdar & Sain, 2008), whereas the low value (about 30-40%) has been obtained for beet pulp MFC (Heux, Dinand, & Vignon, 1999). In addition, the degree of crystallinity also depends on the treatment method used for MFC preparation. Iwamoto et al. (2007) reported the degree of crystallinity of MFC obtained after different numbers of passes through grinder. The results show that the crystallinity index decreases with an increase in the number of passes from 1 to 30 passes. Similar results are also observed for the isolation of MFC from sugarcane bagasse (Li, Wei, Wang, Chen, Chang, Kong, et al., 2012) and prickly pear fruit peels (Habibi et al., 2009) by high-pressure homogenization. It is indicated that the intermolecular hydrogen bonds of cellulose were broken, causing the collapse of crystal structure during the homogenization process.

The crystalline structure of MFC can be observed using an X-ray diffractometer in a powder measurement mode, which means MFC has to be dried prior to analysis. The X-ray diffractometer analyzes crystalline states under normal atmospheric conditions. This method is non-destructive. X-rays focused on a

sample fixed on the axis of the spectrometer (goniometer) are diffracted by the sample. The changes in the diffracted X-ray intensities are measured, recorded and plotted against the rotation angles of the sample. The result is referred to as the X-ray diffraction pattern of the sample. Computer analysis of the peak positions and intensities associated with this pattern enables qualitative analysis, lattice constant determination and/or stress determination of the sample. Qualitative analysis may be conducted on the basis of peak height or peak area. The peak angles and profiles may be used to determine particle diameters and degree of crystallization, and are useful in conducting precise X-ray structural analysis.

#### **(iv) Rheological properties**

The term “rheology” is the science devoted to the study of deformation and flow of matter. The rheological tests rely on applying a specific force to a material and measuring the resulting flow and/or deformation (Rao, 1999). In an aqueous environment, MFC has specific rheological properties that can be described in terms of pseudoplasticity and shear-thinning behavior. This shear-thinning behavior is of importance in industrial processing and particularly in coating application. An ideal gel behaves elastically, and  $G'$  is independent of angular frequency, and  $G' \gg G''$  (Klemm et al., 2011). MFC suspension displays a gel-like behavior even at low concentration and the  $G'$  is rather high. The high elastic modulus is due to the long fibrils, which form an entangled network structure. The  $G'$  value is almost 10 times higher than the loss modulus ( $G''$ ). The  $G'$  value is particularly strongly dependent on the MFC concentration. An increase in MFC concentration from 0.125 to 5.900 % resulted in an increase in the  $G'$  value by five orders of magnitude (Pääkkö et al., 2007).

In addition, the shear-thinning behavior of enzymatic pretreated MFC depends on pH. Enzymatic method preserves the total charge of the original pulp. It is widely known that all charges are due to the presence of hemicellulose. At lower pH, the hydrogen ions neutralize the charges of the hemicellulose associated with the MFC which reduces the electrostatic repulsion, resulting in a higher interfibrillar interaction and a higher viscosity. At higher pH, on

the other hand, the number of charges increases leading to a higher electrostatic repulsion resulting in a lower interaction and a lower viscosity. (Pääkkö et al., 2007).

#### **2.2.1.4 Potential applications of microfibrillated cellulose**

Although the colloidal and rheological properties of MFC have been studied by many groups of researcher, there are today very few large-scale commercial applications. However, the treatments and modification procedures described above along with a general renaissance of interest in renewable biomaterials with micro/nanometer-sized dimension, have led to renewed interest in possible applications.

##### **(i) Paper and paperboard applications**

Microfibrillated cellulose acts as a strengthening agent and as a reinforcing agent to enhance the strength of pulps produced by thermo-mechanical processing (Eriksen, Syverud, & Gregerson, 2008). In addition, MFC can be used as a barrier in greaseproof paper, for which the film forming properties of MFC are utilized (Syverud & Stenius, 2009).

##### **(ii) Composite applications**

Microfibrillated cellulose extracted from tunicin can be used as a component of paints when combined with latex particles. Rubber latex is blended with MFC, followed by vulcanization and drying, to make natural rubber products. The hardness and resistance to cut and abrasion of the rubber products are improved (Klemm et al., 2011).

##### **(iii) Food applications**

Microfibrillated cellulose and other cellulose derivatives have long been used in fabricating formulated foods. Four important roles for the physically or chemically modified cellulose derivatives in foods are the controlling of rheological properties, water retention capacity, emulsification, and stabilizing of foams. The applicability of MFC and other cellulose derivatives for specific food applications can be determined from their physicochemical properties. A

number of parameters must be considered: (i) the chemical structure of the polymer, (ii) the molecular weight of the polymer, (iii) the presence of other active ingredients in the food matrix (e.g. salt), (iv) the processing operation that the food will be subjected, and (v) the physical properties (e.g. fiber dimension) of the polymer (Stephen, 1995). Food packaging is one area in which MFC reinforced polymer films is of interest and it is possible to create the films with high transparency and with improved oxygen barrier (Siró & Plackett, 2010). Most numerous literatures are claimed that it can be used as a low-calories thickener and stabilizer in food applications (Klemm et al., 2011).

#### **(iv) Other applications**

Microfibrillated cellulose has led to a wide range of proposed applications, due to its nontoxic, hydrophilic, and rheological properties. MFC is of great interest in pharmaceutical (e.g. as a component of drug tablets) and cosmetic industries. The strength and absorptive properties of finely divided cellulose lead to application in sanitary products, coating agents, and wound dressing. Interestingly, the grafting of quaternary ammonium groups to MFC can be made antimicrobial films (Klemm et al, 2011).

### **2.2.1.5 Limitation of using MFC**

#### **(i) Hornification**

The main problem of applying MFC in real situation is the difficulty of MFC redispersion after drying because irreversible aggregation of the fibrils occurs in a process known as “*hornification*”. Hornification of fibrils results in a material with ivory-like properties that can neither be used in rheological application nor dispersed for composite applications. This is the reason why a lot of researches designed to use MFC immediately after preparation step. The main strategies to prevent hornification have been introduction of a steric barrier (e.g. glycosides, carbohydrate gums, cellulose derivatives, oligosaccharides, and glycol compounds) and functional groups (e.g. carboxymethylation) to the cellulose to block cooperative hydrogen bonding of the cellulose chains. However, large amount of such

steric barrier compounds seem to be necessary to prevent hornification (Klemm et al., 2011).

### **(ii) High energy consumption**

Although MFC can successfully be produced at laboratory scale, there are several challenges to solve to be able to produce and use MFC at the industrial scale. As mention above, the production of MFC using only mechanical treatment (e.g. high-pressure homogenizer) uses a high level of energy consumption. However, by combining the mechanical treatment with certain chemical or enzymatic pre-treatment, a number of researcher groups have shown that it is possible to decrease energy consumption significantly (Siró & Plackett, 2010).

### **(iii) MFC network formation and aggregation**

Focusing on stabilizing effect of MFC in emulsions, Kalashnikova, Bizot, Cathala, and Capron (2011) suggested that because of the long length of MFC chain compared to the size of the droplets, the stabilizing effect of MFC in o/w emulsion tends to produce networks rather than stabilized individual oil droplets. As a consequence, the physicochemical and rheological properties of the emulsion will be affected by the properties of MFC, especially rheological properties. In addition, the microfibrils have great tendency to aggregate. In order to control the emulsion characteristics, the rheological properties of MFC itself should be concerned.

## **2.2.2 Emulsions**

### **2.2.2.1 Definition and classification**

An emulsion is a system consisting of two immiscible liquids which one of the liquids dispersed as small droplets (dispersed phase) in the other (continuous phase). The particle size of most food emulsions is in the range of 0.01-100  $\mu\text{m}$  (McClements, 2005). There are many types of emulsions that can be simply classified according to the relative spatial distribution of the oil and aqueous phase. A system that consists of oil droplets dispersed in an aqueous phase is called an oil-in-water (o/w) emulsion, for example, dressing, milk, beverage, and sauce. A system

consists of water droplets dispersed in an oil phase is named a water-in-oil (w/o) emulsion, for example, margarine and butter. In addition to the simple o/w and w/o emulsions described above, it is possible to prepare multiple emulsions, for example, oil-in-water-in-oil (o/w/o) or water-in-oil-in-water (w/o/w) emulsions. For example, the w/o/w emulsion consists of water droplets dispersed in oil droplets which themselves finally disperse in water, continuous phase.

#### **2.2.2.2 Pickering emulsion**

Emulsions can be stabilized not only by proteins or surfactants, but also by solid particles, hence, they are termed “Pickering emulsions” after the pioneering work of Pickering (1907). Food systems commonly contain particulate material that accumulate at oil-water interfaces and contributes to the colloidal stabilization of emulsions. According to the conventional explanation for emulsion stabilized by solid particles (Dickinson, 2010; Kalashnikova et al., 2011), there is an accumulation of solid particles at the oil-water interface in the form of a densely packed layer that prevents droplet flocculation and coalescence by a steric mechanism or physical barrier (Ramsden, 1904; Pickering, 1907). The steric barrier is more effective for adsorbed particles which are preferentially wetted by the continuous phase, and which lie predominantly on the outer surface of the dispersed droplets (Aveyard, Binks, & Clint, 2003; Dickinson, 2010, 2012). The wettability of the particles at the oil-water interface is quantified by the contact angle that the particle makes with it. Hydrophilic particles ( $< 90^\circ$ ) therefore tend to form oil-in-water (o/w) emulsions (Figure 2.7) whereas hydrophobic particles ( $> 90^\circ$ ) form water-in-oil (w/o) emulsions. Examples of Pickering food emulsions are homogenized and reconstituted milks (o/w emulsions stabilized by casein micelles) and margarines (w/o emulsions stabilized by triglyceride crystals). For the particles of intermediate wettability with not too close to  $0^\circ$  or  $180^\circ$ , it can be regarded as being irreversibly adsorbed due to an extremely high free energy of adsorption compared with the thermal energy (Aveyard, Binks, & Clint, 2003; Dickinson, 2010, 2012). Therefore, one of the most important features of the particle-stabilized emulsions is that they are extremely stable to coalescence even when the emulsion droplets are quite large.

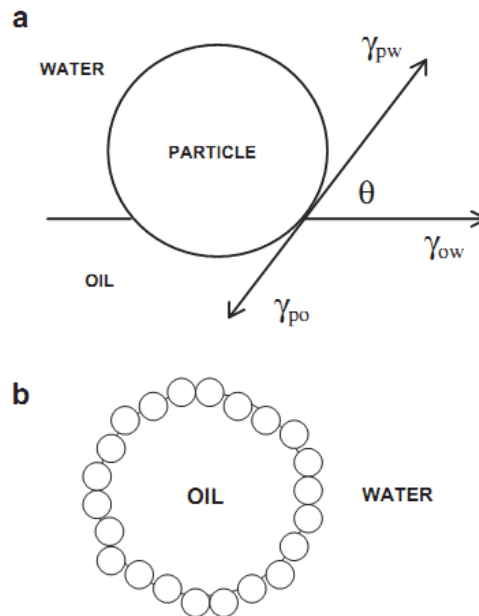


**Figure 2.7** Schematic representation of Pickering stabilization of o/w emulsion by spherical particles. (a) Single hydrophilic particle at the oil-water interface, with contact angle  $\theta$  formed at the junction of the three phases: particle (p), oil (o), and water (w). Quantities  $\gamma_{po}$ ,  $\gamma_{pw}$ , and  $\gamma_{ow}$  are the tension at the three boundaries. (b) Close-packed monolayer of particles at surface of dispersed oil droplet. (Dickinson 2012)

It has been experimentally observed that particle-stabilized emulsion can be produced without full monolayer coverage of particles around the droplets (Binks, Clint, Mackenzie, Simcock, & Whitby, 2005; Binks & Horozov, 2006). When two particle-coated droplets come close together, the arrangements of particles at oil-water interface can be classified into 3 types as shown in Figure 2.8 (Dickinson, 2012).

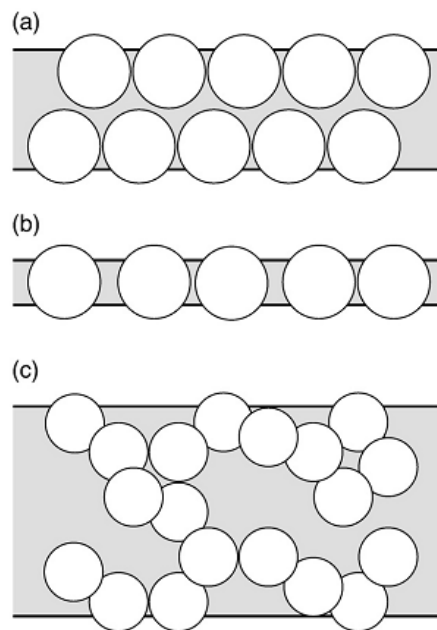


**Figure 2.8** Schematic representations of alternative stabilizing arrangements of particles in a thin film between closely approaching emulsion droplets: (a) separate closely packed monolayers on the two oil–water interfaces; (b) single dense layer of bridging particles; and (c) low-density network layer of aggregated particles (Dickinson, 2010).

**(i) Separate closely packed monolayer on the two oil-water interfaces** (Figure 2.8a): Aggregation or flocculation of the droplets typically involve in the emulsion structure.

**(ii) Single dense layer of bridging particles** (Figure 2.8b): This structure can be found when each particle is wetted by both dispersed phase, but still with the major portion of each particle lying in the continuous phase. Steric hindrance effect plays an important role in preventing oil droplets from coalescence (Binks & Horozov, 2006; Dickinson, 2012).

**(iii) Low density network layer of aggregated particles** (Figure 2.8c): Simply, the droplets are stabilized through the adsorption of aggregated colloidal particles. In this case, the steric barrier is not a simple bilayer or monolayer but it consists of a rigid disordered network of particles, adsorbed to the

oil-water interfaces. The attractive interparticle forces play a crucial role in holding the whole aggregated structure together (Dickinson, 2012).

Over the past 10 years, there is a lot of research conducted on Pickering emulsions, including both organic and inorganic particles (Aveyard, Binks & Clint, 2003) because this system is not only present good mechanical properties, but much fewer solids particles are needed to form emulsion with good stability, so leading to a reduction in the use of hazardous or synthetic emulsifiers. However, fairly few of them are directly related to foods. This is probably due to some kinds of particles studied, such as silica, latexes, bacteria particles, would seem to be unsuitable for food use (Dickinson, 2010; Tzoumaki, Moschakis, Kiosseoglou, & Biliaderis, 2011). Research efforts are being focused on the production of nanoparticles and microparticles that are not only effective to stabilized emulsions, but also acceptable for used in food products (Dickinson, 2010). Natural biopolymers, like polysaccharides, are becoming an interesting source of particulate material for food use, for examples, hydrophobically modified starch granules (Yusoff & Murray, 2011), chitin nanocrystal particles (Tzoumaki et al, 2011), bacterial cellulose nanocrystals (Kalashnikova et al., 2011; Kalashnikova, Bizot, Cathala, & Capron, 2012), and microfibrillated cellulose (Ougiya, Watanabe, Morinaga, & Yoshinaga, 1997), as shown in Table 2.2.

**Table 2.2** Example of microparticles and nanoparticles of biological origin stabilized o/w emulsions by Pickering mechanism.

Particle type	Particle size	References
Chitin nanocrystal particles	240 nm × 20 nm	Tzoumaki et al., 2011
Flavonoid (tiliroside) particles	~ 100 nm	Luo, Murray, Yusoff, Morgan, Povey, & Day 2011
Cellulose nanocrystals	850 nm × 10 nm	Kalashnikova et al., 2011
Hydrophobically modified starch granules	0.5 – 15 μm	Yusoff & Murray, 2011
Microcrystalline cellulose	0.2 μm	Oza & Frank, 1986
Microfibrillated cellulose	–	Ougiya et al., 1997

A key ongoing challenge of studying Pickering emulsion for food manufacture is to be able to produce nanoparticles and microparticles that are both effective as Pickering stabilizers and also acceptable for use in food products on the commercial scale. In addition, it is necessary to design the desired emulsion system. There have been many groups of researchers to investigate and improve understanding of the properties and stability of food emulsions, leading to create low-cost high-quality food products in a more systematic and reliable fashion.

### **2.2.2.3 Emulsion formation**

The emulsification process includes two steps, including deformation and disruption of droplets, and following by stabilization of the newly formed interfaces. In general, emulsions are unstable and thus do not form spontaneously. The process of converting two immiscible liquids into an emulsion is widely known as homogenization using a mechanical device named a homogenizer. Over time, emulsions tend to adopt their thermodynamically most stable state, which consists of a layer of oil on top of a layer of water because the presence of a large interfacial area between these molecules of different polarity is thermodynamically unfavorable. Emulsions are thermodynamically unstable. Thus, emulsion instability can adversely affect the shelf life and quality of product. A surfactant (also known as an emulsifier or stabilizer) is a substance which forms and stabilizes an emulsion. Surfactant is capable of adsorbing to an oil-water interface and protecting emulsion droplet from aggregation (McClements, 2005).

There are two stages in the preparation of an emulsion by homogenization (Figure 2.9); (i) the creation of an emulsion directly from two separate liquids into a “coarse emulsion” with fairly large droplets will be defined as a primary emulsion, and (ii) the reduction in size of the oil droplets in an already existing emulsion will be defined as a secondary emulsion or fine emulsion using another technique (e.g. high-pressure systems) (Phipps, 1985; McClements, 2005). The physicochemical properties, microstructure, and stability of final emulsions depend on many variables related to the processing conditions (e.g., type and geometry of the emulsification equipment, agitation speed, residence time, etc.), or to

the nature of the phases involved (e.g., rheological properties, and concentration of the continuous and disperse phases, etc.).

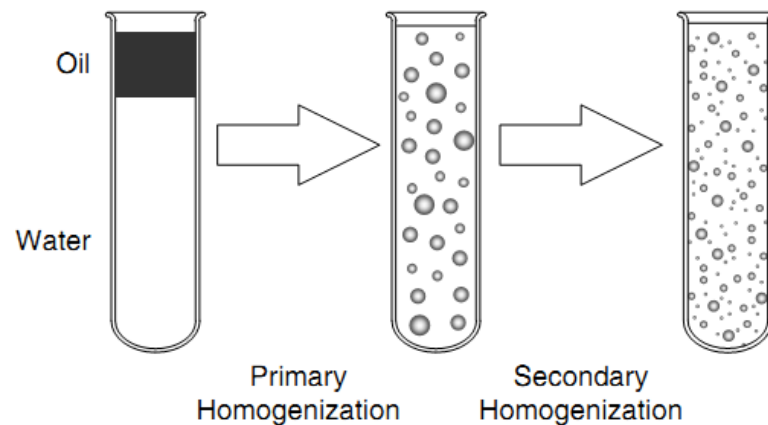


**Figure 2.9** Homogenization can be divided into primary and secondary homogenization. Primary homogenization is the conversion of two bulk liquids into an emulsion, while secondary homogenization is the reduction in size of the droplets in an existing emulsion (McClements, 2005).

In laboratory studies and most emulsion preparations, it is more convenient and efficient to produce the coarse emulsion by rotor stator device. For the rotor stator device, as it rotates, it generates a lower pressure to draw the liquid in and out of the assembly, resulting in circulation and emulsification (Maa & Hsu, 1996). The forces which involved in the reduction of droplet size are the mechanical impingement against the wall due to high fluid acceleration and the shear stress in the gap between rotor and stator, which is generated by the rapid rotation of the rotor. High-pressure valve homogenizers (Figure 2.10) are the common devices for producing fine emulsion in the food manufacture. The instruments are more effective at reducing the droplet size in a preexisting emulsion, than at creating an emulsion directly from two immiscible liquids (Pandolfe, 1995). The principle of high-pressure homogenization is that a coarse emulsion produced using a rotor-stator device is fed directly into the input chamber of the high-pressure valve homogenizer. The emulsion is then forced under pressure through a narrow valve. The combination of the intense

shear, cavitation, and turbulent flow conditions in this valve leads to the disruption of oil droplets (McClements, 2005). In this study, a “two-stage” homogenization process was used to create the emulsion. The emulsion is forced through two consecutive valves. For the first valve, at high pressure, it is responsible for breaking up the oil droplets, whereas for the second valve, at low pressure, it is mainly responsible for disrupting any flocculated droplets which are formed during the first stage.

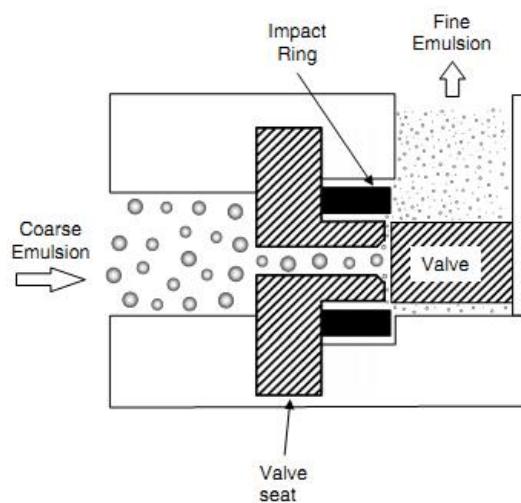


**Figure 2.10** High-pressure valve homogenizers are used to produce emulsions with fine droplet sizes (McClements, 2005).

#### 2.2.2.4 Emulsion properties

##### (i) Particle size and size distribution

Droplet size and size distribution in emulsion plays an important role in determining its stability, appearance, texture and flavor. In a monodisperse emulsion all the droplets have the same size, but in a polydisperse emulsion they have a range of different sizes (Figure 2.11). The droplet size of a monodisperse emulsion can be reported by a single number, such as diameter ( $d$ ) or radius ( $r$ ), whereas real food emulsions usually contain a distribution of droplet sizes. It is necessary to have information about the full particle size distribution of an emulsion. The full particle size distribution refers to the fraction of oil droplets in different specified size ranges (McClements, 2005).

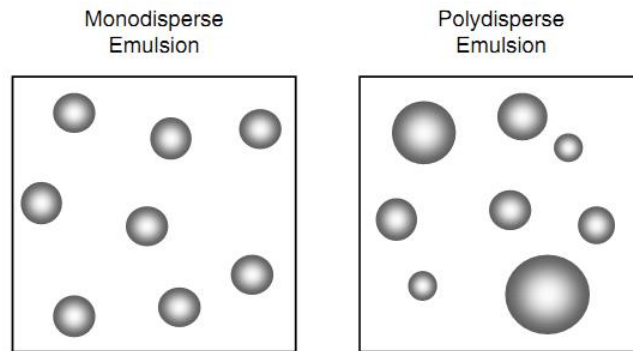


**Figure 2.11** Schematic representation of monodisperse and polydisperse emulsions (McClements, 2005).

The most useful number for representing the size of the droplets are the mean particle size ( $\bar{d}$ ) and the standard deviation ( $\sigma$ ), which is a measure of the central tendency of the distribution and a measure of the width of the distribution, respectively (McClements, 2005). These two parameters can be calculated using the following equations:

$$\bar{d} = \frac{\sum_{i=1} n_i d_i}{N} \quad (2.2)$$

$$\sigma = \sqrt{\frac{\sum_{i=1} n_i (d_i - \bar{d})^2}{N}} \quad (2.3)$$

where  $n_i$  is the number of droplets with diameter  $d_i$  and  $N$  is the total number of droplets. Most of emulsion research, particle size can be reported as the surface-weighted mean particle diameter ( $d_{32}$ ) and the volume-weighted mean diameter ( $d_{43}$ ), defined by the following equations:

$$d_{32} = \frac{\sum n_i d_i^3}{\sum n_i d_i^2} \quad (2.4)$$

$$d_{43} = \frac{\sum n_i d_i^4}{\sum n_i d_i^3} \quad (2.5)$$

Both  $d_{32}$  and  $d_{43}$  are sensitive to different aspects of the particle size distribution (McClements, 2005):  $d_{32}$  is more sensitive to the presence of small particles, whereas  $d_{43}$  is more sensitive to the presence of large particles

(Surh, Decker, & McClements, 2006). Moreover, particle size distribution can be presented as a smooth curve, as shown in Figure 2.12.

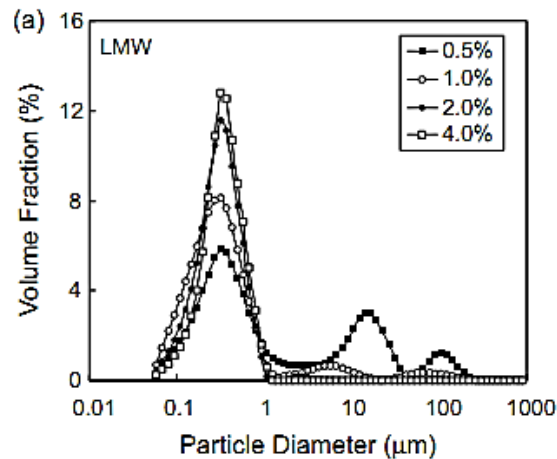


**Figure 2.12** Example of bimodal and multimodal distributions of o/w emulsions stabilized by fish gelatin at various concentrations (modified from Surh, Decker, & McClements, 2006).

Static light scattering (SLS) and dynamic light scattering (DLS) techniques are widely used for particle size and size distribution measurement. For SLS, this technique is based on the principle that particles in a laser beam scatter laser light at angles which are inversely proportional to the size of the particles (i.e. large particles scatter light at small angles whereas small particles scatter light at wider angles). Mie theory is used to interpret the scattering patterns of emulsions containing spherical droplets of any size (Kerker, 1969). It should be noted that the Mie theory assumes that the light waves are only scattered by a single particle. Therefore, to avoid multiple light scattering, the emulsion must be diluted before analysis. This instrument is fully automated simple to use and rapid. The particle size range is between 0.02 - 2000 μm. When the sizes of the particles are below the lower detection limit of SLS technique, DLS technique is a useful method for measuring very small particles typically between 3 nm and 3 μm (i.e. small emulsion droplets, surfactant micelles, etc.) (Horne, 1995; Dalgleish, West, & Hallett, 1997). DLS is based measurement of the translational diffusion coefficient of droplets, velocity of the

Brownian motion, determined by the interaction between a laser beam and emulsion droplets (Hunter, 1986; Horne, 1995). DLS measures Brownian motion which relates to the size of the particles (i.e. the larger particle, the slower Brownian motion). The particle size can be calculated by using the Stokes-Einstein equation:

$$r = \frac{kT}{6\pi\eta_1 D} \quad (2.6)$$

where  $r$  is the hydrodynamic radius,  $k$  is the Boltzmann's constant,  $T$  is the absolute temperature,  $\eta_1$  is the viscosity of the continuous phase, and  $D$  is the translational diffusion coefficient.

### (ii) Electrical charge of droplets

The magnitude and sign of the electrical charge on the droplets play a crucial role in controlling properties and stability of food emulsions. The origin of the electrical charge is normally to be due to the ionization of surface groups on the droplets and the adsorption of emulsifier molecules that are ionized or ionizable (McClements, 2005). In 2003, Pashely reported that nonionic surfactant stabilized oil droplets also have an electrical charge because the oil preferentially adsorbs either  $\text{OH}^-$  or  $\text{H}_3\text{O}^+$  ion from water or contains ionic impurities (Pashely, 2003). Different types of emulsifier show different effects on the electrical charge of the droplets (i.e. surface-active polysaccharides may have an electrical charge depending on the functional groups along their backbone or proteins may also be neutral, negative, or positive charged depending on the pH of the solution compared to their isoelectric point). The electrical charge on a droplet can be measured in a number of different ways (Hunter 1986). In this study, we measure the electrical charge of the oil droplet via the  $\zeta$ -potential value ( $\zeta$ ). The  $\zeta$ -potential is the effective surface potential of a droplet suspended in a medium, which should be noted that charged species in the surrounding medium may adsorb to the surface of the droplet and alter its net charge.

In this study,  $\zeta$ -potential of the emulsions were measured using a Zetasizer Nano ZS instrument, which is a commercial instrument that combine particle electrophoresis measurement with dynamic light scattering

measurements so that both the droplet charge and size distribution can be determined using the same instrument. It is a principle of this instrument that an oscillating electric field is applied across the dispersion and the  $\zeta$ -potential value is then determined from the droplet velocity move toward the oppositely charged electrode. This instrument calculates the  $\zeta$ -potential by determining the electrophoresis mobility and the Henry's equation (equation 2.7) is then applied.

$$U_E = \frac{2\varepsilon z f(ka)}{3\eta} \quad (2.7)$$

where  $z$  is the  $\zeta$ -potential,  $\varepsilon$  is the dielectric constant,  $\eta$  is the viscosity of the liquid and  $f(ka)$  is the Henry's function, and  $U_E$  is the electrophoresis mobility.

The important of  $\zeta$ -potential is their magnitude which gives an indication of the potential stability of emulsion system. The fact that the emulsion droplets are coated by a biopolymer or surfactant with an appreciable electrical charge leads to that electrostatic repulsion may play an important role in stabilizing them against droplet aggregation (McClements, 2005; Surh et al., 2006). A dividing region between stable and unstable droplet dispersions is generally taken at either +30 or -30 mV. For example, oil droplets with  $\zeta$ -potential value higher than +30 mV or lower than -30 mV are considered stable. As  $\zeta$ -potential value closes to zero, droplets tend to aggregate (Malvern Instrument Ltd., 2004). In addition, ionic strength and pH have a strong effect on the droplet charge, especially for emulsion stabilized by ionized emulsifier. For example, if the pH of the aqueous phase is adjusted so that the emulsifier loses its charge, or if salt is added to "screen" the electrostatic interactions between the oil droplets, resulting to the repulsive forces may not strong enough to prevent the droplet flocculation.

### (iii) Microstructure

Emulsion microstructure provides very useful information of emulsion properties (e.g. particle size and shape, interfacial membrane morphology, and three-dimensional network of aggregated polymer in an aqueous phase, etc.) and emulsion stability (e.g. size and shape of flocs, coalescence of oil droplet, and interaction of oil droplets, etc.). There are several optical techniques,

including optical microscopy, electron microscopy, and confocal laser scanning microscopy, etc. used for examination of the microstructure of emulsion (Kirby, Gunning, & Morris, 1995; McClements, 2005). Any type of microscope must have three qualities if it is going to be used for examination of the structure of small objects: resolution (the ability to distinguish between two objects that are close to each other), magnification (the number of times that the image is greater than the specimen being examined), and contrast (how well an object can be distinguish from its background) (Aguilera and Stanley, 1990).

#### Conventional optical microscopy

An optical microscope contains a series of lenses that direct light through the specimen and magnify the resulting image. The resolution of an optical microscope is determined by the wavelength of light used and the mechanical design of the instrument. This technique provides valuable information about the droplet size distribution in emulsions which contain large droplets, and can be used to distinguish between flocculation and coalescence. The limitation of using optical microscopy are stated following; (i) in practical, it is difficult to obtain reliable measurement below 1  $\mu\text{m}$  (Hunter, 1993), (ii) the Brownian motion of small droplets or particles cause images to appear blurred (McClements, 2005), (iii) the natural contrast between the major components in food emulsions is fairly poor, which makes it difficult to distinguish them from each other, so that chemical strains can be applied to overcome this problem, and (iv) the sample preparation can alter the structure of the specimen being analyzed (Kalab, Allan-Wojtas, Miller, 1995).

#### Scanning electron microscope (SEM)

SEM is commonly used to provide images of the surface topography and microstructure of emulsion systems. The emulsions with small droplet size ( $< 1 \mu\text{m}$ ) and other structural components (i.e. protein aggregates, biopolymer microfibrils, and micelles, etc.) can be examined by this instrument (Aguilera & Stanley, 1990; Munoz & Mikula, 1997; McClement, 2005). SEM relies on the measurement of secondary electrons generated by specimen when it is bombarded by an electron beam, rather than the electron that have traveled directly through the specimen. SEM micrograph has a three-dimensional appearance. It is widely known that the major limitation of SEM is the difficulty in preparing

specimens without altering the structure and the use of high energy electron beams cause the damage and changes in the structure of delicate specimens. The recent advances in the design of electron microscope and sample preparation technique, such as cryo-SEM and/or critical point dryer, respectively, help to overcome these problems (McClements, 2005).

#### *Confocal laser scanning microscopy (CLSM)*

CLSM focuses an extremely narrow laser beam at a particular point in the specimen being analyzed and a detector measures the intensity of the resulting signal (McClements, 2005). A two-dimensional micrograph is obtained by measuring at different points in the  $x$ - $y$  plane, either by moving the laser beam or by moving the specimen, whereas a three-dimensional micrograph is obtained by focusing the laser beam at different vertical depths ( $z$ -plane) and then scanning in the horizontal direction ( $x$ - $y$  plane). This technique can be used to observe the microstructure of multicomponent systems using the fluorescent dyes which selectively bind to specific components (Larison, 1992); for example, Nile red dye and oil (McClements, 2005), Congo red dye and cellulose (Winuprasith & Suphantharika, 2013). CLSM not only provides higher clarity images than optical microscopy but also generate the three-dimensional micrograph without the need to section the specimen. Nevertheless, CLSM technique has some of the sample problems as optical microscopy, but it has a better resolution and sensitivity.

The use of the microscopic techniques to observe microstructure of emulsions is the direct method. However, there are other indirect techniques such as rheological test, which also provide the information of microstructure and interaction of components in the system.

#### **(iv) Rheological properties of emulsions**

The term “rheology” is the science devoted to the study of deformation and flow of matter. The rheological tests rely on applying a specific force to a material and measuring the resulting flow and/or deformation (Rao, 1999). The rheological properties of emulsions are great of interest not only for fundamental scientific understanding but also for practical industrial applications, for example, processing operation design, product development, sensory, quality, and

stability of emulsion-based food products. Food emulsions are complex system that can exhibit different rheological behaviors, i.e. fairly hard solids (e.g. butter and margarine), viscoelastic gels (e.g. yogurt and mayonnaise), and low viscosity fluid (e.g. milk and beverages). Most of food emulsions exhibit a variety of non-Newtonian effects, such as shear thinning, yield stress, viscoelasticity, and time-dependency (McClements, 2005). Non-ideal rheological behavior may manifest itself in a different ways in liquids (i.e. the viscosity of a liquids may depend on the shear rate and/or time over the applied shear stress). There are two categories of non-ideal behavior, including shear-rate dependent and time dependent non-ideal behavior.

- For “*shear-rate dependent non-ideal behavior*”, the apparent viscosity of emulsion may either decrease or increase as the shear rate is increased but is independent of the shearing time as shown in Figure 2.13 (Dickinson, 1992). The two most common types of shear-rate dependent non-ideal liquids are *pseudoplastic fluid* (a decrease in the apparent viscosity as the shear rate is increased, known as *shear thinning*) and *dilatant fluid* (an increase in the apparent viscosity as the shear rate is increased, known as *shear thickening*).

- For “*time-dependent non-ideal behavior*”, the apparent viscosity may either increase or decrease with time during the application of shear. It is possible either reversible or irreversible changes of emulsion rheological characteristics after a sufficiently long period standing. Time-dependent non-ideal fluids can be classified into two categories, including *thixotropic behavior* and *rheopectic behavior*. For thixotropic fluid, when a material is sheared at a constant shear rate, the viscosity is decreased over a period of time, as a result of a progressive breakdown of particles that are aggregated by weak forces, whereas rheopectic fluid manifests the opposite sort of behavior (McClements, 2005).

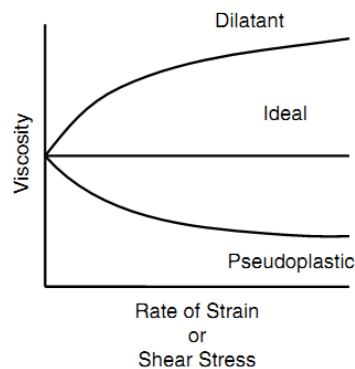


**Figure 2.13** Apparent viscosity as a function of rate of shear strain or shear stress (modified from McClements, 2005).

A variety of instrumental method has been developed to characterize emulsion rheological properties. In this study, a dynamic shear rotational rheometer was used to measure viscoelastic properties of materials. It can measure not only viscosity but also other parameters, such as yield stress, kinetic properties, complex viscosity, modulus, creep, and recovery. Basically, the sample is placed in a thermostated measurement cell, where it is subjected to a controlled shear stress or strain. The resulting strain or stress is then measured by the instrument. The rheological properties of the material can be determined from the stress-strain relationship using a computational program (McClements, 2005). There are many kinds of measurement cells (e.g. concentric cylinder, cone and plate, and parallel plate) which can be used to contain the sample during an experiment (Mckenna & Lyng, 2003). In this study, the measurement cells were selected depending on the viscosity of the materials. Cone and plate was used for high-viscosity emulsion, whereas cylinder measurement cell was designed for low-viscosity emulsion. Figure 2.14 illustrates the different types of measurement cells.

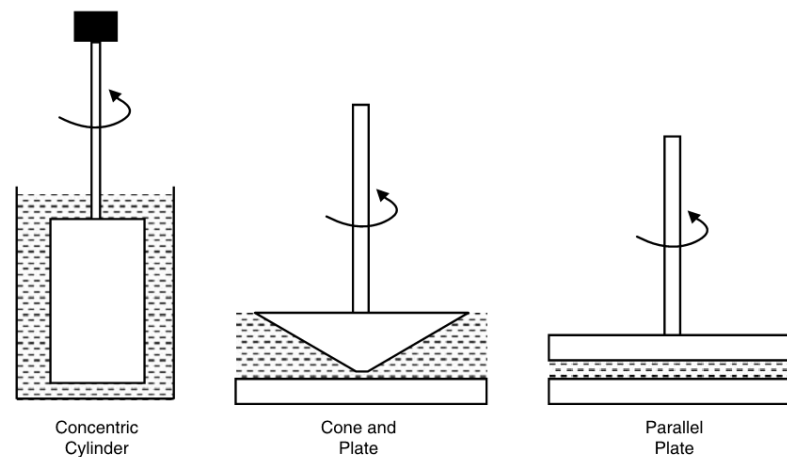


**Figure 2.14** Different types of measurement cells commonly used with dynamic shear rheometers (McClements, 2005).

#### 2.2.2.5 Emulsion stability

The quality of an emulsion is related to its stability. The term “emulsion stability” is widely known as the ability of emulsion to resist changes in its properties over time. An emulsion may become unstable due to physical (e.g., creaming, flocculation, and coalescence, etc.), chemical (e.g., oxidation and hydrolysis), and microbiological processes (e.g., bacterial and mold growth) (McClements, 2005; Surh et al., 2006). The stability of emulsions depends on its composition and microstructure, as well as on the environmental conditions such as temperature variation, mechanical agitation, and storage conditions. A number of the most important physical instability responsible for emulsion destabilization refer to creaming, flocculation, coalescence, and phase inversion (Figure 2.15).

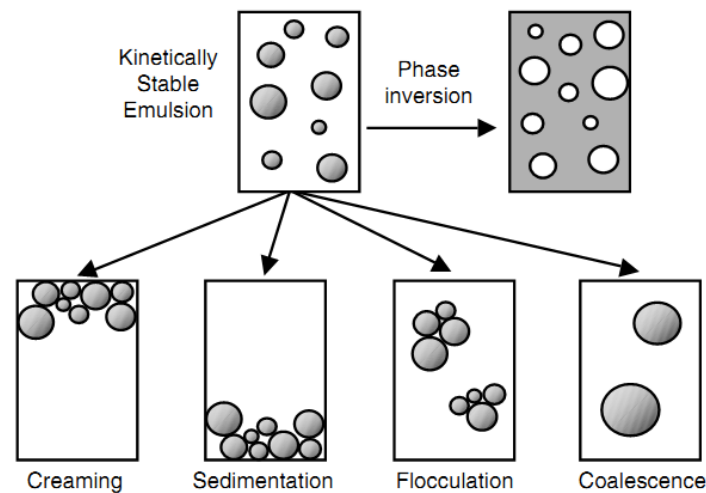


**Figure 2.15** Physical instability of emulsion (McClements, 2005).

#### (i) Creaming and sedimentation

The most obvious manifestation of emulsion instability is creaming and sedimentation. Gravity or centrifugal field induces creaming and sedimentation process, which the droplets tend to move upward or downward, respectively, because the droplets in an emulsion have a different density to that of the liquid that surrounds them. In general, the densities of most edible oils in liquid state are lower than that of water, so there is a tendency for oil to accumulate at the top of emulsion and water at the bottom (Dickinson & Stainsby, 1982; Dickinson, 1992; Walstra, 1996). Thus, o/w emulsion tends to cream (Figure 2.16), whereas w/o emulsion tends to sediment. Creaming and sedimentation are reversible. The original uniform distribution of droplet can be obtained by gentle mixing. This instability is usually regarded as having an adverse effect on the food emulsion quality, i.e. texture, appearance, and mouthfeel. In addition, gravitational separation can also lead to enhance flocculation and coalescence, and eventually to oiling-off, which is the formation of a layer of pure oil on top of the emulsion. Therefore, it is important for the food manufacture to understand the gravitational separation mechanism (Dickinson, 1992; McClements, 2005).

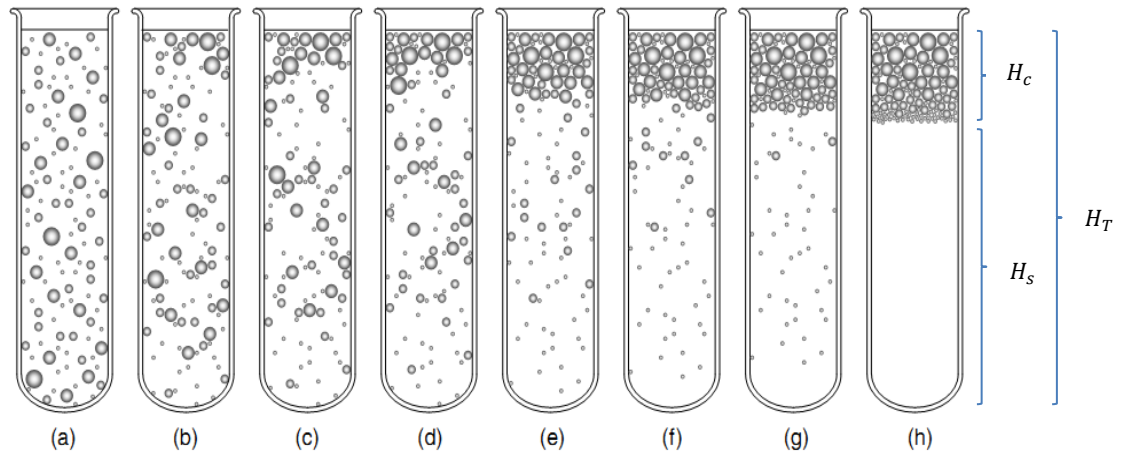


**Figure 2.16** Time dependence of droplet creaming in o/w emulsions. Droplets move upward until they cannot move any further and then form a “creamed” layer. Larger droplets tend to move upward faster than smaller ones (modified from McClements, 2005).

According to the Stokes’ law (equation 2.7) describes the dependence of the individual droplet size and the rate of creaming.

$$v_{Stokes} = \frac{2gr^2(\rho_2 - \rho_1)}{9\eta_1} \tag{2.7}$$

where  $v_{Stokes}$  is the creaming velocity,  $\eta_1$  is the shear viscosity.  $\rho_2 - \rho_1$  is the different density between of the continuous and dispersed phase,  $g$  is the acceleration due to gravity, and  $r$  is the radius of droplets. From the Stokes’ law, there are several effective approaches of controlling gravitational separation. First, density difference between oil and aqueous phase should be minimize by mixing oil-soluble “weighting agents” that have a higher density than water with the oil phase prior to homogenization, so that the final density of the oil becomes similar to that of the aqueous phase. Second, the droplet size should be reduced using a suitable ratio of emulsifier to oil and homogenization condition. Third, the viscosity of the continuous phase should be increased by adding a thickening agent or biopolymers that form a gel or a three-dimensional network in the aqueous phase. Finally, the rate of gravitational separation can be retarded by increasing the droplet concentration. The droplets are

prevented from moving because they are so closely packed together (Dickinson, 1992; McClements, 2005).

The stability of an o/w emulsion to creaming can be easily measured by placing an emulsion in a transparent test tube, storing for a certain length of time, and then measuring the height of the interface between the opaque creamed layer and the transparent serum layer (Keowmaneechai & McClements, 2002). The creaming index of emulsion can be calculated using equation 2.8.

$$\text{Creaming index (\%)} = 100(H_s/H_T) \quad (2.8)$$

where  $H_s$  is the height of the serum layer and  $H_T$  is the total height of the emulsion (Figure 2.16). However, there are limitations for this technique. (i) It does not give information about the full vertical concentration profile of the droplets. (ii) In some systems it is difficult to clearly locate each layer. (iii) It may take very long time before the layer is observable (McClements, 2005).

### **(ii) Flocculation**

Flocculation, the process whereby two or more droplets come together to form an aggregate in which the droplets retain their individual integrity, is the major types of aggregations in food emulsion (McClements, 2005). Droplet flocculation has a pronounced effect on microstructure, rheological properties and stability of food emulsion. The flocculation rate depends on two factors: (i) the frequency of collisions between the droplets which is induced by Brownian movement, gravitational separation, or applied mechanical forces (ii) the efficiency of collision which is the height of repulsive energy barrier. To prevent droplets from flocculating it is necessary to have a sufficiently high repulsive barrier to stop them from coming too close together (Ivanov, Danov, & Kralchevsky, 1999). Biopolymer or polysaccharide can induce the flocculation of emulsion droplets via bridging and depletion flocculation mechanism (Figure 2.17).

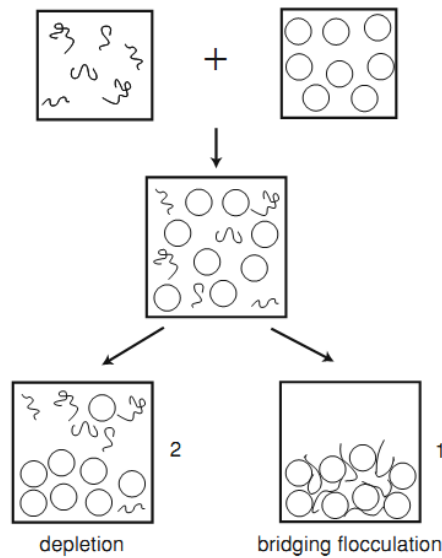


**Figure 2.17** Types of instability that occur after mixing a colloidal dispersion with a polymer solution, including bridging and depletion flocculation (Lekkerkerker & Tuinier, 2011).

#### Bridging flocculation

Bridging flocculation occurs when segments of the same biopolymer molecule adsorb onto surface of different droplets via electrostatic and hydrophobic interaction, resulting in linking oil droplets together (Figure 2.17). In case of emulsion, this type of flocculation tends to occur when biopolymers, which is used as an emulsifier, is not enough to completely cover the oil-water interface formed during homogenization or when a biopolymer in the aqueous phase has an electrical charge that is opposite to that of droplets (Dickinson, 2003). Thus, bridging flocculation can be avoided (or can easily be disrupted) by ensuring that the concentration of biopolymer is sufficient to completely cover the oil droplets and/or both biopolymer and droplets have similar charge (Dickinson, 2003; McClements, 2005).

#### Depletion flocculation

When the biopolymer does not adsorb, depletion leads to partitioning of colloids and polymers over different phases (Figure 2.17). The presence of non-adsorbing biopolymer in an aqueous phase of an emulsion causes an

increase in the attractive force between the droplets due to an osmotic effect associated with the exclusion of polymer from a narrow region surrounding each droplet. This attractive may become large enough to overcome the repulsive interaction between the droplets, causing flocculation (Jenkins & Snowden, 1996; McClements, 2005). The increase in mean particle size brought about by droplet flocculation leads to rapid creaming. However, at higher biopolymer concentrations the creaming rate is decreased, even though there is still a strong depletion flocculation between the droplets, because the viscosity of continuous phase increase so much, resulting in retardation of the droplet movement.

Emulsion containing flocs causes an increase of emulsion viscosity comparing with one containing the same concentration of non-flocculated droplets. This is because the presence of the continuous phase trapped within the flocs increases the effective volume fraction of the floc to be greater than the sum of the volume fractions of the individual droplets. Interestingly, emulsions that contain flocculated droplets tend to exhibit pronounced shear thinning behavior, that is, the viscosity decreases as the shear rate increases. Figure 2.18 shows flocs become increasingly deformed and disrupted with increasing shear stress (or rate), which leads to a decrease in emulsion viscosity. In addition, flocculation leads to the formation of a three-dimensional network of aggregated droplets that extends throughout the emulsion, referred to as a particle gel. The three-dimensional network of aggregated droplets prevents the droplets from moving, resulting in less creaming whereas flocculation increases the creaming rate in dilute emulsions (Manoj, Fillery-Travis, Watson, Hibberd, & Robins, 1998; Berli, Quemada, & Parker, 2003).

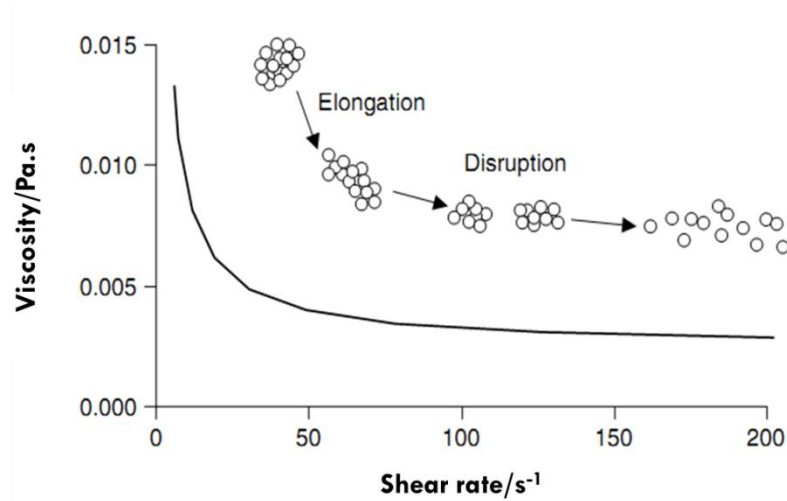


**Figure 2.18** Schematic diagram of events that occur during the shearing of a flocculated emulsion and their effect on emulsion viscosity (McClements, 2005).

A wide variety of experimental techniques are used for monitoring the flocculation occurred in emulsions. Microscopic studies using an optical or electron microscope are the most direct method. However, the major drawback of this technique is that the procedure used to prepare the samples for observation often disturbs the flocs and it is difficult to distinguish whether two droplets are flocculated or just in close proximity. The changes in the particle size observed using particle sizing instrument (i.e. light scattering) can be used as a combination technique. In addition, the rheological properties of emulsion, including the change in viscosity or shear modulus, can often monitor the flocculation (Manoj et al, 1998; Tadros, 2004). There are several ways to retard the flocculation, i.e. decelerating droplet movements by increasing the viscosity of continuous phase, decreasing the droplet concentration, narrowing the size distribution, etc.

### (iii) Coalescence

Coalescence is the process whereby two or more droplets merge to form a single larger droplet because the energy of adhesion between two droplets is larger than the turbulent energy causing dispersion, the thin film between the droplets is then ruptured. In an o/w emulsion, coalescence eventually leads to a growth in the mean droplet diameter and a formation of a layer of oil on the

top of emulsion, which is called oiling off or destabilized oil because the thermodynamically stable state involves in a decrease in the contact area between the oil and water (McClements, 2005). Coalescence is an irreversible process (Dickinson, 1992; McClements & Dungan, 1993). A basic schematic of this instability is illustrated in Figure 2.19.

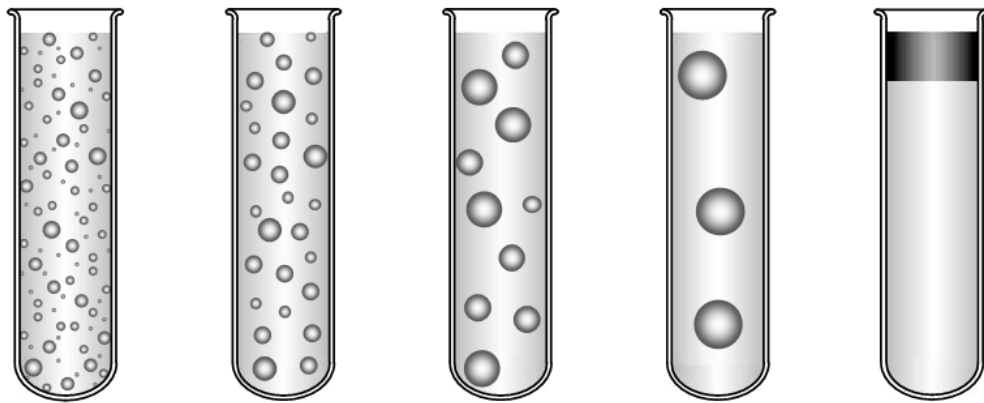


**Figure 2.19** Droplet coalescence leads to a growth in the mean droplet diameter and may eventually lead to complete separation of the oil and aqueous phases (McClements, 2005).

The nature of the emulsifier (e.g. protein, small molecule surfactant, etc.) and environmental conditions (e.g. shear force, ionic strength, etc.) in the system are the key to this process. For example, coalescence of emulsion stabilized by small molecule surfactant is largely governed by their ability to keep droplets apart, rather than the resistance of the droplet membrane to rupture. In case of solid stabilized or Pickering emulsion, shear force induced coalescence should be concerned because shear force or mechanical stress applied to emulsion system cause film stretching or film tearing leading to the merging of two interfacial membranes of the droplets, a spherical larger droplet is then formed (Dickinson, 2012; McClements, 2005). Coalescence of partially covered droplets is generally accompanied by bridging flocculation, for example, the sharing of adsorbed particles, macromolecules, or biopolymers between pairs of adjacent droplets (Dickinson, 2012).

Experimental characterization of droplet coalescence can be performed using both direct and indirect techniques, many of

which are similar to those used to characterize droplet flocculation, including microscopic studies (e.g. optical microscope, electron microscope, and confocal laser scanning microscope) and changes in particle size during storage using light scattering technique (e.g. particle size analyzer).

#### **(iv) Ostwald ripening**

Ostwald ripening is the process that large droplets grow at the expense of smaller ones (Figure 2.20) because of mass transport of dispersed phase from one droplet to another through the intervening continuous phase or because of the difference in chemical potential of the material within the droplets (Taylor, 1995). The driving force for this process is the fact that the solubility of a substance within a droplet in the continuous phase surrounding it increases with decreasing droplet radius. This process does not require the droplets to be close. Ostwald ripening plays an important role in o/w emulsions which contain water-soluble lipids (e.g. flavor oil) or when the aqueous phase contains alcohol (e.g. cream liquors). There are several strategies which can retard this instability by ensuring that: (i) droplet size distribution is small, and that the droplets are quite big, (ii) dispersed phase used has a low solubility in continuous phase (McClement, 1994; Weiss, & McClements, 2000), (iii) emulsifier used is highly effective at reducing interfacial tension, (iv) the thickness of interfacial membrane is increased (McClements, 2005).

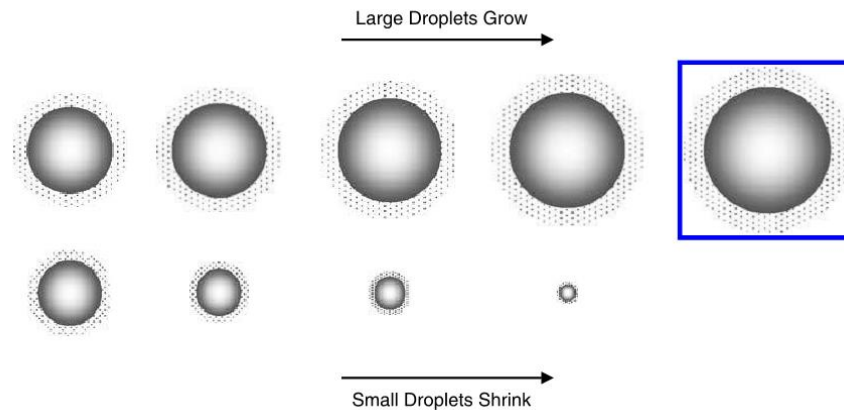


**Figure 2.20** Ostwald ripening involves the growth of large droplets at the expense of smaller ones due to diffusion of dispersed phase through the continuous phase (McClements, 2005).

Experimental characterization of Ostwald ripening is the technique that measures the changes in droplet size distribution with time. If the droplets are large enough, the optical microscopy can be used, otherwise, instrumental particle sizing techniques can be applied. However, it is difficult to distinguish between coalescence and Ostwald ripening because of increasing in particle size occurred in these two stabilities. It should be examined the factors that influence the growth rate of oil droplets as well (Kabalnov & Shchukin, 1992; McClements, 2005).

#### (v) Phase inversion

Phase inversion is the process which an o/w emulsion is converted into a w/o emulsion or vice versa. After phase inversion take place, the system may be kinetic stable or unstable. This mechanism is an essential step in butter and margarine production with desirable product characteristics, including appearance, texture, stability, and taste. Phase inversion is usually triggered by several alterations in the composition and environmental condition of an emulsion, including dispersed phase volume fraction, emulsifier type and concentration, temperature, solvent condition, and mechanical agitation. At the point where phase inversion occurs, which is called the “balance point”, the emulsion system is believed to be extremely complex, involving o/w emulsion, w/o emulsion, multiple emulsion, and bicontinuous phases (McClement, 2005).

Phase inversion process can be monitored by measuring; (i) the changes in emulsion viscosity because the viscosity of an emulsion is mainly affected by the viscosity of the continuous phase, (ii) the changes in electrical conductivity (i.e. there is a reduction in the electrical conductivity of an o/w emulsion when phase inversion occurs), (iii) the changes in droplet size using a particle sizing technique and microscope, and (iv) the changes in interfacial tension between oil and water phases as a function of temperature (Lehnert, Tarabishi, Leuenberger, 1994; Pacek, Moore, Nienow, & Calabrese, 1994; McClements, 2005).

### **2.2.3 Emulsion stabilized by cellulose materials**

It has long been known that effective stabilization against coalescence of emulsion droplets can be obtained by using a certain finely divided cellulose materials as emulsifying agents. As mention above, o/w and w/o emulsions can be formed depending on the nature of cellulose surfaces (hydrophilic or hydrophobic). The examples of emulsion stabilized by cellulose micro/nanomaterial are shown as follows.

In 1986, Oza and Frank demonstrated the ability of microcrystalline cellulose (MCC) to form and stabilize o/w emulsions. This study indicated that the MCC forms a network around emulsified oil droplets. This structure provides a mechanical barrier (steric barrier) which stabilizes emulsion without the necessary for decreasing interfacial tension, as in conventional surfactant stabilized emulsion (e.g. proteins and small molecules surfactants). Rheological properties of prepared emulsions containing MCC had a considerable degree of thixotropy which contributed to their stability and also exhibited shear-thinning behavior.

Almost ten years later, Ougiya, Watanabe, Morinaga, and Yoshinaga (1997) compared the ability of bacterial cellulose (BC), MFC, and MCC to stabilize o/w emulsions. They suggested that the BC produced in an agitated culture showed the highest emulsion-stabilizing activity among all cellulose materials. They also concluded that a mechanical barrier and a scaffolding structure composed of fine fibrils of BC interrupted the coalescence of oil droplets. Moreover, the BC-stabilized emulsions was stable against the environmental stresses, including pH, ionic strength, and temperature.

In 2011, Kalashnikova et al. studied o/w emulsions stabilized by bacterial cellulose nanocrystals (BCN) obtained by hydrochloric acid hydrolysis of BC. The BCNs have an elongated shape, low surface charge density, and forming a colloidal suspension in water. The BCNs can stabilize hexadecane/water interface with monodispersed distribution of oil droplets around 4  $\mu\text{m}$  in diameter. The researchers also suggested that the high stability of prepared emulsion was attributed to the irreversible adsorption of the BCNs associated with the formation of network.

Most of the studies carried out on the stabilization of emulsions by microcrystalline cellulose (MCC) (Oza & Frank, 1986; Kalashnikova et al., 2012), and bacterial cellulose (BC) (Ougiya et al., 1997; Kalashnikova et al., 2011) described o/w emulsions, due to the highly hydrophilic nature of cellulose. However, there are no reports on the effect of preparation conditions and concentration of MFC on the physical and rheological properties and stability of emulsion.

## **2.3 $\beta$ -lactoglobulin coated gold nanoparticles**

### **2.3.1 $\beta$ -lactoglobulin ( $\beta\text{Lg}$ )**

In our study, we also used another biopolymer, which is  $\beta$ -lactoglobulin ( $\beta\text{Lg}$ ) to stabilize another colloidal system, which is gold colloidal nanoparticle (GNPs). This system is called  $\beta\text{Lg}$ -coated GNPs. We also take an advantage of this system as a model of  $\beta\text{Lg}$ -adsorbed onto oil-water interface to explain the changes in conformation of  $\beta\text{Lg}$  after adsorption.  $\beta\text{Lg}$  is the globular protein in bovine milk and its structure, properties, and biological role are well established.  $\beta\text{Lg}$  is a small protein which usually exists as a dimer at neutral pH, but dissociates into monomers below pH 3, between pH 3 and 5.2 the dimer tetramerizes to give an octamer, and above pH 7 the dimer associates with a concomitant conformational change to give an expanded monomer. It can be stated that the interactions of  $\beta\text{Lg}$  are dependent on pH. Each monomer comprises 162 amino acid residues, with one free cysteine and two disulfide bridges. Each  $\beta\text{Lg}$  molecule consists of an 8-stranded, antiparallel  $\beta$ -barrel with a 3-turn  $\alpha$ -helix on the outer surface and a ninth  $\beta$ -strand flanking the first strand (Figure 2.21). The molecular weight is 18,350 Da. The secondary structure of native  $\beta\text{Lg}$  is

mainly composed of  $\beta$ -sheet (54%) and  $\alpha$ -helices (17%) (Link, Mohamed, & El-Sayed, 1999; Van Der Zande, Böehmer, Fokkink, & Schöenenberger, 2000; El-Sayed, 2001). This protein folds intramolecular, thereby burying most of their hydrophobic residues so that extensive self-association or interaction with other protein does not occur.

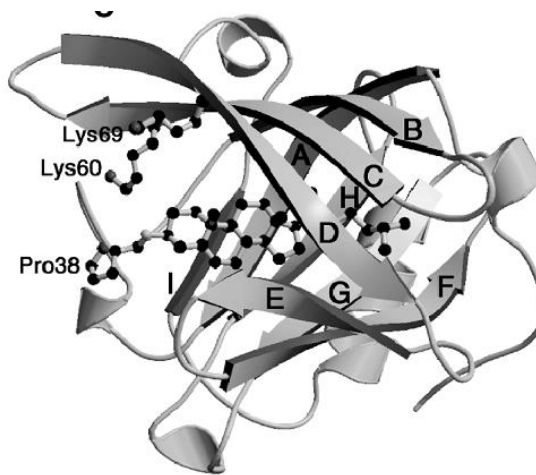


**Figure 2.21** An illustration showing  $\beta$ -lactoglobulin structure (Kontopidis, Holt, & Sawyer, 2003).

$\beta$ Lg is one of two components of whey protein (i.e. compose of  $\beta$ Lg and  $\alpha$ -lactalbumin) obtained from cheese-making industry. In the past, whey was often discarded, however, it is now economically feasible to concentrate and extract the components that exhibit excellent functionality (e.g. emulsifying activity) and nutritional properties.  $\beta$ Lg-stabilized o/w emulsions have been studied by a number of researchers (McClements, 2005). The mechanism of  $\beta$ Lg to form an emulsion is adsorbing at o/w interface and lowering the interfacial tension. Thus, it is important to know the structural conformation of  $\beta$ Lg at the interface to be better understanding the role of formation and stability of the produced emulsion.

### 2.3.2 Protein adsorption onto particle surfaces

The adsorption of globular proteins to the surfaces of particles is important in a number of physicochemical and biological phenomena relevant to the development of high quality, safe, and healthy foods. Proteins undergo structural

changes after adsorption onto the interfaces depending on its concentration, adsorption rate, pH, ionic strength, and temperature, etc. Proteins can be adsorbed to the surface of many kinds of materials. Proteins adsorb to the surfaces of fat droplets and gas bubbles during the production of emulsions and foams, which plays an important role in their stability to particle growth and aggregation (Dickinson, 2003; McClements, 2005). Proteins adsorb to the surfaces of ice crystals during their formation and subsequent growth, which is important in the development of anti-freeze systems (Venketesh & Dayananda, 2008). Lipases are a group of digestive enzymes that adsorb to the surfaces of fat droplets within the gastrointestinal tract and promote lipid digestion (Wilde & Chu, 2011). Other enzymes may be immobilized on the surfaces of solid particles to improve their utilization or activity (Talbert & Goddard, 2012). Proteins may adsorb onto the surfaces of ingested metallic nanoparticles (such as gold or silver) in foods, thereby altering the biological fate of both the proteins and nanoparticles. It is therefore important to understand the influence of protein adsorption onto particle surfaces on both protein and particle properties.

### **2.3.3 Gold colloidal nanoparticles**

In this study, we designed to use gold nanoparticles (GNPs) in solution or gold colloid as a model of oil droplets in protein stabilized o/w emulsions because we need to perform the experiment using a novel instrument called “surface-enhanced Raman scattering (SERS)” and it is necessary to mimic the interference of oil peaks from the spectra, resulting in the protein peaks are then enhanced. Therefore, the protein conformational changes induced by adsorption process and bile salts can be obtained.

Various nanometer-sized gold particles of uniform shape and size are invaluable tools in nanotechnology (assembled arrays), light scattering (elastic - plasmon resonance; inelastic - Raman effect) and for single molecule detection. Gold nanoparticles can be attached to proteins, alkanethiols and DNA by various methods.

#### **2.3.3.1 Gold nanoparticle formation and properties**

Since Faraday’s pioneering work (1857), several procedures have been developed to synthesize colloidal nanostructures. A number of research

articles show that the most popular method to prepare nanospheres of gold, for their use as SERS enhancer, are the reduction of the metal cations from their salts (Aroca, Alvarez-Puebla, Pieczonka, Sanchez-Cortez, & Garcia-Ramos, 2005), which is called wet chemistry that yield metal nanoparticle colloids. For GNPs, it is the reaction between  $\text{HAuCl}_4$  or  $\text{KAuCl}_4$  with sodium citrate or sodium borohydride. GNPs can be prepared as follows: 0.1 ml of  $\text{HAuCl}_4$  solution (4% w/v) is added to 40 ml of triply distilled water, then 1 ml of trisodium citrate solution (1%, w/v) is added dropwise with stirring. The mixture is boiled for 5 min. The formation of GNPs is revealed by a deep wine red color observed after 10 min, with a surface plasmon absorption maximum at about 520 nm and a homogeneous particle distribution (Camafeita, Sanchez-Cortes, & Garcia-Ramos, 1995). The diameter of prepared GNPs depends on the method of production, reducing agent, temperature, metal ion concentration, and duration used during production. Normally, the size regime relevant to SERS experiments is between 10 and 80 nm (Aroca et al., 2005), but in our study, we used 200 nm GNPs due to the reason that in most real food systems, the diameter of the oil droplets or other solid particles are usually larger than 100 nm (McClements, 2005). The GNPs will thus exhibit different localized surface plasmon resonance depending on the size, shape, and the dielectric constant of the metal.

The plasmon absorption and the optical image of a GNPs colloid dried in air are shown in Figure 2.22. The GNPs on glass and quartz form fractal-like structure and strong SERS signals are normally obtained in the branches of these structures (Aroca, 2006).

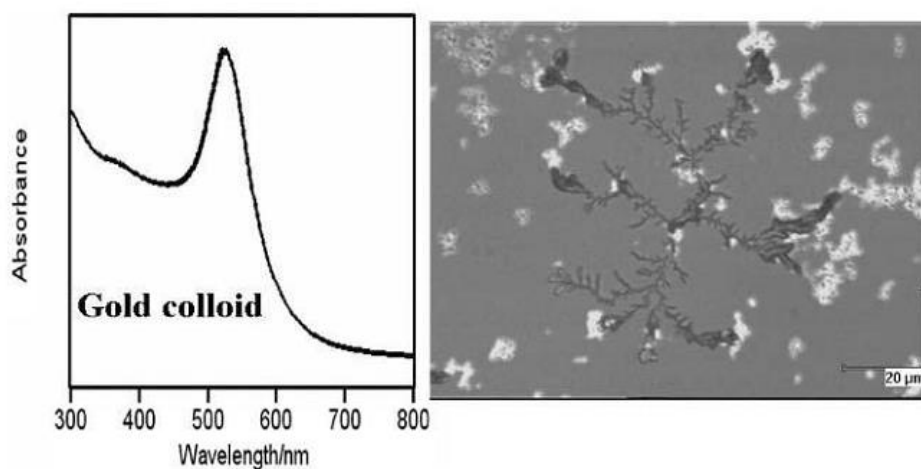


**Figure 2.22** Plasmon absorption spectrum of GNPs and the optical image of cast GNPs on glass and dried in air (Aroca, 2006).

Figure 2.23 shows the effect of particle diameter of GNPs on the color of solutions. The 2 nm GNPs is too small to scatter light and the solution is clear. The remaining sizes scatter light to different degrees and the solution color changes with increasing particle size.



**Figure 2.23** Solutions containing GNPs with various particle sizes (Ted Pella, Inc.)

GNP colloids prepared by the conventional chemical reduction method described above are highly stable for months or even years because the counter ions existing on the GNP surface coming from the ionic species added to the mixture during the preparation plays an important role to stabilize GNPs. These ions are normally adsorbed on the GNP surface, resulting in enough surface charge on GNP surface to maintain them suspended in the dispersion medium (refers to inter-particle

repulsion forces) (Aroca et al., 2005). Brewer, Glomm, Johnson, Knag, and Franzen (2005) suggested that citrate is a common electrostatic stabilizing agent for GNPs because the particles are synthesized through a citric acid reduction reaction. Electrostatic stabilization arises from a charged repulsion between neighboring GNPs that occurs as a result of the negative surface charge of the citrate layer. The stability of GNPs stabilized by citrate have been studied by Alvarez-Puebla, Arceo, Goulet, Garrido, and Aroca, (2005) using a photon correlation spectroscopy as a function of pH. The  $\zeta$ -potential of GNPs varies from -44 mV at pH 2 to -61 mV at pH 11. In addition, this electrostatic barrier also helps the chemisorption of analytes, such as protein and DNA.

### **2.3.3.2 Formation of conjugated gold-protein**

Two possible mechanisms of globular protein (e.g. bovine serum albumin, BSA and  $\beta$ -lactoglobulin,  $\beta$ lg) have been suggested which is either “end-on” or “side-on” binding. Depending on the protein concentration, the end-on binding results in a higher surface coverage of protein molecules on the surface (Brewer et al, 2005). Figure 2.24 represents the possible ways (side-on or end-on) of globular protein molecules attached onto the surface. During the formation of an adsorbed layer on the surface, each protein molecule normally passes through three following steps; (i) transport toward the surface, (ii) attachment to the surface, and (iii) spreading on the surface (Malmsten, 2003). These three steps are related with the two possible hypotheses for the interaction between nanoparticles and protein molecules, including an electrostatic binding hypothesis and a displacement hypothesis.

#### **(i) Electrostatic binding hypothesis**

One of the most important factors affecting the interaction of proteins with GNPs is pH, since this will influence the electrical characteristics of both the proteins and GNPs. The net charge on protein molecules goes from positive to negative as the pH is increased from below to above the proteins isoelectric point ( $pI$ ). Electrostatic attraction plays an important role in promoting adsorption of protein molecules to GNP surfaces, since the protein is cationic and the citrate-GNPs are anionic at  $pH < pI$  (Winuprasith, Suphantharika, McClements, & He,

2014). In this hypothesis, the protein attaches itself to the passivation layer on the gold surface, with little direct interaction between protein molecule and gold surface.

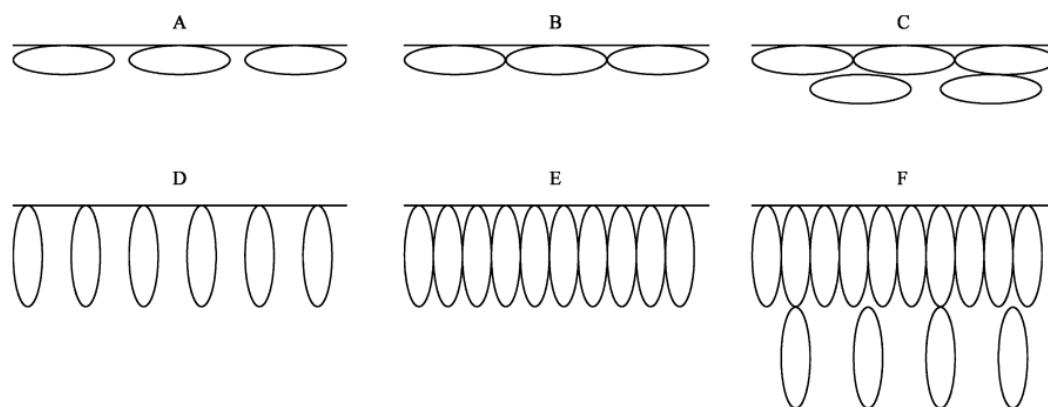


**Figure 2.24** Schematic representations of several likely arrangements of bovine serum albumin (BSA) at the interface; (A) monolayer, side-on (axis parallel to the surface), not close-packed; (B) monolayer, side-on, close-packed; (C) bilayer, side-on, second layer less concentrated than A; D, E, and F are the same as A, B, and C, but for end-on (axis perpendicular to the surface) orientations. Other possibilities include arrangements similar to C and F, but with first layer not close-packed, and other orientations with the axis neither parallel nor perpendicular (McClellan & Franses, 2003).

### (ii) Displacement hypothesis

The displacement mechanism requires citrate to be displaced by protein during adsorption, with amino acids functional groups, such as lysine (amine), histidine (imidazole), and cysteine (thiol) among others that interact directly with the gold surface. Spreading or structural changes in the adsorbing protein on the surface can lower the free energy of the system. Changes in protein conformation are most often the result of denaturation that occurs during the displacement of the citrate stabilizer. For the protein denaturation, the protein molecules unfold near the surface and expose their hydrophobic residues and present specific functional groups that interact with gold surface (Brewer et al., 2005).

The interaction of the protein molecules with a GNP surface can involve these two possibilities. Interestingly, the steric interactions of a protein

with a surface layer (e.g. citrate) provide greater colloidal stability to a colloidal suspension than pure electrostatic interaction, for example, electrostatic interaction alone will fail to stabilize the colloid at the  $pI$  of the protein. However, protein-coated GNPs can be stabilized by the interaction of protein side chain or domains, resulting in a reduction in entropy and a loss of solvation enthalpy. Both of these result exhibits an intercolloid repulsion (Brewer et al, 2005). The fact is that the protein molecules can be bound to GNPs even at the  $pI$  of protein. Brewer et al, 2005 reported that at pH 4.6, BSA contains the large number of protonated surface lysines, which act as a polycation. These lysine groups can, therefore, interact with citrate by salt-bridge interaction.

## **2.4 Raman spectroscopy**

Raman spectroscopy has been used as analytical tool for many decades in cosmetic, pharmaceutical, and food industry because this technique can obtain board chemical profiles of the reaction, biotransformation, or impurities in real time, ultimately on-line. The interaction of electromagnetic radiation with electron and molecule nuclei gives rise to a host of spectroscopic techniques that are based on absorption, emission, and scattering processes (Li-chan, 1996).

Raman spectroscopy is a novel and promising technique to observe the conformation of biomolecules, since it is non-destructive and rapid method. The detection limit of parts per billion (ppb) have been achieved, even a single molecule can be detected (Aroca et al., 2005). SERS also provides the fingerprint of the molecules and the capability to analyze compounds in aqueous solution with minimal interference from water adsorption, which is a critical factor when considering biological application (Brewster, 2009).

### **2.4.1 Basic principles**

Raman spectroscopy is a branch of vibrational spectroscopy, which involves measuring lights that is inelastically scattered from an analyte upon illumination with an intense monochromatic source. The analyte is normally exposed

and illuminated with a laser (in the UV, visible or IR regions of the electromagnetic spectrum). As a consequence, the interaction of photons from the light source with molecules in the sample induces a series of molecular vibrations.

Figure 2.25 shows several scenarios of light scattering processes which photon will be either Rayleigh (elastically) scattered or Raman (inelastically) scattered. The resultant Raman spectrum is a measure of how much energy that photon has gained (anti-Stokes Raman scattering) or lost (Stokes Raman scattering). This value is expressed as the difference in energy between the incident and scattered light in units of the reciprocal wavelength or  $\text{cm}^{-1}$  (Figure 2.26). Brewster et al. (2009) stated that Stokes Raman scattering is most often recorded because a majority of molecules have an energy in the lowest vibrational level of the molecular ground state (about 90%), resulting in the probability of a Stokes event is much greater than anti-Stokes Raman scattering. The discrete vibrational transitions occur in the ground state of molecules, corresponding to various stretching and bending deformation modes of individual chemical bonds. Li-chan (1996) suggested that Raman scattering depends on changes in the polarizability of functional groups as the atoms vibrate. Hence, polar group (e.g. C=O, N-H, and O-H) have strong IR stretching vibrations, while nonpolar groups (e.g. C=C, C-C, and S-S) have intense Raman bands. Water is a polar molecule that possesses strong IR absorption whereas water has weak Raman scattering properties and produces less interference in Raman spectroscopy. As a consequence, Raman technique is usually more suitable for the biological systems, for example, food systems, which are primarily aqueous in nature. Figure 2.27 illustrates DXR Raman spectroscopy and a gold multi-spot microscope slide.

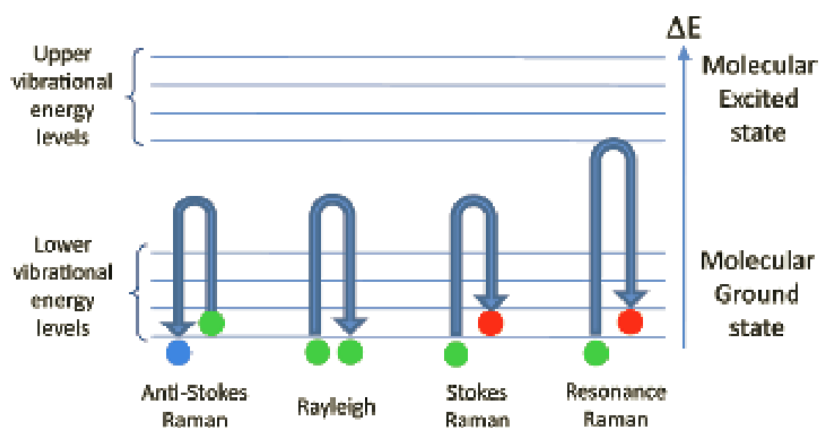


**Figure 2.25** Energy level diagram depicting light scattering processes (Brewster, Jarvis, & Goodacre, 2009)

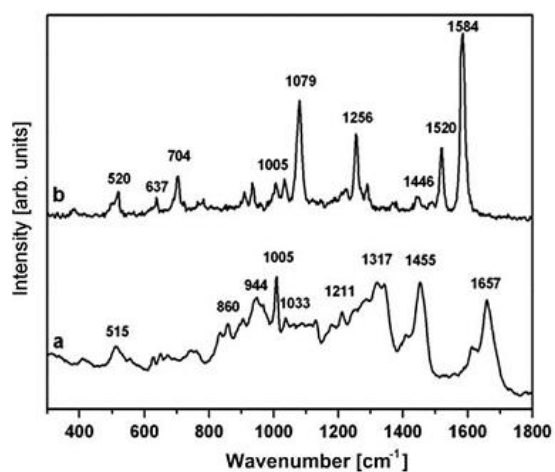


**Figure 2.26** Raman spectrum of solid BSA (a) and SERS spectrum of bioconjugates gold nanospheres-BSA (b) (Iosin, Toderas, Baldeck, & Astilean, 2009).



**Figure 2.27** DXR Raman spectroscopy (left), and a gold multi-spot microscope slide (right).

### 2.4.2 Surface-enhanced Raman scattering (SERS)

Raman scattering intensities are typically weak, with approximately only 1 in every  $10^6 - 10^8$  photon being inelastically scattered. Fortunately, there are a number of ways to enhance the Raman signal. Here, we are focusing in a surface-enhanced Raman scattering (SERS) technique, which has an ability to increase the Raman signal of an analyte (up to 15 orders of magnitude in comparison to the normal Raman scattering). SERS involves in the analyte being in close proximity to, or adsorbed onto, a roughened metal surface or a colloidal solution (e.g. Ag, Au, and Cu). Increase in Raman intensity due to the SERS effect is occurred because the interaction of the electric field of the incident light with the metal gives rise to the surface plasmon, which is believed to enable an electromagnetic enhancement effect via surface-plasmon polariton (SPP) resonances. In addition, a part of the SERS enhancement is due to the so-called charge transfer enhancement effect that resembles the ordinary resonance Raman process occurring in metal-ligand complexes (Aroca, 2006). Metal substrates for SERS measurement must be nanostructured. In the last decade, in order to improve stability and reproducibility of SERS substrates and to increase the achievable SERS enhancement factors, more shape-controlled and shape reproducible metallic nanoparticles have been concerned.

#### 2.4.2.1 SERS substrate preparation

To enhance the Raman intensity of the sample molecules, there are two common sample preparation techniques for SERS measurement using

nanoparticle (e.g. Ag dendrites or citrate-gold nanoparticles), namely substrate method and solution method. These two methods are very useful in different applications (He, Haynes, Diez-Gonzalez, & Labuza, 2010).

(i) Substrate method Nanoparticles (NPs), such as gold or silver, are deposited onto a glass slide first and air-dried, then the sample solution is deposited on the dried NPs. The substrate method is simpler and faster to collect the SERS ‘fingerprint’ spectra of the sample and very useful when there is only trace amount of sample.

(ii) Solution method Nanoparticle colloids and sample solution are mixed under rotation for a certain period of time, then the NPs are collected by natural precipitation or slowly spinning down. The solution method is based on the interaction of the sample molecules and NPs. If the sample molecule is able to be bound onto the NPs, then the signal of sample molecule can be enhanced through chemical enhancement (Haynes, McFarland, & Van Duyne, 2005). If the sample molecules cannot be bound onto the NPs, after washing, there is little/no signal measured from the sample molecule.

In this study, we took an advantages of solution method and we also measured the GNPs dispersed in solution because the presence of a solution tend to minimize the burning of the sample allowing the use of higher laser powers, and the use of more energetic laser lines. In addition, the use of solution permits the acquisition of an average spectrum due to the Brownian movement that governs the colloidal dispersions. This averaging of signal can be further improved upon by the use of systems that force the recirculation of the sample (Kim, Lee, & Kim, 2004).

#### **2.4.2.2 Critical factors of SERS experiment**

##### **(i) Shape, size, aggregates of metal colloids**

In order to increase the electromagnetic field enhancement, some non-spherical geometry has been created and tested, such as triangles, ellipsoids, cylinders, etc. The morphology of the prepared colloids can be affected by the experimental condition used during the metal production. In particular, the temperature, reactant concentrations, counter ions and the total volume play an important role for controlling the size, shape, and stability of the systems. For

example, Jana, Gearheart, and Murphy (2001) prepared gold nanorods and this shape of nanoparticles had been used for SERS by Nikoobakht and El-Sayed (2003) with optimum results. This gold nanorods show the surface plasmon bands at 525 and 885 nm due to the excitation of the transversal and longitudinal plasmons, respectively.

Although spherical and spheroidal particles exhibit an excellent model system and exact solutions are available for their interactions with electromagnetic radiation (Aroca, 2006), the most important factor for SERS enhancement is aggregation of nanoparticles or fractal structures. The localized resonances in fractal carry large quality factors and seem to increase in number of processing from the visible to the near-infrared region. These elusive localized spot of small dimensions, which are smaller than the wavelength of the incident radiation, are the source of extremely highly enhanced local fields, resulting in SERS enhancement factors of  $10^{12}$  or higher. These are so-called “hot-spot” detected in SERS experiments (Sanchez-Cortes, Garcia-Ramos, & Morcillo, 1994; Sanchez-Cortes, Garcia-Ramos, Morcillo, & Tinti, 1995).

#### **(ii) Distance dependence**

SERS distance dependence is critical both mechanistically and practically. SERS does not require the molecule to be in direct contact with the surface but within a certain sensing volume. Aroca (2006) suggested that the local field enhancement is maximum for a molecule attached to the surface (first-layer effect) and it also has a long-range component that extends its effect up to about 10 nm away from the interface. If the molecules form isolated thick clumps rather than a smooth surface coverage, the electromagnetic enhancement and chemical charge transfer mechanism are reduced which reduce the SERS intensity from a molecules.

### **2.4.3 Applications of Raman spectroscopy in Foods**

The examples have been chosen to illustrate areas of application that highlight unique advantages of Raman spectroscopy to study various components in food systems (Table 2.3).

In this decade, there are many publications related to attempts to take an advantage of Raman spectroscopy in food applications. However, Li-Chan (1996) suggested that before choosing this technique for a particular analysis, one must consider its relative strengths in comparison with other analytical methods, and also the limitations, imposed by the target concentration, as well as complexity, optical properties, and nature of surrounding matrix. In our experiments, we are interested in protein conformation, so the next topic is then focusing on the interpretation of Raman spectra related to protein conformation.

**Table 2.3** Examples of Raman spectroscopy applications in food systems.

Analyte	Application	References
Protein	Infrared and Raman spectroscopic study of casein in cheese: Effect of freezing and frozen storage	Fontecha, Bellanato, & Juarez (1993)
Protein	Study of BSA–gold nanoparticle conjugates by fuorescence and surface-enhanced Raman scattering	Iosin et al. (2009)
Lipid	The Polymorphism of diglycerides	Shannon, Fenerty, Hamilton, & Padley (1992)
Lipid	Fast determination of milk fat content using Raman spectroscopy	El-Abassy, Eravuchira, Donfack, von der Kammer, & Materny (2011)
Lipid	Composition of bovine milk fat globules by confocal Raman microscopy	Gallier, Gordon, Jiménez-Flores, & Everett (2011)

**Table 2.3** (Continued) Examples of Raman spectroscopy applications in food systems.

Analyte	Application	References
Protein/lipid	Study of protein–lipid interactions at the bovine serum albumin/oil interface by Raman microspectroscopy	Meng, Chan, Rousseau, & Li-Chan (2005)
Carbohydrate	Structure of $\alpha$ - and $\beta$ -anomers of glucose	Corbett, Zichy, Góral, & Passingham (1991)
Protein/ Carbohydrate	Raman spectroscopic characterization of structural changes in heated whey protein isolate upon soluble complex formation with pectin at near neutral pH	Zhang, Zhang, Lin, & Vardhanabhuti (2012)
Pigment	Resonance Raman spectroscopic studies of anthocyanins and anthocyanidins in aqueous solutions	Merlin, Statoua, Cornard, Saidi-Idrissi, & Brouillard (1994)
Protein/ pigment	A surface enhanced Raman spectroscopic study of interactions between casein and polymethoxyflavones	He, Zheng, Labuzab, & Xiao (2012)

#### **2.4.4 Interpretation of Raman spectra related to protein conformation**

Proteins and their components are widely used as a classical example of applying Raman spectroscopy to the analysis of biomolecules. The obtained information can be related to the microenvironment and chemistry of the side chains as well as on the conformation of the polypeptide backbone. Some of importance Raman modes that are very useful in the interpretation of the protein structure are listed in Table 2.4. The lists include vibrational transitions assigned to several amino acid side chain (i.e. the S–S, and S–H groups of cysteine and cysteine, the aromatic rings of tryptophan, tyrosine, and phenylalanine, the C–H groups of aliphatic amino acids, the COO<sup>-</sup> and COOH groups of aspartic and glutamic acids, and the amidazole ring of histidine). Band of amide I, amide III, and skeletal stretching modes can be used to characterize backbone conformation, corresponding to the relative proportions of different types of secondary structure in proteins as well as protein denaturation (Li-Chan, 1996).

##### **2.4.4.1 Aromatic amino acid side chains**

Aromatic amino acid side chains are useful to monitor the polarity of the microenvironment, or involvement in hydrogen bonding. For example, if tryptophan residues from a buried, hydrophobic microenvironment become exposed to the polar aqueous phase solvent, resulting in a decrease in the intensity of a band near 760 cm<sup>-1</sup>. In case of tyrosine residues, the intensity ratio of a doublet near 850 cm<sup>-1</sup> and 830 cm<sup>-1</sup> is also a good indicator of the environment as well as the hydrogen bonding of the phenolic hydroxyl groups. For example, the involvement of tyrosine residues in the gelation of  $\alpha$ -lactalbumin was indicated by a decrease in the intensity ratio of  $I_{850}/I_{830}$ , corresponding to an increase in how well buried the tyrosine residues are within the gel network (Nonaka, Li-Chan, & Nakai, 1993). On the other hand, the phenylalanine band is reported to be insensitive to conformation and microenvironment. Thus, the sharp band of phenylalanine at 1006 cm<sup>-1</sup> is often used as a reference of the protein Raman spectra (Li-Chan, 1996).

**Table 2.4** Raman bands useful in the interpretation of protein structure (adapted from Li-Chan, 1996).

Origin	Wavenumber ( $\Delta \text{ cm}^{-1}$ )	Assignment	Structural information obtained
Cystine, cysteine, methionine	510	S–S stretch	Presence of <i>gauche-gauche-gauche</i> conformation; band broadening and/or shifts may indicate conformational heterogeneity of cystine residues
	525	S–S stretch	<i>Gauche-gauche-trans</i> conformation
	545	S–S stretch	<i>Trans-gauche-trans</i> conformation
	630-670	C–S stretch	Gauche conformation
	700-745	C–S stretch	Trans conformation
	2550-2580	S–H stretch	Presence of thiol of cysteine residues
Tyrosine	850/830	Fermi resonance between ring fundamental and overtone	State of phenolic OH group (exposed or buried, hydrogen-bond donor or acceptor)
Tryptophan	760, 880, 1360	Indole ring	Sharp intense band indicates buried residues; sensitive to environment polarity
Phenylal- anine	1006	Ring breathe	Conformation insensitive; useful as an internal intensity standard
Histidine	1409	<i>N</i> -deuteroimidazole	Probe of ionization state, metalloprotein structure, proton transfer in deuterated solution
Aspartic and glutamic acids	1400-1430	C=O stretch of $\text{COO}^-$	Ionized carboxyl groups
	1700-1750	C=O stretch of COOH or COOR	Undissociated carboxyl, ester or metal complexation
Aliphatic residues	1450-1465	C–H bending	Microenvironment, polarity
	2800-3000	C–H stretching	Microenvironment, polarity

**Table 2.4** (continued) Raman bands useful in the interpretation of protein structure (adapted from Li-Chan, 1996).

Origin	Wavenumber ( $\Delta \text{ cm}^{-1}$ )	Assignment	Structural information obtained
Amide I	1655 $\pm$ 5	Amide C=O stretch, N-H wag	$\alpha$ -helix
	1670 $\pm$ 3	Amide C=O stretch, N-H wag	Anti-parallel $\beta$ -sheet
	1665 $\pm$ 3	Amide C=O stretch, N-H wag	Disordered structure (solvated)
	1685	Amide C=O stretch, N-H wag	Disordered structure (non-hydrogen bonded)
	>1275	N-H in plane bend, C-H stretch	$\alpha$ -helix
Amide III	1235 $\pm$ 5 (sharp)	N-H in plane bend, C-H stretch	Anti-parallel $\beta$ -sheet
	1245 $\pm$ 4 (board)	N-H in plane bend, C-H stretch	Disordered structure (solvated)
	1235	N-H in plane bend, C-H stretch	Disordered structure (non-hydrogen bonded)

#### **2.4.4.2 Aliphatic amino acid residues**

Aliphatic amino acid residues exhibit C–H stretching and bending mode at 2800-3000 and 1440-1465  $\text{cm}^{-1}$ , respectively. The latter methylene deformation bend have reported on the changes in band intensity as a function of polarity of the solvent or microenvironment. This band can be used to monitor hydrophobic interactions between aliphatic residues. In the same way, shifts of the C–H stretching band near 2940  $\text{cm}^{-1}$  to higher wavelength indicate the sensitivity of this band to the polarity of the microenvironment and to protein denaturation (Li-Chan, 1996).

#### **2.4.4.3 Charged amino acid residues**

The presence of the bands at 1700-1750 and 1400-1430  $\text{cm}^{-1}$  provide valuable information on the state of ionization, corresponding to undissociated carboxyl, ester or metal complexation, and ionized carboxyl groups, respectively. In addition, imidazole rings of histidine residues are generally weak in the spectra of globular protein, but when observed they give a good indication of the ionization state (Li-Chan, 1996).

#### **2.4.4.4 Amide (peptide) bond**

The amide bond of the proteins has several vibrational modes. Amide I and amide III bands are normally used for the investigation of secondary structure of the proteins (e.g.  $\alpha$ -helix,  $\beta$ -sheet, disordered structure, etc.) as a function of heat-induced gelation, frozen stage, interaction with surfaces, or salt/pH-induced conformation changes. For example, the shift of the amide I band, which is characteristic corresponded to the  $\alpha$ -helix content in albumin, from 1657 to 1649  $\text{cm}^{-1}$  refers to some of the  $\alpha$ -helix structure of BSA may become modified to a  $\beta$ -sheet or random coil conformation due to the interaction with GNP surface (Iosin, Canpean, & Astilean, 2011).

In addition to its use in the analysis of the food constituents described above, Raman spectroscopy could potentially be applied to many other areas of food science (e.g. trace components, nucleic acids, whole cells, tissues, and

microorganisms) and others, such as medical and pharmaceutical application (e.g. cancer cells). However, the practical and instrumental limitations of the various forms of Raman spectroscopy need to be understood to obtain the desired information. Furthermore, the unique advantages of Raman spectroscopy, in comparison with other analytical tools, should be carefully considered to justify it as the method of choice for particular applications.

## CHAPTER III

### EXPERIMENTAL METHODS

#### 3.1 Preparation of microfibrillated cellulose

Mangosteen (*Garcinia mangostana* L.) rind, a residue from mangosteen-canning factory, was supplied by a local manufacturer (Chanthaburi, Thailand). The obtained mangosteen rind was washed with distilled water for 3 times and cut into small pieces. Then, it was dried at 60 °C using hot-air oven overnight. After that the dried mangosteen rind was ground using a laboratory mill (Brabender<sup>®</sup> GmbH & Co. KG, Duisburg, Germany). Then, the ground mangosteen rind was sieved through a 100 mesh sieve using a vibratory sieve shaker (Endecotts Ltd, London, UK). The resulting mangosteen rind powder was extracted for cellulose using alkaline extraction according to the procedure described elsewhere (Prakongpan, Nitithamyong, & Luangpituksa, 2002). Briefly, the material (100 g) was dispersed in distilled water at a ratio of 1:25 (w/w) and adjusted to pH 12 using 25% NaOH. The slurry was stirred at room temperature (25 °C) overnight and heated to 90 °C for 2 h and 45 min in a water bath shaker (Memmert GmbH, Schwabach, Germany). After cooling to room temperature, the resulting slurry was filtered through a Whatman 541 filter paper (hardened, ashless cellulose with 22 µm pore size) then washed with distilled water. After that, the material was re-dispersed in distilled water at a ratio of 1:2.32 (w/w) and adjusted to pH 7 using 85% H<sub>3</sub>PO<sub>4</sub>. Bleaching treatment was performed by adding 30% H<sub>2</sub>O<sub>2</sub> into the suspension at a ratio of 0.0134:1 (w/w) of the total suspension. The mixture was heated at 90 °C for 3 h and filtered through a Whatman 541 filter paper. The yellow-brown, water swollen cellulose was obtained and stored wet in a refrigerator at 4 °C. The resulting purified cellulose was used for the preparation of microfibrillated cellulose (MFC) by re-dispersing in distilled water at a concentration of 1% w/w and then passing through a high pressure homogenizer (type Panda, Niro-Soavi S.p.A, Parma, Italy) at a pressure of 500 bar for 1, 5, and 20 passes at room

temperature. The MFC obtained by 1, 5, and 20 homogenization passes were denoted by 1P-MFC, 5P-MFC, and 20P-MFC, respectively whereas the purified cellulose before homogenization was denoted by 0P-MFC. All the homogenized materials (MFC) are yellow-brown gel-like aqueous matters, having an MFC concentration of 1% w/w and exhibiting neither flocculate nor sediment when diluted with water.

## 3.2 Characterization of microfibrillated cellulose

### 3.2.1 Chemical analysis

Total nitrogen, fat, carbohydrate, moisture, and ash contents of dried mangosteen rind and its purified cellulose were determined using AOAC Official Methods (AOAC, 2000). Cellulose content was also determined following the FCC assay method (FCC, 1981). All chemical analyses were performed in duplicate.

### 3.2.2 X-ray powder diffraction (XRD) analysis

Dried ground mangosteen rind, its purified cellulose, and microfibrillated cellulose (MFC) were characterized for crystalline structure with an X-ray diffractometer (model D8-Advance, Bruker AXS GmbH, Karlsruhe, Germany) using Cu-K $\alpha$  radiation (wavelength = 1.542 Å) in a powder measurement mode. Samples were scanned from 3 to 30° 2 theta in 0.05° step at 8 s per step. Samples were equilibrated at room temperature and 50% relative humidity (magnesium nitrate, Mg(NO<sub>3</sub>)<sub>2</sub> powder) for 3 days prior to analysis. The crystallinity index was measured by Segal's empirical method (Segal, Creely, Martin, & Conrad, 1959), with the following equation:

$$\text{Crystallinity index (\%)} = \frac{I_{200} - I_{am}}{I_{200}} \times 100 \quad (3.1)$$

where  $I_{200}$  is the intensity value for the crystalline cellulose ( $2\theta = 22.5^\circ$ ), while  $I_{am}$  is the intensity value for the amorphous cellulose ( $2\theta = 18^\circ$ ).

### 3.2.3 Determination of degree of polymerization

The MFC samples obtained with different number of homogenization passes were dissolved in 1 M  $C_2H_6CuN_2$ . The viscosimetric average degree of polymerization ( $DP$ ) of MFC samples was calculated from the intrinsic viscosities  $[\eta]$  of the corresponding solutions at 25 °C, using the following equation (Dinand *et al.*, 1999):

$$[\eta] = 0.891DP^{0.936} \quad (3.2)$$

## 3.3 Preparation of MFC-stabilized emulsions

MFC aqueous suspensions were prepared at appropriate concentrations by dilution of the stock 1% w/w MFC suspensions using distilled water. The MFC concentrations reported in this paper refer to the aqueous phase and not to the whole emulsion. MFC-stabilized oil-in-water (o/w) emulsions (500 g each) were prepared by blending an appropriate concentration of soybean oil and MFC aqueous suspensions together using a rotor-stator (model Ultra Turrax T18, IKA Works, Inc., Wilmington, NC, USA) at 11,000 rpm for 1 min and followed by 15,000 rpm for another 4 min at room temperature.  $NaN_3$  (0.01% w/w) was added to the emulsions as an antimicrobial agent. These coarse emulsions were then passed through a two-stage high-pressure homogenizer (type Panda, Niro-Soavi S.p.A, Parma, Italy) at pressures of 500/50 bar for the first/second stages homogenizing valves, respectively for 3 passes at room temperature. The samples were stored at room temperature for 24 h before being analyzed.

In this study, firstly, the effect of number of homogenization passes used in the MFC preparation on the properties of MFC itself as well as the properties and stability of MFC-stabilized o/w emulsions was studied (CHAPTER IV). Secondly, the effect of concentration of MFC obtained by an appropriated homogenization pass, which gave the highest emulsion stability, on the properties and stability of MFC-stabilized o/w emulsions was examined (CHAPTER V).

### 3.4 Characterization of MFC-stabilized emulsions

#### 3.4.1 Particle size determination

To avoid multiple scattering effects, the emulsion samples were diluted to a concentration of approximately 0.005% w/w using distilled water and stirred gently by a spatula until completely dispersed. Samples were analyzed by a laser diffraction particle size analyzer (Mastersizer 2000; Malvern Instruments Ltd., Worcestershire, UK). The sample solution was dispersed in distilled water at 1,200 rpm until an obscuration rate of 10 - 15% was obtained. Background and sample were measured for 10 s. Optical properties of the sample were defined as follows: refractive indices of oil and water were 1.46 and 1.33, respectively and absorption was assumed to be 0. Particle size distribution was measured based on light scattering theory. Particle size was reported as the surface-weighted mean particle diameter ( $d_{32}$ ) and the volume-weighted mean particle diameter ( $d_{43}$ ), defined by the following equation:

$$d_{32} = \frac{\sum n_i d_i^3}{\sum n_i d_i^2} \quad (3.3)$$

$$d_{43} = \frac{\sum n_i d_i^4}{\sum n_i d_i^3} \quad (3.4)$$

where  $n_i$  is the number of particles with diameter  $d_i$ . All measurements were performed in triplicate.

#### 3.4.2 Scanning electron microscopy

Scanning electron microscopy (SEM) was carried out to visualize microstructure of the MFC-stabilized emulsions. A drop of the emulsion samples was placed on a piece of glass cover slip and post fixed in 2% osmium tetroxide for 30 min. The samples were critical point dried through CO<sub>2</sub> in a critical point dryer (model CPD 020, Balzers, Bal-Tec GmbH, Germany). The dried samples were then affixed to aluminum stubs using carbon filled tape and the assemblies were coated with gold using an ion sputter instrument (model SCD 040, Balzers, Bal-Tec GmbH, Germany). An observation was recorded using a scanning electron microscope (model JSM-5410LV, JEOL, Tokyo, Japan).

### 3.4.3 Confocal laser scanning microscopy

Confocal laser scanning microscopy (CLSM) was performed in an attempt to localize the MFC particles in the emulsions. The freshly made MFC-stabilized o/w emulsion (5 mL) was mixed with an aliquot of 40  $\mu\text{L}$  of 0.01% w/v aqueous solution of Congo red dye resulting in a final concentration of 0.8 mg dye/mL solution. The mixture was thoroughly stirred for 5 min and incubated overnight in the dark at room temperature. Then, the stained sample was placed into a microscope slide. A cover slip was placed on top of the sample, ensuring that no air bubbles were trapped between the sample and the cover slip. Micrographs of the emulsion were acquired using a confocal laser scanning microscope (Fluoview FV1000, Olympus Corporation, Tokyo, Japan) operating in a fluorescence mode. A 60 $\times$  oil-immersion objective and additional zoom of 5 $\times$  was used to scan the images at approximately 20-30  $\mu\text{m}$  below the cover slip. Fluorescence from the sample was excited with 488-nm line of an Ar laser, and a 605-nm band-pass filter was used for emission. As the Congo red dye stained the MFC particles, regions rich in the MFC appeared as bright patches on the dark background of the micrographs.

### 3.4.4 Rheology measurements

Rheological properties of the freshly prepared MFC gels and MFC-stabilized o/w emulsions were measured at 25  $^{\circ}\text{C}$  using a controlled-strain rheometer (PhysicaMCR 301, Anton Paar GmbH, Graz, Austria) equipped with a cone and plate sensor (1 $^{\circ}$  cone angle, 50 mm diameter, and 0.05 mm gap) or a double gap cylinders sensor (the inner and outer cylinders had a diameter of 36.0 mm and 43.4 mm, respectively). For dynamic viscoelastic measurements, the linear viscoelastic range was determined with a strain sweep (0.01-100%) at a fixed frequency of 10 rad/s. After that, a dynamic frequency sweep was conducted by applying a constant strain of 0.5% which was within the linear region, over a frequency range between 0.1 and 100 rad/s. The dynamic mechanical spectra were obtained recording the storage modulus  $G'$ , and the loss modulus  $G''$  as a function of frequency.

For steady flow tests, the cone or the inner cylinder of the measuring sensor was programmed to linearly increase the shear rate from 0.1  $\text{s}^{-1}$  – 300  $\text{s}^{-1}$  in 3 min followed immediately by a reduction from 300  $\text{s}^{-1}$  to 0.1  $\text{s}^{-1}$  in the next 3 min. The

shear stress - shear rate data (flow curves) of the former are referred to as upward flow curves and the latter as downward flow curves. All the flow curves were analyzed using the Herschel-Bulkley model as following equation:

$$\sigma = \sigma_0 + K\dot{\gamma}^n \quad (3.5)$$

where,  $\sigma$  is the shear stress (Pa),  $\sigma_0$  is the yield stress (Pa),  $\dot{\gamma}$  is the shear rate ( $s^{-1}$ ),  $K$  is the consistency coefficient ( $Pa\ s^n$ ), and  $n$  is the flow behavior index (dimensionless). Apparent viscosity ( $\eta_a$ ) was calculated from the flow curve data using the equipment software and presented as a function of shear rate.

### 3.4.5 $\zeta$ -potential measurements

The  $\zeta$ -potential of MFC suspension and MFC-stabilized emulsion was measured using a particle electrophoresis instrument (Zetasizer Nano ZS, Malvern Instruments Ltd., Malvern, Worcestershire, UK). Immediately prior to measurements, the samples were diluted to a concentration of approximately 0.006% w/w using buffer solutions (pH 3 - 8) or NaCl solutions (0 - 250mM) to avoid multiple scattering effects. Optical properties of the sample were defined as follows: refractive indices of oil and water were 1.46 and 1.33, respectively and absorption was assumed to be 0. The  $\zeta$ -potential was reported as the average and standard deviation of measurements made on three freshly prepared samples, with three readings taken per sample.

### 3.4.6 Visual assessment of creaming

Creaming stability was determined to evaluate the relative stability of o/w emulsions. Immediately after preparation, the emulsions (15 g) were poured into 20-mm diameter and 70-mm height glass test tubes and were sealed with plastic caps to prevent evaporation. The sample tubes were kept at room temperature and the movement of any creaming boundary was tracked with time for 80 days. During storage, most of the emulsions tended to separate into a strongly turbid or cream layer at the top and a serum layer at the bottom. The total emulsion height ( $H_T$ ) and the serum layer height ( $H_S$ ) were measured. The extent of creaming was reported as creaming index ( $CI$ ), defined by the following equation:

$$CI = \frac{H_s}{H_T} \times 100 \quad (3.6)$$

### 3.4.7 Statistical analysis

All measurements were performed in triplicate for each sample with the exception of chemical analyses which were done in duplicate. Results are expressed as mean  $\pm$  standard deviations. A one-way analysis of variance (ANOVA) and Duncan's multiple range test were used to establish the significance of differences ( $p \leq 0.05$ ) among the mean values. The statistical analyses were performed using SPSS version 14.0 Windows program (SPSS Inc., Chicago, IL, USA).

## 3.5 Preparation of $\beta$ Lg-coated GNPs

A  $\beta$ -lactoglobulin ( $\beta$ Lg) solution was prepared at ambient temperature (22 °C) by dissolving powdered  $\beta$ Lg in 5 mM acetate buffer solution (pH 3) or 5 mM phosphate buffer (pH 7). The solutions of  $\beta$ Lg with concentrations of 0-6000  $\mu$ M were prepared. The  $\beta$ Lg solutions were stirred gently for 3 h to ensure complete protein dissolution. If required the pH of these solutions was readjusted to pH 3 or pH 7 using either 1 M HCl and/or 1 M NaOH.

The interaction of the globular proteins with the gold nanoparticles (GNPs) was studied by adding 20  $\mu$ L of  $\beta$ Lg solution into a 1.5 mL microcentrifuge tube. Then, 1000  $\mu$ L of GNP solution was added drop wise under vigorous mixing for 5 min. Thus, the original protein concentration was reduced by a factor of 20/1020, and the original GNP concentration was reduced by a factor of 1000/1020. The mixture was incubated overnight under consistent orbital rotation at ambient temperature (22 °C). The pH of mixture was kept constant at pH 3 or pH 7. After overnight incubation, the mixed  $\beta$ Lg-GNP suspensions were analyzed.

In this study, firstly, the effect of  $\beta$ Lg concentration on the surface coverage and aggregation of GNPs at pH 3 was examined (CHAPTER VI). The  $\beta$ Lg concentration, which could be saturated the GNP surface, was then selected to be used in further study. Secondly, the impact of bile salts on the protein corona around GNPs

at pH 7 was then tested to better understanding the role of orogenic mechanism (CHAPTER VII).

### **3.6 $\beta$ Lg-coated GNPs interaction with bile salts**

After  $\beta$ Lg-coated GNPs preparation at pH 7, the bile salt solution was added to the mixture of  $\beta$ Lg-coated GNPs. The bile salt concentration was varied from 0-20 mg/mL to cover a range of potential physiological situations. The mixture was kept constant at pH 7.0 and incubated with continuous shaking at 100 rpm at 37 °C for up to 2 h. Each treatment was prepared in triplicate. The mixture of  $\beta$ Lg-coated GNPs and  $\beta$ Lg-coated GNPs with bile salts were denoted “GNPs- $\beta$ Lg” and “GNPs- $\beta$ Lg-BS”, respectively.

### **3.7 Characterization of GNPs mixtures**

#### **3.7.1 Particle size and charge measurements**

The particle size and charge of bare and coated GNPs were determined using a commercial dynamic light scattering/particle electrophoresis device (Nano-ZS, Malvern Instruments, Worcestershire, UK). The particle size data were reported as the Z-average diameter, while the particle charge data were reported as the  $\zeta$ -potential. Measurements were performed at ambient temperature (22 °C) and results were reported as the average of 6 measurements.

#### **3.7.2 UV–visible spectrophotometer**

The ultraviolet spectrum (250–900 nm) of the  $\beta$ Lg coated GNPs was recorded with a UV/Vis scanning spectrophotometer (model UV-2101 PC, Shimadzu Scientific Instruments Inc., Columbia, MD) to determine the peak of the gold plasmon band.

### **3.7.3 Transmission electron microscopy (TEM)**

The morphology and distribution of the  $\beta$ Lg-coated GNPs were analyzed using a transmission electron microscope (model 2000FX, JEOL, Tokyo, Japan) operated at an accelerating voltage of 200 kV. The samples for TEM were prepared by placing a drop of gold colloidal solution onto carbon-coated copper grids and dried at room temperature.

### **3.7.4 Surface-enhanced Raman scattering (SERS)**

The samples for SERS measurement were prepared by placing a drop of  $\beta$ Lg-coated GNPs solution (5  $\mu$ L) onto a gold multi-spot microscope slide. The SERS measurement was then conducted immediately using a DXR Raman microscope (Thermo Scientific Madison, WI) equipped with a 10 $\times$  microscope objective. The spectra were recorded using a 780 nm excitation laser with 5 s scanning time. The laser power was maintained at 13 mV throughout all the experiments.

**CHAPTER IV**  
**MICROFIBRILLATED CELLULOSE FROM MANGOSTEEN**  
**(*Garcinia mangostana* L.) RIND: PREPARATION,**  
**CHARACTERIZATION, AND EVALUATION**  
**AS AN EMULSION STABILIZER**

#### **4.1 Abstract**

Aqueous microfibrillated cellulose (MFC) suspensions were prepared by extraction of ground mangosteen (*Garcinia mangostana* L.) rind with hot aqueous sodium hydroxide, bleaching with hydrogen peroxide, and subsequent shearing in a high pressure homogenizer. The cellulose content of the material markedly increased after the alkali and bleaching pre-treatments. The influences of number of passes through the homogenizer on characteristics of the resulting MFC were investigated. Results show that crystallinity index, degree of polymerization, viscoelasticity, and viscosity of the MFC suspensions decreased as the number of homogenization passes increased, indicating that fiber degradation occurred during homogenization. The emulsion stabilizing properties of MFC, on the other hand, were improved when the number of homogenization passes was increased. The oil-in-water emulsions stabilized by MFC (30% w/w soybean oil, 0.7% w/w MFC in aqueous phase, emulsion pH range ~ 6.8–7.2) obtained at the higher number of homogenization passes exhibited smaller oil droplets, stronger three-dimensional network structures, and more stable to creaming than those stabilized by MFC obtained at the lower number of homogenization passes. The creaming stability of the MFC-stabilized emulsions was reduced at low pH or high salt concentration due to electrostatic screening of the negatively charged MFC particles. Thermal treatment had little influence on the creaming stability of these emulsions. These results should improve understanding of the relationships between processing and characteristics of MFC from a novel

lignocellulosic material, i.e. mangosteen rind, and lead to a potential application as an emulsion stabilizer.

## 4.2 Introduction

Microfibrillated cellulose (MFC) or cellulose gel is isolated and purified cellulose fibers recovered from original cellulose filamentous structure, as cellulose fibers consist of nanometer-scale microfibrils (2–10 nm thick, several tens of micrometers length). The MFC typically consists of partially disintegrated microfibril aggregates with a lateral dimension in the scale of tens of nanometers (typically in the range of 20–40 nm) and lengths of several micrometers (Lavoine, et al, 2012; Siró & Plackett, 2010), and can thus be regarded as nanofibers. MFC possesses several interesting properties, such as a very large specific surface area, very high aspect ratios, high strength and stiffness, low weight, biodegradability, and renewability which has found applications as rheology modifiers in foods, paints, cosmetics, and pharmaceutical products (Turbak, Snyder, & Sandberg, 1983) and as fillers in composite materials (Lavoine et al., 2012; Siró & Plackett, 2010). A progress in preparation and application of MFC has been recently reviewed in the literature (Lavoine et al., 2012; Siró & Plackett, 2010). MFC can be produced in a number of different ways. It is possible to mechanically treat cellulosic fibers so that microfibrils as well as their aggregates are isolated. However, a major obstacle that needs to be overcome is the high energy consumption connected to the mechanical disintegration of the fibers into MFC, which often involves several passes through the disintegration device (Lavoine et al., 2012; Siró & Plackett, 2010). By combining the mechanical treatment with certain pre-treatments, e.g. chemical or enzymatic pre-treatment it is possible to decrease the energy consumption significantly. Isolation of MFC from various lignocellulosic materials such as softwood pulp (Henriksson, Berglund, & Lindström, 2007; Iwamoto, Nakagaito, & Yano, 2007; Pääkkö et al., 2007; Quiévy, Jacquet, Sclavons, Deroanne, Paquot, & Devaux, 2010; Turbak, Snyder, & Sandberg, 1984), bamboo pulp (Zhang et al., 2012), sugarcane bagasse (Li et al., 2012; Mandal & Chakrabarty, 2011), sugar beet pulp (Agoda-Tandjawa et al., 2010; Dinand,

Chanzy, & Vignon, 1999), corn cobs (Shogren, et al., 2011), raw banana, jute, and pineapple leaf fibers (Abraham et al., 2011), and prickly pear fruit peels (Habibi, Mahrouz, & Vignon, 2009) have been studied. It is important to use MFC that originate in plants such as wood, agricultural crops and by-products, which are the most abundant resources on earth and are underutilized source of cellulose. This also offers an opportunity to the effective disposal of the waste.

Mangosteen (*Garcinia mangostana* L.) is one of the most delicious and best flavored tropical fruits, known as the queen of fruits. Its edible portion is only about 40% of the whole fruit and the rest is rind (Chen, Huang, Huang, & Cai, 2011). The edible fruit pulp is mostly used as a dessert, but can also be canned or made into juice or preserves. The mangosteen rind contains polyphenolic compounds known as xanthenes, which provide a powerful antioxidant activity (Wittenauer, Falk, Schweiggert-Weisz, & Carle, 2012). The antioxidants extracted from mangosteen rind are utilized by pharmaceutical industry. The mangosteen rind is a residue produced in large quantities each year by the food and pharmaceutical industries. The mangosteen rind waste has about 60–70% cellulose content comparable to those of the other agricultural by-products such as raw banana, jute, and pineapple leaf (Abraham et al., 2011). Hence for the cost effective production of MFC, the mangosteen rind is a potential candidate. To the best of our knowledge, there is no literature describing the use of mangosteen rind to produce MFC so far.

An emulsion is a system consisting of dispersed droplets of one immiscible liquid in another immiscible liquid. The emulsions can be formed and stabilized not only by proteins or surfactants, but also by solid particles to form the so-called ‘Pickering emulsions’ after the pioneering work of Pickering (1907). The particles accumulate at the oil-water interface to form a physical (steric) barrier that protects the emulsion droplets against coalescence. The steric barrier is more effective for adsorbed particles which are preferentially wetted by the continuous phase, and which lie predominantly on the outer surface of the dispersed droplets (Aveyard, Binks, & Clint, 2003; Dickinson, 2010, 2012). The wettability of the particles at the oil–water interface is quantified by the contact angle  $\theta$  that the particle makes with it. Hydrophilic particles ( $\theta < 90^\circ$ ) therefore tend to form oil-in-water (o/w) emulsions whereas hydrophobic particles ( $\theta > 90^\circ$ ) form water-in-oil (w/o) emulsions. For the

particles of intermediate wettability with not too close to  $0^\circ$  or  $180^\circ$ , it can be regarded as being irreversibly adsorbed due to an extremely high free energy of adsorption compared with the thermal energy (Aveyard, Binks, & Clint, 2003; Dickinson, 2010, 2012). Therefore, one of the most important features of the particle-stabilized emulsions is that they are extremely stable to coalescence even when the emulsion droplets are quite large. Both organic and inorganic particles have been used as emulsion stabilizers (Aveyard, Binks, & Clint, 2003), among them also particles of cellulose. However, little investigation has been done on the mechanism for the emulsion-stabilizing effect of microfibrillated cellulose. Most of the studies carried out on the stabilization of emulsions by microcrystalline cellulose (MCC) (Kalashnikova, Bizot, Cathala, & Capron, 2012; Oza & Frank, 1986), microfibrillated cellulose (MFC) (Turbak, Snyder, & Sandberg 1983; Xhanari, Syverud, Chinga-Carrasco, Paso, & Stenius, 2011), or bacterial cellulose (BC) (Kalashnikova, et al., 2011; Ougiya, et al., 1997) described o/w emulsions, due to the highly hydrophilic nature of cellulose. However, there is no report on the effect of preparation conditions on the emulsion stabilizing properties of MFC from mangosteen rind.

This work aimed mainly to explore the feasibility of using mangosteen rind as a new potential lignocellulosic precursor for production of microfibrillated cellulose (MFC) in an attempt to convert this waste into value-added products. The influences of the main processing parameter, i.e. the number of passes through a high pressure homogenizer, on physicochemical and rheological properties of MFC were investigated. The emulsion stabilizing properties of MFC obtained with various homogenization passes were also evaluated in terms of physical and rheological properties and stability to creaming of the MFC-stabilized o/w emulsions.

## **4.3 Materials and methods**

### **4.3.1 Materials**

Dried mangosteen rind (*G. mangostana* L.), a residue from mangosteen-canning factory, was supplied by a local manufacturer (Chanthaburi, Thailand).

Sodium hydroxide (NaOH) and phosphoric acid (H<sub>3</sub>PO<sub>4</sub>) were purchased from Mallinckrodt Baker, Inc. (Phillipsburg, NJ, USA). Hydrogen peroxide (H<sub>2</sub>O<sub>2</sub>), sodium chloride (NaCl), hydrochloric acid (HCl), and Congo red (C.I. 22120) were purchased from Merck KGaA (Darmstadt, Germany). Sodium azide (NaN<sub>3</sub>) and cupriethylenediamine (C<sub>2</sub>H<sub>6</sub>CuN<sub>2</sub>) were purchased from Sigma Chemical Company (St Louis, MO, USA). All reagents were of analytical grade and distilled water was used for preparation of all solution. Soybean oil was purchased from a local supermarket and used without further purification.

### **4.3.2 Microfibrillated cellulose preparation**

The preparation of microfibrillated cellulose (MFC) from dried mangosteen rind was described in Section 3.1. Briefly, the mangosteen rind was ground and sieved through a 100 mesh sieve. MFC from the resulting mangosteen rind powder was prepared using hot alkaline extraction and subsequent shearing in a high pressure homogenizer at a pressure of 500 bar for 1, 5, and 20 passes at room temperature. The MFC obtained by 1, 5, and 20 homogenization passes were denoted by 1P-MFC, 5P-MFC, and 20P-MFC, respectively whereas the purified cellulose before homogenization was denoted by 0P-MFC. All the homogenized materials (MFC) are yellow-brown gel-like aqueous matters, having an MFC concentration of 1% w/w and exhibiting neither flocculate nor sediment when diluted with water.

### **4.3.3 Characterization of microfibrillated cellulose**

#### **4.3.3.1 Chemical analysis**

Total nitrogen, fat, carbohydrate, moisture, and ash contents of dried mangosteen rind and its purified cellulose were determined using AOAC Official Methods (AOAC, 2000). Cellulose content was also determined following the FCC assay method (FCC, 1981). All chemical analyses were performed in duplicate.

#### **4.3.3.2 X-ray powder diffraction (XRD) analysis**

Dried ground mangosteen rind, its purified cellulose, and microfibrillated cellulose (MFC) were characterized for crystalline structure with an X-ray diffractometer (model D8-Advance, Bruker AXS GmbH, Karlsruhe, Germany).

The crystallinity index was then calculated by Segal's empirical method (Segal, Creely, Martin, & Conrad, 1959), as described in Section 3.2.2.

#### **4.3.3.3 Determination of degree of polymerization**

The MFC samples obtained with different number of homogenization passes were dissolved in 1 M  $C_2H_6CuN_2$ . The viscosimetric average degree of polymerization ( $DP$ ) of MFC samples was calculated from the intrinsic viscosities  $[\eta]$  of the corresponding solutions at 25 °C, as described in Section 3.2.3.

#### **4.3.4 Preparation of MFC-stabilized emulsions**

MFC aqueous suspensions obtained with different number of homogenization passes were prepared at a concentration of 0.7% w/w by dilution of the stock 1% w/w MFC suspensions using distilled water. The MFC concentrations reported in this paper refer to the aqueous phase and not to the whole emulsion. MFC-stabilized oil-in-water (o/w) emulsions (500 g each) were prepared by blending 30% w/w soybean oil and 70% w/w MFC aqueous suspensions together at room temperature (Section 3.3). The samples were stored at room temperature for 24 h before being analyzed.

#### **4.3.5 Characterization of MFC-stabilized emulsions**

##### **4.3.5.1 Particle size determination**

The emulsion samples were analyzed for particle size and particle size distribution of oil droplets using a laser diffraction particle size analyzer (Mastersizer 2000; Malvern Instruments Ltd., Worcestershire, UK), as described in Section 3.4.1. Particle size was reported as the volume-weighted mean particle diameter ( $d_{43}$ ).

##### **4.3.5.2 Scanning electron microscopy**

Scanning electron microscopy (SEM) was carried out to visualize microstructure of the MFC-stabilized emulsions. The emulsion samples were observed by using a scanning electron microscope (model JSM-5410LV, JEOL, Tokyo, Japan) (Section 3.4.2).

#### **4.3.5.3 Confocal laser scanning microscopy**

Confocal laser scanning microscopy (CLSM) was performed in an attempt to localize the MFC particles, which were stained by Congo red dye, in the emulsions. Confocal micrographs of the emulsion were acquired using a confocal laser scanning microscope (Fluoview FV1000, Olympus Corporation, Tokyo, Japan) operating in a fluorescence mode, as described in Section 3.4.3. As the Congo red dye stained the MFC particles, regions rich in the MFC appeared as bright patches on the dark background of the micrographs.

#### **4.3.5.4 Rheology measurements**

Rheological properties of the freshly prepared MFC aqueous suspensions and MFC-stabilized o/w emulsions were measured at 25 °C using a controlled-strain rheometer (PhysicaMCR 301, Anton Paar GmbH, Graz, Austria) equipped with a cone and plate sensor (1° cone angle, 50 mm diameter, and 0.05 mm gap) by the procedure described in Section 3.4.4.

#### **4.3.5.5 $\zeta$ -potential measurements**

The  $\zeta$ -potential of 20P-MFC suspension and 20P-MFC-stabilized emulsion was measured using a particle electrophoresis instrument (Zetasizer Nano ZS, Malvern Instruments Ltd., Malvern, Worcestershire, UK) (Section 3.4.5).

#### **4.3.5.6 Visual assessment of creaming**

Creaming stability was determined to evaluate the relative stability of o/w emulsions by the procedure described in Section 3.4.6. The samples were kept at room temperature and the movement of any creaming boundary was tracked with time for 80 days.

#### **4.3.5.7 Determination of stability to environmental stresses**

The influences of environmental stresses (pH, ionic strength, and temperature) on the creaming stability of the MFC-stabilized emulsions were examined. The emulsions were prepared as described above using 30% soybean oil

and 70% MFC suspensions with various concentrations, i.e. 0.05, 0.10, 0.30, 0.50, and 0.70% w/w MFC. These emulsions were then diluted to a droplet concentration of 10% w/w using distilled water for the stability tests to pH and temperature and NaCl solutions for the stability tests to ionic strength. Thus, the MFC concentrations in the diluted emulsions were 0.017, 0.033, 0.100, 0.167, and 0.233%, respectively. The diluted emulsions (15 g) were transferred into 20-mm diameter and 70-mm height glass test tubes for all stability tests. For the thermal stability test, the diluted emulsions were incubated in a water bath for 30 min at 30, 50, 70, and 90 °C. The pH stability test was performed by adjusting pH of the distilled water diluted emulsions to 3, 4, 5, 6, 7, and 8 using either 0.1 M NaOH or 0.1 M HCl solution. For the stability tests to ionic strength, the emulsions were diluted using NaCl solutions to a final concentration of 0-250 mM NaCl. After each treatment, the treated emulsions were stored at room temperature for 24 h prior to determination of creaming index.

#### **4.3.6 Statistical analysis**

All measurements were performed in triplicate for each sample with the exception of chemical analyses which were done in duplicate. Results are expressed as mean  $\pm$  standard deviations. A one-way analysis of variance (ANOVA) and Duncan's multiple range test were used to establish the significance of differences ( $p \leq 0.05$ ) among the mean values. The statistical analyses were performed using SPSS version 14.0 Windows program (SPSS Inc., Chicago, IL, USA).

## **4.4 Results and Discussions**

### **4.4.1 Purified cellulose and microfibrillated cellulose**

#### **4.4.1.1 Chemical compositions**

Chemical compositions of mangosteen rind and its purified and bleached cellulose are shown in Table 4.1. The mangosteen rind consisted of a high percentage of cellulose (68%), indicating a good source of cellulose. With the treatment of alkali and bleaching agents, protein and fat were removed in which the residue of these components of less than 1% was found in the purified cellulose.

Moreover, it is well recognized that a substantial proportion of the other non-cellulosic materials such as lignin, hemicelluloses, and pectins were also removed by these treatments (Abraham et al., 2011; Agoda-Tandjawa et al., 2010; Siró & Plackett, 2010). The removal of these components resulted in an increase of the percentage of cellulose in the purified cellulose up to 94% which is in good agreement with those reported by other researchers (Abraham et al., 2011). It has been reported that the mechanical treatment, i.e. homogenization, used to convert the purified cellulose into microfibrillated cellulose (MFC) did not substantially affect the chemical composition of the cellulose starting material (Turbak, Snyder, & Sandberg, 1984). Therefore, we can assume that the chemical composition of MFC is the same as that of the purified cellulose.

**Table 4.1** Chemical compositions of untreated mangosteen rind and its purified cellulose.<sup>a</sup>

Composition (% w/w, dry basis)	Dried mangosteen rind	Purified cellulose
Moisture <sup>b</sup>	10.82 ± 0.28	15.65 ± 0.52
Protein (N × 6.25)	7.48 ± 0.09	0.84 ± 0.02
Fat	6.45 ± 0.04	0.20 ± 0.01
Ash	4.47 ± 0.07	2.41 ± 0.02
Carbohydrate	81.60 ± 0.03	96.55 ± 0.01
Total dietary fiber	92.69 ± 0.76	97.29 ± 2.65
Insoluble dietary fiber	77.93 ± 0.39	95.42 ± 1.06
Cellulose	67.69 ± 0.13	93.73 ± 0.48

<sup>a</sup> Assays were performed in duplicate.

<sup>b</sup> % w/w, wet basis.

#### 4.4.1.2 X-ray diffraction patterns

Figure 4.1 shows x-ray diffraction patterns of the mangosteen rind, its purified cellulose, and MFC. For these materials, peaks were observed at 16.0 and 22.5° two theta. This pattern is characteristic of cellulose I which is a crystal form of native cellulose (Abraham et al., 2011). This is typical of cellulose isolated from other sources, i.e. corn cobs (Shogren et al., 2011) and sugar beet pulp (Agoda-

Tandjawa et al., 2010). The x-ray pattern for mangosteen rind is broader due to the presence of non-crystalline lignin, hemicelluloses, and pectins. Upon removal of these materials by treatment with alkali and bleaching agents, the calculated crystallinity index increased from 32% for the mangosteen rind to 56% for the purified cellulose. However, after homogenization the crystallinity index significantly decreased to 36% for MFC. It is indicated that the intermolecular hydrogen bonds of cellulose were broken, causing the collapse of crystal structure during the homogenization process. Similar results were also observed for the isolation of MFC from sugarcane bagasse (Li et al., 2012) and prickly pear fruit peels (Habibi, Mahrouz, & Vignon, 2009) by high pressure homogenization.

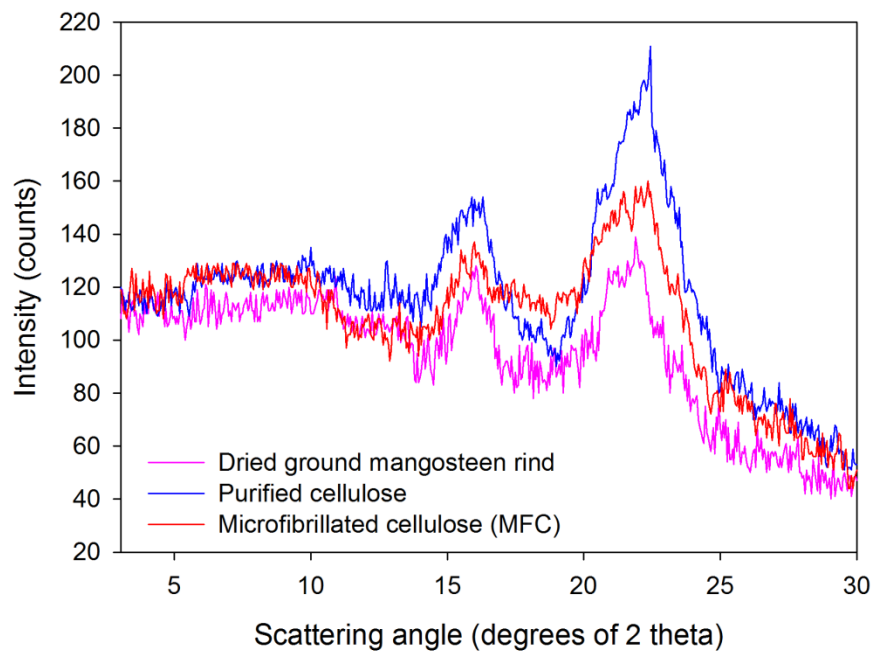


**Figure 4.1** X-ray diffraction patterns of dried ground mangosteen rind, purified cellulose, and mechanical treated (20 passes through the homogenizer) cellulose, i.e. microfibrillated cellulose (MFC).

#### 4.4.1.3 Degree of polymerization (*DP*)

There is a significant ( $p \leq 0.05$ ) decrease in degree of polymerization (*DP*) of MFC during homogenization. The *DP* of one-pass, five-pass, and twenty-pass MFC which were denoted by 1P-MFC, 5P-MFC, and 20P-MFC, respectively, was 1003, 850, and 711, respectively. The *DP* is reported to correlate

strongly with the aspect ratio of the nanofibers; longer fibrils are associated with higher  $DP$  (Siró & Plackett, 2010). The decrease of  $DP$  indicates the breakage along the fiber direction (Iwamoto, Nakagaito, & Yano, 2007). Depending on the nature of the starting material and the preparation conditions, the  $DP$  of MFC may be even lower. A reduction of about 30-50% in  $DP$  of MFC was reported when the 2% enzymatically treated softwood pulp ( $DP = 1200$ ) suspensions were subjected to homogenization of a high pressure homogenizer for 20 passes (Henriksson et al., 2007). Generally, our results are in good agreement with those previously reported by Iwamoto, Nakagaito, and Yano (2007), who found that both  $DP$  and degree of crystallinity decreased in a similar manner as the number of passes through the grinder increased.

#### 4.4.1.4 Rheological properties

For rheological analysis, the dynamic mechanical spectra of the 1P-MFC, 5P-MFC, and 20P-MFC aqueous suspensions at a concentration of 1% w/w are depicted in Figure 4.2A. All MFC suspensions exhibited the storage modulus ( $G'$ ) to be higher than the loss modulus ( $G''$ ) within the measured angular frequency range.  $G'$  and  $G''$  were only slightly dependent of the angular frequency, evidencing a gel-like behavior (Clark & Ross-Murphy, 1987). Interestingly, prior to homogenization, the two-phase nature of the water-fiber suspension was apparent since sedimentation occurred rapidly for the purified cellulose suspension. After homogenization, even for only one pass, the resulting MFC suspensions became gels which were stable and did not sediment or flocculate. The gelation of MFC could be attributed to the formation of strongly entangled and disordered network structure of the MFC with very high aspect ratio (Pääkkö et al., 2007). Moreover, the negative charge carried by the MFC nanofibers allows the fibers to electrostatically repulse each other, increasing the organization and the stability of the gels (Agoda-Tandjawa et al., 2010). Other authors have established that the presence of residual hemicelluloses and pectins on the microfibril surface is necessary to obtain a stable MFC gels in water (Habibi, Mahrouz, & Vignon, 2009). It can be seen from Figure 4.2A that  $G'$  of the MFC gels decreased with increasing the number of passes through the homogenizer. It is likely that partially disintegrated microfibrillar aggregates present in the MFC samples

obtained from the low number of homogenization passes could form strong entanglements and junction zones in the gel networks. Further homogenization, however, disrupts these aggregates and possibly breaks the MFC chains into smaller cellulose microfibrils and fragments, as evidenced partly by the lower  $DP$ , which form weaker gels (Shogren et al., 2011).

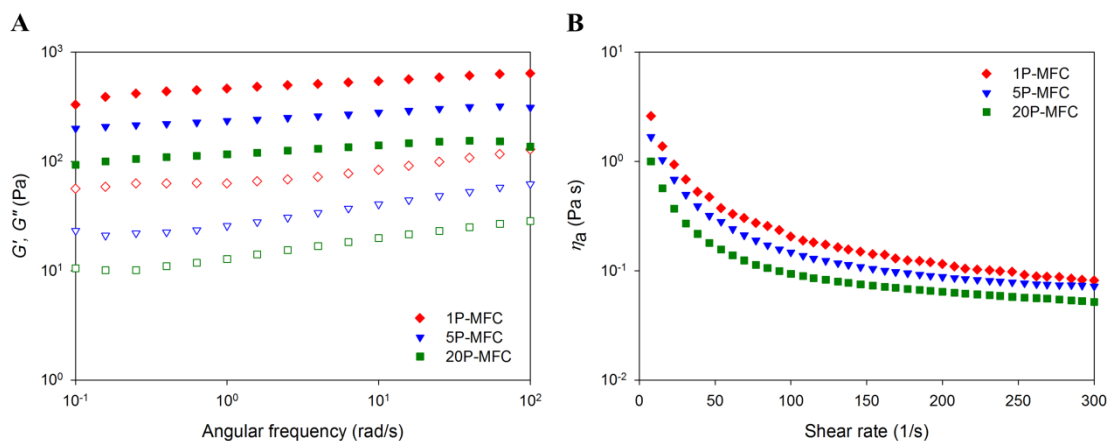


**Figure 4.2** Influence of number of passes through the homogenizer on rheological properties of 1% w/w fresh MFC suspensions, measured at 25 °C (A) mechanical spectra, i.e. storage modulus,  $G'$ , (closed symbols) and loss modulus,  $G''$ , (open symbols) as a function of angular frequency, measured at 0.5% strain; (B) Apparent viscosity ( $\eta_a$ ) (calculated from the downward flow curve data) as a function of shear rate. Refer to Table 4.2 for the sample codes of MFC obtained from various homogenization passes.

In addition, the apparent viscosities calculated from the downward flow curve data of all MFC suspensions were investigated as a function of shear rate (Figure 4.2B). All suspensions behaved like a typical aggregated system, as indicated by their shear-thinning rheological behavior, i.e. viscosity decreases with increasing shear rate. The shear-thinning of MFC suspensions was already early recognized in the literature for the materials prepared by enzymatic hydrolysis combined with high pressure homogenization (Pääkkö et al., 2007). The apparent viscosity data show the evidence of structural difference for different types of MFC. Not surprisingly, the MFC obtained with the higher number of homogenization passes exhibited lower viscosities than those produced at the lower number of passes, for

example, at a shear rate of  $10 \text{ s}^{-1}$ , the viscosities of 1P-MFC, 5P-MFC, and 20P-MFC were 2.11, 1.42, and 0.89 Pa s, respectively. In the case of the weakly bonded networks of low aspect ratio MFC, e.g. 20P-MFC, upon exposing increased shear rate, the network falls apart easily and individual elements start to flow. In the case of the more entangled networks of MFC, e.g. 1P-MFC and 5P-MFC, the viscosity remains higher.

It has been found that drying of the MFC gel modifies its properties and is moreover relatively costly. After drying, even the freeze-drying, re-dispersion of the MFC in water does not allow the recovery of the rheological properties of the initial suspension (Agoda-Tandjawa et al., 2010; Quiévy et al., 2010). Therefore, in this study, the MFC gels have been used directly after preparation in its never-dried form, as an aqueous suspension.

#### **4.4.2 Characterization of MFC-stabilized o/w emulsions: Effect of number of passes through homogenizer of MFC**

##### **4.4.2.1 Particle size and particle size distribution**

The initial droplet size distributions of the o/w emulsions stabilized by the three types of MFC, i.e. 1P-MFC, 5P-MFC, and 20P-MFC as well as the purified cellulose (0P-MFC) are shown in Figure 4.3A. Bimodal distributions with two ranges were encountered with all the MFC-stabilized emulsions. When the number of homogenization passes during the preparation of MFC increased from 0 to 20 passes, the emulsion droplets in the smaller size range ( $<10 \mu\text{m}$ ) increased, whereas the droplets in the larger size range ( $>10 \mu\text{m}$ ) decreased. Average droplet diameters ( $d_{43}$ ) significantly decreased from 61.2 to 24.3  $\mu\text{m}$  with increasing the number of homogenization passes from 0 to 20 passes (Figure 4.3B). It appears that at the lower number of passes, the high viscosity of the resulting MFC suspensions (Figure 4.2B) may have reduced the efficiency of the homogenization process and resulted in the formation of larger oil droplets (Huang, Kakuda, & Cui, 2001). Moreover, it is well recognized that the smaller the particles, the higher the emulsion stabilizing efficiency (Denkov, Ivanov, Kralchevsky, & Wasan, 1992). Therefore, the MFC obtained at the higher number of homogenization passes having smaller particle sizes could stabilize the emulsion more efficiently than those obtained at the lower number of passes and

resulted in the smaller emulsion droplets. Similar results were also reported by Binks and Lumsdon (2001), who found that the average emulsion droplet diameters decreased from 75 to 35  $\mu\text{m}$  with decreasing particle diameter.

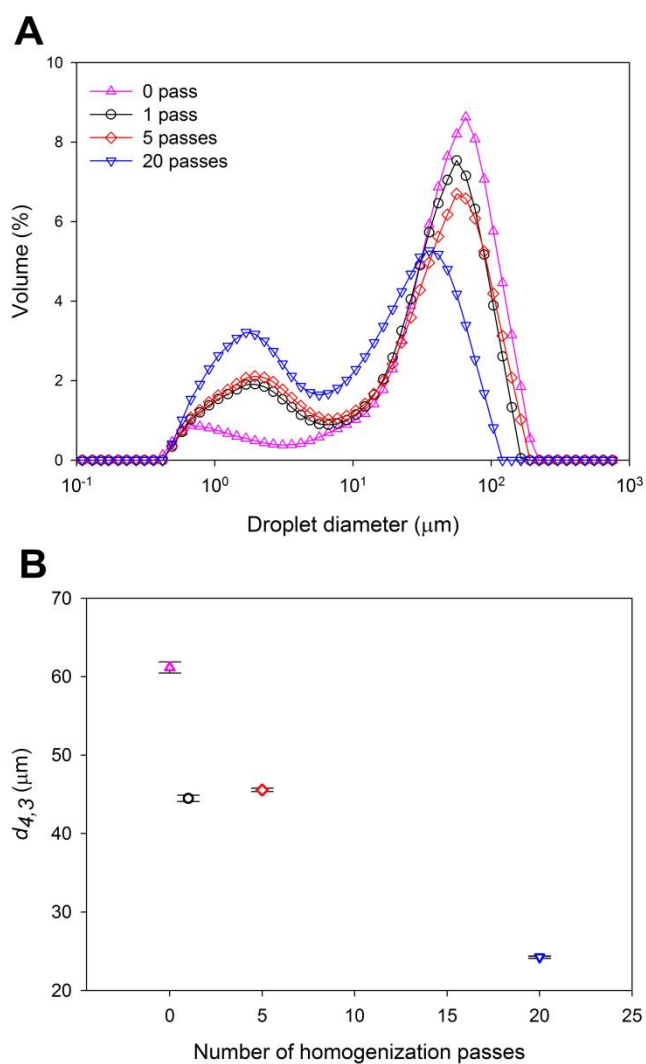


**Figure 4.3** Influence of number of passes through the homogenizer of MFC on (A) particle size distribution and (B) average particle size ( $d_{4,3}$ ) of MFC-stabilized o/w emulsions (30% w/w oil, 0.7% w/w MFC in aqueous phase). Refer to Table 4.2 for the sample codes of MFC obtained with various homogenization passes.

#### 4.4.2.2 Microstructure

Microstructure of the MFC-stabilized o/w emulsions and respective localization of the MFC particles in the emulsions were visualized by SEM

and CLSM, respectively (Figure 4.4). SEM images of these emulsions were easily distinguished by the presence of relatively open, loose network structures of aggregated droplets in the 1P-MFC emulsion (Figure 4.4A), whereas the much denser network structures of MFC in which most of the droplets were embedded occurred in the 20P-MFC emulsion (Figure 4.4B). The 1P-MFC emulsion droplets partially resided in the continuous MFC matrix (Figure 4.4C), while those of the 20P-MFC emulsion were completely trapped in the MFC network (Figure 4.4D). CLSM image allows for direct visualization of the location of MFC particles in the emulsions. The round-shaped bright fluorescence of MFC was observed at the perimeter of the emulsion droplets, while the inside remained dark (Figure 4.4E). The low fluorescence intensity was also observed in the aqueous phase, indicating the presence of excess MFC in the continuous aqueous phase. It has been clarified that the MFC particles were mainly located at the interface of the emulsion droplets resulting in a particle-stabilized emulsion. It was concluded that the MFC provided its functionality by forming a solid-like network in the continuous aqueous phase, i.e. network stabilization combined with adsorbing at the oil-water interface, i.e. Pickering stabilization.

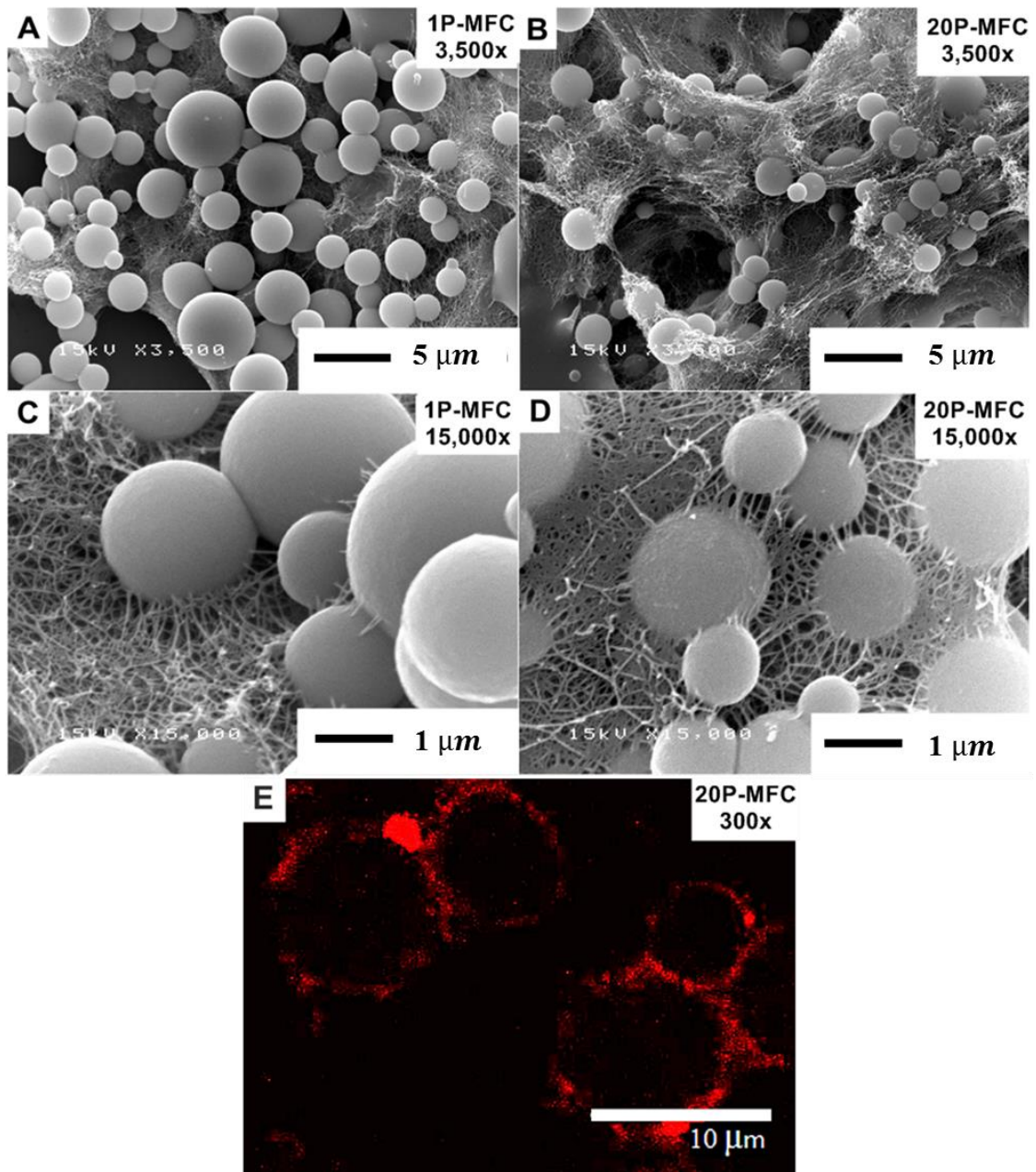


**Figure 4.4** SEM micrographs of o/w emulsions stabilized by MFC (30% w/w oil, 0.7% w/w MFC in aqueous phase) obtained with 1 pass (A, C) and 20 passes (B, D) through the homogenizer. CLSM micrograph (E) of emulsion droplets stabilized by MFC obtained with 20 homogenization passes.

#### 4.4.2.3 Rheological properties

Rheological characterization of the MFC-stabilized o/w emulsions was performed by measuring their dynamic and steady shear behaviors. The dynamic mechanical spectra and the steady flow curves of the emulsions stabilized by

different types of MFC are presented in Figure 4.5A and B, respectively. As it can be seen from Figure 4.5A, for all MFC-stabilized emulsions,  $G'$  was always higher than  $G''$  in the frequency range explored and both moduli were almost independent of frequency. This is typical for gel-like behavior (Clark & Ross-Murphy, 1987). Moreover, with increasing the number of homogenization passes for MFC preparation from 0 to 20 passes, the  $G'$  values of the corresponding emulsion are raised, indicating a more structured of the emulsion gel network. For the steady flow tests (Figure 4.5B), all emulsions exhibited mainly time-dependent shear-thinning (thixotropic) with yield stress behavior in the range of shear rates tested. Both upward and downward flow curves, except upward curve of the 20P-MFC emulsion, were well fitted by the Herschel-Bulkley model. The Herschel-Bulkley rheological parameters along with the coefficients of determination for each upward or downward flow curve and the hysteresis loop areas between these two curves are summarized in Table 4.2. In general, all the emulsions show both a considerable degree of thixotropy and the presence of spurs at low shear rates on the upward flow curves which signify three-dimensional structure that breaks down at higher shear rates. The spurs define the static yield stress values (i.e. the yield stress values calculated from the upward curve data) of the emulsions, which in turn can be related to the strength of the network structure that must be broken to cause flow (Oza & Frank, 1986). As expected, the static yield stress values were higher than the dynamic yield stress, i.e. the yield stress calculated from the downward curve data. The thixotropy hysteresis loop is commonly attributed to the breakdown and alignment of the three-dimensional network structure in the emulsions. That is when the emulsion having stronger network structure is deformed, a relatively longer time is required for it to return to its original structure upon removal of shear stress. Therefore, the greater the loop area, the more structured a system is, or vice versa. All samples show a flow behavior index ( $n$ ) less than 1, indicative of a non-Newtonian and shear-thinning flow behavior. Moreover, it appeared that the thixotropic character was more pronounced as evidenced by significantly higher values of hysteresis area and yield stress when the emulsions were stabilized by MFC obtained at higher number of homogenization passes, suggesting a higher degree of three-dimensional structure in these emulsions. As expected, an increase in the values of yield stress and hysteresis area obtained from the steady shear

tests with increasing the number of homogenization passes of MFC is consistent with an increase in the  $G'$  values of the dynamic shear measurements as described above. Based on these rheological measurements, it was concluded that an additional stabilizing mechanism in these o/w emulsions was the development of a gel-like microstructure composed of flocculated oil droplets and a viscoelastic network of MFC particles in the aqueous medium between the droplets which was supported by SEM micrographs of the undiluted emulsions (Figure 4.4). These observations were similar to those reported by Tzoumaki, et al. (2011) for o/w emulsions stabilized by chitin nanocrystal particles.

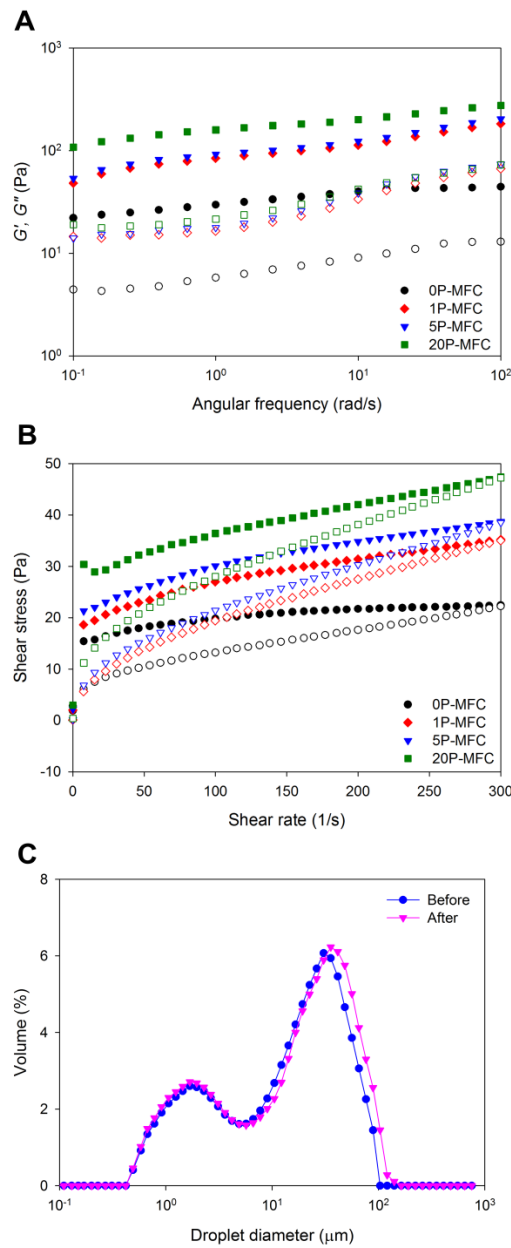


**Figure 4.5** Influence of number of passes through the homogenizer of MFC on (A) mechanical spectra, i.e. storage modulus,  $G'$ , (closed symbols) and loss modulus,  $G''$ , (open symbols) as a function of angular frequency, measured at 0.5% strain and (B) flow curves, i.e. shear stress as a function of shear rate, in which closed symbols represent the ascending part and open symbols represent the descending part of the flow curves of fresh o/w emulsions stabilized by MFC (30% w/w oil, 0.7% w/w MFC in aqueous phase), measured at 25 °C. Particle size distributions (C) of 20P-MFC-stabilized emulsion before and after steady flow tests. Refer to Table 4.2 for the sample codes of MFC obtained with various homogenization passes.

**Table 4.2** The Herschel-Bulkley rheological parameters of emulsions stabilized by MFC (30% w/w oil, 0.7% w/w MFC in aqueous phase) obtained with different number of passes through the homogenizer.<sup>a</sup>

Number of passes through homogenizer <sup>b</sup>	Upward curve					Downward curve				
	Hysteresis area (Pa/s)	$\sigma_0$ (Pa)	$K$ (Pa s <sup>n</sup> )	$n$ (-)	$R^2$	$\sigma_0$ (Pa)	$K$ (Pa s <sup>n</sup> )	$n$ (-)	$R^2$	
0 (0P-MFC)	1772.16 ± 139.56b	13.30±0.27c	1.88±0.11b	0.43±0.01c	0.998	2.43±0.53cd	1.08±0.11a	0.59±0.02a	0.996	
1 (1P-MFC)	2024.85 ± 90.17ab	14.43±0.62b	2.40±0.27a	0.41±0.02b	0.999	3.97±0.74b	1.19±0.31a	0.59±0.04a	0.998	
5 (5P-MFC)	2340.38 ± 231.87a	20.64±0.52a	2.45±0.10a	0.38±0.01a	0.998	3.27±1.00bc	1.41±0.28a	0.58±0.06a	0.999	
20 (20P-MFC) <sup>c</sup>	2450.31 ± 341.18a	-	-	-	-	6.52±0.62a	1.49±0.17a	0.58±0.02a	0.999	

<sup>a</sup> Assays were performed in triplicate. Mean ± standard deviation values in the same column followed by different letters are significantly different ( $p \leq 0.05$ ).

<sup>b</sup> The sample codes were denoted in parentheses.

<sup>c</sup> Herschel-Bulkley equation was not fitted to the upward curve of flow.

As it is well recognized that the Pickering emulsions are susceptible to shear-induced coalescence (Whitby, Fischer, Fornasiero, & Ralston, 2011), the average droplet sizes and droplet size distributions of the emulsions at the end of the steady flow tests were also determined. The 20P-MFC-stabilized emulsion with an average droplet size ( $d_{43}$ ) of 24  $\mu\text{m}$ , for example, shows a slight increase in  $d_{43}$  to 27  $\mu\text{m}$  at the end of the steady flow tests. A small change in droplet size distribution of this emulsion (Figure 4.5C), in which the droplets in the larger size range ( $>10 \mu\text{m}$ ) slightly increased after shearing, was observed. These results indicate that the MFC-stabilized emulsions are relatively stable to coalescence under the shear conditions applied during the flow tests and therefore their flow behaviors should not be significantly affected by the shear-induced coalescence. Shearing is known to disrupt the three-dimensional droplet-particle network, increase the number of droplet collisions, and presumably enhance the rate of coalescence. Generally, the emulsion stability to coalescence increases with decreasing particle size (Denkov et al., 1992) or increasing aspect ratio (Madivala, Vandebril, Fransaer, & Vermant, 2009) of the solid particles. The o/w emulsions stabilized by silica particles exhibited significant coalescence at shear rates of  $10 \text{ s}^{-1}$  and above (Whitby et al., 2011), whereas those stabilized by cellulose nanocrystals were very stable, without change in droplet size, even under various mechanical treatments such as vortex or rotor-stator blender at 15,000 rpm (Kalashnikova et al., 2011). The excellent ability of these cellulose nanocrystals as well as MFC (as is the case here) to stabilize the o/w emulsions could be attributed to their small particle size with high aspect ratio and flexibility which allows network formation at the oil-water interface of the emulsion droplets (Xhanari et al., 2011). These particle networks formed around the droplets respond elastically in shear and compression and thus prohibit the coalescence of these droplets (Madivala et al., 2009).

#### 4.4.2.4 $\zeta$ -potential

The role of electrostatic interactions in stabilizing emulsions was examined by measuring the electrical charge ( $\zeta$ -potential) of the droplets. The dependence of  $\zeta$ -potential of the droplets in 20P-MFC-stabilized emulsion on the ionic environment (pH and NaCl concentration) is similar to that of the 20P-MFC particles

themselves as shown in Figure 4.6. This is expected since the MFC particles have fairly uniform surfaces (i.e. they are not amphiphilic). This implies that the surfaces of particle-coated droplets have properties similar to those of the particles themselves (Dickinson, 2010). However, it should be noted that the absolute value of the  $\zeta$ -potential of the emulsion droplets across the whole ranges of pH and NaCl concentration remained relatively lower than those of the MFC particles. The low net charge on the droplets can be explained in terms of the relatively low surface load of MFC and/or because of ionic impurities in the samples that adsorbed to the surface of the oil droplets and changed their electrical charge (Surh, Decker, & McClements, 2006). In addition, whether the droplet surface is coated by a dense layer of MFC particles or is only sparsely covered can be sensitively influenced by adjusting the pH and/or ionic strength (Dickinson, 2010). Clearly the  $\zeta$ -potential of the MFC-coated droplets and MFC particles remained negative at all pH values (Figure 4.6A), possibly because of the negatively charged ( $-\text{COO}^-$ ) groups on the MFC particles. The MFC has no cationic groups and therefore did not become positively charged at any pH. An increase in pH from 3 to 8 caused an increase in the magnitude of negative charge on the droplets from  $-9.9$  to  $-30.9$  mV, which was probably due to deprotonation of some of the protonated carboxyl groups ( $\text{COOH} \rightarrow \text{COO}^- + \text{H}^+$ ). The examination of the influence of ionic strength (0–250 mM NaCl) (Figure 4.6B) shows that the magnitude of  $\zeta$ -potential of the emulsion droplets decreased with increasing the concentration of NaCl from  $-25.4$  mV with no added salt to  $-12.1$  mV at 250 mM NaCl due to the electrostatic screening of the charged ( $-\text{COO}^-$ ) groups by the counter-ions ( $\text{Na}^+$  in this case). It is conventionally recognized that the larger the absolute magnitude of  $\zeta$ -potential, the greater is the electrostatic repulsion between droplets, and therefore the better the stability (Dickinson, 2009).

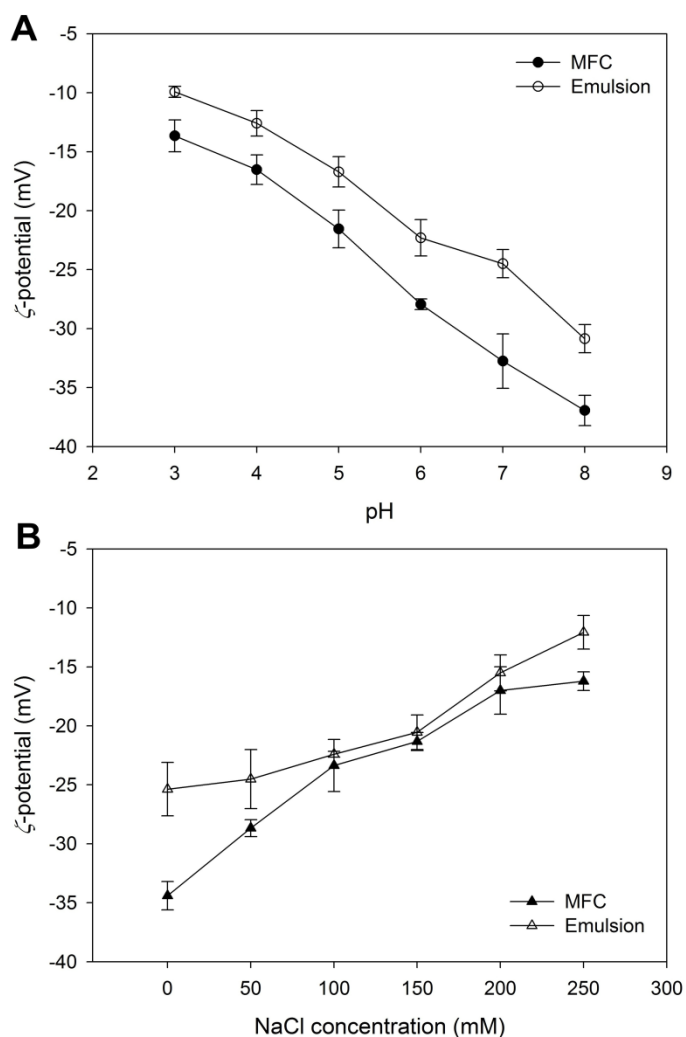
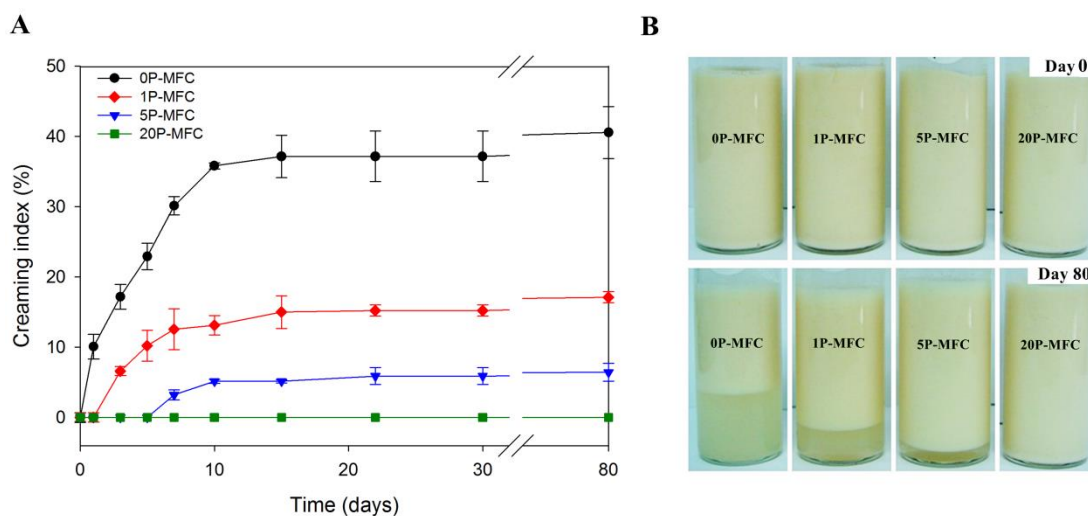


**Figure 4.6** Effects of (A) pH and (B) NaCl concentration on  $\zeta$ -potential of MFC suspensions and MFC-stabilized o/w emulsions (30% w/w oil, 0.7% w/w MFC in aqueous phase, pH 7). The 20-pass MFC (20P-MFC) was used in these experiments.

#### 4.4.2.5 Creaming stability

Figure 4.7A shows the creaming behavior of the emulsions stabilized by different types of MFC as well as the purified cellulose (0P-MFC). The 0P-MFC-stabilized emulsion was the first to show creaming. The emulsions stabilized by 1P-MFC and 5P-MFC showed a delayed creaming with a delay period of 1 and 5 days, respectively. Interestingly, the 20P-MFC-stabilized emulsion never creamed throughout the storage period of 80 days. For the creamed emulsions, during the first 30 days storage, the creaming index (CI) of 0P-MFC, 1P-MFC, and 5P-MFC emulsions reached their plateau values of 37.1, 15.2, and 5.9% after storage for 15, 22,

and 22 days followed by a slight increase to 40.5, 17.1, and 6.4%, respectively after storage for 80 days. As expected, the 0P-MFC emulsion showed the highest creaming rate as well as the highest final *CI* value that undoubtedly due to its largest droplets (Figure 4.3B) as well as the weakest emulsion structure as evidenced by its lowest yield stress (Table 4.2) and  $G'$  (Figure 4.5A) values. This led to a very high droplet mobility and subsequently high degree of creaming. Actually, this emulsion creamed readily within a few hours after preparation. For the other emulsions with a delayed creaming, the delay could be attributed to the depletion-flocculated network which was formed in the presence of non-adsorbing MFC particles (Manoj, et al., 1998). The highest stability to creaming was observed for the 20P-MFC emulsion due to its smallest droplets (Figure 4.3B) most of which were entrapped in the strongest three-dimensional network of droplets and MFC particles (Figure 4.4B) as evidenced by its highest yield stress (Table 4.2) and  $G'$  (Figure 4.5A) values. This viscoelastic network (or gel) of MFC particles surrounding the droplets immobilizes the droplets thereby preventing completely creaming. This emulsion therefore has an extremely long shelf-life and is aesthetically attractive. It is generally suggested that emulsion droplets are made as small as possible in order to minimize gravity creaming effects (Dickinson, 2009).



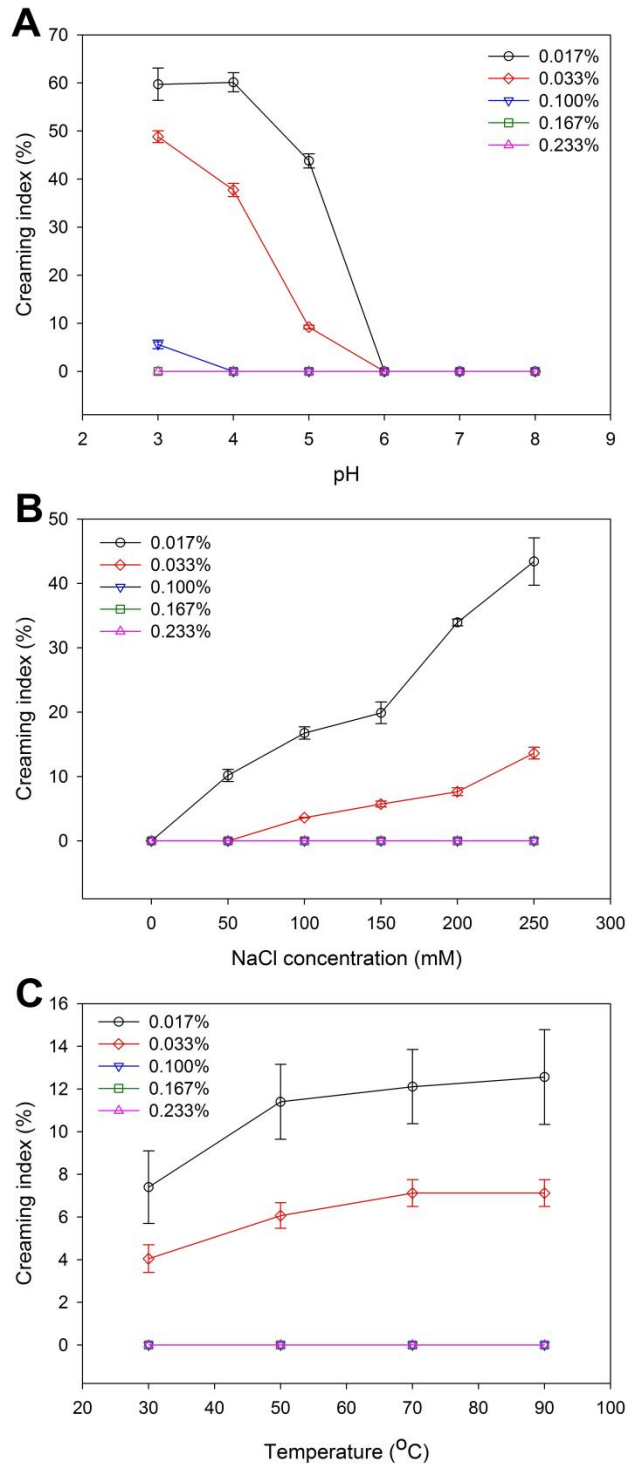
**Figure 4.7** Creaming profiles (A) and photographs (B) of MFC-stabilized o/w emulsions (30% w/w oil, 0.7% w/w MFC in aqueous phase) during storage at room temperature (25 °C) for 80 days. Refer to Table 4.2 for the sample codes of MFC obtained with various homogenization passes.

Figure 4.7B shows a photograph of all emulsions taken immediately after preparation (day 0) and after storage at room temperature for 80 days (day 80). No creaming was observed in any of the freshly prepared emulsions. However after storage for 80 days, the emulsions stabilized by 0P-MFC, 1P-MFC, and 5P-MFC displayed a sharp boundary between a top cream layer and a bottom serum layer. In the case of 0P-MFC and 1P-MFC emulsions, the serum was slightly cloudy, indicating the presence of a small residual amount of suspended individual oil droplets (Manoj et al., 1998), but the 5P-MFC emulsion creamed to leave transparent serum. The turbidity of serum gives an indication of whether the system is fully flocculated or contained flocs in coexistence with unflocculated droplets. It is generally known that the higher the degree of droplet flocculation, the serum phase becoming more transparent (Manoj et al., 1998). Therefore, the 0P-MFC and 1P-MFC emulsions exhibited creaming of individual droplets or discrete flocs and the serum phase remained cloudy throughout the storage time, whereas the 5P-MFC emulsion creamed by gravity-induced collapse of an emulsion gel which left behind a transparent serum layer from the beginning. Our results show that the stability to creaming of all emulsions increased progressively with increasing the number of homogenization

passes during MFC preparation in line with the decrease in droplet sizes and increase in yield stress and  $G'$  values.

#### 4.4.2.6 Environmental stresses

Figure 4.8 shows the influence of environmental stresses, i.e. pH, ionic strength, and temperature, on the creaming stability of diluted o/w emulsions (10% oil) stabilized by 20P-MFC at various concentrations ranged from 0.017% to 0.233%. Our results show that the creaming stability of the emulsions depended not only on the environmental stresses but also on the concentration of MFC used to stabilize the emulsions. That is the higher the MFC concentrations used, the more stable emulsions were obtained. Interestingly, the emulsions containing 0.10% MFC and above did not cream ( $CI = 0\%$ ) under the whole range of environmental stresses applied in this study. The emulsions containing 0.017% and 0.033% MFC exhibited an increase in the  $CI$  values with decreasing pH to the maximum values of about 60% and 49%, respectively at pH 3 (Figure 4.8A). However, no creaming was observed at  $pH \geq 6$  for all emulsions. The  $CI$  values of the 0.017% and 0.033% MFC emulsions also increased with increasing NaCl concentration to the maximum values of 43% and 14%, respectively at 250 mM NaCl (Figure 4.8B). As mentioned earlier, we would have expected a poor creaming stability of the emulsions stored at low pH or high salt content because of the relatively low electrostatic repulsion, i.e. low absolute values of  $\zeta$ -potential (Figure 4.6), between the droplets, and therefore promoting droplet flocculation and accelerating creaming.



**Figure 4.8** Influences of environmental stresses, i.e. (A) pH, (B) NaCl concentration, and (C) temperature, on creaming profiles of 10% o/w emulsions stabilized by MFC at different concentrations. The 20-pass MFC (20P-MFC) was used in these experiments.

Thermal treatment had little influence on the creaming stability of the emulsions stabilized by MFC (Figure 4.8C). This suggested that the majority of the droplets in the emulsions were unaffected by heating. The maximum *CI* value of only 13% was observed at a temperature of 90 °C for the emulsion stabilized by 0.017% MFC. The cause of this instability is unknown, but may have been due to some partial desorption of MFC particles from the droplet surfaces at elevated temperatures that led to flocculation and consequently creaming (Surh, Decker, & McClements, 2006). The emulsions stabilized by MFC at high concentrations ( $\geq 0.10\%$ ) remained relatively stable to creaming even at low pH or high ionic strength where electrostatic interactions should be highly screened. Based on rheological measurements, this good creaming stability can be attributed to the development of a gel-like microstructure composed of flocculated oil droplets and a viscoelastic network of MFC particles in the aqueous medium between the droplets (Tzoumaki et al., 2011). Hence, we can conclude that at low concentrations of MFC ( $< 0.10\%$ ) the electrostatic interaction between the droplets plays a major role in creaming stability of the emulsions, whereas at high MFC concentrations ( $\geq 0.10\%$ ) the formation of the three-dimensional droplet-particle network plays a major role in preventing creaming of the emulsions.

## 4.5 Conclusions

In this study, the microfibrillated cellulose (MFC) from waste mangosteen rind was prepared by high pressure homogenization coupled with an alkaline extraction and bleaching pre-treatment. The percentage of cellulose components was found to be increased during the alkaline extraction and bleaching process. It was also found that the high pressure homogenization contributed to markedly change in the properties of MFC. With an increase in the number of passes through the homogenizer, the cellulose fibers were subjected to degradation, which can be explained by the decrease in the degree of crystallinity and the degree of polymerization of cellulose. The degradation of the cellulose fibers led to the decrease of mechanical properties and viscosity of the resulting MFC suspensions. The

stabilizing properties of MFC in o/w Pickering emulsions were evaluated. The emulsions stabilized by MFC obtained at the higher number of homogenization passes exhibited smaller droplets, more pronounced elastic responses, higher degree of thixotropy and yield stress, and higher stability to creaming. These results indicate that the smaller the MFC particles, the higher efficiency of MFC adsorption at the oil–water interfaces and the stronger inter-droplet network and MFC network in the continuous phase were formed. Additionally, the creaming stability of the MFC-stabilized emulsions was decreased at low pH or high salt concentration due to the electrostatic screening effect, while this property was less affected by thermal treatment. However, when the MFC concentration was increased up to 0.10%, the creaming stability of the emulsions was not affected by any environmental stresses studied due to a predominant role of the formation of three-dimensional droplet-particle network in preventing creaming. Thus, the MFC from mangosteen rind is a useful stabilizer for o/w emulsions. The roles of MFC concentration on the physical and rheological properties as well as stability to either creaming or coalescence of the o/w Pickering emulsions are being further reported in next Chapter (Chapter V).

## **CHAPTER V**

### **PROPERTIES AND STABILITY OF OIL-IN-WATER EMULSIONS STABILIZED BY MICROFIBRILLATED CELLULOSE FROM MANGOSTEEN RIND**

#### **5.1 Abstract**

The influence of concentration of microfibrillated cellulose (MFC) extracted from mangosteen (*Garcinia mangostana* L.) rind on the properties and stability of 10% w/w soybean oil-in-water (o/w) Pickering emulsions (pH  $\approx$  7.0) was examined. The MFC concentration in the aqueous phase was varied from 0.05 to 0.70% w/w. The mean droplet size and the color intensity of the emulsions increased with increasing MFC concentration. Microscopic observations revealed that the MFC particles mainly adsorbed at the oil-water interface of the emulsion droplets, whereas the amount of excess non-adsorbing MFC particles, forming a three-dimensional network in the continuous phase, increased with increasing MFC concentration. The rheological data provided evidence for network formation in the emulsions with increasing MFC concentration. Such a gel-like behavior was attributed to an inter-droplet network structure and the formation of a MFC network in the continuous phase. All emulsions were stable to coalescence for a period of 80 days but the stability to creaming decreased progressively with decreasing MFC concentration. These results have important implications for the rational design and production of particle-stabilized food emulsions.

## 5.2 Introduction

A large number of emulsion-based products are of great interest because they play an important role in food, cosmetics, and pharmaceutical industries. An emulsion is a dispersed system that consists of two or more completely or partially immiscible liquids where one of the liquids dispersed as small spherical droplets in the other (McClements, 2005; Zarena, Bhattacharya, & Kadimi, 2012). The emulsions can be formed and stabilized not only by surface-active compounds, e.g. surfactants or proteins, but also by solid particles to form the so-called 'Pickering emulsions' after the original work of Pickering (1907). The mechanism of solid particles stabilized emulsion is the effective and irreversible adsorption of dispersed particles at the oil-water interface to form mechanical (steric) barriers around the emulsion droplets, which prevents their coalescence (Dickinson, 2010, 2012; Chevalier & Bolzinger, 2013). Several characteristics of the solid particles such as particle size (Binks & Lumsdon, 2001), particle shape (Madivala, Vandebriel, Fransaeer, & Vermant, 2009; Kalashnikova, Bizot, Bertoncini, Cathala, & Capron, 2013), particle wettability (Xhanari et al., 2011; Kalashnikova et al., 2012), particle concentration (Frelichowska, Bolzinger, & Chevalier, 2010; Kalashnikova et al., 2011), and particle interactions and assemblies (Wongkongkatap et al., 2012; Lee, Son, Cho, Choi, Kim, & Kim, 2014) have been reported to play an important role in the properties and stability of the particle-stabilized emulsions. It is generally known that the smaller the solid particle, the higher aspect ratio, and the intermediate wettability, the higher the emulsifying properties of the particle. At relatively low particle concentrations, the emulsion droplet size decreases with increasing particle concentration because more solid particles are available to stabilize smaller oil droplets. On the contrary, at higher particle concentrations, an increase in droplet size may occur due to the higher viscosity of the continuous phase that may reduce the efficiency of emulsification process. The emulsion stability is also enhanced by the interactions of solid particles at the droplet interfaces.

Research efforts are being focused on the production of different types of nanoparticles and microparticles, varying from inorganic to organic, that are not only effective to stabilize emulsions, but also acceptable for use in food products

(Dickinson, 2010, 2012). Natural biopolymers, like polysaccharides, for examples, hydrophobically modified starch granules (Yusoff & Murray, 2011), chitin nanocrystal particles (Tzoumaki et al., 2011), and bacterial cellulose nanocrystals (Kalashnikova et al., 2011, 2012) are becoming an interesting source of particulate material for food use.

Cellulose is the most abundant biopolymers on earth and is an excellent candidate for interfacial stabilization because of its renewability, sustainability, biodegradability, and nontoxicity (Kalashnikova et al., 2011, 2013). Cellulose is a linear homobiopolymer consisting of glucan chains with repeating  $\beta$ -(1 $\rightarrow$ 4)-D-glucopyranose units. These chains form parallel bundles, the microfibrils, which again aggregate to form cellulose fiber. The isolation of cellulose fibril aggregates using a homogenization process has first been described by Turbak et al. (1983). The resulting cellulose fibers are moderately degraded and opened into their substructural fibrils and microfibrils, which is called microfibrillated cellulose (MFC). MFCs are generally produced from cellulosic plant materials such as wood, agricultural crops and by-products, which are the most abundant resources and are underutilized sources of cellulose. Mangosteen rind, which is about two thirds of the whole fruit weight, is usually disposed as agricultural waste (Zarena et al., 2012). These wastes are rich in cellulose and have been used for the production of MFC (Winuprasith & Supphantharika, 2013). MFCs have many interesting properties, such as stable aqueous suspension, extremely large specific surface area, and very high longitudinal aspect ratios, providing an opportunity for multiple uses as dietary fibers, thickeners, emulsifiers or additives in food products (Habibi, Mahrouz, & Vignon 2009). Due to the hydrophilic nature of cellulose, MFCs are better wet by water than oil, and, thus, tend to stabilize oil-in-water (o/w) emulsions (Xhanari et al., 2011).

In a previous study (Chapter IV), we have examined the influence of preparation conditions, i.e. the number of homogenization passes, on the emulsion stabilizing properties of MFC from mangosteen rind (Winuprasith & Supphantharika, 2013). This study has shown that the o/w emulsions stabilized by MFC obtained with higher number of homogenization passes had smaller oil droplets, stronger three-dimensional network structures, and more stable to creaming than those stabilized by MFC produced at lower number of homogenization passes. In this study, we

investigated the influence of MFC concentration on the physical and rheological properties as well as stability to either creaming or coalescence of the o/w Pickering emulsions.

## **5.3 Materials and methods**

### **5.3.1 Materials**

Dried mangosteen rind (*Garcinia mangostana* L.), a by-product of mangosteen-canning process, was supplied by a local manufacturer (Chanthaburi, Thailand). Sodium hydroxide (NaOH) and phosphoric acid (H<sub>3</sub>PO<sub>4</sub>) were obtained from Mallinckrodt Baker, Inc. (Phillipsburg, NJ, USA). Hydrogen peroxide (H<sub>2</sub>O<sub>2</sub>) and Congo red (C.I. 22120) were obtained from Merck KGaA (Darmstadt, Germany). Sodium azide (NaN<sub>3</sub>) was obtained from Sigma Chemical Company (St Louis, MO, USA). All reagents were of analytical grade and distilled water was used for preparation of all solution and emulsion. Soybean oil was purchased from a local supermarket and used without further purification.

### **5.3.2 Preparation of microfibrillated cellulose**

Microfibrillated cellulose (MFC) was prepared according to a previously described protocol (Prakongpan, Nitithamyong, & Luangpituksa, 2002) (Section 3.1) using alkaline extraction method (NaOH/H<sub>2</sub>O<sub>2</sub>) and subsequent shearing with a high-pressure homogenizer at a pressure of 500 bar for 20 passes at room temperature (25 °C). The resulting material was yellow-brown gel-like aqueous matter, having a MFC concentration of 1% w/w and exhibiting neither flocculate nor sediment when diluted with water.

### **5.3.3 Preparation of MFC-stabilized emulsions**

MFC aqueous suspensions were prepared at a concentration of 0.05, 0.10, 0.30, 0.50, and 0.70% w/w by dilution of the stock 1% w/w MFC suspension using distilled water. The MFC concentrations reported in this paper refer to the aqueous phase and not to the whole emulsion. MFC-stabilized o/w emulsions were prepared by

blending 10% w/w soybean oil and 90% w/w MFC aqueous suspensions at room temperature (Section 3.3). The samples were stored at room temperature for 24 h before being analyzed.

#### **5.3.4 Particle size measurement**

The freshly prepared (1-day) and 80-day stored emulsions were analyzed for particle size and particle size distribution of the emulsion droplets using a laser diffraction particle size analyzer (Mastersizer 2000, Malvern Instruments Ltd., Worcestershire, UK) as previously described in Section 3.4.1. Particle size was reported as the surface-weighted mean particle diameter ( $d_{32}$ ) and the volume-weighted mean diameter ( $d_{43}$ ).

#### **5.3.5 Color measurement**

The freshly prepared emulsions were measured for color in the  $L^*$ ,  $a^*$ ,  $b^*$  system using a colorimeter (model CR-300, Konica Minolta Business Technologies, Inc., Langenhagen/Hannover, Germany). The colorimeter was calibrated using a white standard porcelain plate ( $L^* = 97.10$ ,  $a^* = -0.07$ ,  $b^* = +1.97$ ). A fixed amount of the emulsion was poured into a measurement cup, which was then surrounded with a black paper strip. In this color system,  $L^*$  represents the lightness, and  $a^*$  and  $b^*$  are color coordinates: where  $+a$  is the red,  $-a$  is the green,  $+b$  is the yellow, and  $-b$  is the blue directions.

#### **5.3.6 Optical microscopy**

The 5% o/w emulsions were prepared by diluting the freshly prepared 10% o/w emulsions with distilled water. The diluted emulsions were gently agitated in a glass test tube before analysis to ensure that they were homogenous. A drop of the emulsion was placed on a microscope slide and then covered with a cover slip. The microstructure of the emulsions was observed using a conventional light microscope (Olympus BX51, equipped with an Olympus PM10-SP digital camera, Tokyo, Japan) operating at 40 $\times$  magnification.

### 5.3.7 Scanning electron microscopy

Scanning electron microscopy (SEM) was carried out to visualize microstructure of the MFC-stabilized emulsions. The emulsion samples were observed using a scanning electron microscope (model JSM-5410LV, JEOL, Tokyo, Japan), as described in Section 3.4.2.

### 5.3.8 Confocal laser scanning microscopy

Confocal laser scanning microscopy (CLSM) was performed in an attempt to localize the MFC particles, which were stained by Congo red dye, in the emulsions. Confocal micrographs of the emulsion were acquired using a confocal laser scanning microscope (Fluoview FV1000, Olympus Corporation, Tokyo, Japan) operating in a fluorescence mode, as described in Section 3.4.3. As the Congo red dye stained the MFC particles, regions rich in the MFC appeared as bright patches on the dark background of the micrographs.

### 5.3.9 Rheology measurement

Rheological properties of the freshly prepared MFC-stabilized emulsions were measured at 25 °C using a controlled-strain rheometer (Physica MCR 301, Anton Paar GmbH, Graz, Austria) equipped with either a cone and plate sensor (1° cone angle, 50 mm diameter, and 0.05 mm gap) or a double gap cylinders sensor (the inner and outer cylinders had a diameter of 36.0 mm and 43.4 mm, respectively). The gel-like 0.30, 0.50, and 0.70% MFC-stabilized emulsions were measured using the cone and plate sensor, whereas the liquid-like 0.05 and 0.10% MFC-stabilized emulsions using the double gap cylinders sensor. The dynamic viscoelastic and steady flow measurements were performed as described in Section 3.4.4. The complex viscosity ( $\eta^* = \sqrt{(G'{}^2 + G''{}^2)}/\omega$ ) as a function of frequency and apparent viscosity ( $\eta_a$ ) as a function of shear rate were obtained using the equipment software.

In addition to the rheology measurement previously described in Section 3.4.4, the superimposition of the shear rate dependence of steady shear viscosity,  $\eta_a(\dot{\gamma})$ , and the frequency dependence of complex viscosity,  $\eta^*(\omega)$ , at equal values of frequency and shear rate, known as the Cox-Merz rule (equation 5.1), was also performed.

$$\eta^*(\omega) = \eta_a(\dot{\gamma})|_{\omega=\dot{\gamma}} \quad (5.1)$$

This rule provides insight on the structure of materials. Deviation from Cox-Merz rule is an indication of structural heterogeneity in materials. The extent of deviation can be estimated by a shift factor ( $\alpha$ ) for correcting the frequency. The expression is known as the modified Cox-Merz rule (equation 5.2):

$$\eta^*(\alpha\omega) = \eta_a(\dot{\gamma})|_{\omega=\dot{\gamma}} \quad (5.2)$$

### 5.3.10 Visual assessment of creaming

Creaming stability was determined to evaluate the relative stability of o/w emulsions by the procedure described in Section 3.4.6. The samples were kept at room temperature and the movement of any creaming boundary was tracked with time for 80 days.

### 5.3.11 Statistical analysis

All measurements were performed in triplicate for each sample. Results are expressed as mean  $\pm$  standard deviations. A one-way analysis of variance (ANOVA) and Duncan's multiple range test were used to establish the significance of differences ( $p \leq 0.05$ ) among the mean values. Paired-samples  $t$ -test ( $p \leq 0.05$ ) was used to compare the mean oil droplet sizes of a particular emulsion measured after storage for 1 day and 80 days. The statistical analyses were performed using SPSS version 14.0 Windows program (SPSS Inc., Chicago, IL, USA).

## 5.4 Results and Discussion

### 5.4.1 Particle size and particle size distribution

The initial (day 1) surface-weighted ( $d_{32}$ ) and volume-weighted ( $d_{43}$ ) mean droplet diameters of the 10% o/w emulsions stabilized by MFC at different concentrations measured by light scattering are shown in Table 5.1. There was a significant increase in both  $d_{32}$  and  $d_{43}$  when the MFC concentration in the continuous

aqueous phase was increased from 0.05 to 0.70%. For each emulsion, the  $d_{43}$  value was much higher than the  $d_{32}$  value. The reason for this difference is that they are sensitive to different aspects of the particle size distribution, i.e.  $d_{32}$  is more sensitive to the presence of small particles, whereas  $d_{43}$  is more sensitive to the presence of large particles in the size distribution (McClements, 2005). This can be seen when the full particle size distributions of the emulsions are examined (Figure 5.1). Bimodal distributions with two size ranges were observed for all the MFC-stabilized emulsions. When the MFC concentration was increased, the emulsion droplets in the smaller size range ( $<4 \mu\text{m}$ ) decreased, whereas the droplets in the larger size range ( $>4 \mu\text{m}$ ) increased. The visual inspection of droplet size in the emulsions under a light microscope (inset Figure 5.1) proved to be in good agreement with the data from light scattering (Table 5.1). It appears that at higher MFC concentrations, an increase in viscosity of the continuous phase may have reduced the efficiency of homogenization process and resulted in the formation of larger oil droplets (Huang, Kakuda, & Cui 2001; Tzoumaki et al., 2011). The apparent viscosity of the MFC aqueous suspensions measured at a shear rate of  $100 \text{ s}^{-1}$  and  $25 \text{ }^\circ\text{C}$  significantly increased from 6.3 to 87.0 mPa.s when the MFC concentration was increased from 0.05 to 0.70%. The higher viscosity of the continuous phase may hinder the MFC movement during emulsification and their final deposition at the oil-water interface. Moreover, it was noticed that the MFC-stabilized emulsions and in general of particle-stabilized emulsions have relatively large droplet sizes compared to those produced by small-molecule surfactants and proteins which is mainly due to the low surface activity of most solid particles at the oil-water interface (Oza & Frank, 1986; Dickinson, 2010, 2012; Chevalier & Bolzinger, 2013).

**Table 5.1** Influence of MFC concentration on surface-weighted ( $d_{32}$ ) and volume-weighted ( $d_{43}$ ) mean droplet diameters of 10% o/w MFC-stabilized emulsions measured after storage for 1 day and 80 days at room temperature.

MFC concentration (%)	$d_{32}$ ( $\mu\text{m}$ )		$d_{43}$ ( $\mu\text{m}$ )	
	Day 1	Day 80	Day 1	Day 80
0.05	1.33±0.01B,e	1.53±0.04A,e	2.89±0.03A,e	3.03±0.03A,e
0.10	2.19±0.01B,d	2.50±0.04A,d	7.67±0.01A,d	8.92±0.03A,d
0.30	6.79±0.06A,c	6.64±0.07A,c	31.45±0.20A,c	32.11±0.23A,c
0.50	8.27±0.14A,b	8.05±0.16A,b	41.20±0.41A,b	40.98±0.24A,b
0.70	11.16±0.11A,a	11.04±0.08A,a	50.92±0.29A,a	50.22±0.26A,a

Assays were performed in triplicate.

Capital letters (A-B) and lowercase letters (a-e) represent the effect of storage time and MFC concentration, respectively. Mean  $\pm$  standard deviation values in the same row or column with different letters are significantly different ( $p \leq 0.05$ ).

**Table 5.2** Influence of MFC concentration on color ( $L^*$ ,  $a^*$ ,  $b^*$ ) of fresh 10% o/w MFC-stabilized emulsions.

MFC concentration (%)	Color		
	$L^*$ (lightness)	$a^*$ (redness)	$b^*$ (yellowness)
0.05	87.60±1.20a	-1.29±0.07e	8.07±0.13e
0.10	87.80±0.13a	-0.97±0.01d	10.46±0.08d
0.30	83.76±0.21b	-0.03±0.01c	16.32±0.09c
0.50	80.84±0.05c	0.85±0.01b	19.76±0.09b
0.70	78.53±0.23d	1.58±0.03a	21.74±0.12a

Assays were performed in triplicate. Mean  $\pm$  standard deviation values in the same column followed by different letters are significantly different ( $p \leq 0.05$ ).

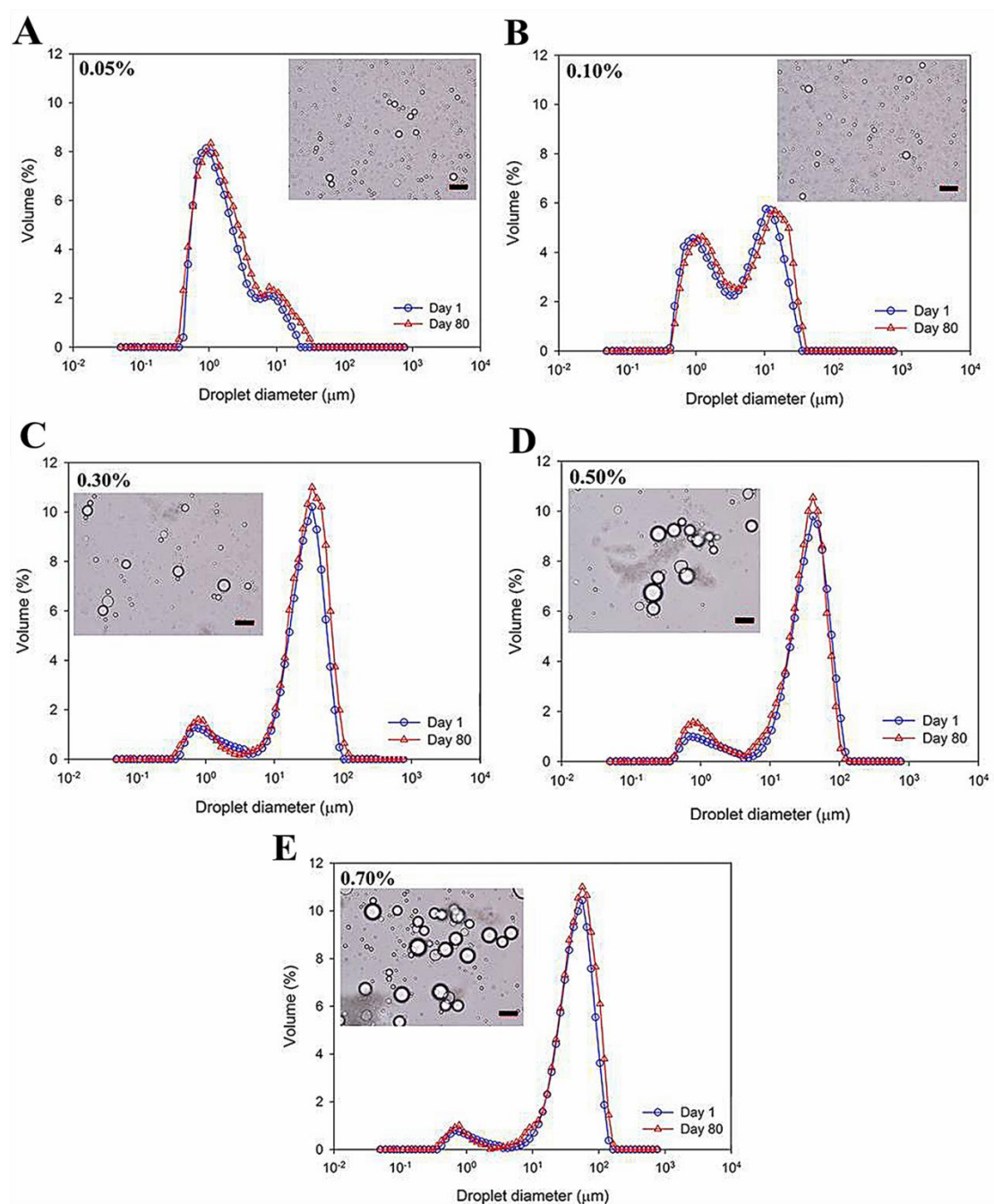


**Figure 5.1** Particle size distributions of 10% o/w emulsions stabilized by MFC at different concentrations, i.e. 0.05% (A), 0.10% (B), 0.30% (C), 0.50% (D), and 0.70% (E), measured after storage for 1 day and 80 days at room temperature. The insets represent optical micrographs (40 $\times$ ; scale bars represent 20  $\mu\text{m}$ ) of the 1-day stored emulsions.

#### 5.4.2 Color of emulsions

The color of emulsions stabilized by MFC at different concentrations presented in the form of  $L^*$ ,  $a^*$ ,  $b^*$  tristimulus system is shown in Table 5.2. The lightness ( $L^*$  value) decreased and the magnitude of  $a^*$  and  $b^*$  values significantly ( $p \leq 0.05$ ) increased with increasing MFC concentration. This means the emulsions became darker, and their color tended to be more intense as the MFC concentration increased. Generally, it is well recognized that the lightness and color of an emulsion are determined by scattering and absorption of the incident white light by the emulsion, respectively, which are in turn influenced by the emulsion droplet size and concentration and the presence of colorants in the emulsion (Chantrapornchai, Clydesdale, & McClements, 1999). As the MFC concentration increased, the droplet size significantly increased (Table 5.1) and the emulsions became flocculated (Figure 5.2). The light scattering efficiency of the droplet decreased with increasing droplet diameter and so the light could penetrate further into the emulsion and was absorbed to a greater extent, which resulted in a decrease in the lightness ( $L^*$ ) and an increase in the color ( $a^*$  and  $b^*$ ) of the emulsions.

The increase in color intensity of the emulsions with increasing MFC concentration may also have been caused by the higher amount of MFC in the emulsions, since MFC itself had a yellow-brown color ( $L^* = 31.73$ ,  $a^* = +0.74$ ,  $b^* = +8.37$  at 0.70% concentration). In the presence of MFC, some of the light was absorbed by the chromophores in the MFC and therefore did not contribute to the light scattering, resulting in a lower lightness and a higher color intensity. A variety of studies have shown that the lightness decreases and the color intensity increases as the concentration of chromophoric material in the emulsion increases (McClements, 2005). However, it has been reported that the color of emulsions was less sensitive to droplet flocculation (Chantrapornchai, Clydesdale, & McClements, 2001), which in this case occurred at high MFC concentrations. The reason is that the individual emulsion droplets are spherical, homogeneous particles, whereas flocs are nonspherical, heterogeneous particles that have many internal boundaries, and therefore one cannot expect a floc to behave like a droplet of the same diameter (Chantrapornchai et al., 2001).

### 5.4.3 Microstructure of emulsions

Due to the presence of the MFC adsorbing on the oil droplet surface was not clearly revealed using a scanning electron microscope (SEM) as a result of its limited resolution. Hence, a confocal laser scanning microscope (CLSM) become more effective tool to visualize the location of MFC in the emulsions. In this experiment, the microstructure of MFC-stabilized o/w emulsions was observed using SEM (Figure 5.2A-C) and the location of MFC particles in the emulsions was checked by CLSM (Figure 5.2D-F).

The SEM micrographs of these emulsions were easily distinguished by the extent of three-dimensional networks formed by excess MFC in the continuous aqueous phase of the emulsions. The emulsion stabilized by 0.05% MFC (Figure 5.2A) displayed no MFC network formed in the continuous phase, whereas a slight network formation was found in the 0.30% MFC-stabilized emulsion (Figure 5.2B). But with increasing MFC concentration up to 0.70%, the extent of network formation in the continuous phase became very pronounced (Figure 5.2C). These results revealed an increase in the amount of excess MFC in the continuous phase with increasing MFC concentration used for emulsion stabilization.

The CLSM micrographs show bright fluorescence of MFC, whereas regions completely depleted of the MFC particles appear dark. For all emulsions, the round-shaped bright fluorescence was observed at the perimeter of the emulsion droplets, while the inside remained dark, indicating that the MFC particles were predominantly adsorbed at the oil-water interface of the emulsion droplets (Figure 5.2D-F). The fluorescence intensity observed in the continuous phase also increased with increasing MFC concentration in the emulsions, confirming an increase in excess MFC in the continuous phase.

Overall, it was concluded that the MFC particles were mainly located at the interface of the emulsion droplets, regardless of the MFC concentration used, resulting in a particle-stabilized emulsion, i.e. Pickering emulsion. At higher MFC concentrations, the excess non-adsorbing MFC particles provided an additional functionality by forming three-dimensional networks in the continuous phase, i.e. network stabilization, which played a major role in the properties and stability of these emulsions.

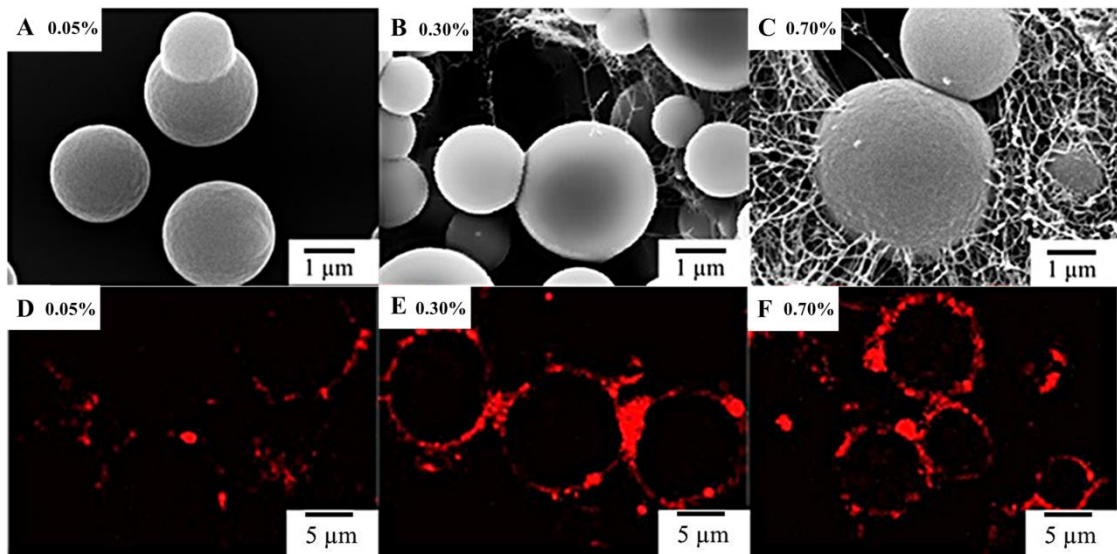


**Figure 5.2** SEM and CLSM micrographs of fresh 10% o/w emulsions stabilized by MFC at different concentrations, i. e. 0.05% (A, D), 0.30% (B, E), and 0.70% (C, F).

#### 5.4.4 Rheological properties

Rheological properties of the MFC-stabilized o/w emulsions as a function of MFC concentration were investigated by measuring their dynamic and steady shear behaviors. Small amplitude oscillatory shear measurement was performed to determine viscoelastic properties of the MFC-stabilized emulsions. The dynamic mechanical spectra of all emulsions show  $G' > G''$  with no crossover throughout the tested frequency range (Figure 5.3A). This behavior could be classified as a typical gel-like behavior (Clark & Ross-Murphy, 1987). The magnitudes of  $G'$  and  $G''$  increased, whereas their frequency dependence decreased with increasing MFC concentration, indicating an increase in the strength of emulsion microstructure with increasing MFC concentration. Moreover, the magnitudes of dynamic mechanical loss tangent ( $\tan \delta = G''/G'$ ) of all emulsions tested were much smaller than unity indicates predominantly elastic behavior (Figure 5.3B). The magnitude of  $\tan \delta$  also decreased with increasing MFC concentration, indicating a more elasticity of the emulsions stabilized by higher MFC concentrations.

For the steady shear measurement, flow curves of all MFC-stabilized emulsions exhibited mainly time-dependent shear-thinning (thixotropic) with yield stress behavior in the shear rate range tested (Figure 5.3C). Herschel-Bulkley model was found to be well fitted to both upward and downward flow curves of all

emulsions, except the upward flow curve of the emulsion stabilized by 0.70% MFC. The Herschel-Bulkley rheological parameters along with the coefficients of determination for each upward and downward flow curve and the hysteresis loop areas between these two curves are summarized in Table 5.3. The degree of thixotropy considerably increased with MFC concentration in which the presence of spurs at low shear rates on the upward flow curves of the emulsions containing  $\geq 0.03\%$  MFC was observed. The spurs define the magnitudes of static yield stress, i.e. the yield stress calculated from the upward flow curve data of the emulsions, which in turn can be related to the strength of the three-dimensional network structure that must be broken down at higher shear rates to cause flow (Oza & Frank, 1986). As expected, the magnitude of static yield stress was higher than that of the dynamic yield stress, i. e. the yield stress calculated from the downward flow curve data. The thixotropic hysteresis loop area is attributed to the breakdown and alignment of the emulsion network structure. That is when the stronger emulsion network structure is deformed, a relatively longer time is required for it to return to its original structure upon removal of shear stress. Therefore, the greater the loop area, the more structured an emulsion is, or vice versa. The results show that the flow behavior index ( $n$ ) values of all tested emulsions were less than unity and decreased with increasing MFC concentration, which suggested that the shear-thinning behavior became more pronounced at higher MFC concentrations. The apparent viscosity ( $\eta_a$ ) of all emulsions decreased with increasing shear rate and increased with MFC concentration (Figure 5.3D) as did the  $G'$  values (Figure 5.3A). The shear-thinning behavior is a typical characteristic of an emulsion containing flocculated droplets, in which the changes in floc size and shape are induced by shearing action (McClements, 2005). These results indicate that a stronger floc structure was formed in the emulsions containing higher MFC concentrations. Moreover, in our previous study (Chapter IV), we have demonstrated that the MFC-stabilized emulsions were not susceptible to shear-induced coalescence under the shear conditions applied during the steady shear measurement. Therefore, the steady shear results obtained in this study should not be significantly affected by the shear-induced coalescence.

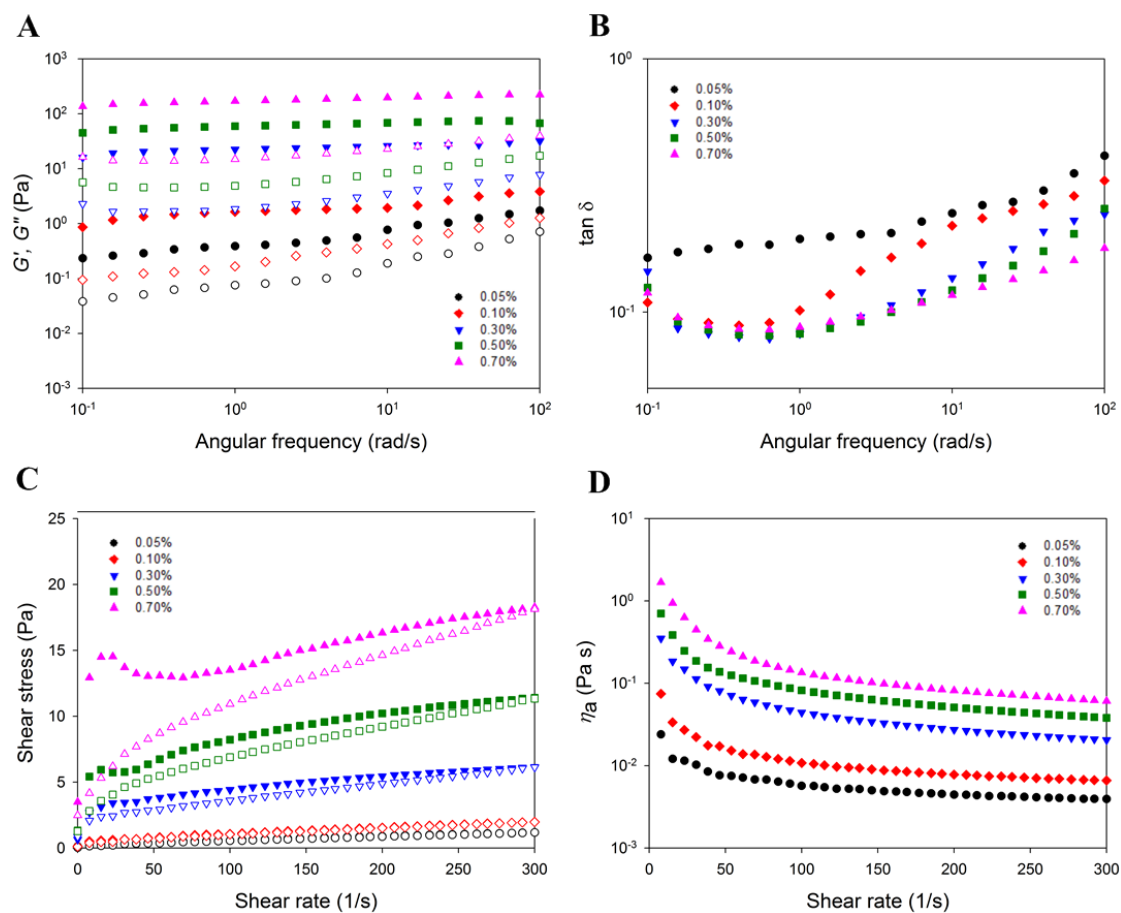


**Figure 5.3** Influence of MFC concentration on (A) mechanical spectra, i. e. storage modulus,  $G'$ , (closed symbols) and loss modulus,  $G''$ , (open symbols) as a function of angular frequency, (B) loss tangent ( $\tan \delta$ ) as a function of angular frequency, (C) flow curves, i. e. shear stress as a function of shear rate, in which closed symbols represent the upward curves and open symbols represent the downward curves, and (D) apparent viscosity,  $\eta_a$ , as a function of shear rate of fresh 10% o/w MFC-stabilized emulsions. All measurements were performed at 25 °C.

**Table 5.3** Influence of MFC concentration on the Herschel-Bulkley parameters of fresh 10% o/w MFC-stabilized emulsions.

MFC concentration (%)	Hysteresis area (Pa/s)	Upward curve			Downward curve				
		$\sigma_0$ (Pa)	$K$ (Pa s <sup>n</sup> )	$n$ (-)	$R^2$	$\sigma_0$ (Pa)	$K$ (Pa s <sup>n</sup> )	$n$ (-)	$R^2$
0.05	8.92±3.18d	0.10±0.002d	0.02±0.001c	0.73±0.002a	0.998	0.07±0.001d	0.01±0.001c	0.76±0.01b	0.996
0.10	16.86±1.38d	0.34±0.003c	0.03±0.001c	0.71±0.01b	0.999	0.27±0.004c	0.03±0.01c	0.73±0.002c	0.998
0.30	182.96±5.93c	2.25±0.13b	0.20±0.01b	0.52±0.01c	0.998	1.99±0.07b	0.04±0.01c	0.81±0.02a	0.999
0.50	324.67±12.19b	3.82±0.18a	0.43±0.01a	0.51±0.01c	0.991	1.90±0.10b	0.38±0.03b	0.56±0.01d	0.999
0.70 <sup>a</sup>	808.45±28.49a	-	-	-	-	2.57±0.04a	0.73±0.03a	0.54±0.001e	0.999

Assays were performed in triplicate. Mean ± standard deviation values in the same column followed by different letters are significantly different ( $p \leq 0.05$ ).

<sup>a</sup>Herschel-Bulkley equation is not fitted to the upward curve of flow.

To further investigate the rheology-structure relationship of the MFC-stabilized emulsions, a comparison between the steady shear viscosity ( $\eta_a$ ) and complex viscosity ( $\eta^*$ ) of the emulsions was performed using the Cox-Merz rule (Cox & Merz, 1958). This rule provides insight on the structure of the sample. Polymer entanglement solutions obey the Cox-Merz rule whereas hyperentanglements or aggregated structures do not (Rao, 2007). The Cox-Merz plots of all emulsions are shown in Figure 5.4A. It was observed that none of the emulsions obeyed the Cox-Merz rule, suggesting that all emulsions exhibited viscoelastic behavior of a weak gel-like structure. The magnitudes of  $\eta^*$  were higher than those of  $\eta_a$ , indicating that network structures are more sensitive to shear forces than to oscillatory movements (Santipanichwong & Suphantharika, 2009). However, the two lines were parallel to each other. Further, by multiplying  $\omega$  in the original Cox-Merz equation by a shift factor ( $\alpha$ ), the two lines could be made to follow a single line with high correlation coefficients ( $R^2 > 0.96$ ) (data not shown). As shown in Figure 5.4B, the shift factors significantly decreased from 0.3000 to 0.0597 as the MFC concentration increased from 0.05 to 0.70%. These results revealed that the deviation from the Cox-Merz rule of the MFC-stabilized emulsions was MFC concentration-dependent, i.e. the deviation between steady shear and dynamic viscosities of the emulsions increased as the MFC concentration increased. From these results, it was concluded that a weak droplet network structure occurred in all tested emulsions, especially at high MFC concentrations (0.30-0.70%) where there was a sufficiently high concentration of colloidal MFC particles presented in the continuous aqueous phase of the emulsions.

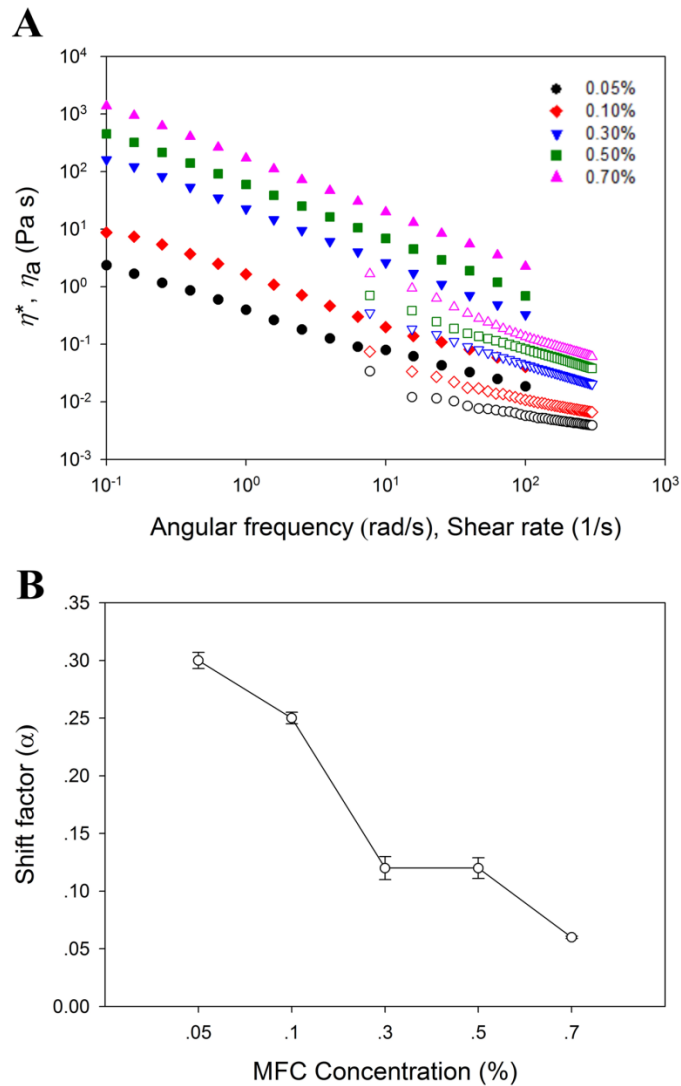


**Figure 5.4** Influence of MFC concentration on (A) Cox-Merz plot, i. e. complex viscosity,  $\eta^*$ , (closed symbols) versus steady shear viscosity or apparent viscosity,  $\eta_a$ , (open symbols) and (B) shift factors of fresh 10% o/w MFC-stabilized emulsions.

Overall, there was a good relationship between the rheology of the emulsions determined by both dynamic and steady shear measurements and their microstructures visualized using SEM and CLSM. Based on these rheological measurements and microscopic observations (Figure 5.2), it was proposed that the MFC particles provide their functionality by adsorbing at the oil-water interface (Pickering stabilization) or by developing a gel-like microstructure composed of flocculated oil droplets and a viscoelastic network of the MFC particles in the aqueous

phase between the droplets (network stabilization), or by a combination of these processes.

### **5.4.5 Emulsion stability**

#### **5.4.5.1 Stability against coalescence**

Comparisons of the mean droplet sizes and droplet size distributions between the 1- and 80-day stored emulsions are shown in Table 5.1 and Figure 5.1, respectively. There was no significant change in  $d_{32}$  and  $d_{43}$  with storage time, except  $d_{32}$  of the emulsions stabilized by low MFC concentrations (0.05-0.10%), which significantly increased (Table 5.1). However, it should be noted that  $d_{43}$  is more sensitive to the presence of large particles in an emulsion than  $d_{32}$ , hence it is often more sensitive to phenomenon such as coalescence (McClements, 2005). Therefore,  $d_{43}$  should be more appropriate and more accurate in determining change in droplet size due to droplet coalescence. The emulsions did not show any change in the droplet size distributions on storage for 80 days (Figure 5.1). These results imply negligible droplet coalescence over the entire storage period. It is well recognized that the high resistance to coalescence is a major benefit of the emulsion stabilized by solid particles (Chevalier & Bolzinger, 2013). For the particles of intermediate wettability, they are effectively and irreversibly adsorbed at the oil-water interface due to an extremely high free energy of adsorption compared with the thermal energy (Aveyard, Binks, & Clint, 2003; Dickinson, 2010, 2012). These adsorbed solid particles act as a steric (mechanical) barrier against droplet-droplet coalescence. Therefore, the particle-stabilized emulsions are extremely stable to coalescence even when the emulsion droplets are quite large. These results are in good agreement with those of the o/w emulsions stabilized by chitin nanoparticles (Tzoumaki et al., 2011) and modified starch particles (Yusoff & Murray, 2011) at various concentrations, in which the mean particle size of oil droplets did not exhibit any change after storage for 30 days and 90 days, respectively.

#### **5.4.5.2 Stability against creaming**

Creaming behavior of the o/w emulsions stabilized by MFC at different concentrations is shown in Figure 5.5A. The emulsions stabilized by low

MFC concentrations ( $\leq 0.30\%$ ) creamed readily, in which the creaming rate and extent increased with decreasing MFC concentration. On the contrary, the emulsions stabilized by high MFC concentrations ( $\geq 0.50\%$ ) did not cream throughout the entire storage period of 80 days. For the creamed emulsions, the creaming index (*CI*) of the emulsions stabilized by 0.05, 0.10, and 0.30% MFC reached their plateau values of 45.0, 33.0, and 9.6%, respectively at the same storage time of 22 days followed by a slight increase to 47.1, 33.8, and 9.7%, respectively after storage for 80 days. As expected, the emulsions stabilized by lower MFC concentrations had lower stability against creaming due to their lower degree of three-dimensional structures as evidenced by their lower yield stress (Table 5.3) and  $G'$  (Figure 5.3A) values compared to those of the emulsions stabilized by higher MFC concentrations. This led to a higher mobility of droplets and consequently higher degree of creaming. Despite the emulsions stabilized by high MFC concentrations had significantly larger droplet sizes than the ones stabilized by low MFC concentrations (Table 5.1), they had extremely high stability against creaming ( $CI = 0$ ) during storage for 80 days. This could be attributed to the depletion-flocculated network, i.e. a three-dimensional network of droplets and MFC particles, formed in the presence of non-adsorbing excess MFC particles (Figure 5.2C), which was evidenced by their higher yield stress (Table 5.3) and  $G'$  (Figure 5.3A) values (Winuprasith & Suphantharika, 2013). Therefore, the inhibition of creaming was probably due to immobilization of the dispersed oil droplets in a weak gel-like network of aggregated droplets, i.e. an emulsion gel (Dickinson, 2003; Tzoumaki et al., 2011). These emulsions therefore had an extremely long shelf-life and were aesthetically attractive. In summary, the emulsions containing high MFC concentrations ( $\geq 0.50\%$ ) exhibited a good stability against creaming, mainly due to their high viscosity, whereas the droplet size did not play an important role in creaming.

Photographs of the MFC-stabilized emulsions taken after storage at room temperature for 1 day and 80 days are shown in Figure 5.5B. The emulsions stabilized by  $\leq 0.30\%$  MFC showed a slight creaming after storage for 1 day which was followed by a significant increase in creaming after 80 days storage, whereas those stabilized by  $\geq 0.50\%$  MFC exhibited no creaming throughout the entire storage period. The creamed emulsions displayed a sharp boundary between a top

cream layer and a bottom serum layer. The turbidity of serum increased with decreasing MFC concentration. The serum turbidity gives an indication of whether the emulsion is fully flocculated or contains flocs in coexistence with unflocculated droplets. It is generally known that the higher the degree of droplet flocculation, the serum phase becoming more transparent (Manoj, et al., 1998). Therefore, the 0.05% and 0.10% MFC-stabilized emulsions exhibited creaming of individual droplets or discrete flocs and the serum phase remained cloudy throughout the storage period, indicating the presence of a small residue amount of suspended individual oil droplets, whereas the 0.30% MFC-stabilized emulsion creamed by gravity-induced collapse of an emulsion gel which left behind a transparent serum layer from the beginning. These results confirmed that the degree of droplet flocculation in the MFC-stabilized emulsions increased with MFC concentration.

It is generally recognized that creaming or flocculation is not considered as an indication of instability unless it is associated with droplet coalescence since the emulsion droplets can be easily re-dispersed by means of gentle stirring (Oza & Frank, 1986; Kalashnikova et al., 2011; Chevalier & Bolzinger, 2013).

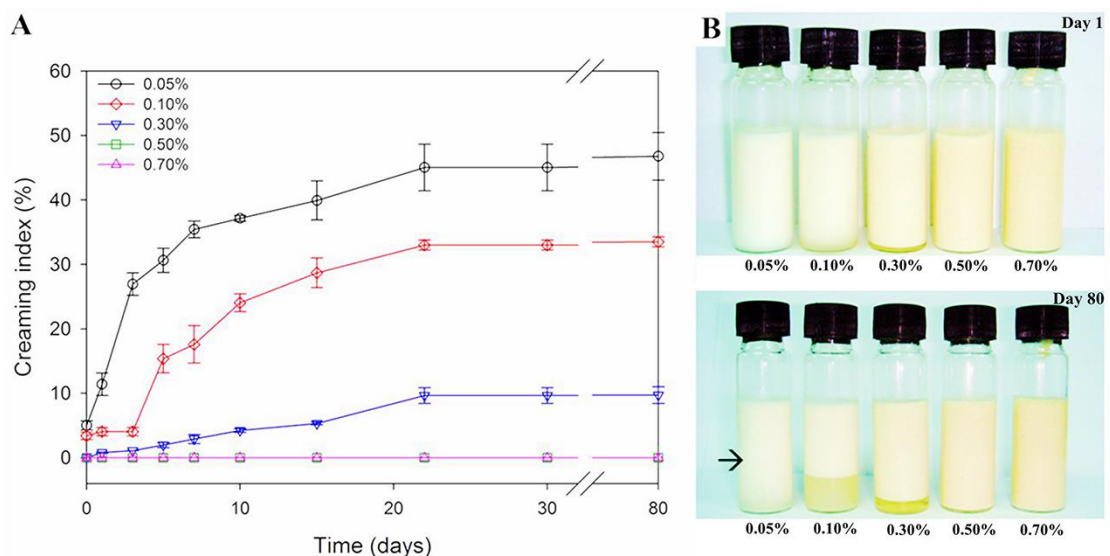


**Figure 5.5** Influence of MFC concentration on creaming profiles of 10% o/w MFC-stabilized emulsions during storage at room temperature for 80 days (A). Photographs of the 1- and 80-day stored emulsions (B). Arrow marks cream-serum boundary.

## 5.5 Conclusions

The physical and rheological properties and stability of the MFC-stabilized emulsions were strongly influenced by the concentration of MFC. An increase in MFC concentration led to larger droplets, darker and more color, more pronounced elastic responses, and higher stability to creaming of the emulsions. However, all emulsions, regardless of the MFC concentration used, possessed long-term storage stability against droplet coalescence. A possible mechanism of MFC for o/w emulsion formation and stabilization could be due to the adsorption of MFC at the oil-water interfaces, providing a steric (mechanical) barrier against droplet coalescence by the Pickering mechanism. Additionally, with an increase in MFC concentration, the formation of a three-dimensional network of the excess MFC particles in the continuous aqueous phase immobilized the droplets thereby preventing creaming. This study provides practical information that may increase the utilization of MFC as natural emulsifying and stabilizing ingredients in food products. Then, we have focused on biopolymer-stabilized solid particles, namely  $\beta$ -lactoglobulin-coated gold nanoparticles and used as a model of protein-coated oil emulsion droplets to increase understanding about the role of stabilizing mechanism and protein conformational changes after adsorption onto the surfaces. In Chapter VI, the difference analytical approaches from this Chapter (polysaccharide-stabilized liquid surfaces) were performed to study the interaction between protein and gold nanoparticles (protein-stabilized solid particles), such as determination of surface plasmon resonance, and surface-enhanced Raman scattering, etc.

## **CHAPTER VI**

### **SPECTROSCOPIC STUDIES OF CONFORMATIONAL CHANGES OF $\beta$ -LACTOGLOBULIN ADSORBED ON GOLD NANOPARTICLE SURFACES**

#### **6.1 Abstract**

In this work, we investigated the conformational changes of a globular protein ( $\beta$ -lactoglobulin,  $\beta$ Lg) coated on the surface of 200 nm gold nanoparticles (GNPs) using a number of analytical techniques: dynamic light scattering (DLS); particle electrophoresis ( $\zeta$ -potential); localized surface plasmon resonance (LSPR) spectroscopy; transmission electron microscopy (TEM); and surface-enhanced Raman scattering (SERS). The  $\beta$ Lg (pH 3) concentration had a pronounced effect on the aggregation and surface charge of  $\beta$ Lg-coated GNPs. The surface charge of GNPs changed from negative to positive as increasing amounts of  $\beta$ Lg molecule were added, indicating that the globular protein molecules adsorbed to the surfaces of the particles. Extensive particle aggregation occurred when  $\beta$ Lg did not saturate the GNP surfaces, which was attributed to electrostatic bridging flocculation. Modifications in LSPR and SERS spectra after addition of  $\beta$ Lg to the GNP suspensions supported the adsorption of  $\beta$ Lg to the particle surfaces. Moreover, SERS highlighted the importance of a number of specific molecular groups in the binding interaction, and suggested conformational changes of the globular protein after adsorption. This research provides useful information for characterizing and understanding the interactions between globular proteins and colloidal particles.

## 6.2 Introduction

The adsorption of globular proteins to the surfaces of particles is important in a number of physicochemical and biological phenomena relevant to the development of high quality, safe, and healthy foods. Proteins adsorb to the surfaces of fat droplets and gas bubbles during the production of emulsions and foams, which plays an important role in their stability to particle growth and aggregation (Dickinson, 2003; McClements, 2005; Kralova & Sjoblom, 2009). Proteins adsorb to the surfaces of ice crystals during their formation and subsequent growth, which is important in the development of anti-freeze systems (Venketesh & Dayananda, 2008). Lipases are a group of digestive enzymes that adsorb to the surfaces of fat droplets within the gastrointestinal tract and promote lipid digestion (Wilde & Chu, 2011). Other enzymes may be immobilized on the surfaces of solid particles to improve their utilization or activity (Talbert & Goddard, 2012). Proteins may adsorb onto the surfaces of ingested metallic nanoparticles (such as gold or silver) in foods, thereby altering the biological fate of both the proteins and nanoparticles (Hussain, Jaitley, & Florence, 2001; Powell et al., 2010). It is therefore important to understand the influence of protein adsorption onto particle surfaces on both protein and particle properties.

A globular protein may undergo structural changes after adsorption to the surfaces of particles, which alters its functional properties (Adams, Higgins, & Jones, 2002; Iosin, Toderas, Baldeck, & Astilean, 2009; Mezzenga & Fischer, 2013). On the other hand, protein adsorption may influence the aggregation state of the particles, by inducing bridging or depletion flocculation (Dickinson, 2010; Lesmes, Sandra, Decker, & McClements, 2010; Schmelz, Lesmes, Weiss, & McClements, 2011). In this study, we used  $\beta$ -lactoglobulin as a model globular protein and 200 nm gold nanoparticles (GNPs) as model colloidal particles to study protein-particle interactions.  $\beta$ -Lactoglobulin ( $\beta$ Lg) is the major globular protein in bovine milk and its structure, properties, and biological role are well established. This protein usually exists as a dimer at neutral pH, but dissociates into monomers below pH 3. Each monomer comprises 162 amino acid residues, with one free cysteine and two disulfide bridges. The molecular weight is 18,350 Da. The secondary structure of native  $\beta$ Lg is mainly composed of  $\beta$ -sheet (54%) and  $\alpha$ -helices (17%) (Link, Mohamed, & El-

Sayed, 1999; Van Der Zande, Böehmer, Fokkink, & Schöenenberger, 2000; El-Sayed, 2001).

GNPs are attractive for many biological and medical applications due to their chemical stability, biocompatibility, and unique optical properties (Blanch, Hecht, & Barron, 1999; Ngarize, Herman, Adams, & Howell, 2004; Ding, Chen, Xie, & Guo, 2008; Seo, Hédoux, Guinet, Paccou, Affouard, Lerbret et al., 2010). Typical diameters of GNPs are between 1 and 100 nm. The experiments were performed using 200 nm GNPs due to the reason that in most real food systems, the diameter of the oil droplets or other solid particles are usually larger than 100 nm (McClements, 2005). In addition, we took the advantage of surface enhanced Raman scattering (SERS) property of GNPs to study the protein conformation adsorbed onto the GNPs. Raman spectroscopy is a vibrational spectroscopic technique, which is widely used for molecular identification and structural characterization. Raman techniques have been applied widely to study protein conformation both in solid states and in solution with varying environmental conditions, such as temperature, and pH (Wang, He, Labuza, & Ismail, 2013). Raman spectroscopy can provide information related to protein backbone conformation and the molecular environment of certain side chains, as well as the transitions from ordered to disordered structure upon protein denaturation. The Raman scattering is also sensitive to changes in covalent bonds, such as disulfide linkages, and non-covalent bonds, such as electrostatic and hydrophobic interactions (Li-Chan, 1996). When an analyst is in close proximity to a metallic (typically silver or gold) nano-surface, an enhanced Raman scattering is produced, so called surface-enhanced Raman scattering (SERS). The enhancement has been attributed to electromagnetic enhancement and chemical charge transfer mechanism (Brewster, Jarvis, & Goodacre, 2009). SERS is therefore a sensitive and promising technique to observe the molecular conformational change of biopolymers on a nanosubstrate.

In this study, we used a variety of analytical techniques to better understand protein-particle interactions: dynamic light scattering (DLS), particle electrophoresis ( $\zeta$ -potential), localized surface plasmon resonance (LSPR), transmission electron microscopy (TEM), and surface-enhanced Raman scattering (SERS). This study focuses on the influence of  $\beta$ Lg concentration on protein conformational changes and particle aggregation. This research provides useful

information for understanding and characterizing the interactions of globular proteins with colloidal particles.

## **6.3 Materials and methods**

### **6.3.1 Materials**

Powdered  $\beta$ Lg was obtained from Davisco Foods International (Lot JE 001-0-415, Le Sueur, MN). As stated by the manufacturer, the protein content was 97.4% w/w (dry basis), the purity was 95% w/w,  $\beta$ Lg and the nitrogen content was 15.6% w/w. A suspension of 200 nm gold nanoparticles ( $7 \times 10^8$  particles/mL) in citrate buffer (pH 3) was purchased from Ted Pella, Inc. (Redding, CA). Analytical grade acetic acid, hydrochloric acid, sodium acetate, and sodium hydroxide were purchased from Sigma Chemical Company (St. Louis, MO). Double distilled water was used throughout the experiments.

### **6.3.2 $\beta$ Lg solution preparation**

A  $\beta$ Lg solution was prepared at ambient temperature (22 °C) by dissolving powdered  $\beta$ Lg in 5 mM acetate buffer solution (pH 3). A series of solutions with  $\beta$ Lg concentrations ranging from 0 to 6000  $\mu$ M was prepared. The  $\beta$ Lg solutions were stirred gently for 3 h to ensure complete protein dissolution. If required the pH of these solutions was readjusted to pH 3.0 using either 1 M HCl and/or 1 M NaOH.

### **6.3.3 Gold nanoparticle (GNPs) interaction with $\beta$ Lg**

The interaction of the globular proteins with the gold nanoparticles (GNPs) was studied by adding 20  $\mu$ L of  $\beta$ Lg solution into a 1.5 mL microcentrifuge tube. Then, 1000  $\mu$ L of GNP solution was added drop wise under vigorous mixing for 5 min. Thus, the original protein concentration was reduced by a factor of 20/1020, and the original GNP concentration was reduced by a factor of 1000/1020. The mixture was incubated overnight under consistent orbital rotation at ambient temperature (22 °C). The pH of mixture was kept constant at pH 3. At pH 3,  $\beta$ Lg is positively charged while GNPs are negatively charged, and so they can interact with each other through

electrostatic attraction. After incubation, the mixed  $\beta$ Lg–GNP suspensions were analyzed.

#### **6.3.4 Particle size and charge measurement**

The particle size and charge of bare and coated GNPs were determined using a commercial dynamic light scattering/particle electrophoresis device (Nano-ZS, Malvern Instruments, Worcestershire, UK), as described in Section 3.7.1.

#### **6.3.5 UV–visible spectrophotometer**

The ultraviolet spectrum (250–900 nm) of the  $\beta$ Lg-coated GNPs was recorded with a UV/Vis scanning spectrophotometer (model UV-2101 PC, Shimadzu Scientific Instruments Inc., Columbia, MD) to determine the peak of the gold plasmon band.

#### **6.3.6 Transmission electron microscopy (TEM)**

The morphology and distribution of the  $\beta$ Lg-coated GNPs were analyzed by transmission electron microscopy (model 2000FX, JEOL, Tokyo, Japan) (Section 3.7.3).

#### **6.3.7 Surface-enhanced Raman spectroscopy (SERS)**

The SERS measurement was then conducted immediately using a DXR Raman microscope (Thermo Scientific, Madison, WI) equipped with a 10 $\times$  microscope objective (Section 3.6.4). The SERS spectra were collected from different points ( $N = 24$ ) on the sample in order to ensure the reproducibility of the measurements.

### **6.4 Results and discussion**

#### **6.4.1 Properties of bare GNPs**

Initially, we characterized the electrical properties ( $\zeta$ -potential) and dimensions (particle diameter) of the bare GNPs used in this study. The bare GNPs

had a  $\zeta$ -potential of  $-56.5$  mV, which can be attributed to the negatively charged citrate side-groups on the particle surfaces (Lee, Kim, Yoon, Gong, Choi, Kim, & Joo, 2004; Iosin et al., 2009; Masereel, Dinguizli, Bouzin, Moniotte, Feron, Gallez, et al., 2010; Seo et al., 2010; Iosin, Canpean, & Astilean, 2011). The high negative charge on the bare GNPs accounts for their good stability to aggregation, since they will be prevented from coming into close proximity due to the strong negative charge on their surfaces. One of the most important factors affecting the interaction of the proteins with the GNPs is the pH, since this will influence the electrical characteristics of both the proteins and particles. Previous studies have shown that the net charge on  $\beta$ Lg molecules goes from positive to negative as the pH is increased from below to above the proteins isoelectric point (Georgescu, Alexov, & Gunner, 2002). The isoelectric point of  $\beta$ Lg has been reported to be around pH 5 (Kontopidis, Holt, & Sawyer, 2004; McClements, 2010). In our case, we mixed the  $\beta$ Lg solution and GNPs at pH 3, and so the protein molecules should have a strong positive charge which will promote their adsorption to the negative GNPs surfaces through electrostatic attraction (Masereel et al., 2010; Seo et al., 2010; He et al., 2013). The initial mean diameter of the bare GNPs determined by dynamic light scattering was around 186 nm.

#### 6.4.2 Particle charge characteristics

The interactions of the protein molecules with the GNPs were initially studied using particle charge measurements (Figure 6.1). The  $\zeta$ -potential went from highly negative to highly positive as the concentration of  $\beta$ Lg added to the GNP suspensions was increased, with a point of zero charge around 2500  $\mu$ M  $\beta$ Lg. At sufficiently high protein concentrations a relatively high constant positive charge (+22 mV) was reached, suggesting that the surfaces of the gold nanoparticles were saturated with protein. The particle charge results suggested that the GNPs were saturated with protein around 5000  $\mu$ M  $\beta$ Lg, since there was no further change in the  $\zeta$ -potential when the protein concentration was increased further. This value was used to estimate the surface load of the protein at the gold surfaces. The surface load at saturation ( $\Gamma_{\text{Sat}}$ ) can be calculated using the following expression (McClements, 2005):

$$\Gamma_{\text{Sat}} = \frac{c_{\text{Sat}}d_{32}}{6\phi} \quad (6.1)$$

Here,  $C_{\text{Sat}}$  is the mass of material adsorbed to the surface of the particles per unit volume of suspension ( $\text{kg m}^{-3}$ ),  $d_{32}$  is the volume-surface mean particle diameter of the bare particles (m), and  $\phi$  is the volume fraction of the GNPs. The mean particle diameter of the GNPs was determined in this study:  $d_{32}$  0.186  $\mu\text{m}$ . The particle volume fraction was estimated from the information about the particle concentration in the GNP suspension. The particle concentration in GNP suspension was calculated according to the absorbance of the suspension at 450 nm (Haiss, Thanh, Aveyard, & Fernig, 2007). The GNP suspension contained  $8.22 \times 10^9$  particles/mL, which is equivalent to a volume fraction of  $2.77 \times 10^{-5}$ . The mass of material adsorbed to the surface of the particles at saturation ( $C_{\text{sat}}$ ) estimated from the  $\zeta$ -potential measurements (i.e.,  $\beta\text{Lg} = 20/1020 \times 5000 \mu\text{M}$ ) was  $0.00545 \text{ kg m}^{-3}$ . These values were used to calculate the surface load from equation 6.1, giving  $\Gamma_{\text{Sat}} = 6.2 \text{ mg m}^{-2}$ . This value is in reasonable accordance with surface load of this protein typically reported for adsorption to the surfaces of lipid droplets (around 1–10  $\text{mg m}^{-2}$ ) (McClements, 2005; Ye & Singh, 2006, 2007; Mao & McClements, 2011).

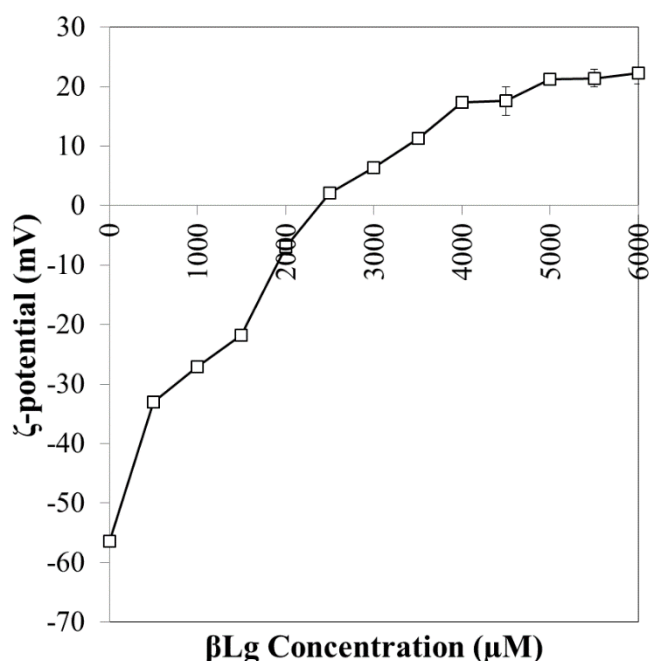


**Figure 6.1**  $\zeta$ -Potential of bare GNPs and  $\beta$ Lg-coated gold nanoparticles with varying  $\beta$ Lg concentrations.

It would have been informative to apply a thermodynamic binding model to our system to provide additional information about the magnitude of the binding constant, and the nature of the binding interactions. However, the concentration of protein adsorbed to the gold nanoparticle surfaces, as well as the concentration of non-adsorbed protein in the continuous phase is needed to apply these models. Unfortunately, we were unable to reliably separate the gold nanoparticles from the aqueous continuous phase and measure the free protein concentration, and therefore we could not apply a full binding model (such as the Langmuir adsorption isotherm). In addition, proteins are known to undergo thermal denaturation and reorganization after adsorption to interfaces, which cannot simply be accounted for in thermodynamic models.

#### 6.4.3 Particle size and aggregation

Visual observations and digital photographs of aqueous GNPs and  $\beta$ Lg–GNP suspensions containing different amounts of protein were carried out (Figure 6.2). Suspensions containing 2000–3500  $\mu$ M  $\beta$ Lg showed evidence of precipitated GNPs at the bottom of the test tubes, while the other samples did not. These results were supported by particle size measurements using dynamic light scattering which showed that the mean particle diameter was appreciably higher at intermediate protein concentrations (Seo et al., 2010). The Z-average increased from 200 to 6800 nm when the  $\beta$ Lg concentration was increased from 0 to 2500  $\mu$ M, then decreased to about 230 nm when the  $\beta$ Lg concentration was further increased to 5000  $\mu$ M. Any further increases in protein concentration did not cause an appreciable change in the mean particle diameter, suggesting that the particles were stable to aggregation at high protein concentrations.

It is convenient to divide our experimental observations into three different regimes depending on the protein concentration ( $C$ ):

(i)  $C = 0$ . The GNPs are stable to aggregation because of the strong electrostatic repulsion between them.

(ii)  $0 < C < C_{\text{Sat}}$ . Charge neutralization and bridging flocculation occurs when the  $\beta$ Lg concentration is insufficient to completely saturate the particle surfaces ( $C_{\text{Sat}}$ ). Charge neutralization leads to a reduced electrostatic

repulsion between the particles, whereas bridging occurs because there are both positive and negative patches on the particle surfaces.

(iii)  $C_{\text{Sat}} < C_{\text{Dep}}$ . The particles should be stable to droplet aggregation when their surfaces are completely saturated with  $\beta$ Lg molecules due to the high electrostatic and steric repulsion between them.

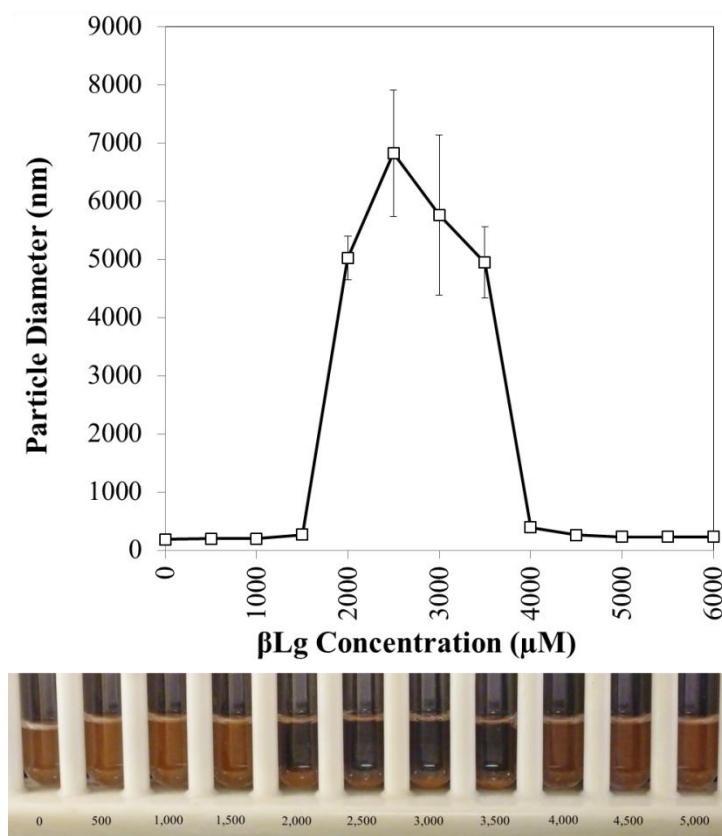


**Figure 6.2** Diameter of bare GNPs and  $\beta$ Lg-coated GNPs with varying  $\beta$ Lg concentrations. The inset shows visual observation of  $\beta$ Lg–GNP mixtures.

Comparing the  $\zeta$ -potential (Figure 6.1) and particle size (Figure 6.2) measurements suggests that the protein concentration required to stabilize the GNPs against aggregation is fairly similar to that required for saturation of the surfaces with protein. At high protein concentration, we postulate that the GNPs were coated by a thin layer of protein, and additional protein was present in the aqueous phase.

#### 6.4.4 UV–visible absorption spectra

To confirm the adsorption of  $\beta$ Lg molecules to the surfaces of the GNPs, the UV–visible absorption spectra of GNPs in the absence and presence of the protein was measured (Figure 6.3). A  $\beta$ Lg solution at concentration of 1000  $\mu$ M was used to carry out this comparison so as to avoid particle aggregation effects. The absorption spectrum of a protein solution in the absence of the gold nanoparticles was also measured. The bare GNPs suspension exhibited a broad surface plasmon resonance band around 579 nm. The  $\beta$ Lg solution exhibited a broad absorption band around 279 nm, which can be attributed to the presence of aromatic residues such as tryptophan and tyrosine. The measurements on the isolated protein and GNPs systems show that their absorption peaks can clearly be distinguished from each other. The spectral position of the peak in the surface plasmon resonance band of the protein-coated GNPs was red-shifted compared to that of the bare GNPs: from 579 to 584 nm. This shift suggests that the protein molecules adsorbed to the surfaces of the GNPs and modified their refractive index thereby altering their absorption and scattering behavior (Li, Guo, & Wang, 2008; Masereel et al., 2010; Iosin, Canpean, & Astilean, 2011; Cañaveras, Madueño, Sevilla, Blázquez, & Pineda, 2012).

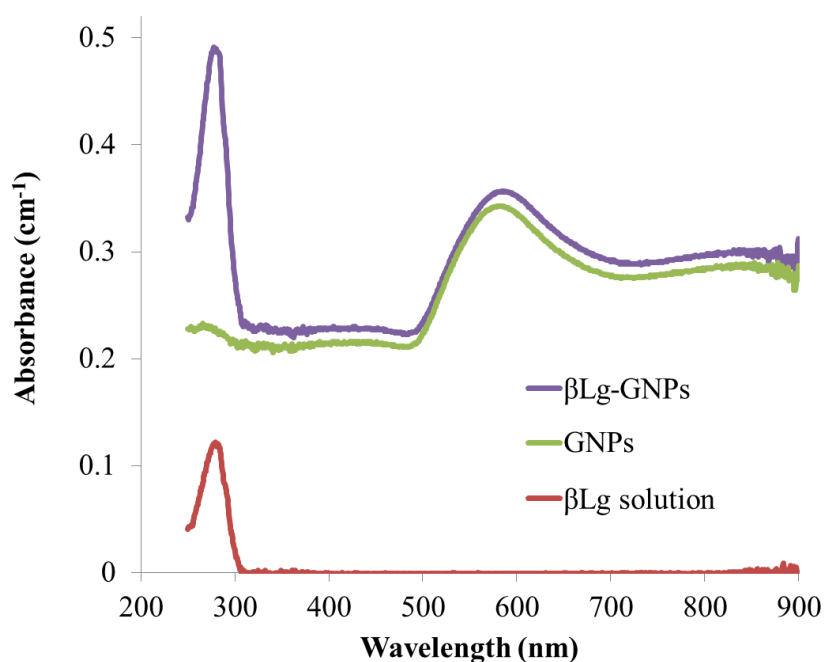


**Figure 6.3** Absorption spectra of  $\beta$ Lg solution at concentration of 1000  $\mu$ M, bare GNPs in solution and  $\beta$ Lg-coated GNPs at 5000  $\mu$ M  $\beta$ Lg concentration.

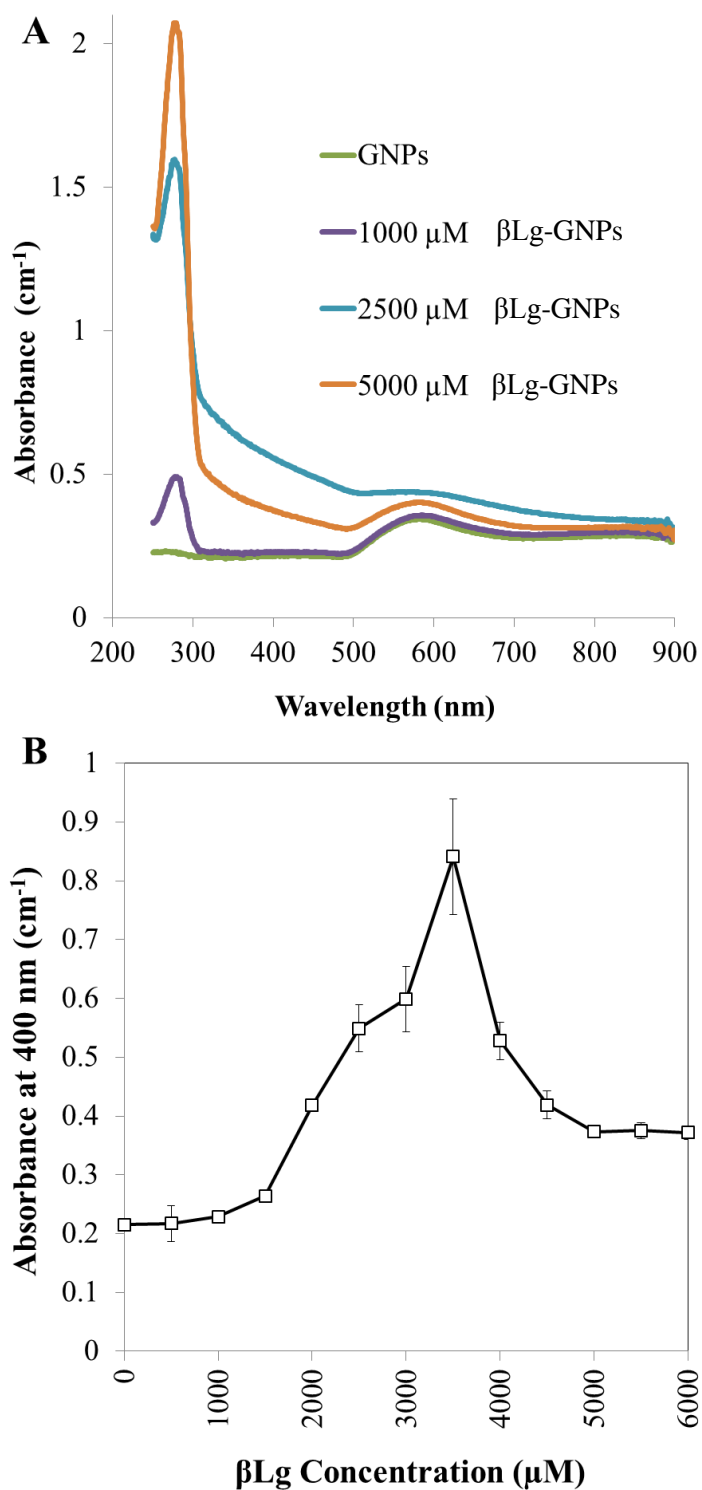


**Figure 6.4** Influence of  $\beta$ Lg concentration on (A) absorption spectra of  $\beta$ Lg-coated GNPs at 1000, 2500 and 5000  $\mu\text{M}$   $\beta$ Lg concentration, and (B) absorbance at 400 nm of  $\beta$ Lg-coated GNPs suspensions.

The  $\beta$ Lg concentration in the protein-GNPs suspensions had a pronounced influence on their absorbance spectra (Figure 6.4A). We therefore plotted the absorbance at 400 nm as a function of protein concentration (Fig 6.4B). The wavelength is between the surface plasmon resonance band for the GNPs and the absorption band for the proteins, and should therefore provide information about particle aggregation. The absorbance was relatively low from 0 to 1500  $\mu$ M  $\beta$ Lg, relatively high from 1500 to 4500  $\mu$ M  $\beta$ Lg, and then relatively low again at higher protein concentrations. These results are in close agreement with the particle size measurements (Figure 6.2), and suggest that measurements at this wavelength are sensitive to particle aggregation.

#### **6.4.5 Transmission electron microscopy (TEM)**

The presence of  $\beta$ Lg at surface of GNPs was confirmed by transmission electron microscopy (TEM). TEM images clearly show particles with a core-shell structure (Figure 6.5D). Presumably, the core is a gold nanoparticle, while the shell is a layer of protein molecules (Chantrapornchai, Clydesdale, & McClements, 1999; Cañaveras et al., 2012). This protein layer has previously been divided into a “soft” component that rapidly exchanges with non-adsorbed proteins, and a “hard” component that has a high affinity for the particle surface (Cedervall, Lynch, Lindman, Berggård, Thulin, & Nilsson, 2007; Cedervall, Lynch, Foy, Berggård, Donnelly, Cagney, et al., 2007). TEM images of GNP suspensions with different protein concentrations were also recorded (Figure 6.5). Limited protein aggregation was observed at low (1000  $\mu$ M) and high (5000  $\mu$ M) protein concentrations, but extensive aggregation was observed at intermediate (2500  $\mu$ M) protein concentration, which can be attributed to charge neutralization and bridging effects mentioned earlier.

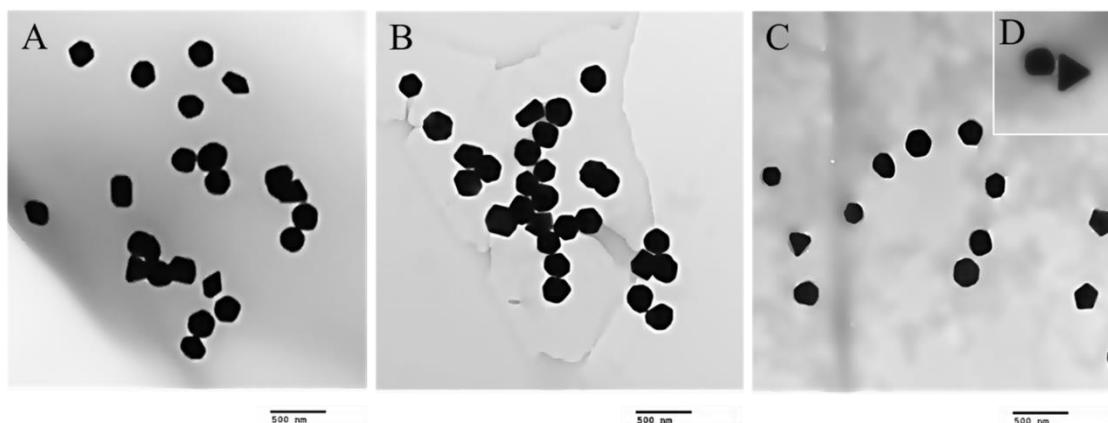


**Figure 6.5** Transmission electron microscopy of  $\beta$ Lg-coated GNPs at 1000  $\mu$ M (A), 2500  $\mu$ M (B), and 5000  $\mu$ M (C)  $\beta$ Lg concentrations. A representative of TEM micrograph of  $\beta$ Lg-coated GNPs with a layer contour of protein corona (D).

#### 6.4.6 Surface-enhanced Raman spectroscopy (SERS)

More specific molecular information about the interactions of the  $\beta$ Lg molecules with the GNP surfaces was obtained using SERS spectroscopy. Proteins have a number of characteristic signals in their spectra with well understood peak assignments (Li-Chan, 1996; Link, Mohamed, & El-Sayed, 1999; Das, Gentile, Coluccio, Perri, Nicastri, Mecarini, et al., 2011; El-Sayed, 2001; Ikeda, 2003; Shang, Wang, Jiang, & Dong, 2007). Initially, the conventional Raman spectrum of  $\beta$ Lg in solution (5000  $\mu$ M, pH 3) was measured in the region 400–2000  $\text{cm}^{-1}$  to determine the characteristic absorption peaks of this protein (Figure 6.6A), and a negative control spectrum of the GNPs in the absence of protein was measured to establish its absorption peaks (Figure 6.6B). The SERS spectra of mixed systems containing GNPs and different amounts of protein were also measured: 1000  $\mu$ M  $\beta$ Lg (spectrum C), 2500  $\mu$ M  $\beta$ Lg (spectrum D), and 5000  $\mu$ M  $\beta$ Lg (spectrum E). These results clearly show that there was an appreciable change in the SERS spectra with increasing protein concentration. A significant difference was observed between all the  $\beta$ Lg-coated GNPs and the bare GNPs, indicating that  $\beta$ Lg was present at the GNP surfaces at all concentrations studied. Significant differences were also found when comparing  $\beta$ Lg on GNPs with  $\beta$ Lg in solution (without GNPs).

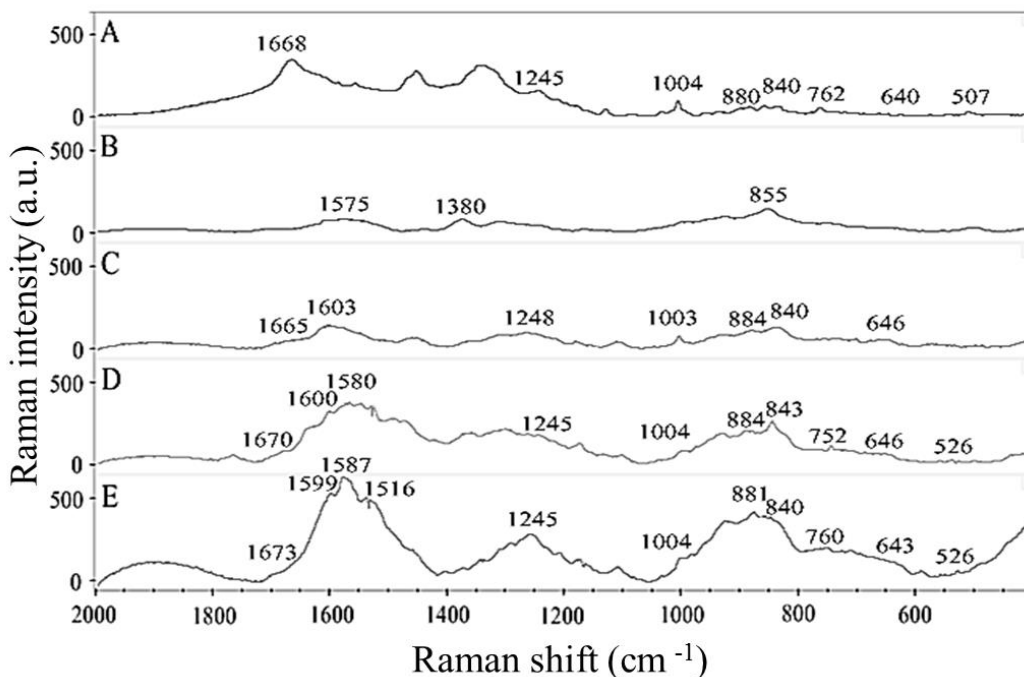


**Figure 6.6** Raman spectrum of  $\beta$ Lg in solution (A) and SERS spectra of  $\beta$ Lg-coated GNP at 1000  $\mu$ M (C), 2500  $\mu$ M (D), and 5000  $\mu$ M (E)  $\beta$ Lg concentrations. Bare GNPs was used as a negative control (B).

(i) A clear concentration dependent trend was found for certain peaks. The  $\text{NH}_2/\text{NH}_3^+$  peaks at 1600, 1587, 1516, 1245, 840  $\text{cm}^{-1}$  significantly increased when increasing the  $\beta$ Lg concentration, especially one  $\text{NH}_3^+$  peak at 1516  $\text{cm}^{-1}$  (assigned as  $\text{NH}_3^+$  deformation) appearing in spectra E (5000  $\mu$ M  $\beta$ Lg). This indicates the interaction between the  $\beta$ Lg and GNPs were mainly through amino groups. These peaks were primarily enhanced due to a chemical enhancement mechanism (Brewster, Javis, & Goodacre, 2009). In addition, some degree of data variance was observed in the ranges for the amino peaks, resulting in noise-like waves in the average spectra, which may be due to multiple binding sites of amino groups to the GNPs. On the other hand, the fact that no significant  $\text{COO}^-$  peak at 1410  $\text{cm}^{-1}$  was observed indicated that the carboxylate groups were not involved in the interactions, presumably due to the electric repulsion between the negative  $\text{COO}^-$  group and the negatively charged gold surface. Other studies on amino acids adsorption to silver nanoparticle surfaces also reported that the amino group was the preferential structure

for binding, although a very small fraction of the C-terminal residues were also reported to be in contact with the metal surface (Garrell, 1991; Chuang & Chen, 2009). In addition, we did not observe a significant intensity increase due to the aggregation of the GNPs (with 2500  $\mu$ M of protein). This may be due to the fact that we used relatively large GNPs (200 nm) and measured them in solution, therefore, the “hot-spot” effects of GNPs aggregation was minimized.

(ii) The secondary structure of  $\beta$ Lg is mainly composed of  $\beta$ -sheets (54%),  $\alpha$ -helices (17%), and other structures (Van Der Zande et al., 2000). The intense band located at 1668  $\text{cm}^{-1}$  in the  $\beta$ Lg solution spectrum is the amide-I band. This band arises mainly from the C–O stretching vibration with minor contributions from N–H wagging. The band shape of the amide-I modes can be considered overlapping bands representing  $\alpha$ -helices,  $\beta$ -sheets, turns, and random structures (Surewicz, Mantsch, & Chapman, 1993; Li-Chan, 1996). The amide-I peaks in the samples containing  $\beta$ Lg and GNP (spectra C–E) were all greatly reduced and slight shifted from 1665 to 1673  $\text{cm}^{-1}$  with increasing protein concentration. This red shift may be interpreted as a more disordered structure (Li-Chan, 1996). A similar reduction of amide-I peak was also observed in the SERS study of bovine serum albumin (pH 2) adsorbed onto 18 nm GNPs (Iosin, Canpean, & Astilean, 2011). The amide-II peaks and amide-III peaks at around 1600–1500 and 1235–1275  $\text{cm}^{-1}$ , respectively, greatly increased at higher concentrations of  $\beta$ Lg primarily due to increased NH/NH<sub>2</sub> vibrations. This data indicates that the secondary structure of  $\beta$ Lg was significantly altered due to its adsorption onto the GNP surfaces.

(iii) The 1004  $\text{cm}^{-1}$  phenylalanine peaks were quite consistent for all three spectra (C–E) mainly due to its conformation insensitivity (Li-Chan, 1996). The peaks at 760, 880, and 1600  $\text{cm}^{-1}$ , which can be attributed to the indole ring structure of tryptophan, increased with increasing  $\beta$ Lg concentration. These peaks are known to be sensitive to environmental polarity: the higher their intensity, the more buried the indole ring is within a non-polar environment. The 1600 and 880  $\text{cm}^{-1}$  peaks overlapped a little with the N–H peaks described previously, making it difficult to interpret. The 760  $\text{cm}^{-1}$  peak was clearly shown in the spectra of the samples containing 2500 and 5000  $\mu$ M  $\beta$ Lg and GNPs (spectrum D and E) while they were absent in the spectra of 1000  $\mu$ M (spectrum C). This data indicates that when

increasing the amount of  $\beta$ Lg, the protein structure formed a more compact chain conformation when adsorbed onto GNPs. It is proposed that the  $\beta$ Lg molecules tend to unfold and spread out more at the GNPs surfaces when they are adsorbed at lower concentrations, but they adopt a more compact structure at higher concentrations due to crowding effects.

(iv) A single  $\beta$ Lg molecule has one free cysteine and two disulfide bridges. It has been reported that the sulfur atom can directly bind onto the GNP surface, resulting in a shift of the C–S peaks at around  $640\text{ cm}^{-1}$  (Brolo, Germain, & Hager, 2002). A possible red shift was observed when increasing the  $\beta$ Lg concentration in this study. However, the intensity of the C–S peaks was too weak to make any firm conclusions.

The S–S peaks that should appear at  $505\text{--}540\text{ cm}^{-1}$  were also weak. The weak intensity of this band for the protein used in this study is related to the relatively low disulfide bridge content. For other proteins, such as bovine serum albumin which contains 17 disulfide bridges, an intense band has been reported at  $515\text{ cm}^{-1}$  (Iosin et al., 2009). Nevertheless, we can observe a noticeable S–S peak in spectra D and E, but not in spectrum C. The red shift of the S–S peak may be due to a conformation change from gauche-gauche-gauche (low energy conformation) to gauche-gauche-trans (higher energy conformation) (Li-Chan, 1996). These changes in the disulfide regions suggest that the native conformation of disulfide linkages in  $\beta$ Lg were altered upon adsorption. The loss of S–S peak in low concentration of protein indicates that the protein was unfolded at lower concentration. The increase of energy conformation of disulfide bonds at higher concentration of protein also indicates that the protein molecules at higher concentration may form more compact structures on GNP surfaces than the ones at low concentration.

Overall, the Raman study confirms that  $\beta$ Lg was adsorbed to GNPs surface mainly through amino groups and could undergo conformational changes with significant alterations in secondary structure. Different protein concentrations appeared to affect the conformation of the molecules at the gold surfaces, with higher concentrations leading to more compact structures. Brewer et al. (2005) studied the interaction between bovine serum albumin (BSA) and citrate coated gold nanoparticles

and concluded the interaction was mainly electrostatic interaction which involves citrate molecules (Brewer et al., 2005). In our study, SERS data shows the changes in the  $\text{NH}_2/\text{NH}_3^+$  peaks, but not the  $\text{COO}^-$  peak, which may also indicate the electrostatic interaction. In addition, protein conformation was significantly changed, suggesting that there were other interactions such as steric or hydrophobic interactions.

## 6.5 Conclusions

In summary, we have studied the interactions between  $\beta$ Lg (pH 3) and GNPs (200 nm) using a variety of analytical methods. Light scattering and electron microscopy indicated that extensive particle aggregation occurs at intermediate protein concentrations, which can be attributed to charge neutralization and bridging flocculation. Particle aggregation promotes rapid phase separation (sedimentation) of the system. Particle electrophoresis, UV–visible spectroscopy, and SERS measurements showed that the proteins adsorbed to the particle surfaces and identified key molecular changes at the surfaces. This study has shown that SERS used in combination with complementary analytical tools can be used to provide fundamental information about the interactions between globular proteins and colloidal particles. Then, we have studied the influence of bile salts addition on the interfacial composition of  $\beta$ Lg-coated GNPs as function of incubation time and bile salts concentration that could be referred to the condition of bile salt secretion in human gastrointestinal tract.

## **CHAPTER VII**

### **ALTERATIONS IN NANOPARTICLE PROTEIN CORONA BY BIOLOGICAL SURFACTANTS: IMPACT OF BILE SALTS ON $\beta$ -LACTOGLOBULIN-COATED GOLD NANOPARTICLES**

#### **7.1 Abstract**

The impact of biological surfactants (bile salts) on the protein ( $\beta$ -lactoglobulin) corona surrounding gold nanoparticles (200 nm) was studied using a variety of analytical techniques at pH 7: dynamic light scattering (DLS); particle electrophoresis ( $\zeta$ -potential); UV-visible (UV) spectroscopy; transmission electron microscope (TEM); and surface-enhanced Raman scattering (SERS). The bile salts were shown to adsorb to the protein-coated nanoparticle surfaces and alter the interfacial composition, charge, and structure. SERS spectra of protein-coated nanoparticles after bile salt addition contained bands from both protein and bile salts, indicating that the protein was not fully displaced by the bile salts. UV, DLS and TEM techniques also indicated that the protein coating was not fully displaced from the nanoparticle surfaces. The impact of the bile salts could be described by an orogenic mechanism: mixed interfaces were formed that consisted of islands of aggregated proteins surrounded by a sea of bile salts. This knowledge is useful for better understanding the interactions between bile salts and protein-coated colloidal particles, which may be important for controlling the fate of delivery systems in the human gastrointestinal tract.

## 7.2 Introduction

Proteins are widely used in the food and pharmaceutical industries as emulsifiers and stabilizing agents. The adsorption of globular proteins to particle surfaces is important in a number of physicochemical and biological phenomena relevant to the development of food and pharmaceutical products. Protein-coated lipid droplets are often used as delivery systems for lipophilic bioactive agents, such as nutraceuticals and drugs (Dickinson, 2003; McClements, 2005; Venketesh & Dayananda, 2008; Kralova & Sjöblom, 2009). Proteins may adsorb to the surfaces of inorganic nanoparticles (such as gold, silver, or titanium dioxide) (Hussain, Jaitley, & Florence, 2001; Powell, Faria, Thomas-McKay, & Pele, 2010), which may alter their gastrointestinal fate (e.g., absorption by epithelium cells or interactions with gut microbiota). Proteins may also adsorb to nanoparticles within the circulatory system of the human body due to a process known as opsonization, which again alters their potential biological fate (Owens & Peppas, 2006; Mahon, Salvati, Baldelli Bombelli, Lynch, & Dawson, 2012). Consequently, there has been much interest in understanding the way in which protein structure and function are altered after adsorption to particle surfaces. Many food and pharmaceutical products contain a mixture of different types of surface active agents, such as proteins, polysaccharides, phospholipids and surfactants. Consequently, the interfacial properties of a protein-coated particle may change in a product over time due to competitive adsorption, co-adsorption or multilayer formation processes. In addition, a protein-coated particle may encounter a compositionally complex environment within the gastrointestinal tract, since the intestinal fluids may also contain a mixture of different surface active agents, such as bile salts, phospholipids, and proteins. There has therefore been substantial interest in understanding the interaction between protein-coated interfaces and surfactants (Nasir & McGuire, 1998; Niño, Wilde, Clark, & Patino, 1998; Fruhner, Wantke, & Lunkenheimer, 2000).

One of the most important classes of surface active agents present within the human gastrointestinal tract are bile salts (BS) (Maldonado-Valderrama, Woodward, Gunning, Ridout, Husband, & Mackie, 2008). Bile salts are surface active mixtures consisting mainly of the sodium salts of taurocholates. They have previously

been shown to be able to displace adsorbed materials from air-water and oil-water interfaces (Wickham, Garrod, Leney, Wilson, & Fillery-Travis, 1998; Mun, Decker, Park, Weiss, & McClements, 2006; Maldonado-Valderrama et al., 2008). Atomic force microscopy (AFM) has been used to characterize the interfacial structures formed by surfactants and proteins at interfaces during competitive adsorption processes, which had led to the proposal of the “orogenic model” for displacement of adsorbed proteins by surfactants (Mackie, Gunning, Wilde, & Morris, 2000a, b; Maldonado-Valderrama et al., 2008; Morris & Gunning, 2008; Maldonado-Valderrama, Gunning, Wilde, & Morris, 2010). In this model, the protein molecules initially have a relatively homogeneous distribution at the interface. When the surfactant molecules are introduced, they adsorb to the interfaces and lead to two-dimensional phase separation: protein-rich regions surrounded by surfactant-rich regions. As the surfactant concentration is increased, the proteins further congregate and form thick islands, which are completely displaced from the interfaces at sufficiently high surfactant concentrations.

In this study, we used  $\beta$ -lactoglobulin ( $\beta$ Lg) as a model globular protein and gold nanoparticles (GNPs) as model colloidal particles to form protein-stabilized nanoparticles.  $\beta$ -Lactoglobulin is the major globular protein in bovine milk and is widely used in the food industry as an emulsifier (McClements, 2005). Its structure, properties, and biological role are well established (Pérez & Calvo, 1995; Croguennec, Mollé, Mehra, & Bouhallab, 2004). This protein usually exists as a dimer at neutral pH with a molecular weight of nearly 36 kDa, but dissociates into monomers below pH 3 (Seo et al., 2010). Its three-dimensional structure consists of an eight-stranded antiparallel  $\beta$ -hydrophobic barrel unit (54%) with an  $\alpha$ -helix (17%) (Kontopidis, Holt, & Sawyer, 2004; Seo, et al., 2010). GNPs are attractive for many biological and medical applications due to their chemical stability, biocompatibility, and unique optical properties (Iosin et al., 2009; Iosin, Canpean, & Astilean, 2011). In this study, we used  $\beta$ -lactoglobulin-coated GNPs (200 nm) as model systems for protein-coated lipid droplets that are found in many food and pharmaceutical systems (McClements, 2005). In addition, we used GNPs as model colloidal particles because we would like to take advantage of the surface enhanced Raman scattering (SERS) characteristics of

GNPs to study the effect of bile salt addition on the interfacial structure of  $\beta$ Lg-coated nanoparticles.

Surface-enhanced Raman scattering (SERS) is a derivative of Raman spectroscopic technique that can be used for sensitive molecular identification and structural characterization (Kudelski, 2008). Enhanced Raman scattering occurs when an analyst is on or in close proximity of a SERS active surface, such as silver or gold nanoparticles. Raman signals can be enhanced tremendously by combining electromagnetic enhancement and chemical charge transfer mechanisms (Brewster, 2009). Detection limits of parts per billion (ppb) have been achieved, and even a single molecule can be detected using this method (Aroca et al., 2005). To study the conformation of biomolecules such as protein, Raman spectroscopy can provide information related to protein backbone conformation and the molecular environment of certain side chains, as well as transitions from ordered to disordered structure upon protein denaturation (Li-Chan, 1996; Wang et al., 2013). Raman scattering is also sensitive to changes in covalent bonds, such as disulfide linkages, and non-covalent bonds, such as electrostatic and hydrophobic interactions (Li-Chan, 1996). Raman spectroscopy also provides the capability to analyze compounds in aqueous solutions with minimal interference from water adsorption, which is a critical factor when considering biological applications (Brewster, 2009). Enhanced with nanotechniques, SERS is a sensitive and promising technique to observe the molecular conformation of biopolymers or substances on a nanosubstrate.

In this study, we used a variety of analytical techniques to better understanding the interaction between bile salts and protein-coated gold nanoparticles, including dynamic light scattering (DLS), particle electrophoresis ( $\zeta$ -potential), localized surface plasmon (LSPR), transmission electron microscopy (TEM), and surface-enhanced Raman scattering (SERS). Our intention was to unravel the mechanisms of interactions between protein-coated GNP interfaces and surface active bile salts by primarily focusing on the physicochemical and interfacial compositional changes at the particle surfaces.

## **7.3 Materials and methods**

### **7.3.1 Materials**

Powdered  $\beta$ Lg was obtained from Davisco Foods International (Lot JE 001-0-415, Le Sueur, MN). As stated by the manufacturer, the protein content was 97.4% w/w (dry basis), the purity was 95% w/w  $\beta$ Lg and the nitrogen content was 15.6% w/w. A suspension of 200 nm gold nanoparticles ( $7 \times 10^8$  particles/mL) was purchased from Ted Pella, Inc. (Redding, CA). Bile extract (porcine) was also purchased from the Sigma Chemical Company (St. Louis, MO). All other chemicals used were of analytical grade. Double distilled water was used throughout the experiments.

### **7.3.2 $\beta$ Lg solution preparation**

A  $\beta$ Lg solution was prepared at ambient temperature (22 °C) by dissolving powdered  $\beta$ Lg in 5 mM sodium phosphate buffer solution (pH 7). A  $\beta$ Lg solution was prepared at a concentration of 5000  $\mu$ M. The  $\beta$ Lg solutions were stirred gently for 3 h to ensure complete protein dissolution. If required the pH of these solutions was readjusted to pH 7.0 using either 1 M HCl and/or 1 M NaOH.

### **7.3.3 Gold nanoparticle (GNPs) interaction with $\beta$ Lg and bile salts**

The interaction of the globular proteins with the gold nanoparticles (GNPs) was studied by adding 20  $\mu$ L of  $\beta$ Lg solution into a 1.5 mL microcentrifuge tube. Then, 1000  $\mu$ L of GNP solution was added drop wise under vigorous mixing for 5 min. Thus, the original protein concentration was reduced by a factor of 20/1020, and the original GNP concentration was reduced by a factor of 1000/1020. The mixture was incubated overnight under consistent orbital rotation at ambient temperature (22 °C). The pH of the mixture was kept constant at pH 7.

After incubation, the bile salt solution was added to the GNP- $\beta$ Lg suspensions. The bile salt concentration was varied from 0-20 mg/mL to cover a range of potential physiological situations. The mixture was kept constant at pH 7.0 and incubated with continuous shaking at 100 rpm at 37 °C for up to 2 h. Each treatment

was prepared in triplicate. The mixture of  $\beta$ Lg-coated GNPs and  $\beta$ Lg-coated GNPs with bile salts were denoted “GNPs- $\beta$ Lg” and “GNPs- $\beta$ Lg-BS”, respectively.

#### **7.3.4 Particle size and charge measurements**

The particle size and charge of bare and coated GNPs were determined using a commercial dynamic light scattering/particle electrophoresis device (Nano-ZS, Malvern Instruments, Worcestershire, UK) at ambient temperature (22 °C) (see Section 3.7.1).

#### **7.3.5 UV–visible spectrophotometer**

The ultraviolet spectrum (250–800 nm) of the bare GNPs and coated GNPs was recorded with a UV/Vis scanning spectrophotometer (model UV-2101 PC, Shimadzu Scientific Instruments Inc., Columbia, MD) to determine the peak of protein and gold plasmon band.

To determine the change of the interfacial composition of the coated GNPs after bile salt addition for 2 h, the unabsorbed  $\beta$ Lg (present in the aqueous phase) was examined by centrifuging mixtures for 20 min at 13,600 g (model 325C, Thermo Scientific, Madison, WI). The centrifuged supernatants were carefully collected. Then, the absorbance of supernatants was measured at 279 nm which represented the protein band.

#### **7.3.6 Transmission electron microscopy (TEM)**

The morphology and distribution of the bare and coated GNPs were analyzed by transmission electron microscopy (model 2000FX, JEOL, Tokyo, Japan), as described in Section 3.7.3.

#### **7.3.7 Surface-enhanced Raman spectroscopy (SERS)**

The SERS measurement was conducted using a DXR Raman microscope (Thermo Scientific, Madison, WI) equipped with a 10 $\times$  microscope objective (Section 3.7.4).

## 7.4 Results and discussion

### 7.4.1 Properties of bare GNPs

Initially, the electrical properties ( $\zeta$ -potential) and dimensions (particle diameter) of bare GNPs were measured. The bare GNPs had a  $\zeta$ -potential of around -56.5 mV at pH 7 (Figure 7.1A), which can be attributed to the negative charge associated with the citrate functional groups used to prevent particle aggregation (Lee et al., 2004; Iosin et al., 2009; Masereel et al., 2010; Seo et al., 2010; Iosin, Canpean, & Astilean, 2011). The initial mean diameter of the bare GNPs determined by dynamic light scattering was around 186 nm at pH 7 (Figure 7.1B), which is fairly close to the value of 200 nm reported by the manufacturer. The GNP suspensions were stable to sedimentation during storage for 24 h, with no evidence of precipitated particles at the bottom of the test tubes.

### 7.4.2 Properties of $\beta$ Lg-coated GNPs

Protein-coated gold nanoparticles were formed by mixing a  $\beta$ Lg solution with a suspension of GNPs at pH 7. Our previous study (Chapter VI) showed that GNP surfaces were saturated with protein around 5000  $\mu$ M  $\beta$ Lg since there was no further change in  $\zeta$ -potential was observed when the protein concentration was increased further (See Chapter VI). This value was used to estimate the surface load of the protein at the gold surfaces. The calculated surface load was around 6.2 mg m<sup>-2</sup>, which is in reasonable accordance with the values reported for this protein in the literature, i.e. 1 to 10 mg m<sup>-2</sup> (see Chapter VI). The particles in the GNPs- $\beta$ Lg mixture were anionic (-23.3 mV), had diameters around 216 nm, and had a monomodal size distribution (data not shown). The coated particles were stable to aggregation and did not show any evidence of sedimentation. These results suggest that the protein molecules adsorbed to the nanoparticle surfaces and caused a change in surface charge and particle dimensions. If it is assumed that the nanoparticles did not aggregate in the presence of the protein, we can calculate the effective thickness of the adsorbed protein layer:  $\delta = (d_{\text{protein}} - d_{\text{bare}})/2$ , where  $d_{\text{protein}}$  and  $d_{\text{bare}}$  are the diameter of the particles in the presence and absence of protein, respectively. Using the particle diameters reported earlier we estimated the thickness of the adsorbed protein layer to

be  $\delta = (216 \text{ nm} - 186 \text{ nm})/2 = 15 \text{ nm}$ . This thickness is considerable larger than the dimensions of a single protein molecule (around 2 to 3 nm), which suggests that multiple layers of proteins are adsorbed. The observed decrease in particle charge after protein adsorption can be attributed to the fact that the protein molecules have a lower charge density than the gold nanoparticle surfaces.

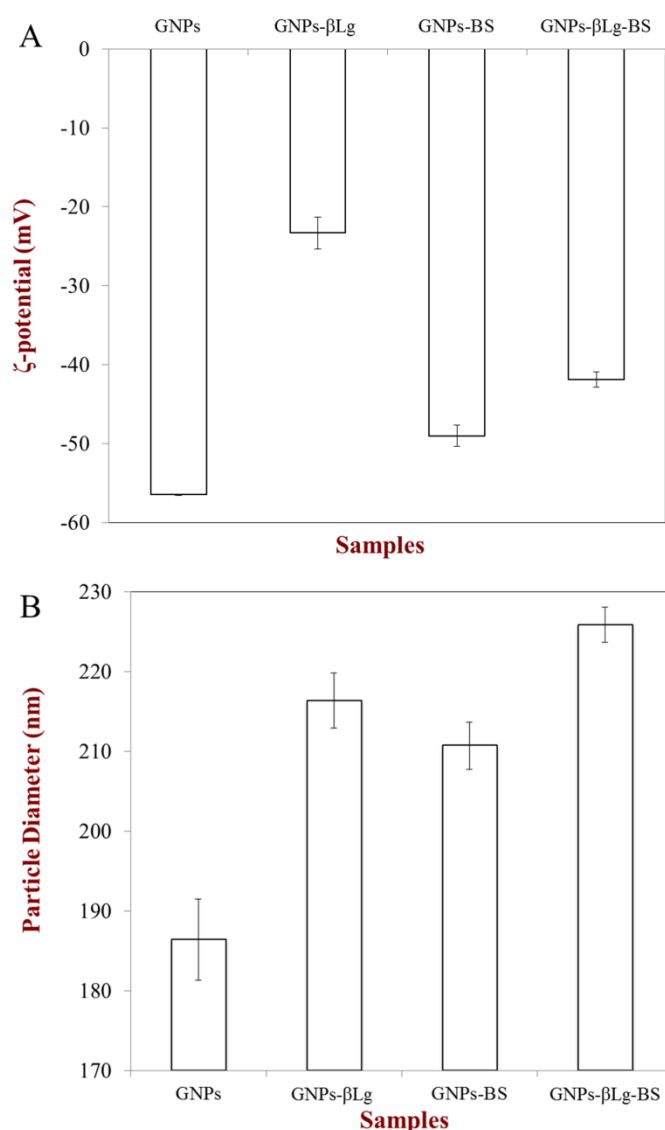


**Figure 7.1**  $\zeta$ -Potential (A) and particle diameter (B) of bare GNPs, GNPs- $\beta$ Lg, GNPs-BS, and GNPs- $\beta$ Lg-BS mixtures. The concentrations of the different components used were  $6.86 \times 10^8$  particles/mL GNPs, 0.098 mM  $\beta$ Lg, and 10 mg/mL BS.

One of the most important factors affecting the interaction of proteins with GNPs is pH, since this will influence the electrical characteristics of both the proteins and gold nanoparticles. The net charge on  $\beta$ Lg molecules goes from positive to negative as the pH is increased from below to above the proteins isoelectric point (Georgescu, Alexov, & Gunner, 2002):  $pI = 5.0$  (Kontopidis, Holt, & Sawyer, 2004; McClements, 2010). In Chapter VI, we previously reported that electrostatic attraction plays an important role in promoting adsorption of  $\beta$ Lg molecules to GNP surfaces at pH 3.0, since the protein is cationic and the GNPs are anionic at  $pH < pI$  (Winuprasith et al., 2014). In the current study, we mixed the  $\beta$ Lg solution and GNPs together at pH 7.0 and so we would expect there to be an electrostatic repulsion since both the protein and nanoparticle are negatively charged at  $pH > pI$ . Nevertheless, our results indicated that protein molecules still adsorbed to nanoparticle surfaces at neutral pH, i.e., there was an appreciable change in particle charge (Figure 7.1A) and dimensions (Figure 7.1B) after mixing the  $\beta$ Lg solution with GNPs. This suggests that non-electrostatic interactions were responsible for protein adsorption under these conditions, such as thiolate linkage or covalent interactions (Gole, Dash, Ramakrishnan, Sainkar, Mandale, Rao et al., 2001; Iosin, Canpean, & Astilean, 2011). In addition, each  $\beta$ Lg molecule has one free cysteine group and two disulfide bridges, which means that sulfur atoms may directly bind to GNP surfaces (see Chapter VI).

### **7.4.3 Influence of bile salts on properties of protein-coated GNPs**

#### **7.4.3.1 Particle charge characteristics**

Knowledge of the interfacial characteristics of nanoparticles is important for understanding their behavior within the gastrointestinal tract. Measurements of the electrical charge of nanoparticles can provide indirect information about changes in their interfacial composition since different adsorbed species usually have different electrical characteristics. Consequently, we measured the influence of bile salt addition on the electrical charge ( $\zeta$ -potential) of  $\beta$ Lg-coated GNPs. The bile salt concentrations used were chosen to represent those typically found physiologically. In the absence of bile salts, the  $\beta$ Lg-coated GNPs had a fairly high negative charge ( $\zeta = -26$  mV). Upon addition of bile salts, the magnitude of the negative charge on the GNPs increased with both incubation time (Figure 7.2A) and

bile salt concentration (Figure 7.2B), which suggested that anionic bile salts adsorbed to the particle surfaces. Interestingly, the negative charge on the GNPs at the longest times and highest bile salt concentrations (-43 mV) did not reach the same  $\zeta$ -potential as bile salt-coated GNPs (-49 mV) (Figure 7.1A). This finding implies that at the bile salt concentrations used in this study, the GNPs were not fully coated by bile, which would mean that they had an interfacial layer that contained both bile and  $\beta$ Lg (Lesmes & McClements, 2012). The  $\zeta$ -potential changed steeply during the first minute of incubation, but then decreased more steadily at longer times (Figure 7.2A), which suggests that the bile salts rapidly adsorbed, but then there was a relatively slow rearrangement of the interfacial structure during the next two hours.

At the pH used in this study (pH 7), both the  $\beta$ Lg-coated GNPs and the bile salts are highly negatively charged, and therefore one would expect an electrostatic repulsion between them that would oppose adsorption. Consequently, there must be another attractive interaction that is strong enough to overcome the repulsive interactions, such as the hydrophobic effect. Thus non-polar groups on the bile salt molecules can bind to non-polar groups on the gold nanoparticle surfaces (Sarkar, Horne, & Singh, 2010).

Previous studies have also reported similar changes in  $\zeta$ -potential of protein-coated particles upon addition of bile salts, which were attributed to co-adsorption of bile and the displacement of protein into the continuous phase (Lesmes et al., 2010; Sarkar, Horne, & Singh, 2010; Schmelz et al., 2011; Lesmes & McClements, 2012). This process has been referred to as the orogenic displacement model. Heterogeneity in the protein film allows surfactant molecules to adsorb into localized defects, and then these nucleated sites grow. Expansion of surfactant-rich regions compresses the protein network, which initially increase in density without increasing in thickness. Once a certain critical surface packing density is reached, the protein layer thickness increases such that the protein film volume is maintained as the surfactant domains expand. At sufficiently high surface pressures the network fails, releasing the protein into the surrounding aqueous phase (Mackie et al., 2000; Maldonado-Valderrama et al., 2008, 2010).

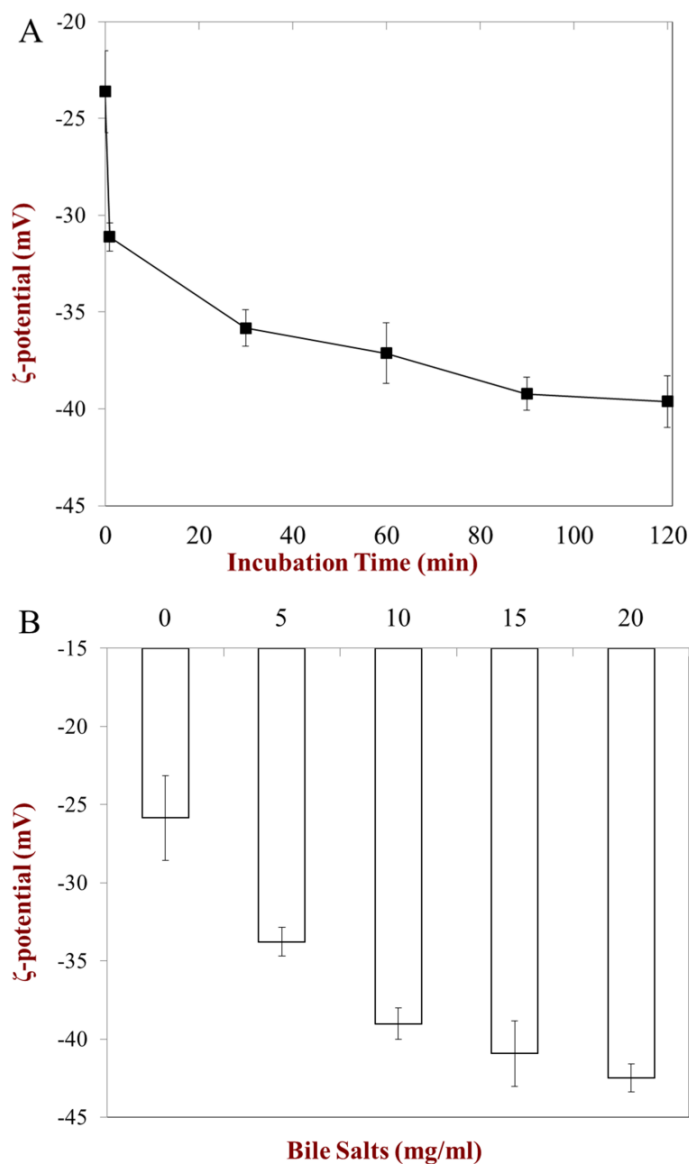


**Figure 7.2** The change in  $\zeta$ -potential of GNPs- $\beta$ Lg-BS on addition of bile salt (10 mg/mL) as a function of time (A) and as a function of bile salt concentration after treatment for 2 h (B). The initial concentrations in the system were  $6.86 \times 10^8$  particles/mL GNPs, and 0.098 mM  $\beta$ Lg.

#### 7.4.3.2 Particle diameter

Measurements of changes in particle diameter upon adsorption of surface-active species can provide valuable information about interfacial thickness and particle aggregation. The influence of bile salts on the mean particle diameter of  $\beta$ Lg-coated GNPs was therefore monitored by dynamic light scattering (DLS). The

particle size distribution remained monomodal (data not shown) and the change in mean particle diameter was relatively small ( $< 6\%$ ) upon addition of bile salts (Figure 7.3A and 7.3B), which suggested that the mixed systems were stable to particle aggregation. There appeared to be a slight increase in mean particle diameter from around 216 to 227 nm when the bile salt concentration was increased from 0 to 20 mg/mL, but this difference was not significant ( $p > 0.05$ ). Sarkar, Horne, and Singh (2010) also reported that the mean droplet diameter of  $\beta$ Lg-stabilized lipid droplets did not significantly change upon addition of bile salts (0-20 mg/mL) (Sarkar, Horne, & Singh, 2010). One would have expected an increase in interfacial thickness with increasing bile salt concentration due to the orogenic mechanism (Mackie, Gunning, Wilde, & Morris, 1999; Mackie et al., 2000a, b; Mackie, Gunning, Ridout, Wilde, & Morris, 2001) described earlier. However, the changes in interfacial thickness were probably too small to measure using the dynamic light scattering instrument used in this study.

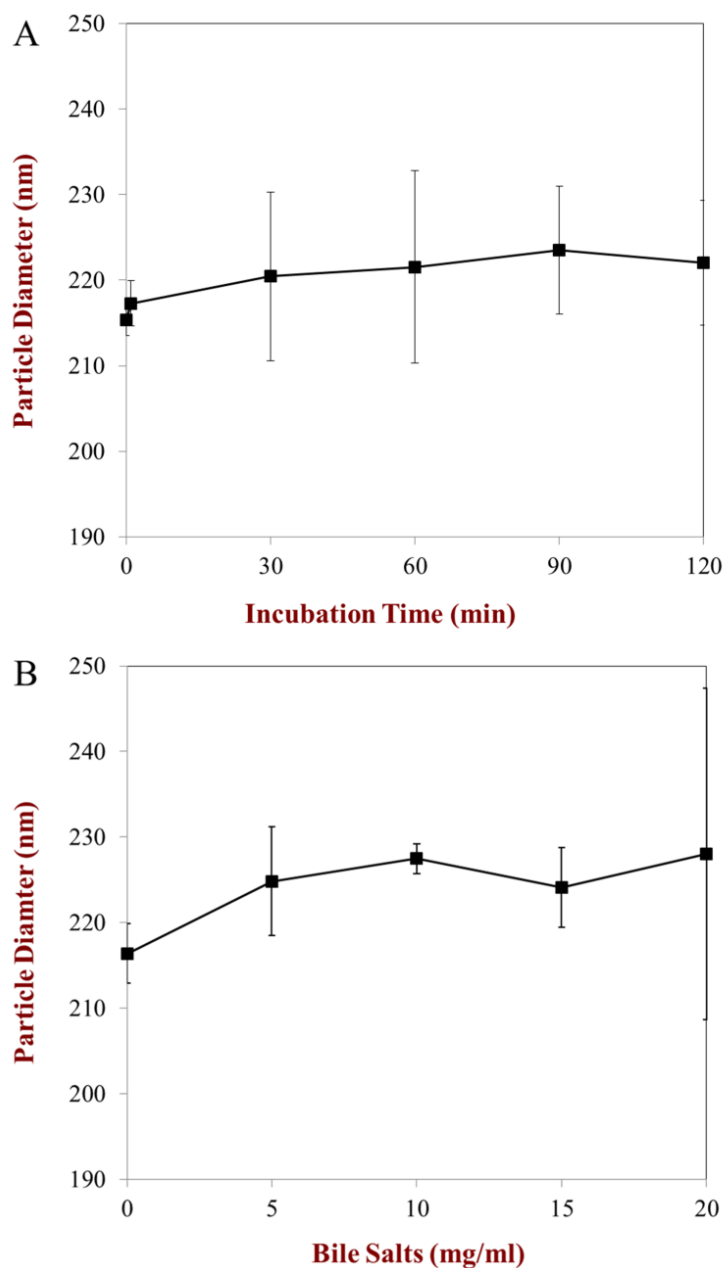


**Figure 7.3** The change in particle diameter of GNPs-βLg-BS on addition of bile salt (10 mg/mL) as a function of time (A) and as a function of bile salt concentration after treatment for 2 h (B). The initial concentrations in the system were  $6.86 \times 10^8$  particles/mL GNPs, and 0.098 mM βLg.

#### 7.4.3.3 UV-visible absorption spectra

UV-visible spectroscopy measurements can be used to measure changes in absorption or scattering of nanoparticle suspensions, which can provide useful information about changes in molecular structure/location or particle

aggregation. UV-visible absorption spectra of GNP suspensions were therefore measured in the absence and presence of  $\beta$ Lg and bile salts (Figure 7.4A). In addition, the UV-visible absorption spectrum of a pure  $\beta$ Lg solution was also measured across the same wavelength range. The suspension containing bare GNPs exhibited a broad absorption band around 579 nm, which can be attributed to surface plasmon resonance. The  $\beta$ Lg solution (containing no GNPs) exhibited a broad absorption band around 279 nm due to the presence of aromatic side groups on tryptophan and tyrosine residues. The large difference in wavelengths of the absorption bands for GNPs and  $\beta$ Lg means that they should not directly interfere with each other. The spectral position of the surface plasmon resonance band of the GNPs red-shifted from 579 nm (bare) to 582 nm (coated) when  $\beta$ Lg was added. This shift suggests that  $\beta$ Lg molecules adsorbed onto the surface of GNPs and modified their refractive index and dielectric constant contrasts, thereby leading to shifts in the absorption and scattering spectra (Li, Guo, & Wang, 2008; Masereel et al., 2010; Iosin, Canpean, & Astilean, 2011). Interestingly, the absorption band at 279 nm associated with the tryptophan and tyrosine residues on  $\beta$ Lg increased appreciably in magnitude when the protein was mixed with GNPs, which again suggests that the protein was at the particle surface, rather than free in solution. The addition of bile salts to the  $\beta$ Lg-coated GNPs caused a change in the magnitude and position of the surface plasmon resonance band (around 580 nm), which suggests that there was a change in interfacial composition. However, the addition of bile salts had little effect on the protein absorption band (around 280 nm), which suggests that the  $\beta$ Lg remained at the droplet surfaces. Taken together, these results suggest that bile salts adsorbed to the GNP surfaces, but that at least some protein remained there.

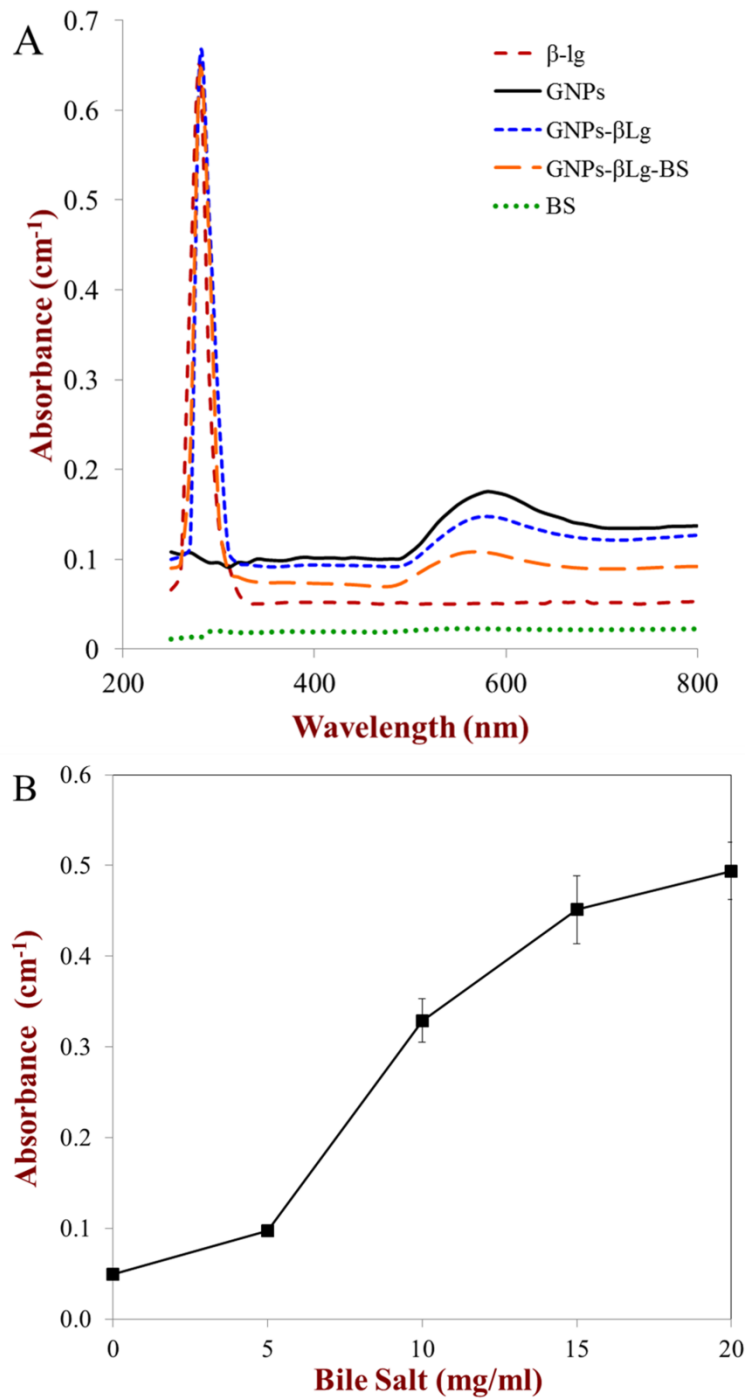


**Figure 7.4** Absorption spectra of  $\beta$ Lg solution, bare GNPs in solution, GNPs- $\beta$ Lg, GNPs- $\beta$ Lg-BS, and BS solutions (A) and absorbance at 279 nm of supernatant obtained from GNPs- $\beta$ Lg-BS with varying bile salt concentrations (B).

Additional information about the mechanism of interaction between  $\beta$ Lg-coated GNPs and bile salts was obtained by using UV-visible

spectroscopy to measure changes in the composition of the aqueous phase surrounding the gold nanoparticles.  $\beta$ Lg-coated GNPs were incubated with different levels of bile salts for 2 h at 37 °C, and then the nanoparticles and surrounding aqueous phase were separated by centrifugation. The aqueous phase was collected and UV-visible absorption spectra were measured. The amount of bile salts added to the suspension of  $\beta$ Lg-coated GNPs had a pronounced influence on the protein concentration in the aqueous phase, as determined by measuring the absorbance at 279 nm. This wavelength corresponds to the adsorption band for proteins, and therefore provides information about the amount of protein displaced from the surfaces of GNPs. There was an appreciable increase in the absorbance of the aqueous phase at 279 nm (Figure 7.4B) with increasing bile salt concentration, which suggests that some of the protein was displaced from the GNP surfaces. The amount of  $\beta$ Lg in the non-adsorbed phase increased about 2 fold at added bile salts concentration of 5 mg/mL and about 10 fold at added bile salts concentration of 20 mg/mL after 2 h incubation. The extinction coefficient of  $\beta$ Lg has been reported to be  $0.96 \text{ L/g/cm}^{-1}$  at 278 nm (Croguennec et al., 2004), and therefore the protein concentration in the aqueous phase at high bile salt levels corresponds to about 0.51 g/L, which was appreciably lower than the original amount added (1.76 g/L). This suggests that the majority of proteins remained at the GNPs surface, even at the highest bile salt concentration used, but that some desorbed.

Our results are in agreement with that of Sarkar et al. (2010) who also reported that  $\beta$ Lg could be displaced from oil droplet surfaces into the aqueous phase in the presence of bile salts, as well as other previous studies of protein displacement from various kinds of particles (Maldonado-Valderrama et al., 2008; Sarkar, Horne, & Singh, 2010; Lesmes & McClements, 2012).

#### **7.4.3.4 Transmission electron microscopy (TEM)**

The presence of  $\beta$ Lg at the surface of the GNPs was confirmed by transmission electron microscopy (TEM), which clearly revealed a diffuse layer of material surrounding the gold nanoparticles in the presence of protein (Figure 7.5B) but not in its absence (Figure 7.5A). This layer has previously been referred to as the “protein corona” (Chantrapornchai, Clydesdale, & McClements, 1999; Warren, Chalmers, Hutchison, Dang, & Pouton, 2006; Cedervall et al., 2007), which has a

“core-shell structure” (Chapter VI). Presumably, the core is a gold nanoparticle, while the shell is a layer of protein molecules. This protein layer has previously been divided into a “soft” component that rapidly exchanges with non-adsorbed proteins, and a “hard” component that has a high affinity for the particle surface (Cedervall et al., 2007). A TEM image of the structure of  $\beta$ Lg-coated GNPs after addition of bile salts was also recorded (Figure 7.5C). These images suggest that there is still a significant amount of protein present at the particle surfaces, but that it forms isolated thick clumps rather than a smooth surface coverage. This structure is consistent with the orogenic displacement mechanism that has been reported for protein-coatings at air-water and oil-water interfaces after addition of surfactants as studied by atomic force microscopy (AFM) (Mackie et al., 2000a, b; Maldonado-Valderrama et al., 2008, 2010).

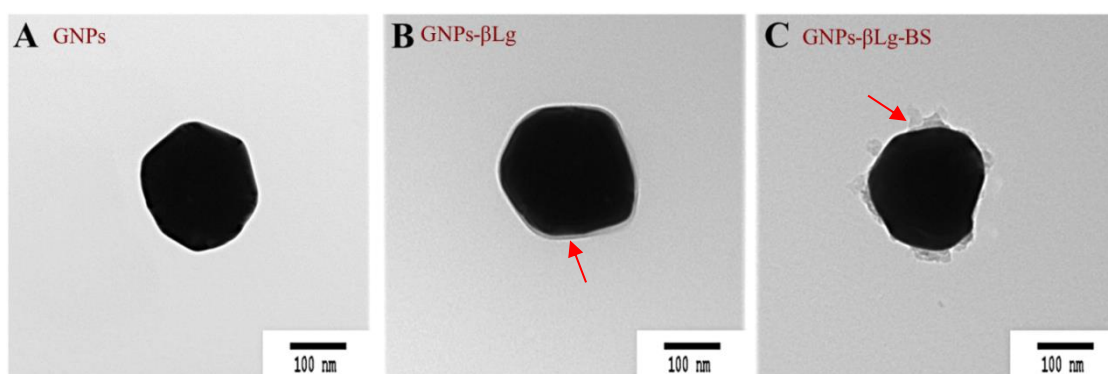


**Figure 7.5** Transmission electron microscopy of GNPs (A), GNPs- $\beta$ Lg (B), GNPs- $\beta$ Lg-BS (C).

The molecular structure of bile salts is very different from the surfactants that consist of a hydrophobic tail and a hydrophilic head group. Rather, bile salts are relatively flat molecules with polar hydroxyl groups located on one side and non-polar methyl groups on the other (Warren et al., 2006). Therefore, they tend to lie flat on the interfaces. This flat conformation of the bile salts on the surfaces may exert different physical forces on the protein network compared to conventional surfactant molecules and may even interfere with the ability of the protein to interact with the surfaces. However, the interfacial properties of bile salts are not yet well

understood (Maldonado-Valderrama et al., 2008), particularly under the complex conditions existing within the human gastrointestinal tract.

#### **7.4.3.5 Surface-enhanced Raman spectroscopy (SERS)**

Finally, more specific information about changes in molecular composition at the nanoparticle surfaces was obtained by SERS spectroscopy, a highly sensitive spectroscopic tool for interfacial studies. SERS spectra were obtained for each sample, and then second derivative transformation was applied to separate overlapping bands and to remove baseline shifts, so that comparisons between different samples could be made more clearly. Average second derivative spectra of suspensions of GNPs, GNPs- $\beta$ Lg, GNPs- $\beta$ Lg-BS, and GNPs-BS were calculated (Figure 7.6). A significant difference was observed between all SERS spectra of coated GNPs and bare GNPs, indicating that  $\beta$ Lg and bile salts were present at the GNP surfaces.

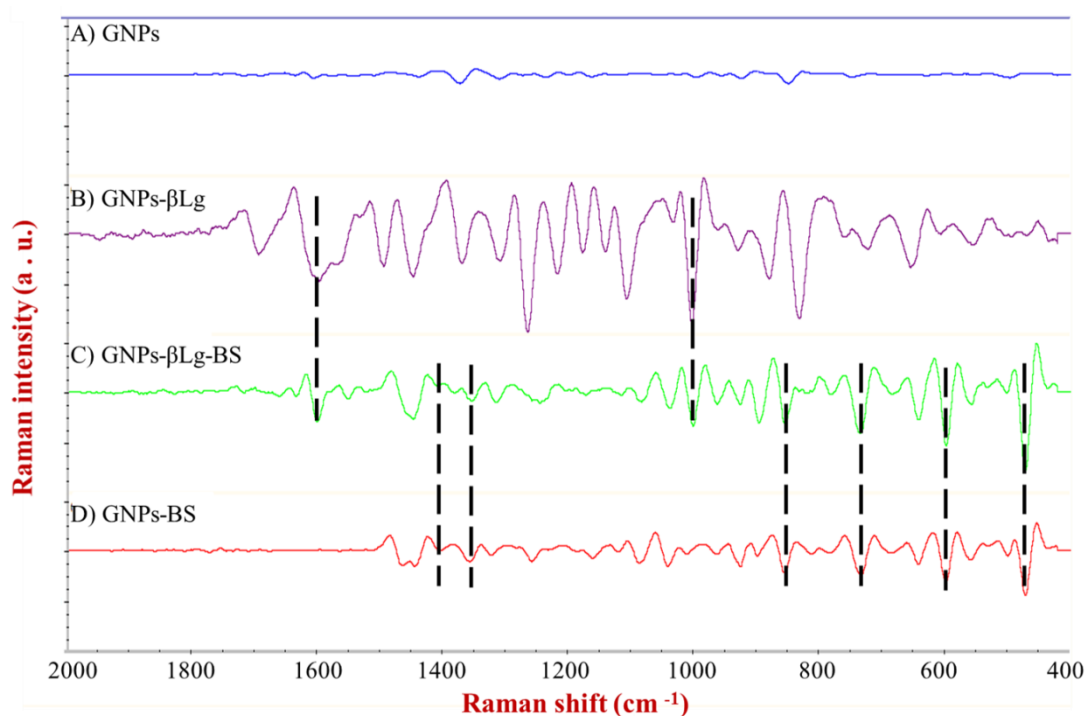


**Figure 7.6** Surface-enhanced Raman scattering (SERS) spectra of GNPs (A), GNPs- $\beta$ Lg (B), GNPs- $\beta$ Lg-BS (C), and GNPs-BS (D). The vertical dashed lines in the spectra highlight regions where key functional groups occur in the bile salts or proteins. The original spectra are shown in Appendix.

For  $\beta$ Lg-coated GNPs at pH 7, both the protein and GNPs are negatively charged at  $\text{pH} > \text{pI}$ . As described earlier, non-electrostatic interaction played an important role for protein adsorption, such as covalent interactions between gold and amino ( $\text{NH}_2$ ) or thiol ( $\text{SH}$ ). From SERS experiment, the strong  $\text{NH}_2$  peaks were observed at 1600, 1269, and 837  $\text{cm}^{-1}$ , which suggests that amino groups involved in the interaction between  $\beta$ Lg and GNPs. The amide-II and amide-III peaks were observed around 1600-1500  $\text{cm}^{-1}$  and 1266  $\text{cm}^{-1}$ , respectively, which arise from  $\text{NH}/\text{NH}_2$  vibrations. Therefore, the origin of this interaction may have been the interaction between  $\text{NH}_2$  groups of the protein and gold surfaces. A  $\text{NH}_3^+$  peak around 1510-1540  $\text{cm}^{-1}$  was not observed, which indicated that the  $\text{NH}_3^+$  groups were not involved in this interaction because at pH 7,  $\beta$ Lg molecules were negatively charged. This finding was totally different from  $\beta$ Lg-coated GNPs at pH 3 (Chapter VI, Section 6.4.6), which electrostatic attraction between positive  $\text{NH}_3^+$  groups of  $\beta$ Lg molecules

and negative citrate groups on the gold surface. In addition, a broad spectrum amide-I band was observed at  $1689\text{ cm}^{-1}$  corresponding to overlapping bands representing  $\alpha$ -helices,  $\beta$ -sheets, turns, and random structures (Surewicz, Mantsch, & Chapman, 1993; Li-Chan, 1996). This band arises from the C=O stretching vibration with minor contributions from N-H wagging. The C-S peak at  $655\text{ cm}^{-1}$  confirmed that the sulfur atom can directly bind onto the GNP surface. On the other hand, S-S peaks (around  $505\text{ cm}^{-1}$ ) were very weak, which suggests that these groups were weakly involved in the interactions, or only a low amount of disulfide bridges were present at the interface. It could be concluded that at pH 7, amine functional groups from  $\beta$ Lg molecules bind to colloidal GNPs through weak covalent interaction and the interaction via thiolate linkages through the cysteine residues as well.

Bile salts can also interact with GNPs. In Figure 7.6D, the bile salts spectra showed primary peaks at  $600\text{ cm}^{-1}$  and  $645\text{ cm}^{-1}$ , which were assigned to be hydroxyl (OH) bending mode. A weak absorption band at  $1408\text{ cm}^{-1}$ , could be assigned to the sodium carboxylate ( $\text{COO}^-$ ) peak of bile salts. This indicates bile salts were able to bind GNPs, possibly via interaction with OH and  $\text{COO}^-$  groups. Kasthuri and Rajendiran (2009) also reported that the carboxylate group of bile salts plays an important role in the interaction between bile salts and nanoparticle surface.

The SERS spectrum obtained from the  $\beta$ Lg-coated GNPs mixed with bile salts (i.e. GNPs- $\beta$ Lg-BS in Figure 7.6C) contained signature peaks of both  $\beta$ Lg-coated GNPs ( $1004\text{ cm}^{-1}$ ) and BS-coated GNPs ( $475\text{ cm}^{-1}$ ,  $600\text{ cm}^{-1}$ ,  $645\text{ cm}^{-1}$ ,  $858\text{ cm}^{-1}$ ,  $1358\text{ cm}^{-1}$ , and  $1408\text{ cm}^{-1}$ , *etc.*). Bile salts may bind to protein directly or replace protein and bind onto the surface of GNPs. From the spectrum of GNPs- $\beta$ Lg-BS (Figure 7.6C), we speculated that both situations happened. The amide-I peaks at  $1666\text{ cm}^{-1}$  were clearly changed after mixing with bile salts, indicating the change of conformation of the protein molecules after interacting with bile salts. Interestingly, the overall intensity of the protein peaks reduced significantly after mixing with bile salts. This may have occurred because of isolated islands of protein due to the orogenic mechanism. The intensity of the SERS signal from a molecule decreases rapidly when one moves away from a gold surface. Hence, the relatively small signal from the protein component may have been because the protein islands protruded into the surrounding aqueous phase, rather than being flat against the gold

surface. This result indicates that the SERS method is sensitive to the actual spatial distribution of the protein molecules at the particle surfaces, not just the total amount adsorbed, which is different from some other analytical methods. Aroca (2006) suggested that the local field enhancement is maximum for a molecule directly attached to the surface (first-layer effect) and it also has a long-range component that extends its effect up to about 10 nm away from the interface (Aroca, 2006; Stiles, Dieringer, Shah, & Van Duyne, 2008). In our case, the thickness of the  $\beta$ Lg surface was greater than 10 nm (confirmed by dynamic light scattering and SEM micrograph). As a consequence, the electromagnetic enhancement and chemical charge transfer mechanism were reduced which affect the intensity of the protein peak. On the other hand, peaks contributed from bile salts were clearly shown in the spectrum of GNPs- $\beta$ Lg-BS with high intensity. This indicates the direct interaction between the bile salts and the GNPs.

## 7.5 Conclusions

In summary, this study provides valuable insights into the orogenic mechanism of interaction of  $\beta$ Lg-coated GNPs with surface active bile salts. Light scattering and electron microscopy indicated an increase in interfacial thickness when bile salt was added. Particle electrophoresis, UV-visible spectroscopy, and SERS measurements showed that the bile salt adsorbed to the particle surfaces of  $\beta$ Lg-coated GNPs and identified key molecular changes at the surfaces. Overall our results confirm that bile salts adsorb to the surfaces of  $\beta$ Lg-coated gold nanoparticles and alter the structural arrangement of the protein molecules. At relatively low bile salt concentrations, a mixed interface is formed that contains islands of aggregated proteins in a sea of bile salts. At higher bile salt concentrations, proteins may be displaced from the particle surfaces. The origin of this effect may be attributed to different physicochemical phenomena: competition of bile salts with protein molecules for sites on the gold surfaces; direct binding of bile salts to protein molecules leading to a decrease in the surface activity of the proteins. This study has shown that SERS used in combination with complementary analytical tools can be

used to provide fundamental information about the interactions between surface active surfactants and protein-coated colloidal particles.

## CHAPTER VIII

### CONCLUSIONS

Most of food products in the market are food emulsions, for example, dressing, milk, and beverages. To develop a novel food emulsion products and technologies, study of the fundamental characteristics of emulsions is needed for food scientist. In this research, we aimed to study the properties and stability of emulsion system stabilized by biopolymer which is microfibrillated cellulose (MFC) and also to apply surface-enhanced Raman scattering technique in emulsion research by using  $\beta$ -lactoglobulin ( $\beta$ Lg)-coated gold nanoparticles (GNPs) as a model system for protein-coated lipid droplets that are found in many food and pharmaceutical systems.

From this research, it was found that mangosteen (*Garcinia mangostana* L.) rind could be used as a raw material for MFC production, due to high cellulose content. MFC was prepared by alkaline extraction and shearing using a high pressure homogenizer. MFC obtained at higher number of passes through the homogenizer has small particle size, which is a desirable characteristic for stabilizing the emulsions. The oil-in-water emulsions stabilized by MFC (30% w/w soybean oil, 0.7% w/w MFC in aqueous phase, emulsion pH range ~ 6.8–7.2) obtained at the higher number of homogenization passes exhibited smaller oil droplets, stronger three-dimensional network structures, and more stable to creaming than those stabilized by MFC obtained at the lower number of homogenization passes. In addition, MFC concentration also played an importance role in stabilization of the emulsions. An increase in MFC concentration from 0.05 to 0.70% w/w led to larger droplets, darker and more color, more pronounced elastic responses, and higher stability to creaming of the emulsions. No phase separation was observed in the emulsions containing 0.50% or 0.70% w/w MFC after storage for 80 days. Microscopic observations revealed that MFC particles mainly adsorbed at the oil-water interface of the emulsion droplets, whereas the amount of excess non-adsorbing MFC particles, forming a three-dimensional network in the continuous phase, increased with increasing MFC

concentration. All tested emulsion exhibited shear-thinning behavior, as a result of three-dimensional network formation of MFC and oil droplets. Overall results indicated that the MFC particles provide their functionality by adsorbing at the oil-water interface (Pickering stabilization) or by developing a gel-like microstructure composed of flocculated oil droplets and a viscoelastic network of the MFC particles in the aqueous phase between the droplets (network stabilization), or by a combination of these processes. Therefore, MFC is an interesting choice for food emulsion application that aims to formulate emulsion system with high stability and also improve the physical properties of the food emulsions. In addition, MFC can be extracted from agricultural by-products. It is therefore classified as a natural stabilizer. At the same time, it also helps to reduce waste from environment.

For  $\beta$ Lg-coated GNPs, we studied the interactions between  $\beta$ Lg and GNPs (200 nm) at pH 3 using a variety of analytical methods.  $\beta$ Lg molecules adsorbed onto GNP surface through electrostatic attraction. The protein molecules should have a strong positive charge at  $\text{pH} < \text{pI}$ , which promote their adsorption to the negative GNPs surfaces. It could be confirmed by changing in the particle charge and shape of UV-Vis spectra. The surface charge of GNPs changed from negative to positive with increasing  $\beta$ Lg concentration, indicating that the globular protein molecules adsorbed to the surfaces of the particles. TEM micrograph also confirmed that protein molecules formed the adsorbed layer around GNPs. Extensive particle aggregation occurred when  $\beta$ Lg did not saturate the GNP surfaces, which was attributed to electrostatic bridging flocculation. The surface load of  $\beta$ Lg molecules onto GNPs was calculated to be  $6.2 \text{ mg m}^{-2}$ . This value is in reasonable accordance with surface load of this protein typically reported for adsorption to the surfaces of lipid droplets (around  $1\text{--}10 \text{ mg m}^{-2}$ ). The Raman study confirms that  $\beta$ Lg was adsorbed to GNPs surface mainly through amino groups and could undergo conformational changes with significant alterations in secondary structure. Different protein concentrations appeared to affect the conformation of the molecules at the gold surfaces, with higher concentrations leading to more compact structures. The changes in the  $\text{NH}_2/\text{NH}_3^+$  peaks, but not the  $\text{COO}^-$  peak, which may also indicate the electrostatic interaction, as mention above. The protein conformation was significantly changed, suggesting that there were other interactions such as steric or hydrophobic interactions.

In addition, bile salts solution was added to  $\beta$ Lg-coated GNPs at pH 7. The results provide valuable insights into the “orogenic mechanism” of interaction of  $\beta$ Lg-coated GNPs at pH 7 with surface active bile salts. At pH 7, amine functional groups from  $\beta$ Lg molecules bind to colloidal GNPs through weak covalent interaction and the interaction via thiolate linkages through the cysteine residues as well, as confirmed by SERS spectra. The bile salts were shown to adsorb to the protein-coated nanoparticle surfaces and alter the interfacial composition, charge, and structure. The increase in interfacial thickness was observed when bile salt was added. From SERS spectra of bile salts-coated GNPs, it is confirmed that bile salt was able to bind GNPs, possibly via interaction with  $\text{OH}^-$  and  $\text{COO}^-$  groups. SERS spectra of protein-coated nanoparticles after bile salt addition contained bands from both protein and bile salts, indicating that the protein was not fully displaced by the bile salts. At relatively low bile salt concentrations, a mixed interface was formed that contains islands of aggregated proteins in a sea of bile salts. At higher bile salt concentrations, proteins might be displaced from the particle surfaces.

For MFC-stabilized emulsions, this study provides practical information that may increase the utilization of MFC as natural emulsifying and stabilizing ingredients in food products. In future studies, the ability of MFC to use as emulsifier and stabilizer in real emulsion-based food products, such as dressing, soup, and ice-cream, etc., should be investigated. The real food emulsions are complicated because they contain several kinds of ingredients, e.g. salts or others stabilizer, which can affect the appearance, and stability of the products. It would be better to understand the role of MFC in stabilizing emulsion in more complex systems. As mentioned above, the emulsion stabilized by MFC exhibited the long term stability against coalescence. Therefore, it could be used this MFC for stabilizing the oil emulsion droplets which incorporate some fat-soluble vitamins or bioactive compounds. Then, it could be controlled the release under gastrointestinal conditions e.g. pH and ionic strength. For future studies about the release in human gastrointestinal tract, it can be done by using an *in vitro* study with the same conditions as human body, for example, a pH-stat instrument for studying the *in vitro* lipid digestion occurred in small intestine.

In future studies of  $\beta$ Lg-coated GNPs, the same analytical approach could be used to study the influence of interfacial engineering approaches on the adsorption of bile salts to particle surfaces under simulated gastrointestinal conditions, e.g., altering emulsifier type, cross-linking interfacial layers, or coating particles with polymer layers. The adsorption of bile salts to lipid droplet surfaces is a key event governing the gastrointestinal fate of ingested lipids. The knowledge gained from this type of study may therefore be useful in the development of foods with controlled functional performance in the gastrointestinal tract, such as increased bioavailability, controlled release, or modulation of satiety response. Some forms of inorganic nanoparticles that are ingested by humans may originally be coated by proteins, and changes in their interfacial composition within the gastrointestinal tract may influence their biological fate.

In addition, SERS is the technique that provides the fundamental knowledge about the interfacial science. This technique could be also applied to study the interaction and conformation of MFC at oil/water interface. It should provide more understanding and information about the long term stability of solid-stabilized emulsion against droplet coalescence. However, an utilization of biopolymer-stabilized solid particles as a model of biopolymer-stabilized oil droplets has some limitation to explain about emulsion instability phenomena, such as coalescence of oil droplets, phase inversion, and Oswald ripening, etc.

## REFERENCES

- Abraham, E., Deepa, B., Pothan, L. A., Jacob, M., Thomas, S., Cvelbar, U., et al. (2011). Extraction of nanocellulose fibrils from lignocellulosic fibres: A novel approach. *Carbohydrate Polymers*, *86*, 1468-1475.
- Adams, S., Higgins, A. M., & Jones, R. A. L. (2002). Surface-mediated folding and misfolding of proteins at lipid/water interfaces. *Langmuir*, *18*, 4854-4861.
- Agoda-Tandjawa, G., Durand, S., Berot, S., Blassel, C., Gaillard, C., Garnier, C., et al. (2010). Rheological characterization of microfibrillated cellulose suspensions after freezing. *Carbohydrate Polymers*, *80*, 677-686.
- Alemdar, A., & Sain, M. (2008). Isolation and characterization of nanofibers from agricultural residues – wheat straw and soy hulls. *Bioresource Technology*, *99*, 1664-1671.
- Andresen, M., Johansson, L. S., Tanem, B. S. & Stenius, P. (2006). Properties and characterization of hydrophobized microfibrillated cellulose. *Cellulose*, *13*, 665-677.
- Ankerfors, M., & Lindström, T. (2007). On the manufacture and uses of nanocellulose. *In the 9th International Conference on Wood & Biofiber Plastic Composites*, May 21-23, 2007, Madison.
- Aguilera, J. M., & Stanley, D. W. (1990). *Microstructural principles of food processing and engineering*. Amsterdam: Elsevier.
- Alvarez-Puebla, R. A., Arceo, E., Goulet, P. J. G., Garrido, J. J., & Aroca, R. F. (2005). Role of nanoparticle surface charge in surface-enhanced Raman scattering. *Journal of Physical Chemistry B*, *109*, 3787-3792.
- Aroca, R. (2006). *Surface-enhanced vibrational spectroscopy*. Chichester, West Sussex: John Wiley & Sons, Ltd.
- Aroca, R. F., Alvarez-Puebla, R. A., Pieczonka, N., Sanchez-Cortez, S., & Garcia-Ramos, J. V. (2005). Surface-enhanced Raman scattering on colloidal nanostructures. *Advances in Colloid and Interface Science*, *116*, 45-61.

- Aveyard, R., Binks, B. P., & Clint, J. H. (2003). Emulsion stabilized solely by colloidal particles. *Advances in Colloid and Interface Science*, *100*, 503-546.
- Barud, H. S., Barrios, C., Regiani, T., Marques, R. F. C., Verelst, M., Dexpert-Ghys, J., et al. (2008). Self-supported silver nanoparticles containing bacterial cellulose membranes. *Materials Science and Engineering C: Materials for Biological Applications*, *28*, 515-518.
- Berli, C. L. A., Quemada, D., & Parker, A. (2003). Gel transition of depletion flocculated emulsions. *Colloids and Surfaces A: Physicochemical and Engineering Aspects*, *215*, 201-204.
- Binks, B. P., Clint, J. H., Mackenzie, G., Simcock, C., & Whitby, C. P. (2005). Naturally occurring spore particles at planar fluid interfaces and in emulsions. *Langmuir*, *21*, 8161-8167.
- Binks, B. P., & Horozov, T. S. (2006). *Colloidal particles at liquid interfaces*. Cambridge: University Press.
- Binks, B. P., & Lumsdon, S. O. (2001). Pickering emulsions stabilized by monodisperse latex particles: effects of particle size. *Langmuir*, *17*, 4540-4547.
- Blanch, E. W., Hecht, L., & Barron, L. D. (1999). New insight into the pH-dependent conformational changes in bovine  $\beta$ -lactoglobulin from Raman optical activity. *Protein Science*, *8*, 1362-1367.
- Bondeson, D., Mathew, A., & Oksman, K. (2006). Optimization of the isolation of nanocrystals from microcrystalline cellulose by acid hydrolysis. *Cellulose*, *13*, 171-180.
- Brewer, S. H., Glomm, W. R., Johnson, M. C., Knag, M. K., & Franzen, S. (2005). Probing BSA binding to citrate-coated gold nanoparticles and surfaces. *Langmuir*, *21*, 9303-9307.
- Brewster, V., Jarvis, R., & Goodacre, R. (2009). Raman spectroscopic techniques for biotechnology and bioprocessing. *European Pharmaceutical Review*, *1*, 48-52.
- Brolo, A. G., Germain, P., & Hager, G. (2002). Investigation of the adsorption of L-cysteine on a polycrystalline silver electrode by surface-enhanced Raman

- scattering (SERS) and surface-enhanced second harmonic generation (SESHG). *Journal of Physical Chemistry B*, *106*, 5982-5987.
- Brown, E. E., & Laborie, M. P. G. (2007). Bioengineering bacterial cellulose/poly (ethylene oxide) nanocomposites. *Biomacromolecules*, *8*, 3074-3081.
- Cao, Y., Wu, J., Zhang, J., Li, H. Q., Zhang, Y., & He, J. S. (2009). Room temperature ionic liquids (RTILs): A new and versatile platform for cellulose processing and derivatization. *Chemical Engineering Journal*, *147*, 13-21.
- Camafeita, L. E., Sanchez-Cortes, S., & Garcia-Ramos, J. V. (1995). SERS of cytosine and its methylated derivatives on gold sols. *Raman Spectroscopy*, *26*, 149-154.
- Cañaveras, F., Madueño, R., Sevilla, J. M., Blázquez, M., & Pineda, T. (2012). Role of the functionalization of the gold nanoparticle surface on the formation of bioconjugates with human serum albumin. *Journal of Physical Chemistry C*, *116*, 10430-10437.
- Cedervall, T., Lynch, I., Lindman, S., Berggård, T., Thulin, E., Nilsson, H. et al. (2007). Understanding the nanoparticle-protein corona using methods to quantify exchange rates and affinities of proteins for nanoparticles. *Proceedings of the National Academy of Sciences of the United States of America*, *104*, 2050-2055.
- Cedervall, T., Lynch, I., Foy, M., Berggård, T., Donnelly, S. C., Cagney, G. et al., (2007). Detailed identification of plasma proteins adsorbed on copolymer nanoparticles. *Angewandte Chemie International Edition*, *46*, 5754-5756.
- Chantrapornchai, W., Clydesdale, F., & McClements, D. J. (2001). Influence of flocculation on optical properties of emulsions. *Journal of Food Science*, *66*, 464-469.
- Chantrapornchai, W., Clydesdale, F., & McClements, D. J. (1999). Influence of droplet characteristics on the optical properties of colored oil-in-water emulsions. *Colloids and Surfaces B: Biointerfaces*, *155*, 373-382.
- Chen, Y., Huang, B., Huang, M., & Cai, B. (2011). On the preparation and characterization of activated carbon from mangosteen shell. *Journal of the Taiwan Institute of Chemical Engineers*, *42*, 837-842.

- Chevalier, Y., & Bolzinger, M. -A. (2013). Emulsions stabilized with solid nanoparticles: Pickering emulsions. *Colloids and Surfaces A: Physicochemical and Engineering Aspects*, 439, 23-34.
- Chuang, C. -H., & Chen, Y. -T. (2009). Raman scattering of L-tryptophan enhanced by surface plasmon of silver nanoparticles: Vibrational assignment and structural determination. *Journal of Raman Spectroscopy*, 40, 150-156.
- Clark, A. H., & Ross-Murphy, S. B. (1987). Structural and mechanical properties of biopolymer gels. *Advances in Polymer Science*, 83, 57-192.
- Corbett, E. C., Zichy, V., Góral, J., & Passingham, C. (1991). Fourier Transform Raman studies of materials and compounds of biological importance-II. The effect of moisture on the molecular structure of the alpha and beta anomers of glucose. *Spectrochimica Acta*, 47A, 1399-1411.
- Cox, W. P., & Merz, E. H. (1958). Correlation of dynamic and steady flow viscosities. *Journal of Polymer Science*, 28, 619-622.
- Croguennec, T., Mollé, D., Mehra, R., & Bouhallab, S. (2004). Spectroscopic characterization of heat-induced nonnative  $\beta$ -lactoglobulin monomers. *Protein Science*, 13, 1340-1346.
- Dalgleish, D. G., West, S. J., & Hallett, F. R. (1997). The characterization of small emulsion droplets made from milk proteins and triglyceride oil. *Colloids and Surfaces A: Physicochemical and Engineering Aspects*, 123, 145-153.
- Das, G., Gentile, F., Coluccio, M. L., Perri, A.M., Nicastrì, A., Mecarini, F., et al. (2011). Principal component analysis based methodology to distinguish protein SERS spectra. *Journal of Molecular Structure*, 993, 500-505.
- Denkov, N. D., Ivanov, I. B., Kralchevsky, P. A., & Wasan, D. T. (1992). A possible mechanism of stabilization of emulsions by solid particles. *Journal of Colloid and Interface Science*, 150, 589-593.
- Dickinson, E. (1992). *Introduction to food colloids*. Oxford, UK: Oxford Science Publishers.
- Dickinson, E. (2003). Hydrocolloids at interfaces and the influence on the properties of dispersed systems. *Food Hydrocolloids*, 17, 25-39.

- Dickinson, E. (2009). Hydrocolloids as emulsifiers and emulsion stabilizers. *Food Hydrocolloids*, 23, 1473-1482.
- Dickinson, E. (2010). Food emulsions and foams: Stabilization by particles. *Current Opinion in Colloid & Interface Science*, 15, 40-49.
- Dickinson, E. (2012). Use of nanoparticles and microparticles in the formation and stabilization of food emulsions. *Trends in Food Science & Technology*, 24, 4-12.
- Dickinson, E., & Stainsby, G. (1982). *Colloids in foods*. London: Elsevier.
- Dinand, E., Chanzy, H., & Vignon, M. R. (1996). Parenchymal cell cellulose from sugar beet pulp. *Cellulose*, 3, 183-188.
- Dinand, E., Chanzy, H., & Vignon, M. R. (1999). Suspensions of cellulose microfibrils from sugar beet pulp. *Food Hydrocolloids*, 13, 275-283.
- Ding, Y., Chen, Z., Xie, J., & Guo, R. (2008). Comparative studies on adsorption behavior of thionine on gold nanoparticles with different sizes. *Journal of Colloid and Interface Science*, 327, 243-250.
- El-Abassy, R. M., Eravuchira, P. J., Donfack, P. von der Kammer, B., & Materny, A. (2011). Fast determination of milk fat content using Raman spectroscopy. *Vibrational Spectroscopy*, 56, 3-8.
- El-Saied, H., Basta, A. H., & Gobran, R. H. (2004). Research progress in friendly environmental technology for the production of cellulose products (bacterial cellulose and its application). *Polymer-Plastics Technology and Engineering*, 43, 797-820.
- Eriksen, Ö., Syverud, K., & Gregerson, Ö. (2008). The use of microfibrillated cellulose produced from kraft pulp as strength enhancer in TMP paper. *Nordic Pulp and Paper Research Journal*, 23, 299-304.
- El-Sayed, M. A. (2001). Some interesting properties of metals confined in time and nanometer space of different shapes. *Accounts of Chemical Research*, 34, 257-264.
- Fontecha, J., Bellanato, J., & Juarez, M. (1993). Infrared and raman spectroscopic study of casein in cheese: Effect of freezing and frozen storage. *Journal of Dairy Science*, 76, 3303-3309.

- Frelichowska, J., Bolzinger, M. –A., & Chevalier, Y. (2010). Effects of solid particle content on properties of o/w Pickering emulsions. *Journal of Colloid and Interface Science*, *351*, 348-356.
- Fruhner, H., Wantke, K. -D., & Lunkenheimer, K. (2000). Relationship between surface dilational properties and foam stability. *Colloids and Surfaces A: Physicochemical and Engineering Aspects*, *162*, 193-202.
- Fukuzumi, H., Saito, T., Iwata, T., Kumamoto, Y., & Isogai, A. (2009). Transparent and high gas barrier films of cellulose nanofibers prepared by TEMPO-mediated oxidation. *Biomacromolecules*, *10*, 162-165.
- Gallier, S., Gordon, K. C., Jiménez-Flores, R., Everett, D. W. (2011). Composition of bovine milk fat globules by confocal Raman microscopy. *International Dairy Journal*, *21*, 402-412.
- Garrell, R. L. (1991). Probing biomolecule-surface interactions with surface-enhanced Raman spectroscopy. *Journal of Bioactive and Compatible Polymers*, *6*, 296-307.
- Georgescu, R. E., Alexov, E. G., & Gunner, M. R. (2002). Combining conformational flexibility and continuum electrostatics for calculating pK<sub>a</sub>s in proteins. *Biophysical Journal*, *83*, 1731-1748.
- Gole, A., Dash, C., Ramakrishnan, V., Sainkar, S. R., Mandale, A. B., Rao, M., et al. (2001). Pepsin-gold colloid conjugates: Preparation, characterization, and enzymatic activity. *Langmuir*, *17*, 1674-1679.
- Habibi, Y., Mahrouz, M., & Vignon, M. R. (2009). Microfibrillated cellulose from the peel of prickly pear fruits. *Food Chemistry*, *115*, 423-429.
- Haiss, W., Thanh, N. T. K., Aveyard, J., & Fernig, D. G. (2007). Determination of size and concentration of gold nanoparticles from UV–Vis spectra. *Analytical Chemistry*, *79*, 4215-4221.
- Haynes, C. L., McFarland, A. D., & Van Duyne, R. P. (2005). Surface-enhanced Raman spectroscopy. *Analytical Chemistry*, *77*, 338a-346a.
- He, J., Cui, S., & Wang, S. -Y. (2008). Preparation and crystalline analysis of high-grade bamboo dissolving pulp for cellulose acetate. *Journal of Applied Polymer Science*, *107*, 1029-1038.

- He, L., Haynes, C., Diez-Gonzalez, F., & Labuza, T. P. (2010). Rapid detection of a foreign protein in milk using IMS–SERS. *Journal of Raman Spectroscopy*, *42*, 1428-1434.
- He, L., Zheng, J., Labuzab, T. P., & Xiao, H. (2013). A surface enhanced Raman spectroscopic study of interactions between casein and polymethoxyflavones. *Journal of Raman Spectroscopy*, *44*, 531-535.
- Henriksson, G., Christiernin, M., & Agnemo, R. (2005). Monocomponent endoglucanase treatment increases the reactivity of softwood sulfite dissolving pulp. *Journal of Industrial Microbiology and Biotechnology*, *32*, 211-214.
- Henriksson, M., Henriksson, G., Berglund, L. A., & Lindström, T. (2007). An environmentally friendly method for enzyme-assisted preparation of microfibrillated cellulose (MFC) nanofibers. *European Polymer Journal*, *43*, 3434-3441.
- Heux, L., Dinand, E., & Vignon, M. R. (1999). Structural aspects in ultrathin cellulose microfibrils followed by <sup>13</sup>C CP-MAS NMR. *Carbohydrate Polymers*, *40*, 115-124.
- Horne, D. S. (1995). Light scattering studies of colloid stability and gelation, In E. Dickinson (Ed.), *New physicochemical techniques for the characterization of complex food systems*, (Chap. 11). London, UK: Blackie Academic & Professional.
- Huang, X., Kakuda, Y., & Cui, W. (2001). Hydrocolloids in emulsions: Particle size distribution and interfacial activity. *Food Hydrocolloids*, *15*, 533-542.
- Hunter, R. J. (1986). *Foundations of colloid science*. Oxford, UK: Oxford University Press.
- Hunter, R. J. (1993). *Introduction to modern colloid science*. Oxford, UK: Oxford University Press.
- Hussain, N., Jaitley, V., & Florence, A. T. (2001). Recent advances in the understanding of uptake of microparticulates across the gastrointestinal lymphatics. *Advanced Drug Delivery Reviews*, *50*, 107-142.

- Ikeda, S. (2003). Atomic force microscopy and Raman scattering spectroscopy studies on heat-induced fibrous aggregates of  $\beta$ -lactoglobulin. *Spectroscopy*, *17*, 195-202.
- Iosin, M., Canpean, V., & Astilean, S. (2011). Spectroscopic studies on pH- and thermally induced conformational changes of Bovine Serum Albumin adsorbed onto gold nanoparticles. *Journal of Photochemistry and Photobiology A: Chemistry*, *217*, 395-401.
- Iosin, M., Toderas, F., Baldeck, P. L., & Astilean, S. (2009). Study of protein-gold nanoparticle conjugates by fluorescence and surface-enhanced Raman scattering. *Journal of Molecular Structure*, *924-926*, 196-200.
- Iwamoto, S., Nakagaito, A. N., & Yano, H. (2007). Nano-fibrillation of pulp fibers for the processing of transparent nanocomposites. *Applied Physics A: Materials Science & Processing*, *89*, 461-466.
- Iwamoto, S., Nakagaito, A. N., Yano, H., & Nogi, M. (2005). Optically transparent composites reinforced with plant fiber-based nanofibers. *Applied Physics A: Materials Science & Processing*, *81*, 1109-1112.
- Ishii, D., Saito, T., & Isogai, A. (2011). Viscoelastic evaluation of average length of cellulose nanofibers prepared by TEMPO-mediated oxidation. *Biomacromolecules*, *12*, 548-550.
- Ivanov, I. B., Danov, K. D., & Kralchevsky, P. A. (1999). Flocculation and coalescence of micron-size emulsion droplets. *Colloids and Surfaces A: Physicochemical and Engineering Aspects*, *152*, 161-182.
- Jana, N. R., Gearheart, L., & Murphy, C. J. (2001). Wet chemical synthesis of high aspect ratio cylindrical gold nanorods. *Journal of Physical Chemistry B*, *105*, 4065-4067.
- Jenkins, P., & Snowden, M. (1996). Depletion flocculation in colloidal dispersions. *Advances in Colloid and Interface Science*, *68*, 57-96.
- Kabalnov, A. S., & Shchukin, E. D. (1992). Ostwald ripening theory: Applications to fluorocarbon emulsion stability. *Advances in Colloid and Interface Science*, *38*, 69-97.

- Kalab, M., Allan-Wojtas, P., & Miller, S. S. (1995). Microscopy and other imaging techniques in food structure analysis. *Trends in Food Science and Technology*, 6, 177-186.
- Kalashnikova, I., Bizot, H., Bertoncini, P., Cathala, B., & Capron, I. (2013). Cellulosic nanorods of various aspect ratios for oil in water Pickering emulsions. *Soft Matter*, 9, 952-959.
- Kalashnikova, I., Bizot, H., Cathala, B., & Capron, I. (2011). New Pickering emulsions stabilized by bacterial cellulose nanocrystals. *Langmuir*, 27, 7471-7479.
- Kalashnikova, I., Bizot, H., Cathala, B., & Capron, I. (2012). Modulation of cellulose nanocrystals amphiphilic properties to stabilize oil/water interface. *Biomacromolecules*, 13, 267-275.
- Kasthuri, J., & Rajendiran, N. (2009). Functionalization of silver and gold nanoparticles using amino acid conjugated bile salts with tunable longitudinal plasmon resonance. *Colloids and Surfaces B: Biointerfaces*, 73, 387-393.
- Keowmaneechai, E. & McClements, D. J. (2002). Influence of EDTA and citrate on physicochemical properties of whey protein-stabilized oil-in-water emulsions containing CaCl<sub>2</sub>. *Journal of Agricultural and Food Chemistry*, 50, 7145-7153.
- Kerker, M. (1969). *The scattering of light and other electromagnetic radiation*. New York: Academic Press.
- Kim, K., Lee, S. J., & Kim, K. L. (2004). Surface-enhanced Raman scattering of 4-nitrothioanisole in Ag sol. *Journal of Physical Chemistry B*, 108, 16208-16212.
- Kirby, A. R., Gunning, A. P., & Morris, V. J. (1995). Atomic force microscopy in food research: A new technique comes of age. *Trends in Food Science and Technology*, 6, 359-365.
- Klemm, D., Heublein, B., Fink, H. P., & Bohn, A. (2005). Cellulose: Fascinating biopolymer and sustainable raw material. *Angewandte Chemie International Edition*, 44, 3358-3393.

- Klemm, D., Kramer, F., Moritz, S., Lindström, T., Ankerfors, M., Gray, D., et al. (2011). Nanocelluloses: a new family of nature-based materials. *Angewandte Chemie International Edition*, 50, 5438-5466.
- Klemm, D., Schumann, D., Kramer, F., Hessler, N., Hornung, M., Schmauder, H. P., et al. (2006). Nanocelluloses as innovative polymers in research and application. *Polysaccharides*, 205, 49-96.
- Kontopidis, G., Holt, C., & Sawyer, L. (2004). Beta-lactoglobulin: Binding properties, structure, and function. *Journal of Dairy Science*, 87, 785-796.
- Kralova, I., & Sjöblom, J. (2009). Surfactants used in food industry: A review. *Journal of Dispersion Science and Technology*, 30, 1363–1383.
- Kudelski, A. (2008). Analytical applications of Raman spectroscopy. *Talanta*, 76, 1-8.
- Larison, K. D. (1992). *Handbook of fluorescent probes and research chemicals*. Eugene, OR: Molecular Probes.
- Lavoine, N., Desloges, I., Dufresne, A., & Bras, J. (2012). Microfibrillated cellulose – its barrier properties and applications in cellulosic materials: A review. *Carbohydrate Polymers*, 90, 735-764.
- Lee, C., Kim, S. I., Yoon, C., Gong, M., Choi, B. K., Kim, K., & Joo, S. -W. (2004). Size-dependent adsorption of 1,4-phenylenediisocyanide onto gold nanoparticle surfaces. *Journal of Colloid and Interface Science*, 271, 41-46.
- Lee, G. J., Son, H. A., Cho, J. W., Choi, S. K., Kim, H. T., & Kim, J. W. (2014). Stabilization of Pickering emulsions by generating complex colloidal layers at liquid-liquid interfaces. *Journal of Colloid and Interface Science*, 413, 100-105.
- Lehnert, S., Tarabishi, H., & Leuenberger, H. (1994). Investigation of thermal phase inversion in emulsions. *Colloids and Surfaces A: Physicochemical and Engineering Aspects*, 91, 227-235.
- Leitner, J., Hinterstoisser, B., Wastyn, M., Keckes, J., & Gindl, W. (2007) Sugar beet cellulose nanofibril-reinforced composites. *Cellulose*, 14, 419-425.
- Lekkerkerker, H. N. W., & Tuinier, R. (2011). *Colloids and the depletion interaction*. New York: Springer.

- Lesmes, U., & McClements, D. J. (2012). Controlling lipid digestibility: response of lipid droplets coated by  $\beta$ -lactoglobulin-dextran maillard conjugates to simulated gastrointestinal conditions. *Food Hydrocolloids*, *26*, 221-230.
- Lesmes, U., Sandra, S., Decker, E. A., & McClements, D. J. (2010). Impact of surface deposition of lactoferrin on physical and chemical stability of omega-3 rich lipid droplets stabilised by caseinate. *Food Chemistry*, *123*, 99-106.
- Li, J., Wei, X., Wang, Q., Chen, J., Chang, G., Kong, L., et al. (2012). Homogenous isolation of nanocellulose from sugarcane bagasse by high pressure homogenization. *Carbohydrate Polymers*, *90*, 1609-1613.
- Li, T., Guo, L., & Wang, Z. (2008). Gold nanoparticle-based surface enhanced Raman scattering spectroscopic assay for the detection of protein-protein interactions. *Analytical Science*, *24*, 907-910.
- Link, S., Mohamed, M. B., & El-Sayed, M. A. (1999). Simulation of the optical absorption spectra of gold nanorods as a function of their aspect ratio and the effect of the medium dielectric constant. *Journal of Physical Chemistry B*, *103*, 3073-3077.
- Li-Chan, E. C. Y. (1996). The applications of Raman spectroscopy in food science. *Trends in Food Science & Technology*, *7*, 361-370.
- Luo, Z., Murray, B. S., Yusoff, A., Morgan, M. R. A., Povey, M. J. W., & Day, A. J. (2011). Particle-stabilizing effects of flavonoids at the oil-water interface. *Journal of Agricultural and Food Chemistry*, *59*, 2636-2645.
- Maa, Y. F., & Hsu, C. (1996). Liquid-liquid emulsification by rotor/stator homogenization. *Journal of Controlled Release*, *38*, 219-228.
- Mackie, A. R., Gunning, A. P., Ridout, M. J., Wilde, P. J., & Morris, V. J. (2001). Orogenic displacement in mixed  $\beta$ -lactoglobulin/ $\beta$ -casein films at the air/water interface. *Langmuir*, *17*, 6593-6598.
- Mackie, A. R., Gunning, A. P., Wilde, P. J., & Morris, V. J. (1999). Orogenic displacement of protein from the air/water interface by competitive adsorption. *Journal of Colloid and Interface Science*, *210*, 157-166.
- Mackie, A. R., Gunning, A. P., Wilde, P. J., & Morris, V. J. (2000a). Orogenic displacement of protein from the oil/water interface. *Langmuir*, *16*, 2242-2247.

- Mackie, A. R., Gunning, A. P., Wilde, P. J., & Morris, V. J. (2000b). Competitive displacement of  $\beta$ -lactoglobulin from the air/water interface by sodium dodecyl sulfate. *Langmuir*, *16*, 8176-8181.
- Madivala, B., Vandebril, S., Fransaeer, J., & Vermant, J. (2009). Exploiting particle shape in solid stabilized emulsions. *Soft Matter*, *5*, 1717-1727.
- Mahon, E., Salvati, A., Baldelli Bombelli, F., Lynch, I., & Dawson, K. A. (2012). Designing the nanoparticle–biomolecule interface for targeting and therapeutic delivery. *Journal of Controlled Release*, *161*, 164-174.
- Maldonado-Valderrama, J., Gunning, A. P., Wilde, P. J., & Morris, V. J. (2010). In vitro gastric digestion of interfacial protein structures: visualization by AFM. *Soft Matter*, *6*, 4908-4915.
- Maldonado-Valderrama, J., Woodward, N. C., Gunning, A. P., Ridout, M. J., Husband, F. A., Mackie, A. R., et al. (2008). Interfacial characterization of  $\beta$ -lactoglobulin networks: Displacement by bile salts. *Langmuir*, *24*, 6759-6767.
- Malmsten, M. (2003). *Biopolymers at interfaces*. New York: Marcel Dekker.
- Malvern-Instrument-Ltd. (2004). *Zetasizer nano series user manual*. Worcestershire, UK.
- Mandal, A., & Chakrabarty, D. (2011). Isolation of nanocellulose from waste sugarcane bagasse (SCB) and its characterization. *Carbohydrate Polymers*, *86*, 1291-1299.
- Manoj, P., Fillery-Travis, A. J., Watson, A. D., Hibberd, D. J., & Robins, M. M. (1998). Characterization of a depletion-flocculated polydisperse emulsion. Part I: Creaming behavior. *Journal of Colloid and Interface Science*, *207*, 283-293.
- Mao, Y., & McClements, D. J. (2011). Modulation of bulk physicochemical properties of emulsions by hetero-aggregation of oppositely charged protein-coated lipid droplets. *Food Hydrocolloids*, *25*, 1201-1209.
- Masereel, B., Dinguizli, M., Bouzin, C., Moniotte, N., Feron, O., Gallez, B. et al. (2010). Antibody immobilization on gold nanoparticles coated layer-by-layer with polyelectrolytes. *Journal of Nanoparticle Research*, *13*, 1573-1580.

- McClellan, S. J., & Franses, E. I. (2003). Effect of concentration and denaturation on adsorption and surface tension of bovine serum albumin. *Colloids and Surfaces B: Biointerfaces*, 28, 63-75.
- McClements, D. J. (2005). *Food emulsions: Principles, practice, and techniques* (2<sup>nd</sup> ed.). Boca Raton, FL: CRC Press.
- McClements, D. J. (2010). Emulsion design to improve the delivery of functional lipophilic components. *Annual Review of Food Science and Technology*, 1, 241-269.
- McClements, D. J., & Dungan, S. R. (1993). Factors that affect the rate of oil exchange between oil-in-water emulsion droplets stabilized by a non-ionic surfactant: Droplet size, surfactant concentration and ionic strength. *Journal of Physical Chemistry*, 97, 7304-7308.
- McKenna, B. M., & Lyng, J. G. (2003). Introduction to food rheology and its measurement, In B.M. McKenna (Ed.), *Texture in foods: Semi-solid foods* (Chap. 6). Boca Raton, FL: CRC Press.
- Meng, G., Chan, J. C. K., Rousseau, D., & Li-Chan, E. C. Y. (2005). Study of protein–lipid interactions at the bovine serum albumin/oil interface by Raman microspectroscopy. *Journal of Agricultural and Food Chemistry*, 53, 845-852.
- Merlin, J. -C., Statoua, A., Cornard, J. -P., Saidi-Ildrissi, M., & Brouillard, R. (1994). Resonance Raman spectroscopic studies of anthocyanins and anthocyanidins in aqueous solutions. *Phytochemistry*, 35, 227-232.
- Mezzenga, R., & Fischer, P. (2013). The self-assembly, aggregation and phase transitions of food protein systems in one, two and three dimensions. *Reports on Progress in Physics*, 76, 046601.
- Morris, V. J., & Gunning, A. P. (2008). Microscopy, microstructure and displacement of proteins from interfaces: Implications for food quality and digestion. *Soft Matter*, 4, 943-951.
- Munoz, V. A., & Mikula, R. J. (1997). Characterization of petroleum industry emulsions and suspensions using microscopy. *Journal of Canadian Petroleum Technology*, 36, 23-36.

- Mun, S., Decker, E. A., Park, Y., Weiss, J., & McClements, D. J. (2006). Influence of interfacial composition on in vitro digestibility of emulsified lipids: Potential mechanism for chitosan's ability to inhibit fat digestion. *Food Biophysics*, *1*, 21-29.
- Nakagaito, A. N., & Yano, H. (2005). Novel high-strength biocomposites based on microfibrillated cellulose having nano-order-unit web-like network structure. *Applied Physics A: Materials Science and Processing*, *80*, 155-159.
- Nasir, A., & McGuire, J. (1998). Sequential and competitive adsorption of bovine serum albumin and  $\beta$ -lactoglobulin, and their resistance to exchange with  $\alpha$ -lactalbumin and  $\beta$ -casein. *Food Hydrocolloids*, *12*, 95-103.
- Ngarize, S., Herman, H., Adams, A., & Howell, N. (2000). Comparison of changes in the secondary structure of unheated, heated, and high-pressure-treated  $\beta$ -lactoglobulin and ovalbumin proteins using Fourier Transform Raman spectroscopy and self-deconvolution. *Journal of Agricultural and Food Chemistry*, *52*, 6470-6477.
- Nikoobakht, B., & El-Sayed, M. A. (2003). Surface-enhanced Raman scattering studies on aggregated gold nanorods. *Journal of Physical Chemistry A*, *107*, 3372-3378.
- Niño, M. R. R., Wilde, P. J., Clark, D. C., & Patino, J. M. R. (1998). Surface dilational properties of protein and lipid films at the air-water interface. *Langmuir*, *14*, 2160-2166.
- Nonaka, M., Li-Chan, E., & Nakai, S. (1993). Raman spectroscopic study of thermally induced celeration of whey proteins. *Journal of Agricultural and Food Chemistry*, *41*, 1176-1181
- Ougiya, H., Watanabe, K., Morinaga, Y., & Yoshinaga, F. (1997). Emulsion-stabilizing effect of bacterial cellulose. *Bioscience, Biotechnology, and Biochemistry*, *61*, 1541-1545.
- Owens, D. E. III, & Peppas, N. A. (2006). Opsonization, biodistribution, and pharmacokinetics of polymeric nanoparticles. *International Journal of Pharmaceutics*, *307*, 93-102.

- Oza, K. P., & Frank, S. G. (1986). Microcrystalline cellulose stabilized emulsions. *Journal of Dispersion Science and Technology*, 7, 543-561.
- Pääkkö, M., Ankerfors, M., Kosonen, H., Nykänen, A., Ahola, S., Österberg, M., et al. (2007). Enzymatic hydrolysis combined with mechanical shearing and high-pressure homogenization for nanoscale cellulose fibrils and strong gels. *Biomacromolecules*, 8, 1934-1941.
- Pacek, A. W., Moore, I. P. T., Nienow, A. W., & Calabrese, R. V. (1994). Video technique for measuring dynamics of liquid-liquid dispersion during phase inversion. *AIChE Journal*, 40, 1940-1949.
- Pandolfe, W. D. (1995). Effect of premix condition, surfactant concentration and oil level on the formation of oil-in-water emulsions by homogenization. *Journal of Dispersion Science and Technology*, 16, 633-650.
- Pashley, R. M. (2003). Effect of degassing on the formation and stability of surfactant-free emulsions and fine teflon dispersions. *Journal of Physical Chemistry B*, 107, 1714-172-.
- Pérez, M. D., & Calvo, M. (1995). Interaction of  $\beta$ -lactoglobulin with retinol and fatty acids and its role as a possible biological function for this protein: A review. *Journal of Dairy Science*, 78, 978-988.
- Phillips, L. G., Whitehead, D. M., & Kinsella, J. E. (1994). *Structure-function properties of food proteins*. San Diego, CA: Academic Press.
- Pickering, S. U. (1907). Emulsions. *Journal of the Chemical Society*, 91, 2001-2021.
- Powell, J. J., Faria, N., Thomas-McKay, E., & Pele, L. C. (2010). Origin and fate of dietary nanoparticles and microparticles in the gastrointestinal tract. *Journal of Autoimmunity*, 34, 226-233.
- Prakongpan, T., Nitithamyong, A., & Luangpituksa, P. (2002). Extraction and application of dietary fiber and cellulose from pineapple cores. *Journal of Food Science*, 67, 1308-1313.
- Quiévy, N., Jacquet, N., Sclavons, M., Deroanne, C., Paquot, M., & Devaux, J. (2010). Influence of homogenization and drying on the thermal stability of microfibrillated cellulose. *Polymer Degradation and Stability*, 95, 306–314.

- Ramsden, W. (1904). Separation of solids in the surface-layers of solutions and suspensions. *Proceedings of the Royal Society of London*, 72, 156-164.
- Rao, M. A. (1999). *Rheology of fluid and semisolid foods: Principles and applications*. Gaithersburg, MD: Aspen Publishers, Inc.
- Rao, M. A. (2007). *Rheology of fluid and semisolid foods: Principles and applications* (2nd ed.). New York: Springer.
- Saito, T., Hirota, M., Tamura, N., Kimura, S., Fukuzumi, H., Heux, L., et al. (2009). Individualization of nano-sized plant cellulose fibrils by direct surface carboxylation using TEMPO catalyst under neutral conditions. *Biomacromolecules*, 10, 1992-1996.
- Sanchez-Cortes, S., Garcia-Ramos, J. V., & Morcillo, G. (1994). Morphological study of metal colloids employed as substrate in the SERS spectroscopy. *Journal of Colloid and Interface Science*, 167, 428-436.
- Sanchez-Cortes, S., Garcia-Ramos, J. V., Morcillo, G., & Tinti, A. (1995). Morphological study of silver colloids employed in surface-enhanced Raman spectroscopy: Activation when exciting in visible and near-infrared regions. *Journal of Colloid and Interface Science*, 175, 358-368.
- Santipanichwong, R., & Supphantharika, M. (2009). Influence of different  $\beta$ -glucans on the physical and rheological properties of egg yolk stabilized oil-in-water emulsions. *Food Hydrocolloids*, 23, 1279-1287.
- Sarkar, A., Horne, D. S., & Singh, H. (2010). Interactions of milk protein-stabilized oil-in-water emulsions with bile salts in a simulated upper intestinal model. *Food Hydrocolloids*, 24, 142-151.
- Schmelz, T., Lesmes, U., Weiss, J., & McClements, D. J. (2011). Modulation of physicochemical properties of lipid droplets using  $\beta$ -lactoglobulin and/or lactoferrin interfacial coatings. *Food Hydrocolloids*, 25, 1181-1189.
- Segal, L., Creely, J. J., Martin, A. E., & Conrad, C. M. (1959). An empirical method for estimating the degree of crystallinity of native cellulose using the X-ray diffractometer. *Textile Research Journal*, 29, 786-794.
- Seo, J. A., Hédoux, A., Guinet, Y., Paccou, L., Affouard, F., Lerbret, A., et al. (2010). Thermal denaturation of beta-lactoglobulin and stabilization mechanism

- by trehalose analyzed from Raman spectroscopy investigations. *Journal of Physical Chemistry B*, *114*, 6675-6684.
- Shang, L., Wang, Y., Jiang, J., & Dong, S. (2007). pH-dependent protein conformational changes in albumin : gold nanoparticle bioconjugates : A spectroscopic study. *Langmuir*, *23*, 2714-2721.
- Shannon, R. J., Fenerty, J., Hamilton, R. J., & Padley, F. B. (1992). The polymorphism of diglycerides. *Journal of the Science of Food and Agriculture*, *60*, 405-417.
- Shogren, R. L., Peterson, S. C., Evans, K. O., & Kenar, J. A. (2011). Preparation and characterization of cellulose gels from corn cobs. *Carbohydrate Polymers*, *86*, 1351-1357.
- Siró, I., & Plackett, D. (2010). Microfibrillated cellulose and new nanocomposites materials: A review. *Cellulose*, *17*, 459-494.
- Spence, K. L., Venditti, R. A., Habibi, Y., Rojas, O. J., & Pawlak, J. J. (2010). The effect of chemical composition on microfibrillar cellulose films from wood pulps: Mechanical processing and physical properties. *Bioresource Technology*, *101*, 5961-5968.
- Stephen, A. M. (1995). *Food polysaccharides and their applications*. New York: Marcel Decker, Inc.
- Stiles, P. L., Dieringer, J. A., Shah, N. C., & Van Duyne, R. P. (2008). Surface-enhanced Raman spectroscopy. *Annual Review of Analytical Chemistry*, *1*, 601-626.
- Sun, X. F., Sun, R. C., Tomkinson, J., & Baird M. S. (2003). Isolation and characterization of lignins, hemicelluloses, and cellulose from wheat straw by alkaline peroxide treatment. *Cellulose Chemistry and Technology*, *37*, 283-304.
- Surewicz, W. K., Mantsch, J. H. H., & Chapman, D. (1993). Perspectives in biochemistry determination of protein secondary structure by Fourier Transform Infrared spectroscopy: A critical assessment. *Biochemistry*, *32*, 389-394.

- Surh, J., Decker, E. A., & McClements, D. J. (2006). Properties and stability of oil-in-water emulsions stabilized by fish gelatin. *Food Hydrocolloids*, *20*, 569-606.
- Svagan, A. J., Samir, M. A. S. A., & Berglund, L. A. (2008). Biomimetic foams of high mechanical performance based on nanostructured cell walls reinforced by native cellulose nanofibrils. *Advanced Materials*, *20*, 1263-1269.
- Syverud, K., & Stenius, P. (2009). Strength and barrier properties of MFC films. *Cellulose*, *16*, 75-85.
- Tadros, T. F. (2004). Application of rheology for assessment and prediction of the long-term physical stability of emulsions. *Advances in Colloid and Interface Science*, *108-109*, 227-258.
- Talbert, J. N., & Goddard, J. M. (2012). Enzymes on material surfaces. *Colloids and Surfaces B: Biointerfaces*, *93*, 8-19.
- Taylor, P. (1995). Ostwald ripening in emulsions. *Colloids and Surfaces A: Physicochemical and Engineering Aspects*, *99*, 175.
- Turbak, A. F., Snyder, F. W., & Sandberg, K. R. (1983). *Suspensions containing microfibrillated cellulose*. U.S. Patent No. 4,378,381.
- Turbak, A. F., Snyder, F. W., & Sandberg, K. R. (1984). *Microfibrillated cellulose*. U.S. Patent No. 4,483,743.
- Tzoumaki, M. V., Moschakis, T., Kiosseoglou, V., & Biliaderis, C. G. (2011). Oil-in-water emulsions stabilized by chitin nanocrystal particles. *Food Hydrocolloids*, *25*, 1521-1529.
- van der Zande, B. M. I., Böhmer, M. R., Fokkink, L. G. J., & Schöenenberger, C. (2000). Colloidal dispersions of gold rods: Synthesis and optical properties. *Langmuir*, *16*, 451-458.
- Venketesh, S., & Dayananda, C. (2008). Properties, potentials, and prospects of antifreeze proteins. *Critical Reviews in Biotechnology*, *28*, 57-82.
- Walstra, P. (1996). *Food chemistry*. New York: Marcel Dekker.
- Walstra, P., & van Vliet, T. (2008). Dispersed systems: Basic considerations, In S. Damodaran, K. L. Parkin, & O. R. Fennema (Eds.), *Food Chemistry* (4<sup>th</sup> ed., pp. 785-786). New York: Marcel Dekker

- Wang, B., & Sain, M. (2007). Dispersion of soybean stock-based nanofiber in a plastic matrix. *Polymer International*, *56*, 538-546.
- Wang, B., Sain, M., & Oksman, K. (2007). Study of structural morphology of hemp fiber from the micro to the nanoscale. *Applied Composite Materials*, *14*, 89-103.
- Wang, Q., He, L., Labuza, T. P., & Ismail, B. (2013). Structural characterisation of partially glycosylated whey protein as influenced by pH and heat using surface-enhanced Raman spectroscopy. *Food Chemistry*, *139*, 313-319.
- Warren, D. B., Chalmers, D. K., Hutchison, K., Dang, W., & Pouton, C. W. (2006). Molecular dynamics simulations of spontaneous bile salt aggregation. *Colloids and Surfaces A: Physicochemical and Engineering Aspects*, *280*, 182-193.
- Weiss, J., & McClements, D. J. (2000). Influence of Ostwald ripening on rheology of oil-in-water emulsions containing electrostatically stabilized droplets. *Langmuir*, *16*, 2145-2150.
- Whitby, C. P., Fischer, F. E., Fornasiero, D., & Ralston, J. (2011). Shear-induced coalescence of oil-in-water Pickering emulsions. *Journal of Colloid and Interface Science*, *361*, 170-177.
- Wickham, M., Garrod, M., Leney, J., Wilson, P. D., & Fillery-Travis, A. (1998). Modification of a phospholipid stabilized emulsion interface by bile salt: Effect on pancreatic lipase activity. *Journal of Lipid Research*, *39*, 623-632.
- Wilde, P. J., & Chu, B. S. (2011). Interfacial & colloidal aspects of lipid digestion. *Advances in Colloid and Interface Science*, *165*, 14-22.
- Winuprasith, T., & Suphantharika, M. (2013). Microfibrillated cellulose from mangosteen (*Garcinia mangostana* L.) rind: Preparation, characterization, and evaluation as an emulsion stabilizer. *Food Hydrocolloids*, *32*, 383-394.
- Winuprasith, T., Suphantharika, M., McClements, D. J., & He, L. (2014). Spectroscopic studies of conformational changes of  $\beta$ -lactoglobulin adsorbed on gold nanoparticle surfaces. *Journal of Colloid and Interface Science*, *416*, 184-189.

- Wittenauer, J., Falk, S., Schweiggert-Weisz, U., & Carle, R. (2012). Characterisation and quantification of xanthenes from the aril and pericarp of mangosteens (*Garcinia mangostana* L.) and a mangosteen containing functional everage by HPLC-DAD- MS<sup>n</sup>. *Food Chemistry*, 134, 445-452.
- Xhanari, K., Syverud, K., Chinga-Carrasco, G., Paso, K., & Stenius, P. (2011). Structure of nanofibrillated cellulose layers at the o/w interface. *Journal of Colloid and Interface Science*, 356, 58-62.
- Ye, A., & Singh, H. (2006). Adsorption behaviour of lactoferrin in oil-in-water emulsions as influenced by interactions with  $\beta$ -lactoglobulin. *Journal of Colloid and Interface Science*, 295, 249-254.
- Ye, A., & Singh, H. (2007). Formation of multilayers at the interface of oil-in-water emulsion via interactions between lactoferrin and  $\beta$ -lactoglobulin. *Food Biophysics*, 2, 125-132.
- Yu, H., Liu, R. G., Shen, D. W., Jiang, Y., & Huang, Y. (2005). Study on morphology and orientation of cellulose in the vascular bundle of wheat straw. *Polymer*, 46, 5689-5694.
- Yusoff, A., & Murray, B. S. (2011). Modified starch granules as particle-stabilizer of oil-in-water emulsions. *Food Hydrocolloid*, 25, 42-55.
- Zarena, A. S., Bhattacharya, S., & Kadimi, U. S. (2012). Mangosteen oil-in-water emulsions: Rheology, creaming, and microstructural characteristics during storage. *Food and Bioprocess Technology*, 5, 3007-3013.
- Zhang, S., Zhang, Z., Lin, M., & Vardhanabhuti, B. (2012). Raman spectroscopic characterization of structural changes in heated whey protein isolate upon soluble complex formation with pectin at near neutral pH. *Journal of Agricultural and Food Chemistry*, 60, 12029-12035.
- Zimmermann, T., Bordeanu, N., & Strub, E. (2010). Properties of nanofibrillated cellulose from different raw materials and its reinforcement potential. *Carbohydrate Polymers*, 79, 1086-1093.
- Zuluaga, R., Putaux, J. L., Restrepo, A., Mondragón, I., & Ganan, P. (2007). Cellulose microfibrils from banana farming residues: Isolation and characterization. *Cellulose*, 14, 585-592.

## **APPENDIX**

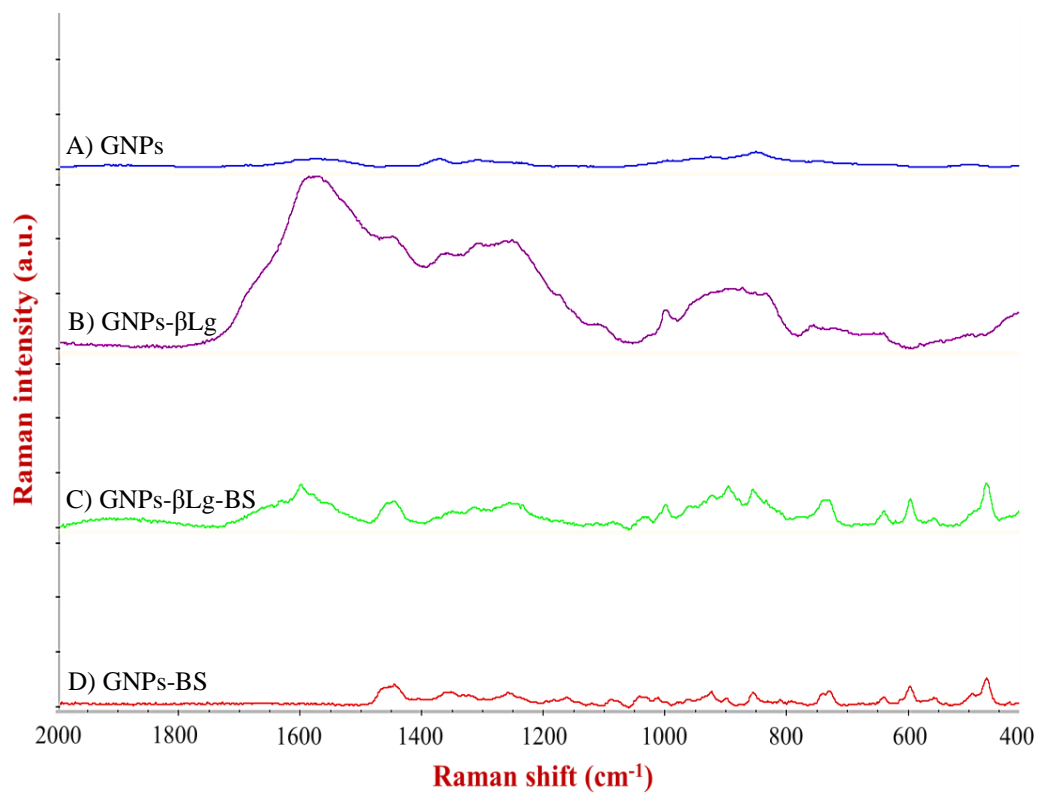


**Figure A.1** Original surface-enhanced Raman scattering (SERS) spectra of GNPs (A), GNPs- $\beta$ Lg (B), GNPs- $\beta$ Lg-BS (C), and GNPs-BS (D).

## **BIOGRAPHY**

<b>NAME</b>	Miss Thunnalin Winuprasith
<b>DATE OF BIRTH</b>	June 16, 1984
<b>PLACE OF BIRTH</b>	Samut Sakhon, Thailand
<b>INSTITUTE ATTENDED</b>	Mahidol University, 2002-2006: Bachelor of Science (Public Health) Mahidol University, 2006-2008: Master of Science (Food and Nutrition for Development) Mahidol University, 2009-2013: Doctor of Philosophy (Biotechnology)
<b>SCHOLARSHIP</b>	The Thailand Research Fund and Mahidol University through the Royal Golden Jubilee Ph.D. Program (Grant No. PHD/0244/2551). The Center of Excellence on Agricultural Biotechnology, Science and Technology Postgraduate Education and Research Development Office, Office of Higher Education Commission, Ministry of Education (AG-BIO/PERDO-CHE).

**EXPERIENCES**

Oct, 2012 – Sep, 2013

“Spectroscopic studies, including surface-enhanced Raman scattering (SERS) technique to study conformational changes of protein coating on gold nanoparticles” at Department of Food Science, University of Massachusetts, Amherst, USA. (Under the supervision of Prof. Dr. David Julian McClements and Dr. Lili He)

**HOME ADDRESS**

1300/601 Norrarachutid Rd., Mahachai,  
Amphoe Mueang, Samut Sakhon,  
Thailand 74000

Tel. +66(8) 9665 9863

Email: [thunnalinw@gmail.com](mailto:thunnalinw@gmail.com)

[thunnalinwi@gmail.com](mailto:thunnalinwi@gmail.com)

**PRESENTATIONS**

1. Winuprasith, T. & Suphantharika, M. (2013, December 4-5). Microfibrillated cellulose from mangosteen (*Garcinia mangostana* L.) rind: Preparation, characterization, and evaluation as an emulsion stabilizer. Oral presented at 2<sup>nd</sup> Malaysia-Thailand Graduate Forum 2013 (MTGF 2013), Universiti of Putra, Malaysia (UPM).
2. Winuprasith, T. & Suphantharika, M. (2014, May 28-30). Evaluation of emulsion stabilizing properties of microfibrillated cellulose from mangosteen rind. Poster presented at the RGJ-Ph.D. Congress XV, Jomtien Palm Beach Resort, Pattaya, Chonburi, Thailand.
3. Winuprasith, T. & Suphantharika, M. (2014, June 21-24). Emulsion stabilizing properties of microfibrillated cellulose from mangosteen (*Garcinia mangostana* L.) rind. Poster presented at the IFT Annual Meeting and

Food Expo 2014 at New Orleans Morial Convention Center, New Orleans, LA, USA.

## **PUBLICATIONS**

1. Winuprasith, T. & Suphantharika, M. (2013). Microfibrillated cellulose from mangosteen (*Garcinia mangostana* L.) rind: Preparation, characterization, and evaluation as an emulsion stabilizer. *Food Hydrocolloids*, 32, 383-394.
2. Winuprasith, T., Suphantharika, M., McClements, D. J. & He, L. (2014). Spectroscopic studies of conformational changes of  $\beta$ -lactoglobulin adsorbed on gold nanoparticle surfaces. *Journal of Colloid and Interface Science*, 416, 184-189.
3. Winuprasith, T., Chantarak, S., Suphantharika, M., He, L. & McClements, D. J. (2014). Alterations in nanoparticle protein corona by biological surfactants: Impact of bile salts on  $\beta$ -lactoglobulin-coated gold nanoparticles. *Journal of Colloid and Interface Science*, 426, 333-340.
4. Winuprasith, T., & Suphantharika, M. (2014). Properties and stability of oil-in-water emulsions stabilized by microfibrillated cellulose from mangosteen rind. *Food Hydrocolloids*, (under review).